Patterns and causes of spatial and temporal variability of dust presence in the central and western Sahara

A thesis submitted to the University of Oxford for the degree of Doctor of Philosophy in Geography and the Environment

Ian Ashpole

St John's College

Trinity 2013

Abstract

Dust is a critical component of the Earth System. The central and western Sahara (CWS) is the dustiest place on Earth during the northern hemisphere summer. Understanding patterns and causes of spatial and temporal variability of dust presence here is essential for its reliable simulation in numerical models of weather and climate. Four papers in this thesis contribute to that objective, utilising a combination of high temporal resolution satellite data and global atmospheric reanalyses for June – August 2004 – 2010 inclusive.

The first paper develops an objective dust detection scheme for the CWS using data from the Spinning Enhanced Visible and Infrared Imager (SEVIRI), which are available every 15 minutes around the clock. These data have shed valuable insight on CWS dust processes, but their subjective application has to date limited their range of applications. The SEVIRI dust flag (SDF) developed here is evaluated against other widely used surface and satellite derived indicators of dustiness and it is found to reliably detect the presence of moderate-heavy dust loadings. The distribution of dust each summer is presented, revealing a high degree of interannual variability in overall dust coverage.

The second paper utilises SDF to create an objective, high spatial resolution dust source map, based on the automated tracking of individual dust plumes. The most active sources are associated predominantly with palaeo-lakes and outwash plains, typically around the Saharan mountains. There is a clear intraseasonal progression of active source areas, controlled by regional climatology. The tracking scheme describes the transport trajectory of dust events following their initiation and the spatial association with deep convection at this time, revealing a clear regional divide in the relative importance of known meteorological mechanisms that drive dust emission from the dominant sources.

The third paper uses an unsupervised clustering algorithm to classify maps of daily dust presence frequency and identify patterns of intraseasonal variability in CWS dust coverage. The resulting idealised dust states vary according to frequency of dust occurrence and its location, demonstrating a clear progression in preferred dust location from June – August and preferred state transitions from one day to the next. High daily dust occurrence frequency corresponds to an advanced West African Monsoon flow and low daily dust occurrence frequency corresponds to a Harmattan-dominated CWS. The overall location of the dust is linked to the location of the Sahara Heat Low, which changes as the summer progresses.

The final paper addresses interannual variability in summertime dust presence frequency by comparing the 2 years with highest (2005) and lowest (2008) dust presence. The key difference is the occurrence of 3 multi-day periods in 2005 characterised by anomalously high dust presence. Case study comparison with the 3 periods of highest dust presence in 2008 identifies the anticyclonic circulation of the midtroposphere as a key control on dust duration over the CWS, dictating whether emitted dust is efficiently transported away from the CWS or whether it remains in suspension over the region for prolonged periods of time, up to several days in the anomalously dusty periods of 2005.

Acknowledgements

A blanket but sincere "thankyou" is all that I can offer to everybody that has contributed to the development of this thesis or its completion; you are too numerous to mention in person. There are however a few who must not go unnamed.

Firstly, I owe huge thanks to my supervisor Richard Washington. Without him this thesis would simply not have happened. Quite beyond being a great source of inspiration, expertise, advice and support, he has encouraged me to develop my own ideas and taught me that time spent thinking or learning with no initial tangible result is not necessarily time wasted. Dave Thomas and Giles Wiggs helped to shape my research in its initial stages and first showed me what awe-inspiring places deserts were on an undergraduate fieldtrip to Tunisia in 2007. I am grateful to Gil Lizcano and Sebastian Engelstaedter, who helped me to learn the necessary tools for climate computing; and also to my many friends and colleagues in the Climate Research Lab. Thanks also to Sebastian Engelstaedter and Rob Bryant for examining this thesis and an enjoyable viva.

I am indebted to St John's College, not only for providing funding for me to undertake this thesis, but also for being a truly special place to study and live. Simon Dadson and Jack Langton, my undergraduate tutors at St John's, encouraged me to embark upon a DPhil, and Simon has provided support throughout its duration, not only as a college advisor but also as a friend. Before them, Tony James and Mike Taylor at Queens' School in Watford first inspired me to study Geography and are among my greatest influences.

At times this thesis has been more than an academic challenge; it has also been a personal trial. Thanks to my family for their unconditional support and love, and to my many incredible friends. Last but by no means least I would like to thank Gaëlle, who has

been my rock, putting up with me no matter how grumpy I've got and always picking me up when I've been struggling – Abigail Bartlet, eat your heart out!

Table of Contents

List of Figures

List of Tables

List of Acronyms

AAI	Absorbing Aerosol Index
AEJ	African Easterly Jet
AERONET	Aerosol Robotic Network
AEW	African Easterly Wave
AI	Aerosol Index
AMMA	African Monsoon Multidisciplinary Analysis
AOD	Aerosol Optical Depth
ASTER	Advanced Spaceborne Thermal Emission and Reflection Radiometer
BoDEx	Bodélé Dust Experiment
BT	Brightness Temperature
BTD	Brightness Temperature Difference
CALIOP	Cloud-Aerosol Lidar with Orthogonal Polarization
CWS	Central and western Sahara
DABEX	Dust and Biomass Experiment
DODO	Dust Outflow and Deposition to Ocean experiment
DSAF	Dust Source Activation Frequency
ECMWF	European Centre for Medium-Range Weather Forecasts
EUMETSAT	European Organisation for the Exploitation of Meteorological Satellites
EO	Earth Observation
EOP	Extended Observation Period
ERA	ECMWF Reanalysis
GERBILS	Geostationary Earth Radiation Budget Intercomparison of Longwave and Shortwave radiation
GES-DISC	Goddard Earth Sciences Data and Information Services Centre
GIOVANNI	GES-DISC Interactive Online Visualisation and Analysis Infrastructure
IOP	Intensive Observation Period
IR	Infrared
ITCZ	Intertropical Convergence Zone
ITD	Intertropical Discontinuity
JJA	June, July and August
LIDAR	Light Detection And Ranging
LLJ	Low Level Jet
MCS	Mesoscale Convective System
METAR	Meteorological Terminal Air Report
MISR	Multi-angle Imaging Spectroradiometer
MODIS	Moderate Resolution Imaging Spectroradiometer
MSG	Meteosat Second Generation

NA	North Africa
NASA	National Aeronautics and Space Administration
NOAA	National Oceanic and Atmospheric Administration
OLR	Outgoing Longwave Radiation
OMI	Ozone Monitoring Instrument
RGB	Red-Green-Blue
SABL	Saharan Atmospheric Boundary Layer
SAMUM	Saharan Mineral Dust Experiment
SDF	SEVIRI Dust Flag
SEVIRI	Spinning Enhanced Visible and Infrared Imager
SHL	Saharan Heat Low
SOM	Self Organised Map
SRTM	Shuttle Radar Topography Mission
SYNOP	Surface Synoptic Observation
TOMS	Total Ozone Mapping Spectrometer
USA	United States of America
UTC	Universal Time Coordinates
UV	Ultraviolet
WAM	West African Monsoon

Chapter 1

Introduction

1.1. Preface

Vast quantities of mineral dust[1] are emitted from the world's arid regions into the atmosphere each year. These tiny particles, typically thought to have diameters below 80 microns [*Bagnold*, 1941], can stay suspended in the atmosphere for considerable amounts of time (often many days) following uplift from the surface and may be transported great distances from source (thousands of kilometres). Dust can therefore impact on many different components of the Earth System including weather, climate and nutrient cycles, and this has been the driving force behind the development of models that predict future dust distribution and quantify its effects. The reliability of these models ultimately hinges upon an adequate representation of dust emissions from the surface, but current simulations show massive disparity in emissions between different models on global and regional scales [Figure 1.1; *Huneeus et al.*, 2011]. This can only be addressed by understanding the characteristics and dynamics of today's globally important dust sources.

Dust emission into the atmosphere is controlled by a range of climatological, meteorological and geomorphological mechanisms that operate across multiple spatial and temporal scales with both natural and human influences [*Bryant*, 2013; *Knippertz and Todd*, 2012; *Ravi et al.*, 2011]. The geographical location of dust sources constrains the overall importance of these processes as well as determining the dust transport

[1] alternatively termed 'atmospheric dust', 'aeolian dust', mineral aerosol, 'dust aerosol' or 'desert dust' in the literature

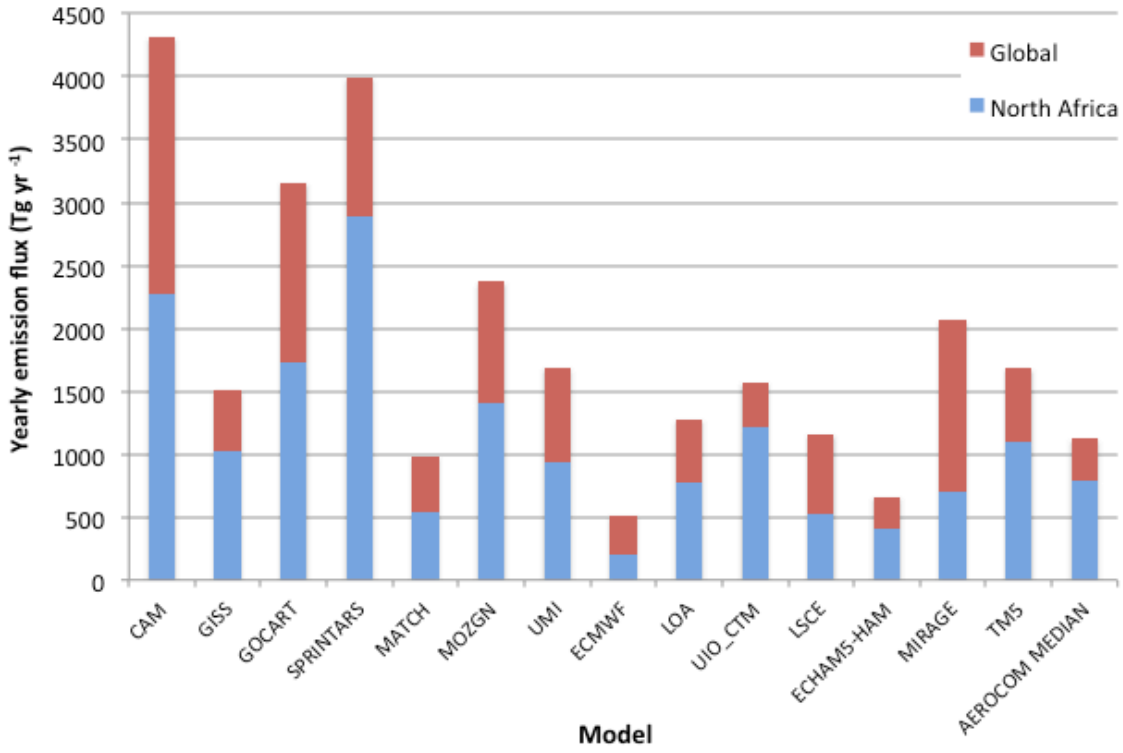

Figure 1.1. Estimated global (red bars) and North African (blue bars) annual dust emissions from 15 different global aerosol models. Data are taken from Tables 3 (global emissions) and 5 (North African emissions) of *Huneeus et al.* [2011]

trajectory following emission. It is also important in dictating the mineralogical and physical characteristics of the dust particles [*Shao et al.*, 2011] that, although subject to modification during transport [*Ryder et al.*, 2013; *Carslaw et al.*, 2010], ultimately determine what effects they can have on the environment [*Durant et al.*, 2009].

North Africa has long been recognised as the world's largest source of dust [*Engelstaedter et al.,* 2006; *Washington et al.*, 2003; *Prospero et al.,* 2002]. The most recent modelling estimates suggest that it contributes some 55 % of global emissions, the vast majority of which come from the predominantly hyper-arid and uninhabited Sahara desert [*Ginoux et al.*, 2012]. There are two principal dust hotspots within the Sahara: The Bodélé Depression in Chad; and a broad area in the central and western Sahara (CWS) covering southern Algeria, northern Mali and parts of Mauritania and northwest Niger (Figure 1.2). Knowledge of the Bodélé and the set of unique characteristics that conspire to make it the strongest single source of dust on Earth has burgeoned, in no small part due to the Bodélé Dust Experiment (BoDEx – *Washington et al.*, [2006]), which saw the first ever in-situ observations of the region. The CWS dust hotspot, which dominates the summertime dust burden [*Engelstaedter and Washington*, 2007], has proven to be somewhat more difficult to understand and is the focus of this thesis.

Owing to its remoteness and inhospitable environment (the CWS has alternatively been termed the 'Saharan Empty Quarter' [*Washington and Wiggs*, 2011]), much of what we know about CWS dust processes comes from the analysis of satellite data. These data are invaluable in providing a view of the distribution of dust across the whole region at a range of spatial and temporal resolutions, although the dust detection algorithms employed suffer from limitations with varying atmospheric conditions, dust layer thickness and vertical location, to name but a few. Nonetheless, they reveal the CWS dust hotspot to be the complex result of emissions from numerous disperse sources,

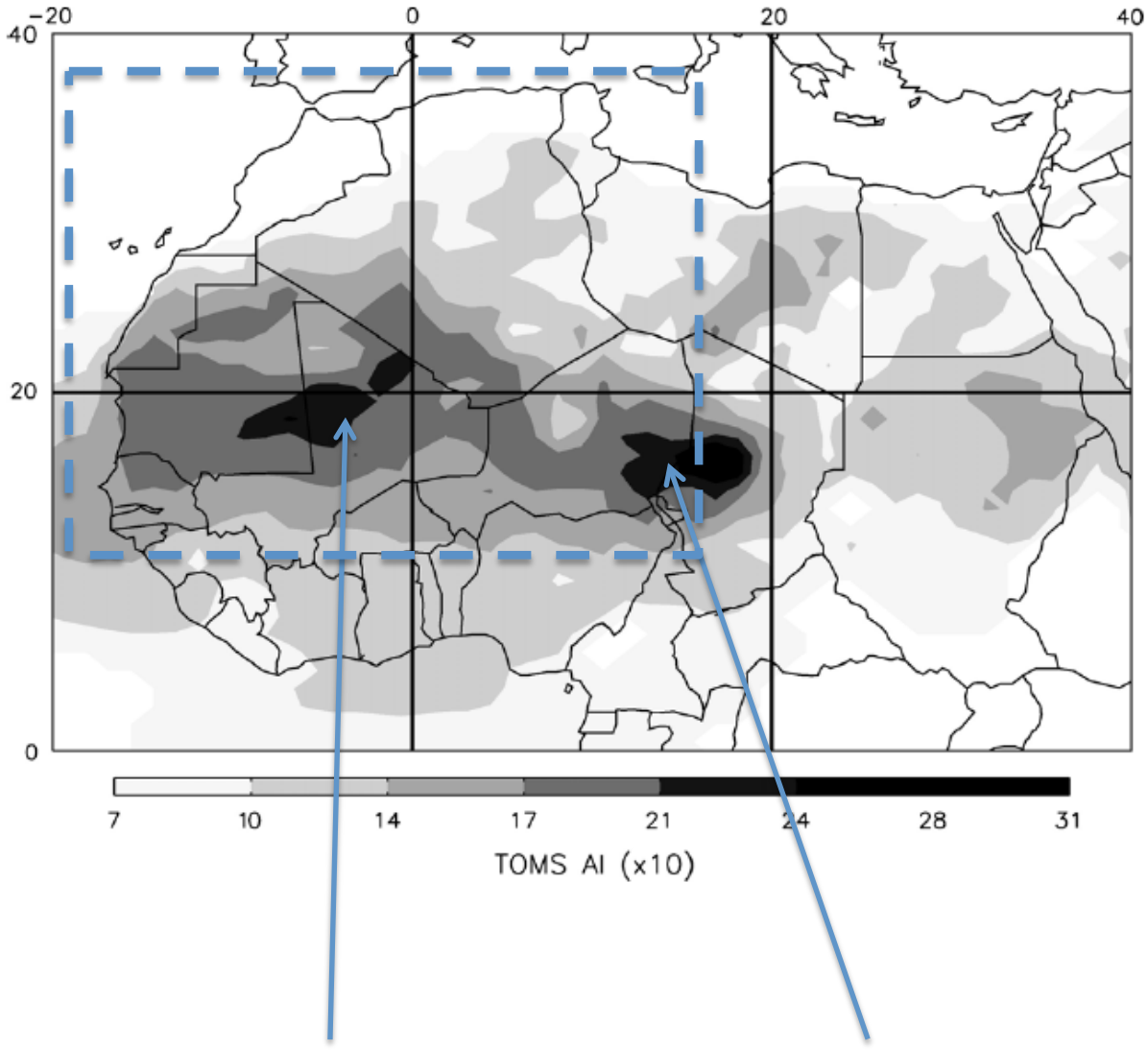

Figure 1.2. Mean Total Ozone Mapping Spectrometer (TOMS) Aerosol Index (AI) (x10) 1980-1992 over North Africa. Dotted blue line corresponds to study region of this thesis. Source: *Engelstaedter et al.* [2006]

driven by a number of different mechanisms in opposing winds that converge into the region during the boreal summer [*Knippertz and Todd*, 2010].

The Spinning Enhanced Visible and Infrared Imager (SEVIRI), which provides an image of the Sahara every 15 minutes throughout the day and night owing to its position in geostationary orbit at 0^{o} latitude 0^{o} longitude, has been crucial in unpicking the CWS dust hotspot by enabling the close monitoring of individual dust events, something which is not possible with other satellite-borne sensors in polar orbit that offer, at best, two observations of the Sahara per day (Figure 1.3). SEVIRI data have revealed that the majority of CWS dust emissions occur either in the early morning, driven by the Low-level Jet (LLJ) mechanism, or in the evening in association with cold pool outflow from deep convection (dust events often known as 'haboobs') that is sometimes present over the region [*Schepanski et al.*, 2009]. These data have also facilitated the identification of individual dust sources within the CWS more accurately than ever before, especially since other sensors typically pass over the region in the early afternoon and thus observe dust that has been in transport for several hours (up to around 20 hours in the case of evening emissions that will not be observed until the following afternoon) [*Schepanski et al.*, 2012].

To date however, the only means of detecting dust with SEVIRI data is by manual inspection of the false colour composite imagery presented in Figure 1.3. Quite aside from the practical reproducibility of results concerning the sources and dynamics of CWS dust being limited by the time-consuming nature of this approach (especially if several years of data are to be analysed), these results will always be subjective since they depend upon a person's interpretation of the dust signal, which is sometimes weak and/or hard to distinguish from the background surface signal. Moreover, the manual back-tracking of dust events to source has only detected source areas to a precision of

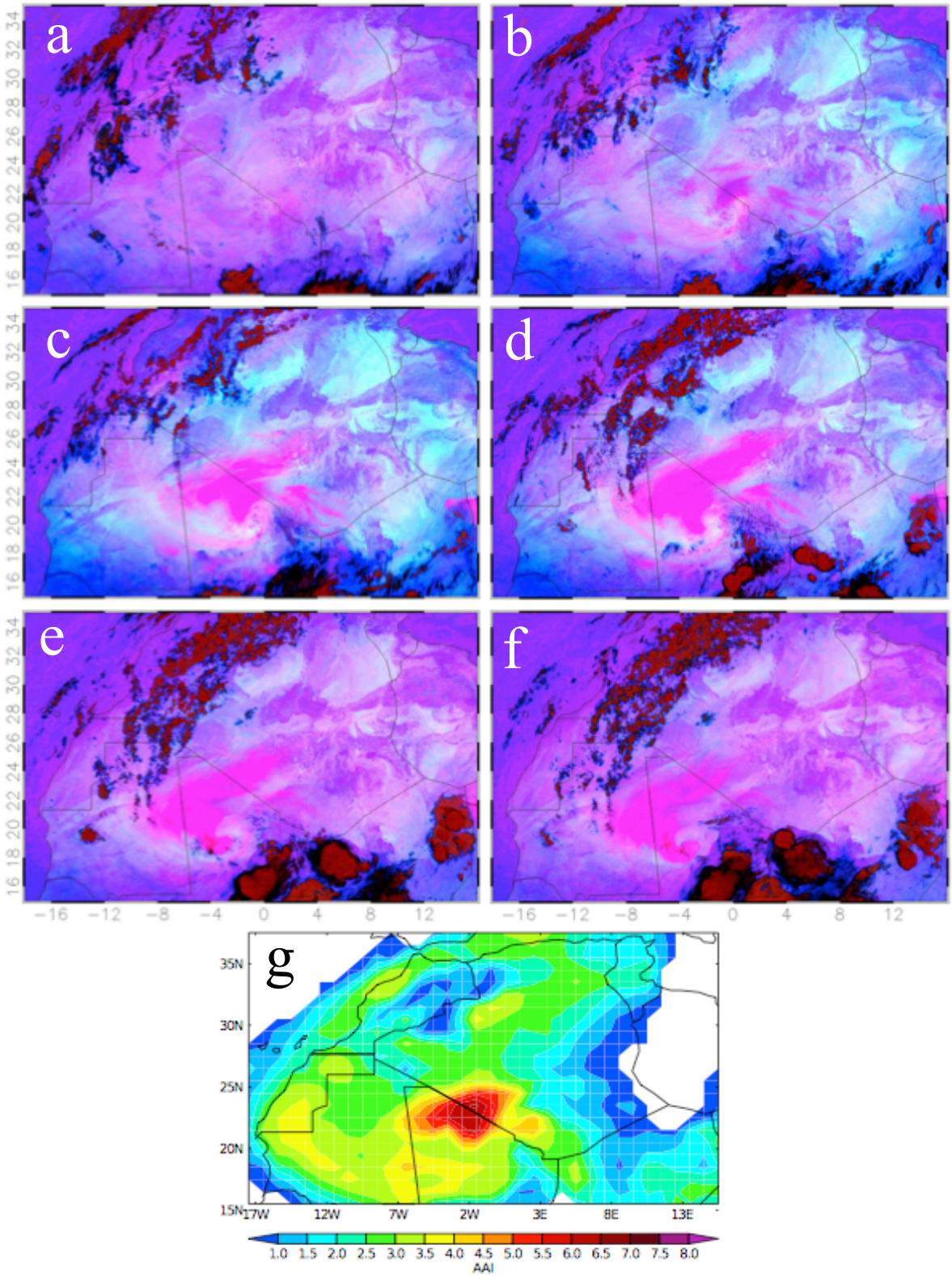

Figure 1.3. SEVIRI dust scheme imagery for 17th July 2005 at: **a.** 07:00; **b.** 10:00; **c.** 13:00; **d.** 16:00; **e.** 19:00; **f.** 22:00. Dust appears pink in these images, deep (shallow) high clouds are red (black) and low clouds blue. **g.** Corresponding AI image for same day from instrument in polar orbit (Ozone Monitoring Instrument (OMI)), acquired at around 13:00. (All times in UTC).

1^{o}x1^{o}, which is far coarser than the maximum possible spatial resolution of 0.03^{o}x0.03^{o} afforded by SEVIRI and prevents the precise identification of the specific surface features from which dust is actually emitted. The manual method also prevents the objective analysis of spatial and temporal variability in dust distributions and the thorough analysis of sensitivities of the dust signal and how this compares to other dust datasets. Central to this thesis therefore is the automation of dust and dust source detection in SEVIRI to remedy these shortcomings and better utilise the full potential of the data.

Dust emission from the surface depends upon the availability of sediment (erodibility) and strong surface winds (erosivity). Sediment availability is modulated by a range of factors including the 'roughness' of the surface (the presence of vegetation, rocks and other nonerodible elements), surface moisture and soil properties such as texture and particle size distribution [*Gillette*, 1979]. Vegetation and precipitation together strongly constrain emissions in most regions [*Zender and Kwon*, 2005], but their influence is likely negated by the hyper-aridity of the CWS (receiving, on average, less than 200 mm rainfall per year) where surface erodibility is expected to be largely invariant. It is reasonable therefore to assume that any variability in the presence of atmospheric dust is controlled by regional atmospheric dynamics. The passage of African Easterly Waves (AEWs), the dominant summertime synoptic scale disturbances over West Africa, has been linked to the occurrence of large CWS dust loadings [*Knippertz and Todd*, 2010]. Key questions remain regarding variability in the presence of dust and its distribution within the CWS on intraseasonal and interannual timescales, however. These are the focus of the second half of this thesis. Analysis of variability on these timescales in other source regions has been central to the identification of broader climatological controls on source activity [*Bryant et al.*, 2007; *Washington and Todd*,

2005] and, in the case of the Bodélé Depression, has facilitated exploration of potential future changes in dust emissions with climate change [*Washington et al.*, 2009].

1.2. Research aims

This CWS is the dustiest place on Earth during the northern hemisphere summer. This thesis therefore focuses on the CWS dust hotspot solely during the months of June – August. The years 2004 – 2010 are studied, primarily due to the availability of SEVIRI data. Other satellite sensors provide a longer time series of dust observations, such as the Total Ozone Mapping Spectrometer (TOMS) Aerosol Index (AI), which is available for from 1978 to 1993 [*Herman et al.*, 1997], but only SEVIRI provides the high temporal resolution necessary to best fulfil the aims of this thesis. The first aim of this thesis is to automate the detection of dust in SEVIRI data, facilitating the development of a scheme to objectively identify source regions within the CWS (aim 2). This dataset is then used to analyse intraseasonal and interannual variability in the dust hotspot and identify potential links to the atmospheric circulation with use of ERA Interim reanalysis data (aims 3 and 4).

The specific aims/research questions addressed in this thesis are:

1) Automate the detection of dust over the CWS during the boreal summer using data from SEVIRI.
    - Evaluate against other widely used indicators of dustiness.

2) Derive an objective map of summertime dust sources in the CWS that utilises the native resolution of SEVIRI.
    - What are the climatological transport pathways associated with the most frequently active sources?
    - What is the spatial association with deep convection?

3) What are the dominant patterns of intraseasonal variability in daily dust coverage over the CWS during the boreal summer?
    - Do they occur with the same frequency throughout the summer and every year?
    - What are the atmospheric controls on these?

4) What role does the atmospheric circulation play in generating substantial interannual variability in the frequency of summertime dust presence over the CWS?

1.3. Thesis structure

This thesis comprises six main chapters. Chapter 2 is a literature review, which is intended to provide a background for the aims proposed above and further context for the thesis. This is followed by four research chapters, each of which are papers that have been published in or submitted to peer-reviewed journals. These address the four main research aims/questions listed above:

- Chapter 3 (*An Automated dust detection using SEVIRI: a multi-year climatology of summertime dustiness in the central and western Sahara*) presents a method to automate the detection of dust using SEVIRI data over the CWS. Results of the detection scheme are compared to dust detection by eye and to other widely used indicators of dust presence. The spatial distribution of CWS dust presence according to this scheme is then presented for June-August 2004-2010. This 'SEVIRI dust flag' (SDF) dataset forms the sampling base for all subsequent chapters.
- Chapter 4 (*A new high-resolution central and western Saharan summertime dust source map from automated satellite dust plume tracking*) outlines a new objective dust source detection method for the CWS, based on the automated tracking of individual dust plumes in the SDF dataset. A map of the sources of all dust plumes tracked is presented and the likely collocated surface features highlighted. It is then compared to the manually derived SEVIRI source map of *Schepanski et al.* [2007; 2009; 2012]. Finally, the transport directions of plumes to originate in the most frequently active source areas are presented, along with their potential association with deep convection.
- Chapter 5 (*Intraseasonal variability and atmospheric controls on daily dust occurrence frequency over the central and western Sahara during the boreal summer*) uses an unsupervised artificial neural network system to classify maps of summertime daily dust occurrence frequency over the CWS. The most commonly occurring dust states are outlined, and their occurrence frequency is broken down by month and by year. Preferred sequences of change between the dust states are then presented, and finally their occurrence is linked to atmospheric controls by analysis of climatological composites from ERA-Interim and deep convection frequency fields.

- Chapter 6 (*Circulation controls on interannual variability in central and western Saharan summertime dust presence*) identifies atmospheric controls on interannual variability in summertime CWS dust presence by comparing the two summers with highest and lowest dust presence. Case study comparison of the largest events to occur in each year explain a large proportion of the difference in dust presence between the two years, and the mean JJA climatologies are compared to demonstrate that the large-scale climate favoured increased dust presence in the dustiest year.

Chapter 7 reviews the results of the research chapters with reference to each aim outlined in Section 1.2, presents general conclusions with regards to these aims and the broader research field, discusses the limitations of the research presented in this thesis and finally proposes logical next steps for the further progression of the work.

1.4. References

Bagnold, R. A. (1941), *The Physics of Blown Sand and Desert Dunes*, Methuen, London.

Bryant, R. G. (2013), Recent advances in our understanding of dust source emission processes, *Progress in Physical Geography*, doi:10.1177/0309133313479391.

Bryant, R. G., G. R. Bigg, N. M. Mahowald, F. D. Eckardt, and S. G. Ross (2007), Dust emission response to climate in southern Africa, *Journal of Geophysical Research*, *112*(D9), D09207, doi:10.1029/2005JD007025.

Carslaw, K. S., O. Boucher, D. V. Spracklen, G. W. Mann, J. G. L. Rae, S. Woodward, and M. Kulmala (2010), A review of natural aerosol interactions and feedbacks within the Earth system, *Atmos. Chem. Phys.*, *10*(4), 1701–1737, doi:10.5194/acp-10-1701-2010.

Durant, A. J., S. P. Harrison, I. M. Watson, and Y. Balkanski (2009), Sensitivity of direct radiative forcing by mineral dust to particle characteristics, *Progress in Physical Geography*, *33*(1), 80–102, doi:10.1177/0309133309105034.

Engelstaedter, S., and R. Washington (2007), Atmospheric controls on the annual cycle of North African dust, *Journal of Geophysical Research*, *112*(D3), D03103, doi:10.1029/2006JD007195.

Engelstaedter, S., I. Tegen, and R. Washington (2006), North African dust emissions and transport, *Earth-Science Reviews*, *79*(1-2), 73–100, doi:10.1016/j.earscirev.2006.06.004.

Gillette, D. A. (1979), Environmental factors affecting dust emission by wind erosion, in *Saharan dust*, edited by C. Morales, pp. 91–91, Wiley, Chichester.

Ginoux, P., J. M. Prospero, T. E. Gill, N. C. Hsu, and M. Zhao (2012), Global-scale attribution of anthropogenic and natureal dust sources and their emission rates based on MODIS Deep Blue aerosol products, *Reviews of Geophysics*, *50*(RG3005), doi:10.1029/2012RG000388.

Herman, J.R., Bhartia, P.K., Torres, O., Hsu, C., Seftor, C., Celarier, E., (1997), Global distribution of UV-absorbing aerosols from Nimbus 7/TOMS data. *Journal of Geophysical Research,102* (D14), 16,911–16,922.

Huneeus, N., M. Schulz, Y. Balkanski, J. Griefsfeller, J. Prospero, S. Kinne, S. Bauer, O. Boucher, M. Chin, F. Dentener, T. Diehl, R. Easter, D. Fillmore, S. Ghan, P. Ginoux, A. Grini, L. Horowitz, D. Koch, M. C. Krol, W. Landing, X. Liu, N. Mahowald, R. Miller, J.-J. Morcrette, G. Myhre, J. Penner, J. Perlwitz, P. Stier, T. Takemura, and C. S. Zender (2011), Global dust model intercomparison in AeroCom phase I, *Atmos. Chem. Phys.*, *11*(15), 7781–7816, doi:10.5194/acp-11-7781-2011.

Knippertz, P., and M. C. Todd (2010), The central west Saharan dust hot spot and its relation to African easterly waves and extratropical disturbances, *Journal of Geophysical Research*, *115*(D12), D12117, doi:10.1029/2009JD012819.

Knippertz, P., and M. C. Todd (2012), Mineral dust aerosols over the Sahara: meteorological controls on emission and transport and implications for modeling, *Reviews of Geophysics*, *50*, doi:10.1029/2011RG000362.1.INTRODUCTION.

Prospero, J.M., Ginoux, P., Torres, O., Nicholson, S.E., Gill, T. E. (2002), Environmental characterization of global sources of atmospheric soil dust identified with the NIMBUS 7 Total Ozone Mapping Spectrometer (TOMS) absorbing aerosol product, *Reviews of Geophysics*, *40*(1), 1002, doi:10.1029/2000RG000095.

Ravi, S., P. D'Odorico, D. D. Breshears, J. P. Field, A. S. Goudie, T. E. Huxman, J. Li, G. S. Okin, R. J. Swap, A. D. Thomas, S. V. Pelt, J. J. Whickler, and T. M. Zobeck (2011), Aeolian Processes and the Biosphere, *Reviews of Geophysics*, *49*(RG3001/2011), 1–45, doi:10.1029/2010RG000328.

Ryder, C. L., E. J. Highwood, T. M. Lai, H. Sodemann, and J. H. Marsham (2013), Impact of atmospheric transport on the evolution of microphysical and optical properties of Saharan dust, *Geophysical Research Letters*, doi:10.1002/grl.50482.

Schepanski, K., I. Tegen, M. C. Todd, B. Heinold, G. Bönisch, B. Laurent, and A. Macke (2009), Meteorological processes forcing Saharan dust emission inferred from MSG-SEVIRI observations of subdaily dust source activation and numerical models, *Journal of Geophysical Research*, *114*(D10201), doi:10.1029/2008JD010325.

Schepanski, K., I. Tegen, and a. Macke (2012), Comparison of satellite based observations of Saharan dust source areas, *Remote Sensing of Environment*, *123*, 90–97, doi:10.1016/j.rse.2012.03.019.

Shao, Y., K.-H. Wyrwoll, A. Chappell, J. Huang, Z. Lin, G. H. McTainsh, M. Mikami, T. Y. Tanaka, X. Wang, and S. Yoon (2011), Dust cycle: An emerging core theme in Earth system science, *Aeolian Research*, *2*(4), 181–204, doi:10.1016/j.aeolia.2011.02.001.

Washington, R., and M. Todd (2005), Atmospheric controls on mineral dust emission from the Bodélé Depression, Chad: The role of the low level jet, *Geophysical Research Letters*, *32*(17), L17701, doi:10.1029/2005GL023597.

Washington, R., and G. S. F. Wiggs (2011), Desert dust, in *Arid Zone Geomorphology: Process, Form and Change in Drylands*, edited by D. S. G. Thomas, pp. 517–537, John Wiley & Sons, Ltd., Oxford.

Washington, R., M. Todd, N. J. Middleton, and A. S. Goudie (2003), Dust-Storm Source Areas Determined by the Total Ozone Monitoring Spectrometer and Surface Observations, *Annals of the Association of American Geographers*, *93*(2), 297–313.

Washington, R., M. C. Todd, S. Engelstaedter, S. Mbainayel, and F. Mitchell (2006), Dust and the low-level circulation over the Bodélé Depression, Chad: Observations from BoDEx 2005, *Journal of Geophysical Research*, *111*(D3), D03201, doi:10.1029/2005JD006502.

Washington, R., C. Bouet, G. Cautenet, E. Mackenzie, I. Ashpole, S. Engelstaedter, G. Lizcano, G. M. Henderson, K. Schepanski, and I. Tegen (2009), Dust as a tipping element : The Bodélé Depression, Chad, *Proceedings of the National Academy of Sciences*, *106*(49), 20564–20571.

Zender, C.S., and E. Y. Kwon (2005), Regional contrasts in dust emission responses to climate, *Journal of Geophysical Research, 110*(D13201), doi:10.1029/2004JD005501

Chapter 2

Literature Review

2.1. Overview and dust definition

This literature review provides a background for the aims proposed in Section 1.2 and further context for the thesis that could not be developed fully in Section 1.1. It is not intended to be an exhaustive review of the current state of the scientific field. It begins by outlining the effects of dust in the Earth System, many of which are important drivers of dust research today. It then moves on to describe the global distribution of dust sources and associated landforms, before considering controls on dust emission in detail. The second half of the literature review focusses on the CWS, starting with a brief overview of the regional climate, before turning to our current knowledge of the sources of dust, processes driving dust emission, and temporal variability in dustiness on intraseasonal and interannual timescales. Finally the sources of data available for the study of dust processes in the CWS are outlined and limitations therein highlighted.

First it is necessary to clarify what is meant by 'dust'. Dust is commonly considered to consist of soil particles with diameters less than 80 μm (0.80 mm) [*Bagnold*, 1941]. Particles of this size can stay airborne for considerable time periods (often many days) once uplifted from surfaces with a supply of sediment available for emission, and can therefore be transported very large distances by the atmospheric circulation. It is interesting to note that recent sampling of airborne dust plumes originating in the Sahara reported particles of up to 300μm in diameter, which is far larger than expected owing to their much higher settling velocities. This is of consequence for estimations of the dust radiative impact [*Ryder et al*, 2013].

2.2. Dust in the Earth System

Atmospheric dust is the most dominant of all atmospheric aerosol species by mass *Textor et al.*, 2006]. Model estimates suggest that around 2000 Megatonnes are emitted into the atmosphere each year [*Shao et al.*, 2011], although these estimates vary by around a factor 5 between models [Figure 1.1; *Huneeus et al.*, 2011]. Once airborne, it may be lifted to great heights and transported over long distances.

Dust aerosol has a direct impact on both the shortwave and longwave radiative flux through scattering and absorption [*Miller and Tegen*, 1998]. This impact is highly variable depending on particle characteristics [*Durant et al.*, 2009], the characteristics of the underlying surface [*Haywood et al.*, 2001; 2011] and on the vertical profile of the dust [*Tanré et al.*, 2003]. Model studies estimate the net global top-of-the-atmosphere direct radiative forcing to be on the order of -0.3 W/m^2 with a range of -0.56 to +0.1 [*Forster et al.*, 2007], which is therefore very likely a net cooling effect across the globe. The temperature forcing is thus sensitive to the amount of dust in the atmosphere, and both are shown to co-vary on a range of timescales [*Winckler et al.*, 2008; *Mahowald et al.*, 2006]. Dust also affects the radiation budget indirectly via modification of cloud properties such as albedo, lifetime and height [*Klüser and Holzer-Popp*, 2010; *McFiggans et al.*, 2006; *Koren et al.*, 2005; *Kaufman et al.*, 2005]. These radiative affects have the potential to affect the general circulation of the atmosphere [*Rodwell and Jung*, 2008], regional circulation and weather [*Lavaysse et al.*, 2011; *Solmon et al.*, 2008; *Tompkins et al.*, 2005] and impact important smaller-scale processes such as tropical storm and cyclone intensities [*Evan et al.*, 2006; *Dunion and Velden*, 2004].

Dust deposition in a range of environments, some distant from source region, impacts on global ecosystems and nutrient cycles, for example affecting oceanic biogeochemistry [*Jickells et al.* 2005] and potentially providing fertilisation for the

Amazon rainforest [*Bristow et al.*, 2010; *Koren et al.* 2006]. Deposition on snow and ice surfaces reduces albedo thus enhancing melt rates [*Painter et al.*, 2007].

In the human realm dust is linked to health problems both proximate to and remote from source regions [*Kellogg et al.*, 2004; *Molesworth et al.*, 2002; *O'Hara et al.*, 2000; *Prospero*, 1999], has implications for the generation of solar power [*Breitkreuz et al.*, 2007], and can disrupt air and road transport and communications [*Criado and Dorta*, 2003].

2.3. Global distribution of dust sources and dust source characteristics

Remotely sensed data affords us a view of the global distribution of dust source regions. Identifying these areas is an important first step to understanding the climatic and geomorphological processes that conspire to generate the vast amounts of dust that are transported around the globe.

The study of long-term (1979-1993) aerosol index (AI) data from the Total Ozone Mapping Spectrometer (TOMS) highlighted that peak dust loadings globally are essentially collocated with desert areas [*Prospero et al.*, 2002; *Washington et al.*, 2003 – see Figure 2.1], where there is an abundance of fine material available for emission into the atmosphere. The Sahara desert is characterised by the highest AI values (i.e. greatest loadings) and broadest areal extent. This is in agreement with results from the analysis of horizontal visibility measurements and dust trajectory studies from a time before satellite data were available, which clearly pointed towards the Sahara desert as the dominant global source of dust [*Engelstaedter et al.*, 2006]. In addition, the Arabian Peninsula and southwest Asia are covered by a broad area of high AI and dust emissions from within these regions have been well documented [e.g. *Middleton,* 1986a,b; *Pease et al.*, 1998],

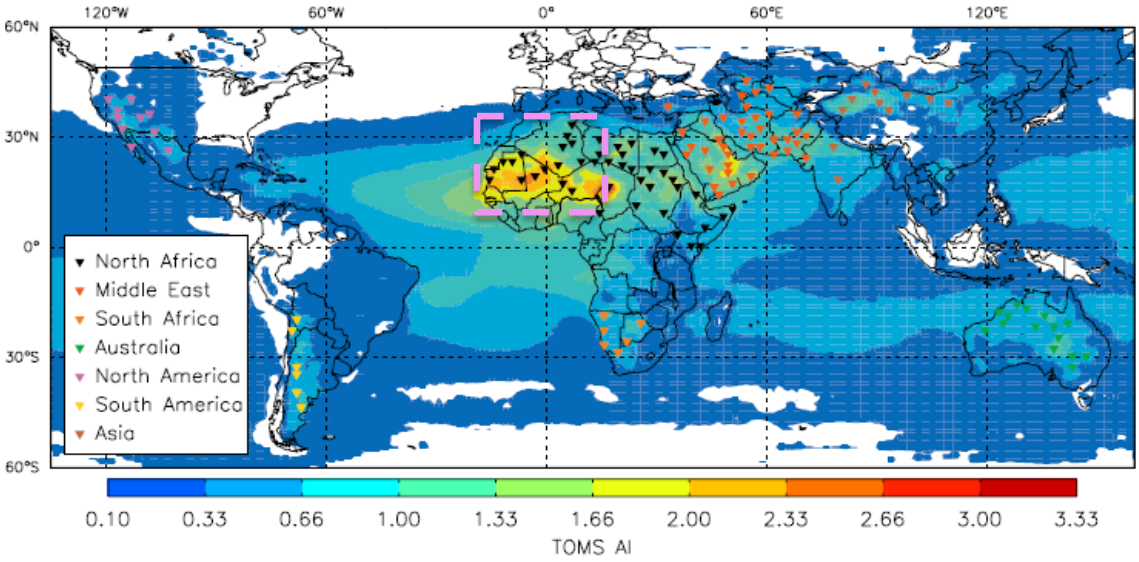

Figure 2.1. Global mean TOMS AI 1984-1990. Symbols correspond to regions mentioned in the text. The pink box outlines the CWS.
Source: *Engelstaedter and Washington* [2007a]

likewise with parts of China and Mongolia (the Gobi and Taklimakan Deserts and the Tarim Basin [e.g. *Sun et al.*, 2001; *Qian et al.*, 2002; *Wang et al.*, 2004]), central Australia (the Lake Eyre basin [e.g. *Bullard et al.*, 2008]) and southern Africa (primarily the Makgadikgadi basin in Botswana and Etosha pan in Namibia but also pans in the south western Kalahari and pans and ephemeral rivers along the Namibian coastline [e.g. *Eckardt and Kuring*, 2005; *Bryant et al.*, 2007; *Vickery et al.*, 2013]). Comparably minor dust activity also occurs in parts of western/southwestern USA (e.g. *Baddock et al.* [2011]; *Bullard et al.* [2011]; *King et al.* [2011]; *Lee et al.* [2012]) and the deserts of South America [e.g. *Gasso et al.*, 2011].

From analysis of satellite-derived dust datasets, it emerged that, within arid regions, most major dust sources are located in topographic depressions [*Prospero et al.*, 2002], primarily in dry lakes and riverbeds where fine alluvial deposits suitable for erosion by the wind can accumulate following intermittent flooding and drying. In the Sahara this wetting-drying process occurs on timescales of many thousands of years [e.g. *Drake et al.*, 2006; *Washington et al.*, 2007] and alluvial deposits are thought to be deep enough to sustain emission without further replenishment, but in ephemeral lake systems, such as the Makgadikgadi pans of Botswana, regular flooding (on interannual timescales) is required to provide erodible sediment suitable for emission in the following years when the waters recede [*Mahowald et al.*, 2003; *Bryant et al.*, 2007]. Other important source geomorphologies include alluvial fans and plains [*Reheis and Kihl*, 1995], sand dunes [*Bullard et al.*, 2008] and stone pavements [*Wang et al.*, 2006]. Even temperate grasslands are potential sources of dust owing to their seasonal growth-decay cycles and potential threats to future vegetation cover posed by climate change and human activities such as animal husbandry and cultivation that may result in land degradation [*Shinoda et*

al., 2011]. Recently, dust emission has also been detected in association with active glacial outwash plains in Iceland [*Prospero et al.*, 2012].

There have been calls to quantify the relative importance of different source geomorphologies to overall dust emissions in order to better understand global dust concentrations under different climatic conditions [*Bullard et al.*, 2011; *Okin et al.*, 2011]. In order to do this, the specific sources that currently contribute to global dust emissions must be identified as precisely as possible so that their surface geomorphologies can be determined. This is facilitated for the CWS by the second aim of this thesis.

2.4. Controls on dust emission

Dust emission occurs when the wind speed (erosivity) exceeds a certain threshold friction velocity that is determined by the properties of the surface (erodibility) [*Bagnold*, 1941; *Shao*, 2008]. Both erosivity and erodibility are highly variable in space and time, acting to constrain when and where dust is emitted.

2.4.1. Erosivity

Erosivity is primarily controlled by climatology and meteorology. It therefore varies along with regional synoptic conditions, which can create distinct seasonality in dust activity. A good example is the Bodélé low-level jet (LLJ), which drives dust emissions from the Bodélé Depression. This is at its strongest during the northern hemisphere winter and weakens into the summer, in phase with Bodélé dustiness. Within the peak Bodélé dust season, the LLJ strengthens in accordance with the Libyan High pressure

system and dustiness responds accordingly [*Washington and Todd*, 2005]. On yet finer temporal scales, erosivity can display a clear diurnal cycle depending on the dynamics of the driving meteorological mechanism. LLJs develop specifically during the night when the desert boundary layer is well stratified, and their momentum is mixed down to the surface during the morning when this stratification is disturbed by the onset of convective turbulence associated with surface heating. Thus, there is a clear morning peak in erosivity and consequently dust emissions over the Bodélé Depression, and indeed anywhere else where LLJs are invoked in driving uplift [*Todd et al.*, 2008].

The climatic control on erosivity means that it is susceptible to climate change. This has been demonstrated in the case of the Bodélé LLJ, with some climate simulations pointing towards increased core wind speeds by the end of the 21st Century in comparison to those at the end of the 20th Century [*Washington et al.*, 2009]. Enhanced erosivity then implies greater dust emissions from the Bodélé Depression at the end of the century, although this is conditional on erodibility, which ultimately determines the availability of sediment and the threshold wind speed above which dust emission can occur if sediment is available, remaining unchanged.

High wind speeds can be driven by processes that occur below the synoptic scale, such as outflows from deep convection that are ultimately governed by convective-scale processes and cause often large-scale and spectacular dust storms known as ‘haboobs’ [*Roberts and Knippertz*, 2012]. At even finer scales convective plumes and dust devils occur, which are short-lived (typically lasting only a matter of minutes), highly localised turbulent circulations that develop over intensely heated surfaces and produce short-lived plumes or vortices associated with dust uplift [e.g. *Warner*, 2004; *Koch and Renno*, 2005; *Ansmann et al.*, 2009]. Predictability of these events is somewhat more problematic than those driven by synoptic-scale dynamics due to their reliance on small-

scale processes that aren't currently represented in models/are very computationally expensive. This represents one of the biggest challenges in dust modelling today [*Knippertz and Todd*, 2012], especially where such events could make a significant contribution to regional dust emissions, as is the case in the CWS.

Meteorology/climatology isn't the only factor controlling erosivity, however. In the case of the Bodélé Depression, the LLJ has been shown from regional model experiments to exist uniquely over the region due to flow acceleration between the Tibesti and Ennedi mountains that lie upwind of the depression [*Washington et al.*, 2006]. Within the Bodélé, erosivity is highly spatially variable, with barchan dunes locally modifying the overlying wind and creating hotspots of dust emission [*Warren et al.*, 2007]. Conversely, erosivity can be decreased by the presence of surface roughness features, which are nonerodible elements (such as rocks and vegetation) that act to provide significant drag on the overlying airflow and decreasing the energy of surface winds [e.g. *Zobeck*, 1991; *Raupach et al.*, 1993]. One such example is vegetation, and it has been argued that declining Sahelian dust emissions since the 1980s are a result of vegetation-related roughness changes [*Cowie et al.*, 2013].

2.4.2. Erodibility

Erodibility is influenced by a range of surface characteristics including roughness features (which can range in size from boulders to pebbles and soil aggregates), soil moisture, crusting, soil texture and particle size distribution [*Gillette*, 1979]. These act either to restrict the availability of sediment suitable for emission or to modify the threshold friction velocity above which dust emission can occur. This threshold is highly spatially variable, even on the individual basin scale, with dust typically emitted

preferentially from small hotspots where surface conditions are optimal, on scales generally of tens of square meters at most [*Houser and Nickling*, 2001]. The effectiveness of roughness features in modifying surface erodibility, for example, depends upon their orientation with respect to the wind [*Ravi et al.,* 2011] as well as their spacing, geometry and density [*Wolfe and Nickling*; 1993].

Vegetation cover and other nonerodible roughness elements ultimately determine the susceptibility of an area to wind erosion directly by physically sheltering the soil surface and indirectly through their impacts on erosivity [*Webb and Strong*, 2011]. Assuming an absence (or relative lack) of vegetation, the properties of the soil itself become the chief controls on surface erodibility. Particle size distribution is particularly important to dust emission. In general, the smaller the particles the less erosive force is required for mobilisation to occur. However, once a certain critical particle size is reached (around 60 μm) this is reversed and the threshold friction velocity begins to increase as particle size decreases, due to increased interparticle cohesion forces between smaller particles [*Bagnold*, 1941; *Iversen and White*, 1982; *Marticorena and Bergametti*, 1995]. Owing to this inverse relationship with wind speed, direct aerodynamic entrainment (suspension) of dust-sized particles is rare, although has been observed in some special cases [*Kjelgaard et al.*, 2004]. Rather, dust emission is thought to be mainly a result of larger saltating sand particles [*Okin et al.*, 2011], which begin to saltate at slower wind speeds and can lead to the production and subsequent suspension of dust-sized particles either by surface bombardment thus ejecting finer particles into the flow or by the disintegration of aggregated saltators, known as ‘sandblasting’ [*Marticorena and Bergametti*, 1995; *Gomes et al.*, 1990]. Dust has also been seen to result directly from collisions between saltating quartz sand particles in dunefields [*Bullard et al.*, 2004].

Erodibility factors can be highly temporally variable. In the case of wet playas in the Mojave Desert, erodibility and sediment availability can change rapidly in response to local changes in groundwater depth and salinity [*Reynolds et al.*, 2007]. In some cases erodibility is so dynamic that it is modified during dust events, one instance being the impact of saltating grains from upwind sand dunes serving to break up wind-resistant crusts developing on playa surfaces [*Gillette et al.*, 2001]. In other cases, surface erodibility is sometimes restricted altogether due to lake inundation, as in the Etosha Pan and Makgadikgadi pans of southern Africa [*Bryant et al.*, 2007]. This highlights an overriding climatic control on erodibility factors that can serve to enhance or limit dust emission on longer time scales from multiannual-decadal, as is observed with increased Sahelian dust emissions corresponding to periods of Sahelian drought due to reduced soil moisture and vegetation coverage [*Prospero and Lamb*, 2003]; to glacial-interglacial, with an order of magnitude more dust during the last glacial maximum likely a result of climatically induced changes in vegetation cover [*Harrison et al.*, 2001]. It is also worth noting that climatic-induced changes in erodibility can have feedbacks on the climate itself. This is hypothesised to be the case in the Sahel, with increases in rainfall and vegetation from the 1980s onwards decreasing the surface erodibility but also causing a drop in wind speeds due to the increased surface roughness (known as 'stilling'), which further reduces the potential for dust emission from this region [*Cowie et al.*, 2013].

Erodibility controls on dust emission are a chief limitation to reliable model simulations, because detailed maps of properties such as surface roughness, soil moisture and soil particle size distribution are unavailable or unreliable at best for key source regions like the Sahara due to a lack of surface observations [*Shao et al.*, 2011]. This has been demonstrated for the Bodélé, with outcrops of highly erodible and emissive diatomite classified as sand in soil maps [*Todd et al.*, 2008b]. As a result, many models

incorporate a preferential source mask, whereby surface areas known to be strong dust sources from satellite observations are effectively prescribed soil and surface characteristics that result in dust emissions that compare well satellite estimates. This can lead to the improved simulation of global [*Ginoux et al.*, 2001] and regional [*Cavazos et al.*, 2009] dust emissions, although this does place a premium on the accuracy of both prescribed dust source locations and meteorology. Moreover, these preferential source areas may not exist as erodibility factors change with climate.

Field data are required to resolve questions concerning erodibility controls on dust emissions and it is therefore beyond the scope of this thesis to address their role in the CWS. Owing to the hyper-aridity of the region however, it is reasonable to assume that erodibility controls such as vegetation and surface moisture are largely stationary from one year to the next and that any variability in dust is likely due to erosivity controls.

2.4.3. Human impacts

Human activity can lead to the creation of 'anthropogenic' dust sources, either directly, for example by removing vegetation cover and desiccating water bodies, or indirectly via modification of climate and the hydrological cycle [*Ginoux et al.*, 2010; *Neff et al.*, 2008; *Zender et al*., 2003]. There is an ongoing debate as to what proportion of global dust emission originates from anthropogenic sources. Recent estimates suggest that globally this amounts to 25%, with high regional variability therein from only 8% in North Africa (predominantly in the Sahel) to 75% in Australia [*Ginoux et al.*, 2012]. It has been suggested that anthropogenic activities have led to a doubling of atmospheric dust loads during the 20th century [*Mahowald et al.*, 2010].

2.5. The central and western Sahara (CWS)

The central and western Sahara (CWS) dominates the global dust budget in the boreal summer (*Engelstaedter and Washington*, 2007). Until relatively recently, knowledge of the specific sources of dust and mechanisms involved in driving emission here has been elusive due to the fact that the dust burden appears to be spread over a large region with no obvious, single contiguous source area and no single dominant wind regime and dust uplift mechanism, as is the case with the Bodélé LLJ. This is largely because the timing of the dust peak coincides with the West African Monsoon (WAM), which juxtaposes multiple different meteorological emission mechanisms and dust transport pathways [*Knippertz and Todd*, 2010]. Analysis of 15-minute SEVIRI imagery and data collected during field campaigns that skirted the CWS have helped to identify the sources and mechanisms involved in creating the dust hotspot.

2.5.1. Summertime climatological context

The CWS is hyper-arid (receives, on average, less than 200 mm of rainfall per year). During the boreal summer its climate is marked by a distinct thermal depression characterised by high surface temperatures and low surface pressures resulting from intense surface heating from solar insolation and dry adiabatic heating associated with large-scale subsidence (the descending limb of the Hadley circulation). This is known as the Saharan Heat Low (SHL), typically occupying a location between the Hoggar and Atlas mountains at this time of year [*Lavaysse et al.*, 2009] (Figure 2.2). The corresponding deep, dry-convective Saharan atmospheric boundary layer (SABL), which frequently reaches heights of up to 6 km above sea level (making it the deepest boundary layer on Earth [*Cuesta et al.*, 2009; *Gamo*, 1996]), governs the often complex vertical

distribution of dust over the Sahara following emission [*Cuesta et al.*, 2009]. From here it is typically transported west across the Atlantic Ocean in the mean easterly flow – the African Easterly Jet (AEJ) – that overlies much of tropical north Africa (occasionally it follows trajectories towards western Europe instead), occurring in pulses every 3 to 5 days associated with African Easterly Waves (AEWs) [*Prospero and Lamb*, 2003], which are the dominant synoptic weather systems in the region during the summer and are characterised by a westward moving trough that passes across the Sahel/southern Sahara, influencing wind characteristics. These have been implicated in organising CWS dust activity [*Knippertz and Todd*, 2010].

Two opposing flows converge across West Africa into the SHL region: the dry northeasterly Harmattan and the moist southwesterly Monsoon flow (Figure 2.2). Their convergence location is known as the Intertropical Discontinuity (ITD), which has a climatological location to southern edge of the CWS, across central/northern Mali, with a northwards protrusion towards the Hoggar in southeast Algeria. During the rest of the year this is located further to the south, and it is this northwards penetration of the convergence that has been linked to the peaking of the CWS dust hotspot in the summer [*Engelstaedter and Washington*, 2007b]. The cyclonic circulation around the low-pressure centre of the SHL is associated with the enhancement of these opposing flows around its south/east and north/west flanks [*Parker et al.*, 2005]. Both of these flows are associated with dust emission.

The climate of the region is highly variable on a range of timescales. As mentioned, on a synoptic scale it is frequently perturbed by AEWs. Their westwards propagation is linked to a north/south displacement of the ITD and is subsequently responsible for transporting moister air and, often, convective complexes into the southern Sahara. These are known as monsoon surges [*Couvreux et al.*, 2010], which can

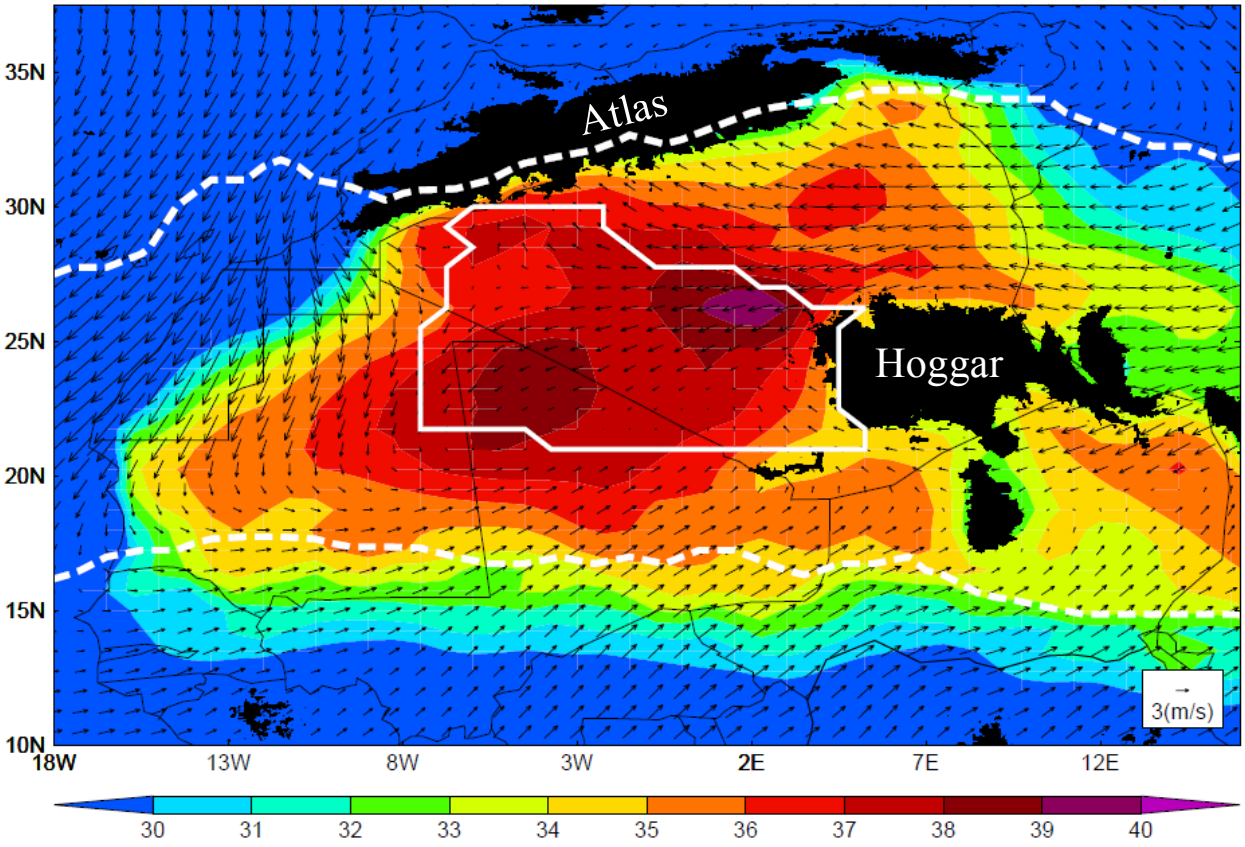

Figure 2.2. Mean summertime climatological context: Temperature in ^{o}C (shading), 925hPa winds (vectors), mean SHL location (white contour, calculated according to *Lavaysse et al.* [2009]), all from ERA Interim. Dotted white line = 0.55 mm/day rainfall contour (approx. 200 mm/year) from GPCP [*Huffman et al.*, 2001]. Black shading = topography > 750 m

also occur without any evidence of AEW interaction, instead resulting from SHL dynamics. The SHL is highly sensitive on intraseasonal timescales to ventilation from the Atlantic and Mediterranean [*Chauvin et al.*, 2010; *Vizy and Cook*, 2009], with cold air surges from the latter associated with large dust outbreaks in the CWS region. The WAM is likewise subject to pronounced intraseasonal [e.g. *Janicot et al.*, 2011] and interannual [e.g. *Rodríguez-Fonseca et al., 2011*] variability, in some cases as a result of global teleconnections. No links have been made between these modes and CWS dustiness although it is reasonable to assume that these may exist given i) distinct corresponding circulation anomalies; and ii) the role of WAM dynamics in driving emission (Section 2.5.3).

2.5.2. Identification of dust sources

Based on the by-eye tracking of dust events to source (defined as the 1x1 degree grid box in which the event is assumed to have originated) in SEVIRI dust scheme composite imagery [*Brindley et al.*, 2012; *Lensky and Rosenfeld,* 2008, *Schepanski et al*. 2007; 2009] identifies multiple disperse regions within the broad CWS domain (Figure 2.3), notably the boundaries of the central Saharan mountains and other topographical features, that are frequent sources of dust. The areas are associated with dry lakebeds, alluvial fans, wadis, sebkhas and chotts, which are assumed to be the specific sources of deflatable material, with sediment being provided by fluvial abrasion. This is in broad agreement with numerous case studies of CWS dust events, which often speculate about the sources of dust based on the SEVIRI imagery.

More recently, *Crouvi et al.* [2012], based on the correlation of number of days each part of the map created by *Schepanski et al.* is identified as a dust source with

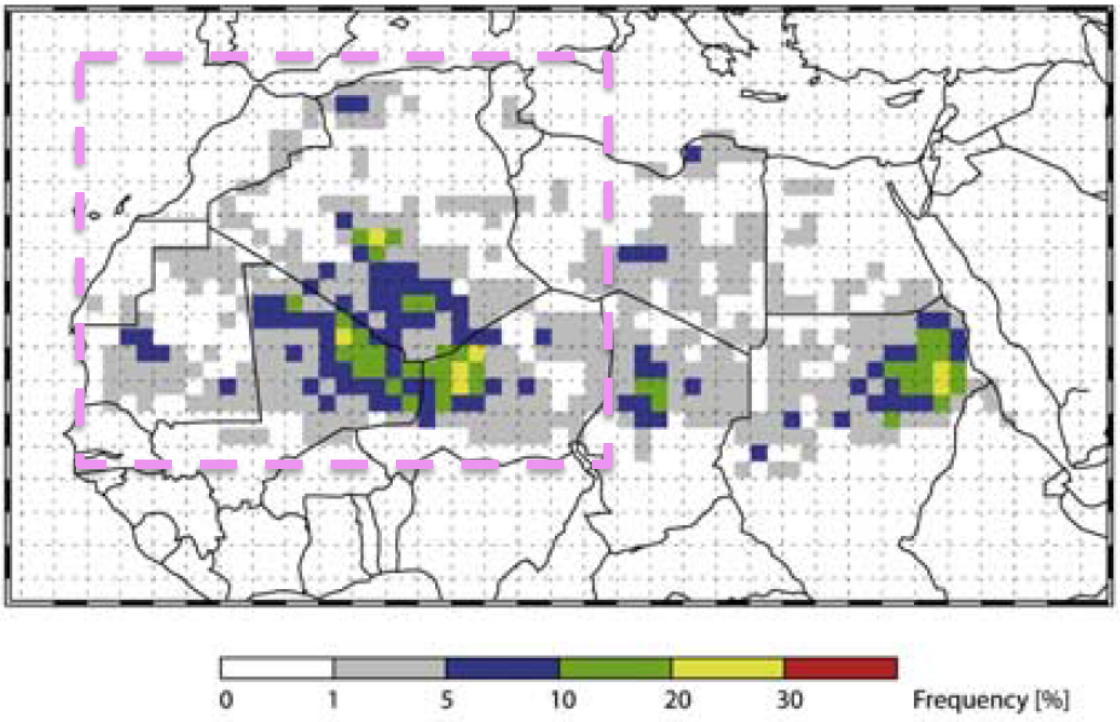

Figure 2.3. Dust source activation frequency from SEVIRI for June – August 2006 determined by manual tracking of dust plumes to source in SEVIRI dust scheme imagery. The pink box highlights the CWS.
Source: *Schepanski et al.* [2007]

information on soil type and geomorphic units, suggests that, actually, active sand dunes are the most persistent dust sources in the Sahara because of their large spatial extent in regions characterised by high winds and high erodibility. They suggest that playas and dry lake beds alone cannot explain the overall distribution of frequency of dust sources and that other dust sources must be considered. This is an obvious contradiction and no additional study of CWS dust sources has been forthcoming to resolve this. A large part of the problem is that the work of *Schepanski et al*. degrades the SEVIRI resolution to 1x1 degree map units, which precludes the identification of specific surface features as sources. This is explicitly addressed under the second aim of this thesis.

2.5.3. Meteorological mechanisms driving dust emission

Several meteorological mechanisms have been observed driving the high windspeeds associated with dust emission in the CWS. The first of these is the low-level jet mechanism. LLJs play a key role in driving dust emission across the Sahara (the Bodélé LLJ being just one example) and there is a high degree of similarity in the spatial distribution of dust source activation frequency and LLJ occurrence frequency [*Schepanski et al.*, 2009]. LLJs form at night in near-surface air layers that become frictionally decoupled from the surface (i.e. are not affected by surface roughness or turbulence, which both modify the geostrophic balance that drives winds), due to stabilisation of the atmospheric column with radiative cooling under clear sky conditions [*Fiedler et al.*, 2013; *Todd et al.*, 2008a]. The flow aloft becomes super geostrophic and windspeeds peak before dawn. Following sunrise, convective turbulence arises as the surface begins to heat and the planetary boundary layer grows, leading to a re-coupling of the flow aloft to surface winds. Momentum from the LLJ is thus mixed downwards,

leading to high surface windspeeds in the morning until the LLJ is degraded. This creates a distinct peak in dust source activation in the morning hours [*Schepanski et al.*, 2009]. LLJs have been detected driving dust emission in both the Harmattan and the Monsoon flows [*Allen et al.*, 2013; *Marsham et al.*, 2013; *Fiedler et al.*, 2013; *Knippertz*, 2008], which converge into the region in the boreal summer.

A substantial proportion of summertime CWS dust source activation is also attributed to strong surface winds in cold pool outflows from moist deep convection [*Allen et al.*, 2013; *Marsham et al.*, 2013; *Marsham et al.*, 2008; *Flamant et al.*, 2007], which drive dust emission on scales of hundreds of kilometres (a dust event sometimes referred to as a 'haboob'). These are typically generated by the subsidence of air cooled by evaporation in the warm, dry Saharan air and consequently are associated with the moister flow of the West African Monsoon. Dust emission associated with cold pool outflows tends to occur in the late afternoon and overnight due to the association with deep convection, which is most prominent in the afternoon and early evening. While the monsoon flow is implicated indirectly in driving dust emission via facilitating deep convection, it has also been associated directly with dust emission as a result of nighttime acceleration of winds at its leading edge [*Bou Karam et al.*, 2008].

On the smallest scales, rotating dust devils and dry convective plumes that occur on days with high insolation and low velocity background winds are also identified as important dust emission mechanisms [*Ansmann et al.*, 2009], but these are generally not detectable in satellite imagery.

Widespread dust emission can also occur in association with synoptically driven high windspeed events, for example as a result of strong background pressure gradients controlled by ridging of the subtropical highs [*Knippertz et al.*, 2011] or in association with Mediterranean Cold Surges [*Vizy and Cook*, 2009].

While the individual mechanisms driving dust emission in the CWS are now quite well understood, the relative contribution that each of these mechanisms makes to the overall CWS dust budget is currently uncertain. Based on observations made at Bordj-Badji Mokhtar (BBM) during the Fennec campaign in June 2011, cold pool outflows are thought to have driven around 50% of dust uplift, with LLJs responsible for about 30% [*Marsham et al.*, 2013], although it is unclear how representative these measurements are of the CWS as a whole across the summer. This is addressed explicitly under the second and third aims of this thesis. A recent model study covering parts of the CWS suggests that cold pools and LLJs are responsible for around 40% of total dust uplift each from late July – September 2006 [*Heinold et al.*, 2013], while another suggests that, Sahara-wide, LLJs drive around 15% of annual dust emissions, although there is a great degree of spatial and temporal variability in this value [*Fiedler et al.*, 2013]. Interestingly, it has been suggested that aged cold pools can trigger LLJ formation, thus indirectly leading to dust emission, in addition to their direct effect [*Heinold et al.*, 2013]. A high importance of cold pool outflows for dust uplift is problematic for the accurate simulation of the CWS dust hotspot, as cold pool outflow driven events are currently inadequately represented in dust models [*Marsham et al.*, 2011].

It has been argued that dry convective plumes and rotating dust devils may contribute significantly to the overall dust burden, based on measurements from the USA [*Koch and Renno*, 2005]. While they contribute much less dust individually than the other mechanisms discussed, they could potentially operate over vast areas such that their cumulative contribution is great. This is currently unresolvable since they are undetectable by satellites and not represented in dust models. In June 2011 at BBM, dry convective plumes contributed only 2% of observed dust emissions [*Allen et al.*, 2013].

2.5.4. Temporal variability in dustiness

Knippertz and Todd, [2010] suggest that the CWS dust hotspot is strongly related to the passage of AEWs. AEWs dominate synoptic scale variability in the WAM region and, based on regression analysis using once-daily area average measures of atmospheric dust content, are thought to contribute to the creation of the CWS dust hotspot through the organisation of dust emission and its subsequent transport over several days. They hypothesise that the southerlies to the east of an AEW trough bring moisture into the southern Sahara, facilitating deep convection and dust emission from northern Mali and Niger in association with cold pool outflows. As the AEW trough migrates west this dust is mixed upwards in the Saharan boundary layer, and then readvected towards the south and west by northerly flow ahead of the next AEW trough. This can drive further emission, in association with the LLJ mechanism. Extratropical influences are also implicated in modulating the amplitude of the AEW. One of the limitations of the study is that SEVIRI is only used for the qualitative monitoring of dust plumes and is unable to be included in the statistical analysis for comparison. Furthermore, this only addresses large dust outbreaks (characterised by AOD/AAI in excess of 2 standard deviations above the climatological 30-day running mean) and does not address the location of the dust since it is based on an area average value. Aim 3 of this thesis intends to build upon the picture developed by *Knippertz and Todd* [2010] and to fill these gaps in their study.

The literature is notably devoid of any further address of intraseasonal variability, or any focus at all on interannual variability in CWS dustiness based on observed data. This is remarkable given the wealth of information that can be gleaned about processes at source from such studies – the Bodélé LLJ was identified as the key driver of dust emissions in that area based on the comparison of the 2 most and least dusty years in the data record [*Washington and Todd,* 2005]. *Barkan et al.* [2004] report multiyear

variability in TOMS AI values over Mali and Mauritania, with the period 1979-1982 characterised by less dusty conditions while 1983-1992 was much dustier, but no extensive analysis or explanation of this has been forthcoming.

Any work that does address interannual variability in Saharan dust more generally focuses on the analysis of dust concentrations over the Atlantic and/or Mediterranean [*Chiapello et al.*, 2005; *Tegen and Miller*, 1998; *Moulin et al.*, 1997] or upon variability in dust concentrations measured at Barbados [*Prospero and Lamb*, 2003]. These generally tend to link interannual variability in dust concentrations to the amount of rainfall in the preceding year in the Sahel, with increased rainfall leading to decreased dustiness the following year due to decreased surface erodibility. While rainfall will play a substantial role in modifying emissions from the Sahel, it is thought unlikely that it will substantially modify emissions from the key CWS sources given the hyper-aridity of the region. It is questionable whether dust measurements at Barbados are a reliable measure of Saharan dustiness in any case, given the strong evidence that other processes, in addition to variability in dust emission from the Saharan sources, contribute to the varying dust concentrations measured there [*Engelstaedter and Washington,* 2009]. A key question to address is whether increased dustiness over the Sahara for any given year is a result of more dust emission events or of issues concerning the transport of the dust, with *Tegen et al.*, [2013] very recently suggesting that years with more observed dust source activations are not characterised by greater OMI AAI than years with less dust source activations. Interannual variability in dust presence is the focus of aim 4 of this thesis.

2.6. Sources of data for the study of CWS dust

Owing to the extreme climate, there is a huge paucity of observational climate and dust data from within the CWS region (Figure 2.4). Targeted field campaigns have tended to skirt the Saharan fringes (with the exception of the recent 'Fennec' project), focussing more on understanding the radiative and mineralogical properties of dust transported from the Sahara (understandably, given that it is these that ultimately affect the net radiation budget, which drives the global climate) as opposed to the meteorological and climatological controls on dust emission and transport and the identification of specific sources. These have nonetheless yielded valuable insights on dust processes. Earth Observation (EO) satellites and reanalysis data are therefore a crucial source of data for the study of Saharan dust distribution and processes.

2.6.1. Satellite observations

Benefits of using EO data are long temporal coverage (in some cases) and broad spatial coverage, as opposed to field campaigns, which usually focus only on a specific few weeks at a single site (although spatial range is often improved by the incorporation of aircraft flights and long-term automated weather stations have recently been deployed throughout the Sahara as part of Fennec). A major drawback to all EO products is the lack of ground-truthing that these products have over desert surfaces, especially in the Sahara. Case study comparison of SEVIRI and OMI AAI fields occasionally reveals quite different dust distributions [e.g. *Knippertz and Todd*, 2010] and there is no clear idea as to which represents the 'truth'. Additionally, no current product is able to view dust beneath thick cloud.

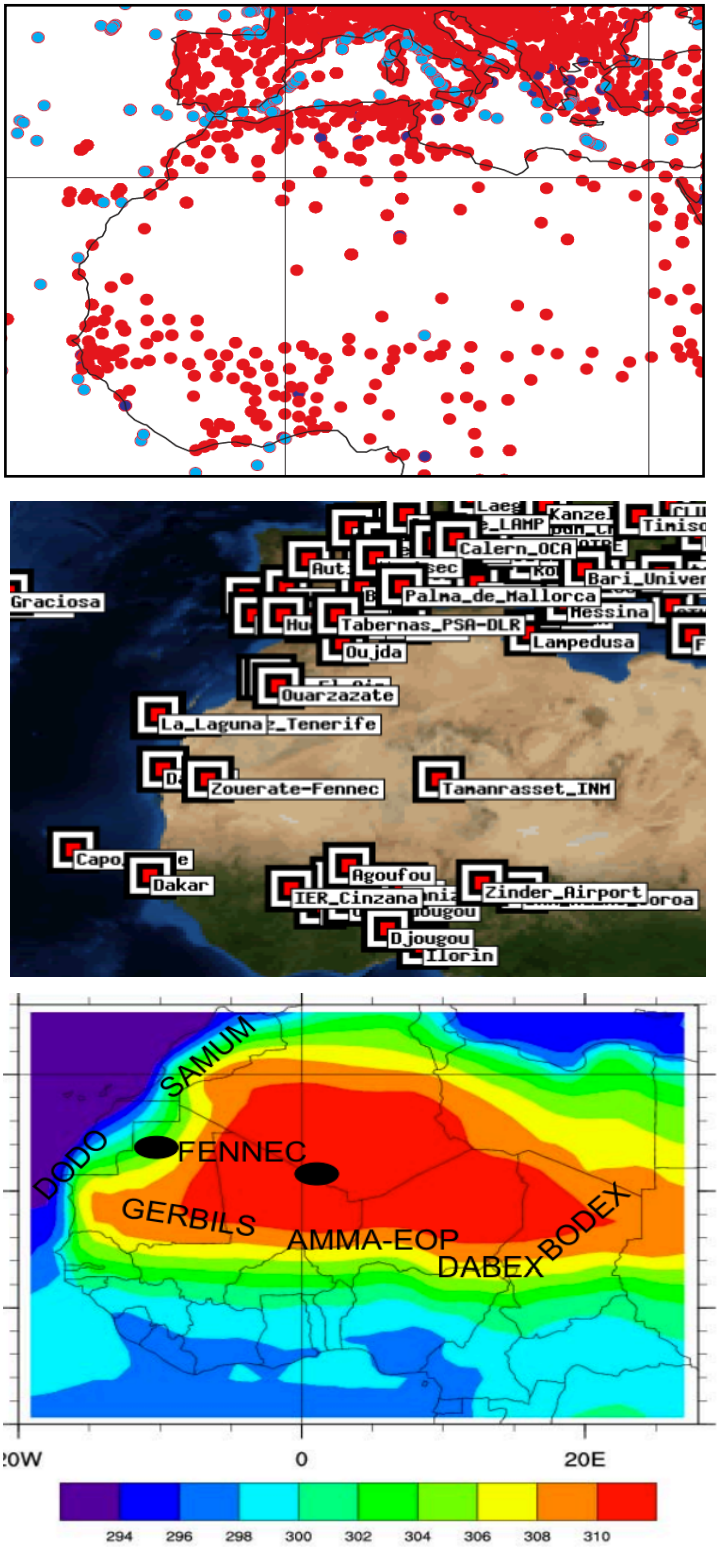

Figure 2.4. Surface observations across the Sahara. Top = location of surface synoptic (SYNOP) observations (red) and meteorological reports (METAR; blue); middle = location of AERONET stations (which provide information of atmospheric dust loadings at a given point, among other variables) with over 1 year of data; bottom = North African field campaign focus areas, overlaid on mean June temperature.
Source: Modified from *Washington* [2012]

There are numerous sensors and products available, differing primarily in their spatial and temporal resolutions and the wavelength of radiation that they detect (Table 2.1). The product used must be suitable for the aim in which it is intended. For example, a comparison of Saharan dust sources detected using different satellite products (SEVIRI, MODIS Deep Blue AOD and OMI AAI) and methods highlights a strong sensitivity of the results to the sensor characteristics [*Schepanski et al.*, 2012]. Temporal resolution, in particular, was found to be key. A drawback of the use of sensors providing only one image per day is that they observe dust that has often been transported away from its source (although it should be noted that a method has been outlined by *Ginoux et al.*, [2010] to determine between aged and freshly emitted dust in MODIS Deep Blue AOD data). The 15-minute resolution of SEVIRI, on the other hand, enables the more precise tracking of a dust plume to its point of origination. Similar results regarding the sensitivity of identified dust sources to sensor characteristics were reported by *Baddock et al.* [2009] in a comparison of techniques over the Lake Eyre Basin, Australia, which concluded that overall the infrared technique (which is used by SEVIRI) was the most consistently reliable if additional information about cloud cover and underlying ground surface characteristics is available. This study also demonstrated however that on a case-by-case basis the most effective technique for source determination varied owing to factors including cloud cover, surface reflectance, dust mineralogy/chemistry and atmospheric dust loadings. It argues therefore that thresholds for dust detection should be adjusted on a regional and/or individual event scale, although it also notes that this may not be possible for studies utilising long timeseries' of data.

The high temporal resolution of SEVIRI means that it can be used for the continuous monitoring of the dust plume location throughout the day, enabling questions about the horizontal location of dust associated with specific events and its residence

Instrument	Wavelength region	Record length	Spatial/ temporal resolution	Comments + example references
TOMS	Ultraviolet	1979-1993; 1996-2005	50km / daily	Quantitative, longest near-continuous record length (can be combined with OMI), sensitive to dust layer height [e.g. *Prospero et al.*, 2002; *Washington et al.*, 2003]
OMI	Ultraviolet	2004-present	13 x 24km/ daily	As TOMS; see also *Knippertz and Todd* [2010] for example of application on case study basis
MODIS (Deep blue)	Visible + UV blue	2002-present	10km / twice daily	Quantitative, cloud-free conditions only however [e.g. *Ginoux et al.*, 2010; 2012]
SEVIRI	Visible and near - thermal infrared	2002-present	3km (at nadir) / 15 minutes	Dust scheme widely used for qualitative indication of dust presence [e.g. *Schepanski et al.*, 2007;2009] but limits on performance [*Brindley et al.*, 2012]. AOD very recently available for whole Sahara between 06UTC-16UTC for 2008 - 2012
CALIOP	Polarization LIDAR	2006-present	30m vertical, 300m horizontal / 16-day repeat cycle	Information on vertical location of dust and AOD, however suffers from cloud contamination and poor temporal sampling *[e.g. Mona et al.*, 2012]

Table 2.1. Widely used satellite instruments for dust detection over the Sahara. Please note, this is not an exhaustive list and is only intended to highlight the most widely used instruments in Saharan dust research.
Source: Modified from *Knippertz and Todd* [2012].

time over the CWS to be addressed. On the other hand, SEVIRI does not yet provide a quantitative measure of dust amount around the clock, although this has very recently become available over the Saharan and Middle Eastern domain half-hourly from around 0600UTC to 1600UTC [*Banks and Brindley,* 2013 – note that these AOD retrievals are dependent upon solar illumination, so no AOD values are present for the CWS until at least 0630UTC]). AAI from TOMS/OMI or AOD from MODIS/MISR are widely used for this purpose, but it should be borne in mind that there is disagreement between different satellite products that do try to quantify dust amount [*Banks et al.*, 2013] and also that AAI arguably shows a bias towards dust loadings that are situated higher up in the atmospheric column, struggling to detect dust in the lowest 1.5 km or so [*Ginoux and Torres*, 2003]. CALIOP provides information on the vertical location of dust [*Mona et al.*, 2012] but this has a poor temporal sampling rate due to its narrow viewing field so is not well suited to source detection (although methods are being developed [*Todd and Cavazos-Guerra,* pers. comm.]).

Despite the lack of quantitative information available, SEVIRI has been widely used in Saharan dust research in recent years to provide qualitative information on dust presence due to the advantages of its high temporal resolution and this has significantly advanced our knowledge of processes occurring over the CWS. It is not without its limitations however. In particular, the SEVIRI dust scheme has recently been shown to be sensitive to the presence of atmospheric water vapour, the altitude of the dust layer, and the lower-tropospheric lapse rate, even for optically very thick dust clouds [*Brindley et al.,* 2012]. These findings were partly facilitated by the results of aim 1 of this thesis.

2.6.2. Reanalysis data

Reanalysis data are widely used for the identification of climatological patterns and trends as they provide a spatially complete and coherent record of the global atmospheric circulation over many years. Reanalyses are favored over archived weather analyses because they incorporate more observations than would have been available at the time of the original analysis. They are, however, model data – i.e. not equivalent to observed data. While they benefit from the assimilation of a wide range of observations, their reliability decreases where observational networks are sparse. This is true of the Sahara, where the observational network is sparse both in space and in time.

There are several reanalysis data sets provided by climate modelling groups around the world. The European Centre for Medium-Range Weather Forecasts (ECMWF) 45-year reanalysis (ERA-40) has been widely used in Saharan dust and climate research and where results have been compared to other reanalysis products they have been found to be very similar [e.g. *Knippertz and Todd*, 2010]. The ERA-Interim reanalysis is the latest global atmospheric reanalysis from ECMWF, which features improved data assimilation and a horizontal resolution of approx 0.75 degrees latitude/longitude (T255 grid) [*Dee et al.*, 2011].

2.7. References

Allen, C. J. T., R. Washington, and S. Engelstaedter (2013), Dust emission and transport mechanisms in the central Sahara: Fennec ground-based observations from Bordj Badji Mokhtar, June 2011, *Journal of Geophysical Research: Atmospheres*, *118,* doi:10.1002/jgrd.50534.

Ansmann, A., M. Tesche, P. Knippertz, E. Bierwirth, D. Althausen, D. Müller, and O. Schulz (2009), Vertical profiling of convective dust plumes in southern Morocco during SAMUM, *Tellus B*, *61*(1), 340–353, doi:10.1111/j.1600-0889.2008.00384.x.

Baddock, M. C., J. E. Bullard, and R. G. Bryant (2009), Dust source identification using MODIS: A comparison of techniques applied to the Lake Eyre Basin, Australia, *Remote Sensing of Environment*, *113*(7), 1511–1528, doi:10.1016/j.rse.2009.03.002.

Baddock, M. C., Gill, T. E., Bullard, J. E., Acosta, M. D., & Rivera Rivera, N. I. (2011), Geomorphology of the Chihuahuan Desert based on potential dust emissions, *Journal of Maps, 7*(1), 249–259, doi:10.4113/jom.2011.1178

Bagnold, R. A. (1941), *The Physics of Blown Sand and Desert Dunes*, Methuen, London.

Banks, J. R., and H. E. Brindley (2013), Evaluation of MSG-SEVIRI mineral dust retrieval products over North Africa and the Middle East, *Remote Sensing of Environment*, *128*, 58–73, doi:10.1016/j.rse.2012.07.017.

Banks, J. R., H. E. Brindley, C. Flamant, M. J. Garay, N. C. Hsu, O. V. Kalashnikova, L. Klüser, and A. M. Sayer (2013), Intercomparison of satellite dust retrieval products over the west African Sahara during the Fennec campaign in June 2011, *Remote Sensing of Environment*, *136*(June 2011), 99–116, doi:10.1016/j.rse.2013.05.003.

Barkan, J., H. Kutiel, and P. Alpert (2004), Climatology of Dust Sources in North Africa and the Arabian Peninsula, Based on TOMS Data, *Indoor and Built Environment*, *13*(6), 407–419, doi:10.1177/1420326X04046935.

Bou Karam, D., C. Flamant, P. Knippertz, O. Reitebuch, J. Pelon, and M. Chong (2008), Dust emissions over the Sahel associated with the West African monsoon intertropical discontinuity region : A representative case-study, *Quarterly Journal of the Royal Meteorological Society*, *634*, 621–634, doi:10.1002/qj.

Breitkreuz, H., M. Schroedter-Homscheidt, and T. Holzer-Popp (2007), A case study to prepare for the utilization of aerosol forecasts in solar energy industries, *Solar Energy*, *81*(11), 1377–1385, doi:10.1016/j.solener.2007.01.009.

Brindley, H., P. Knippertz, C. Ryder, and I. Ashpole (2012), A critical evaluation of the ability of the Spinning Enhanced Visible and Infrared Imager (SEVIRI) thermal infrared red-green-blue rendering to identify dust events: Theoretical analysis, *Journal of Geophysical Research*, *117*(D7), D07201, doi:10.1029/2011JD017326.

Bristow, C. S., K. a. Hudson-Edwards, and A. Chappell (2010), Fertilizing the Amazon and equatorial Atlantic with West African dust, *Geophysical Research Letters*, *37*(14), n/a–n/a, doi:10.1029/2010GL043486.

Bryant, R. G., G. R. Bigg, N. M. Mahowald, F. D. Eckardt, and S. G. Ross (2007), Dust emission response to climate in southern Africa, *Journal of Geophysical Research*, *112*(D9), D09207, doi:10.1029/2005JD007025.

Bullard, J. E., G. H. McTainsh, and C. Pudmenzky (2004), Aeolian abrasion and modes of fine particle production from natural red dune sands: an experimental study, *Sedimentology*, *51*(5), 1103–1125, doi:10.1111/j.1365-3091.2004.00662.x.

Bullard, J., M. Baddock, G. McTainsh, and J. Leys (2008), Sub-basin scale dust source geomorphology detected using MODIS, *Geophysical Research Letters*, *35*(15), L15404, doi:10.1029/2008GL033928.

Bullard, J. E., S. P. Harrison, M. C. Baddock, N. Drake, T. E. Gill, G. McTainsh, and Y. Sun (2011), Preferential dust sources: A geomorphological classification designed for use in global dust-cycle models, *Journal of Geophysical Research*, *116*(F4), F04034, doi:10.1029/2011JF002061.

Cavazos, C., M. C. Todd, and K. Schepanski (2009), Numerical model simulation of the Saharan dust event of 6–11 March 2006 using the Regional Climate Model version 3 (RegCM3), *Journal of Geophysical Research*, *114*(D12), D12109, doi:10.1029/2008JD011078.

Chauvin, F., R. Roehrig, and J.-P. Lafore (2010), Intraseasonal Variability of the Saharan Heat Low and Its Link with Midlatitudes, *Journal of Climate*, *23*(10), 2544–2561, doi:10.1175/2010JCLI3093.1.

Chiapello, I., C. Moulin, and J. M. Prospero (2005), Understanding the long-term variability of African dust transport across the Atlantic as recorded in both Barbados surface concentrations and large-scale Total Ozone Mapping Spectrometer (TOMS) optical thickness, *Journal of Geophysical Research*, *110*(D18), D18S10, doi:10.1029/2004JD005132.

Couvreux, F., F. Guichard, O. Bock, B. Campistron, J.-P. Lafore, and J.-L. Redelsperger (2010), Synoptic variability of the monsoon flux over West Africa prior to the onset, *Quarterly Journal of the Royal Meteorological Society*, *136*(S1), 159–173, doi:10.1002/qj.473.

Cowie, S. M., P. Knippertz, and J. H. Marsham (2013), Are vegetation-related roughness changes the cause of the recent decrease in dust emission from the Sahel?, *Geophysical Research Letters*, *40*, doi:10.1002/grl.50273.

Criado, C., and P. Dorta (2003), An unusual “blood rain” over the Canary Islands (Spain). The storm of January 1999, *Journal of Arid Environments*, *55*(4), 765–783, doi:10.1016/S0140-1963(02)00320-8.

Crouvi, O., K. Schepanski, R. Amit, A. R. Gillespie, and Y. Enzel (2012), Multiple dust sources in the Sahara Desert: The importance of sand dunes, *Geophysical Research Letters*, *39*(13), doi:10.1029/2012GL052145.

Cuesta, J., J. H. Marsham, D. J. Parker, and C. Flamant (2009), Dynamical mechanisms controlling the vertical redistribution of dust and the thermodynamic structure of the West Saharan atmospheric boundary layer during summer, *Atmospheric Science Letters*, doi:10.1002/asl.

Dee, D. P., S. M. Uppala, A. J. Simmons, P. Berrisford, P. Poli, S. Kobayashi, U. Andrae, M. A. Balmaseda, G. Balsamo, P. Bauer, P. Bechtold, A. C. M. Beljaars, L. van de Berg, J. Bidlot, N. Bormann, C. Delsol, R. dragani, M. Fuentes, A. J. Geer, L. Haimberger, S. B. Healy, H. Hersbach, E. V. Holm, L. Isaksen, P. Kallberg, M. Kohler, M. Marticardi, A. P. McNally, B. M. Monge-Sanz, J.-J. Morcrette, B.-K. Park, C. Peubey, P. de Rosnay, C. Tavolato, J.-N. Thepaut, and F. Vitart (2011), The ERA-Interim reanalysis: configuration and performance of the data assimilation system, *Quarterly Journal of the Royal Meteorological Society*, *137*(656), 553–597, doi:10.1002/qj.828.

Dunion, J. P., and C. S. Velden (2004), The Impact of the Saharan Air Layer on Atlantic Tropical Cyclone Activity, *Bulletin of the American Meteorological Society*, *85*(3), 353–365, doi:10.1175/BAMS-85-3-353.

Durant, A. J., S. P. Harrison, I. M. Watson, and Y. Balkanski (2009), Sensitivity of direct radiative forcing by mineral dust to particle characteristics, *Progress in Physical Geography*, *33*(1), 80–102, doi:10.1177/0309133309105034.

Eckardt, F. D., and Kuring, N. (2005), SeaWiFS identifies dust sources in the Namib Desert, *International Journal of Remote Sensing*, *26*(19), 4159–4167, doi:10.1080/01431160500113112

Engelstaedter, S., I. Tegen, and R. Washington (2006), North African dust emissions and transport, *Earth-Science Reviews*, *79*(1-2), 73–100, doi:10.1016/j.earscirev.2006.06.004.

Engelstaedter, S., and R. Washington (2007a), Temporal controls on global dust emissions: The role of surface gustiness, *Geophysical Research Letters*, *34*(15), L15805, doi:10.1029/2007GL029971.

Engelstaedter, S., and R. Washington (2007b), Atmospheric controls on the annual cycle of North African dust, *Journal of Geophysical Research*, *112*(D3), D03103, doi:10.1029/2006JD007195.

Engelstaedter, S., R. Washington, and N. Mahowald (2009), Impact of changes in atmospheric conditions in modulating summer dust concentration at Barbados: A back-trajectory analysis, *Journal of Geophysical Research*, *114*(D17), D17111, doi:10.1029/2008JD011180.

Evan, A. T., J. Dunion, J. a. Foley, A. K. Heidinger, and C. S. Velden (2006), New evidence for a relationship between Atlantic tropical cyclone activity and African dust outbreaks, *Geophysical Research Letters*, *33*(19), L19813, doi:10.1029/2006GL026408.

Fiedler, S., K. Schepanski, B. Heinold, P. Knippertz, and I. Tegen (2013), Climatology of Nocturnal Low-Level Jets over North Africa and Implications for Modeling Mineral Dust Emission, *Journal of Geophysical Research: Atmospheres*, doi:10.1002/jgrd.50394.

Flamant, C., J. Chaboureau, D. J. Parker, C. M. Taylor, J. Cammas, and O. Bock (2007), Airborne observations of the impact of a convective system on the planetary boundary layer thermodynamics and aerosol distribution in the inter-tropical discontinuity region of the West African Monsoon, *Quarterly Journal of the Royal Meteorological Society*, *1189*(June), 1175–1189, doi:10.1002/qj.

Forster, P.. V. Ramaswamy, P. Artaxo, T. Bernsten, R. Betts, D. W. Fahey, J. Haywood, J. Lean, D. C. Lowe, G. Myhre, J. Nganga, G. Prinn, M. Schulz, and R. Van Dorland (2007), Changes in Atmospheric Constituents and in Radiative Forcing, in *Climate Change 2007: The Physical Science Basis. Contribution of Working Group 1 to the Fourth Assessment Report of the Intergovernmental Panel on Climate Change*, edited by S. Solomon, D. Qin, Z. Chen, M. Marquis, K. B. Averyt, M. Tignor, and H. Miller, Cambridge University Press, Cambridge.

Gamo, M. (1996), Thickness of the dry convection and large-scale subsidence above deserts, *Boundary-layer Meteorology*, *79*, 265–278.

Gasso, S., D. Gaiero, I. Koren, and H.F. Del Valle (2011), South American Dust and Its Role in Past and Present Climate: Multidisciplinary Workshop on Southern South American Dust; Puerto Madryn, Argentina, 3–5 October 2007, *Eos, 89*(18)

Gillette, D. A. (1979), Environmental factors affecting dust emission by wind erosion, in *Saharan dust*, edited by C. Morales, pp. 91–91, Wiley, Chichester.

Gillette, A., T. C. Niemeyer, and P. J. Helm (2001), Supply-limited horizontal sand drift at an ephemerally crusted, unvegetated saline playa, *Journal of Geophysical Research*, *106*(D16), 18085–18098.

Ginoux, P., M. Chin, I. Tegen, J. M. Prospero, B. Holben, O. Dubovik, and S.-J. Lin (2001), Sources and distributions of dust aerosols simulated with the GOCART model, *Journal of Geophysical Research*, *106*(D17), 20255–20273.

Ginoux, P., and O. Torres (2003), Empirical TOMS index for dust aerosol: Applications to model validation and source characterization, *Journal of Geophysical Research*, *108*(D17), 4534, doi:10.1029/2003JD003470.

Ginoux, P., D. Garbuzov, and N. C. Hsu (2010), Identification of anthropogenic and natural dust sources using Moderate Resolution Imaging Spectroradiometer (MODIS) Deep Blue level 2 data, *Journal of Geophysical Research*, *115*(D5), D05204, doi:10.1029/2009JD012398.

Ginoux, P., J. M. Prospero, T. E. Gill, N. C. Hsu, and M. Zhao (2012), Global-scale attribution of anthropogenic and natureal dust sources and their emission rates based on MODIS Deep Blue aerosol products, *Reviews of Geophysics*, *50*(RG3005), doi:10.1029/2012RG000388.

Gomes, L., G. Bergametti, G. Coude-Gaussen, and P. Rognon (1990), Submicron Desert Dusts ' A Sandblasting Process Sampling winds can usually be related to depressions involving, *Journal of Geophysical Research*, *95*(D9), 13927–13935.

Harrison, S. P., K. E. Kohfeld, C. Roelandt, and T. Claquin (2001), The role of dust in climate changes today, at the last glacial maximum and in the future, *Earth-Science Reviews*, *54*(1-3), 43–80, doi:10.1016/S0012-8252(01)00041-1.

Haywood, J. M., P. N. Francis, M. D. Glew, and J. P. Taylor (2001), Optical properties and direct radiative effect of Saharan dust : study of two Saharan dust outbreaks using aircraft data n particle soot absorption photometer suggest that the single scattering albedo is approximately generally agreement, *Journal of Geophysical Research*, *106*(D16).

Haywood, J. M., B. T. Johnson, S. R. Osborne, J. Mulcahy, M. E. Brooks, M. a. J. Harrison, S. F. Milton, and H. E. Brindley (2011), Observations and modelling of the solar and terrestrial radiative effects of Saharan dust: a radiative closure case-study over oceans during the GERBILS campaign, *Quarterly Journal of the Royal Meteorological Society*, *137*(658), 1211–1226, doi:10.1002/qj.770.

Heinold, B., P. Knippertz, J. H. Marsham, S. Fiedler, N. S. Dixon, K. Schepanski, B. Laurent, and I. Tegen (2013), The role of deep convection and nocturnal low-level jets for dust emission in summertime West Africa: Estimates from convection-permitting simulations, *Journal of Geophysical Research: Atmospheres*, *118* doi:10.1002/jgrd.50402.

Iversen, J.D., and White, B.R. (1982), Saltation threshold on Earth, Mars and Venus, *Sedimentology, (29)*, 111–119.

Houser, C. A., and W. G. Nickling (2001), The factors influencing the abrasion efficiency of saltating grains on a clay-crusted playa, *Earth Surface Processes and Landforms*, *26*(5), 491–505, doi:10.1002/esp.193.

Huffman, G. J., R. F. Adler, M. M. Morrissey, D. T. Bolvin, S. Curtis, R. Joyce, B. McGavock, J. Susskind (2001), Global precipitation at one-degree daily resolution from multisatellite observations, *Journal of Hydrometeorology*, *2*, 36-50

Huneeus, N., M. Schulz, Y. Balkanski, J. Griefsfeller, J. Prospero, S. Kinne, S. Bauer, O. Boucher, M. Chin, F. Dentener, T. Diehl, R. Easter, D. Fillmore, S. Ghan, P. Ginoux, A. Grini, L. Horowitz, D. Koch, M. C. Krol, W. Landing, X. Liu, N. Mahowald, R. Miller, J.-J. Morcrette, G. Myhre, J. Penner, J. Perlwitz, P. Stier, T. Takemura, and C. S. Zender (2011), Global dust model intercomparison in AeroCom phase I, *Atmosphere, Chemistry and Physics*, *11*(15), 7781–7816, doi:10.5194/acp-11-7781-2011.

Janicot, S. G. Caniaux, F. Chauvin, G. de Coetlogon, B. Fontaine, N. Hall, G. Kiladis, J.-P. Lafore, C. Lavaysse, S. L. Lavender, S. Leroux, R. Marteau, F. Mounier, N. Philippon, R. Roehrig, B. Sultan and C.M.Taylor (2011), Intraseasonal variability of

the West African monsoon, *Atmospheric Science Letters*, *12*(1), 58–66, doi:10.1002/asl.280.

Jickells, T. D., Z. S. An, K. K. Andersen, A. R. Baker, G. Bergametti, N. Brooks, J. J. Cao, P. W. Boyd, R. A. Duce, K. A. Hunter, H. Kawahata, N. Kubilay, J. laRoche, P. S. Liss, N. Mahowald, J. M. Prospero, A. J. Ridgwell, I. Tegen, and R. Torres (2005), Global iron connections between desert dust, ocean biogeochemistry, and climate., *Science (New York, N.Y.)*, *308*(5718), 67–71, doi:10.1126/science.1105959.

Kaufman, Y. J., I. Koren, L. a Remer, D. Rosenfeld, and Y. Rudich (2005), The effect of smoke, dust, and pollution aerosol on shallow cloud development over the Atlantic Ocean., *Proc. Natl. Acad. Sci. U. S. A.*, *102*(32), 11207–12, doi:10.1073/pnas.0505191102.

Kellogg, C. A., D. W. Griffin, V. H. Garrison, K. K. Peak, N. Royall, R. R. Smith, and E. A. Shinn (2004), Characterization of aerosolized bacteria and fungi from desert dust events in Mali, West Africa, *Aerobiologia*, *20*, 99–110.

King, J., Etyemezian, V., Sweeney, M., Buck, B. J., and Nikolich, G. (2011), Dust emission variability at the Salton Sea, California, USA, *Aeolian Research, 3*(1), 67–79, doi:10.1016/j.aeolia.2011.03.005

Kjelgaard, J. F., D. G. Chandler, and K. E. Saxton (2004), Evidence for direct suspension of loessial soils on the Columbia Plateau, *Earth Surface Processes and Landforms, 29*(2), 221–236, doi:10.1002/esp.1028.

Klüser, L., and T. Holzer-Popp (2010), Relationships between mineral dust and cloud properties in the West African Sahel, *Atmophere, Chemistry and Physics*, *10*(14), 6901–6915, doi:10.5194/acp-10-6901-2010.

Knippertz, P. (2008), Dust mobilization in the West African heat trough - The role of the diurnal cycle and of extratropical synoptic disturbances, *Meteorologische Zeitschrift*, *17*, 553–563, doi:10.1127/0941- 2948/2008/0315.

Knippertz, P., and M. C. Todd (2010), The central west Saharan dust hot spot and its relation to African easterly waves and extratropical disturbances, *Journal of Geophysical Research*, *115*(D12), D12117, doi:10.1029/2009JD012819.

Knippertz, P., M. Tesche, B. Heinold, K. Kandler, C. Toledano, and M. Esselborn (2011), Dust mobilization and aerosol transport from West Africa to Cape Verde-a meteorological overview of SAMUM-2, *Tellus B*, *63*(4), 430–447, doi:10.1111/j.1600-0889.2011.00544.

Knippertz, P., and M. C. Todd (2012), Mineral dust aerosols over the Sahara: meteorological controls on emission and transport and implications for modeling, *Reviews of Geophysics*, *50*, doi:10.1029/2011RG000362.

Koch, J., and N. O. Renno (2005), The role of convective plumes and vortices on the global aerosol budget, *Geophysical Research Letters*, *32*(18), L18806, doi:10.1029/2005GL023420.

Koren, I., Y. J. Kaufman, D. Rosenfeld, L. A. Remer, and Y. Rudich (2005), Aerosol invigoration and restructuring of Atlantic convective clouds, *Geophysical Research Letters*, *32*(14), L14828, doi:10.1029/2005GL023187.

Koren, I., Y. J. Kaufman, R. Washington, M. C. Todd, Y. Rudich, J. V. Martins, and D. Rosenfeld (2006), The Bodélé depression: a single spot in the Sahara that provides most of the mineral dust to the Amazon forest, *Environmental Research Letters*, *1*(1), 014005, doi:10.1088/1748-9326/1/1/014005.

Lavaysse, C., C. Flamant, S. Janicot, D. J. Parker, J.-P. Lafore, B. Sultan, and J. Pelon (2009), Seasonal evolution of the West African heat low: a climatological perspective, *Climate Dynamics*, *33*(2-3), 313–330, doi:10.1007/s00382-009-0553-4.

Lavaysse, C., J.-P. Chaboureau, and C. Flamant (2011), Dust impact on the West African heat low in summertime, *Quarterly Journal of the Royal Meteorological Society*, *137*(658), 1227–1240, doi:10.1002/qj.844.

Lee, J. A., Baddock, M. C., Mbuh, M. J., and Gill, T. E. (2012), Geomorphic and land cover characteristics of aeolian dust sources in West Texas and eastern New Mexico, USA, *Aeolian Research, 3*(4), 459–466, doi:10.1016/j.aeolia.2011.08.001

Lensky, I. M., and D. Rosenfeld (2008), and Physics Clouds-Aerosols-Precipitation Satellite Analysis Tool (CAPSAT), *Atmosphere, Chemistry and Physics*, (1998), 6739–6753.

Mahowald, N. M., R. G. Bryant, J. del Corral, and L. Steinberger (2003), Ephemeral lakes and desert dust sources, *Geophysical Research Letters, 30*(2), 1074, doi:10.1029/2002GL016041.

Mahowald, N. M., M. Yoshioka, W. D. Collins, A. J. Conley, D. W. Fillmore, and D. B. Coleman (2006), Climate response and radiative forcing from mineral aerosols during the last glacial maximum, pre-industrial, current and doubled-carbon dioxide climates, *Geophysical Research Letters*, *33*(20), L20705, doi:10.1029/2006GL026126.

Mahowald, N. M., S. Kloster, S. Engelstaedter, J. K. Moore, S. Mukhopadhyay, J. R. McConnell, S. Albani, S. C. Doney, A. Bhattacharya, M. A. J. Curran, M. G. Flanner, F. M. Hoffman, D. M. Lawrence, K. Lindsay, P. A. Mayewski, J. Neff, D. Rothenberg, E. Thomas, P. E. Thornton, and C. S. Zender (2010), Observed 20th century desert dust variability: impact on climate and biogeochemistry, *Atmosphere, Chemistry and Physics*, *10*(22), 10875–10893, doi:10.5194/acp-10-10875-2010.

Marsham, J. H., D. J. Parker, C. M. Grams, C. M. Taylor, and J. M. Haywood (2008), Uplift of Saharan dust south of the intertropical discontinuity, *Journal of Geophysical Research*, *113*(D21), D21102, doi:10.1029/2008JD009844.

Marsham, J. H., P. Knippertz, N. S. Dixon, D. J. Parker, and G. M. S. Lister (2011), The importance of the representation of deep convection for modeled dust-generating winds over West Africa during summer, *Geophysical Research Letters*, *38*(16), L16803, doi:10.1029/2011GL048368.

Marsham, J.H., Hobby, M., Allen, C.J.T., Banks, J.R., Bart, M., Brooks, B.J., Cavazos-Guerra, C., Engelstaedter, S., Gascoyne, M., Lima, A.R., Martins, J.V., McQuaid, J.B., O'Leary, A., Ouchene, B., Ouladichir, A., Parker, D.J., Saci, A., Salah-Ferroudj, R. (2013), Meteorology and dust in the central Sahara: Observations from Fennec supersite-1 during the June 2011 Intensive Observation Period, *Journal of Geophysical Research*, doi:10.1002/jgrd.50211.

Marticorena, B., and G. Bergametti (1995), Modeling the atmospheric dust cycle: 1. Design of a soil-derived dust emission scheme, *Journal of Geophysical Research*, *100*(D8), 16415–16430, doi:10.1029/95JD00690.

Mcfiggans, G., P. Artaxo, U. Baltensperger, H. Coe, M. C. Facchini, G. Feingold, S. Fuzzi, M. Gysel, A. Laaksonen, U. Lohmann, T. F. Mentel, D. M. Murphy, C. D. O'Dowd, J. R. Snider, and E. Weingartner (2006), The effect of physical and chemical aerosol properties on warm cloud droplet activation, *Atmophere, Chemistry and Physics.*, *6*, 2593–2649.

Middleton, N. J. (1986a), Dust storms in the Middle East, *Journal of Arid Environments, 10*, 83–96.

Middleton, N. J. (1986b), A geography of dust storms in southwest Asia, *Journal of Climatology, 6*, 183–196, doi:10.1002/joc.3370060207.

Miller, R.L., Tegen, I. (1998), Climate Response to Soil Dust Aerosols, *Journal of Climate*, *11*, 3247–3267.

Molesworth, A. M., L. E. Cuevas, A. P. Morse, J. R. Herman, and M. C. Thomson (2002), Dust clouds and spread of infection, *The Lancet*, *359*(9300), 81–82.

Mona, L., Z. Liu, D. Müller, a. Omar, a. Papayannis, G. Pappalardo, N. Sugimoto, and M. Vaughan (2012), Lidar Measurements for Desert Dust Characterization: An Overview, *Advances in Meteorology*, *2012*, 1–36, doi:10.1155/2012/356265.

Moulin, C., L. C.E, F. Dulac, and U. Dayan (1997), Control of atmospheric export of dust from North Africa by the North Atlantic Oscillation, *Nature*, *387*, 691–694.

Neff, J. C., a. P. Ballantyne, G. L. Farmer, N. M. Mahowald, J. L. Conroy, C. C. Landry, J. T. Overpeck, T. H. Painter, C. R. Lawrence, and R. L. Reynolds (2008), Increasing eolian dust deposition in the western United States linked to human activity, *Nature Geoscience*, *1*(3), 189–195, doi:10.1038/ngeo133.

Okin, G. S., J. E. Bullard, R. L. Reynolds, J.-A. C. Ballantine, K. Schepanski, M. C. Todd, J. Belnap, M. C. Baddock, T. E. Gill, and M. E. Miller (2011), Dust : Small-Scale Processes With Global Consequences, *EOS*, *92*(29), 241–248.

O'Hara, S. L., G. F. Wiggs, B. Mamedov, G. Davidson, and R. B. Hubbard (2000), Exposure to airborne dust contaminated with pesticide in the Aral Sea region., *The Lancet*, *355*(9204), 627–8, doi:10.1016/S0140-6736(99)04753-4.

Painter, T. H., A. P. Barrett, C. C. Landry, J. C. Neff, M. P. Cassidy, C. R. Lawrence, K. E. McBride, and G. L. Farmer (2007), Impact of disturbed desert soils on duration of mountain snow cover, *Geophysical Research Letters*, *34*(12), L12502, doi:10.1029/2007GL030284.

Parker, D. J., C. D. Thorncroft, R. R. Burton, and A. Diongue-Niang (2005), Analysis of the African easterly jet, using aircraft observations from the JET2000 experiment, *Quarterly Journal of the Royal Meteorological Society*, *131*(608), 1461–1482, doi:10.1256/qj.03.189.

Pease, P. P., V. P. Tchakerian, and N. W. Tindale (1998), Aerosols over the Arabian Sea: Geochemistry and source areas for aeolian desert dust, *Journal of Arid Environments, 39*, 477–496, doi:10.1006/jare.1997.0368.

Prospero, J. M. (1999), Assessing the Impact of Advected African Dust on Air Quality and Health in the Eastern United States, *Human and Ecological Risk Assessment*, *5*(3), 471–479, doi:10.1080/108070399.1999.10518872.

Prospero, J.M., Ginoux, P., Torres, O., Nicholson, S.E., Gill, T. E. (2002), Environmental characterization of global sources of atmospheric soil dust identified with the NIMBUS 7 Total Ozone Mapping Spectrometer (TOMS) absorbing aerosol product, *Reviews of Geophysics*, *40*(1), 1002, doi:10.1029/2000RG000095.

Prospero, J. M., and P. J. Lamb (2003), African droughts and dust transport to the Caribbean: climate change implications, *Science*, *302*(5647), 1024–7, doi:10.1126/science.1089915.

Prospero, J. M., J. E. Bullard, and R. Hodgkins (2012), High-latitude dust over the North Atlantic: inputs from Icelandic proglacial dust storms., *Science, 335*(6072), 1078–82, doi:10.1126/science.1217447.

Qian, W., L. Quan, and S. Shi (2002), Variations of the dust storm in China and its climatic control, *Journal of Climate, 15*, 1216–1229.

Raupach, M.R., Gillette, D.A., and Leys, J.F. [1993], The effect of roughness elements on wind erosion threshold, *Journal of Geophysical Research,98*, 3023–3029.

Ravi, S., P. D'Odorico, D. D. Breshears, J. P. Field, A. S. Goudie, T. E. Huxman, J. Li, G. S. Okin, R. J. Swap, A. D. Thomas, S. V. Pelt, J. J. Whickler, and T. M. Zobeck (2011), Aeolian Processes and the Biosphere, *Reviews of Geophysics*, *49*(RG3001/2011), 1–45, doi:10.1029/2010RG000328.

Reheis, M. C., and R. Kihl (1995), Dust deposition in southern Nevada and California, 1984–1989: Relations to climate, source area, and source lithology, *Journal of Geophysical Research*, *100*(D5), 8893, doi:10.1029/94JD03245.

Reynolds, R. L., J. C. Yount, M. Reheis, H. Goldstein, P. Chavez, R. Fulton, J. Whitney, C. Fuller, and R. M. Forester (2007), Dust Emission from Wet and Dry Playas in the Mojave Desert , USA, *Earth Surface Processes and Landforms*, *1827*(32), 1811–1827, doi:10.1002/esp.

Roberts, A., and P. Knippertz (2012), Haboobs : convectively generated dust storms in West Africa, *Weather*, *67*(12), 311–316.

Rodríguez-Fonseca, B., S. Janicot, E. Mohino, T. Losada, J. Bader,C. Caminade, F. Chauvin, B. Fontaine, J. Garcıa-Serrano, S. Gervois, M. Joly, I. Polo, P. Ruti, P. Roucou, and A. Voldoire (2011), Interannual and decadal SST-forced responses of the West African monsoon, *Atmospheric Science Letters*, *12*(1), 67–74, doi:10.1002/asl.308.

Rodwell, M. J., and T. Jung (2008), Understanding the local and global impacts of model physics changes : An aerosol example, *Quarterly Journal of the Royal Meteorological Society*, *134*, 1479–1497, doi:10.1002/qj.

Ryder, C. L. et al. (2013), Optical properties of Saharan dust aerosol and contribution from the coarse mode as measured during the Fennec 2011 aircraft campaign, *Atmosphere, Chemistry and Physics, 13*(1), 303–325, doi:10.5194/acp-13-303-2013.

Schepanski, K., I. Tegen, B. Laurent, B. Heinold, and A. Macke (2007), A new Saharan dust source activation frequency map derived from MSG-SEVIRI IR-channels, *Geophysical Research Letters*, *34*(18), L18803, doi:10.1029/2007GL030168.

Schepanski, K., I. Tegen, M. C. Todd, B. Heinold, G. Bönisch, B. Laurent, and A. Macke (2009), Meteorological processes forcing Saharan dust emission inferred from MSG-SEVIRI observations of subdaily dust source activation and numerical models, *Journal of Geophysical Research*, *114*(D10201), doi:10.1029/2008JD010325.

Schepanski, K., I. Tegen, and A. Macke (2012), Comparison of satellite based observations of Saharan dust source areas, *Remote Sensing of Environment*, *123*, 90–97, doi:10.1016/j.rse.2012.03.019.

Shao, Y. (2008), *Physics and Modeling of Wind Erosion,* 2nd ed., Springer, Dordrecht, Netherlands.

Shao, Y., K.-H. Wyrwoll, A. Chappell, J. Huang, Z. Lin, G. H. McTainsh, M. Mikami, T. Y. Tanaka, X. Wang, and S. Yoon (2011), Dust cycle: An emerging core theme in Earth system science, *Aeolian Research*, *2*(4), 181–204, doi:10.1016/j.aeolia.2011.02.001.

Shinoda, M., J. a. Gillies, M. Mikami, and Y. Shao (2011), Temperate grasslands as a dust source: Knowledge, uncertainties, and challenges, *Aeolian Research*, *3*(3), 271–293, doi:10.1016/j.aeolia.2011.07.001.

Solmon, F., M. Mallet, N. Elguindi, F. Giorgi, A. Zakey, and A. Konaré (2008), Dust aerosol impact on regional precipitation over western Africa, mechanisms and sensitivity to absorption properties, *Geophysical Research Letters*, *35*(24), L24705, doi:10.1029/2008GL035900.

Sun, J., M. Zhang, and T. Liu (2001), Spatial and temporal characteristics of dust storms in China and its surrounding regions, 1960–1999: relations to source area and climate, *Journal of Geophysical Research, 106*, 10,325–10,333

Tanré, D., J. Haywood, J. Pelo, J. F. Léon, B. Chatenet, P. Formenti, P. Francis, P. Goloub, E. J. Highwood, and G. Myhre (2003), Measurement and modeling of the Saharan dust radiative impact: Overview of the Saharan Dust Experiment (SHADE), *Journal of Geophysical Research*, *108*(D18), 8574, doi:10.1029/2002JD003273.

Tegen, I., and R. Miller (1998), A general circulation model study on the interannual variability of soil dust aerosol, *Journal of Geophysical Research*, *103*(D20), 25975, doi:10.1029/98JD02345.

Tegen, I., K. Schepanski, and B. Heinold (2013), Comparing two years of Saharan dust source activation obtained by regional modelling and satellite observations, *Atmosphere, Chemistry Physics*, *13*(5), 2381–2390, doi:10.5194/acp-13-2381-2013.

Textor, C. M. Schulz, S. Guibert, S. Kinne, Y. Balkanski, S. Bauer, T. Berntsen, T. Berglen, O. Boucher, M. Chin, F. Dentener, T. Diehl, R. Easter, H. Feichter, D. Fillmore, S. Ghan, P. Ginoux, S. Gong, A. Grini, J. Hendricks, L. Horowitz, P. Huang, I. Isaksen, T. Iversen, S. Kloster, D. Koch, A. Kirkevag, J. E. Kristjansson, M. Krol, A. Lauer, J. F. Lamarque, X. Liu, V. Montanaro, G. Myhre, J. Penner, G. Pitari, S. Reddy, Ø. Seland, P. Stier, T. Takemura, and X. Tie (2006), Analysis and quantification of the diversities of aerosol life cycles within AeroCom, *Atmosphere, Chemistry and Physics, 6*(7), 1777–1813, doi:10.5194/acp-6-1777-2006.

Todd, M. C., R. Washington, S. Raghavan, G. Lizcano, and P. Knippertz (2008a), Regional Model Simulations of the Bodélé Low-Level Jet of Northern Chad during the Bodélé Dust Experiment (BoDEx 2005), *Journal of Climate*, *21*(5), 995–1012, doi:10.1175/2007JCLI1766.1.

Todd, M. C., D. Bou Karam, C. Cavazos, C. Bouet, B. Heinold, J. M. Baldasano, G. Cautenet, I. Koren, C. Perez, F. Solmon, I. Tegen, P. Tulet, R. Washington, and A. Zakey (2008b), Quantifying uncertainty in estimates of mineral dust flux: An intercomparison of model performance over the Bodélé Depression, northern Chad, *Journal of Geophysical Research*, *113*(D24), D24107, doi:10.1029/2008JD010476.

Tompkins, A. M., C. Cardinali, J.-J. Morcrette, and M. Rodwell (2005), Influence of aerosol climatology on forecasts of the African Easterly Jet, *Geophysical Research Letters*, *32*(10), L10801, doi:10.1029/2004GL022189.

Vickery, K. J., Eckardt, F. D., and Bryant, R. G. (2013), A sub-basin scale dust plume source frequency inventory for southern Africa, 2005–2008, *Geophysical Research Letters, 40*(July), doi:10.1002/grl.50968

Vizy, E. K., and K. H. Cook (2009), A mechanism for African monsoon breaks: Mediterranean cold air surges, *Journal of Geophysical Research*, *114*(D1), D01104, doi:10.1029/2008JD010654.

Wang, X., Dong, Z., Zhang, J., and Liu, L. (2004), Modern dust storms in China: an overview. *Journal of Arid Environments*, *58*(4), 559–574, doi:10.1016/j.jaridenv.2003.11.009

Wang, X., Z. Zhou, and Z. Dong (2006), Control of dust emissions by geomorphic conditions, wind environments and land use in northern China: An examination based on dust storm frequency from 1960 to 2003, *Geomorphology*, *81*(3-4), 292–308, doi:10.1016/j.geomorph.2006.04.015

Warner, T. T. (2004) *Desert Meteorology*, Cambridge University Press, Cambridge.

Warren, A., A. Chappell, M. C. Todd, C. Bristow, N. Drake, S. Engelstaedter, V. Martins, S. M'bainayel, and R. Washington (2007), Dust-raising in the dustiest place on earth, *Geomorphology*, *92*(1-2), 25–37, doi:10.1016/j.geomorph.2007.02.007.

Washington, R., M. Todd, N. J. Middleton, and A. S. Goudie (2003), Dust-Storm Source Areas Determined by the Total Ozone Monitoring Spectrometer and Surface Observations, *Annals of the Association of American Geographers*, *93*(2), 297–313.

Washington, R., and M. Todd (2005), Atmospheric controls on mineral dust emission from the Bodélé Depression, Chad: The role of the low level jet, *Geophysical Research Letters*, *32*(17), L17701, doi:10.1029/2005GL023597.

Washington, R., M. C. Todd, G. Lizcano, I. Tegen, C. Flamant, I. Koren, P. Ginoux, S. Engelstaedter, C. S. Bristow, C. S. Zender, A. S. Goudie, A. Warren, J. M. Prospero (2006), Links between topography, wind, deflation, lakes and dust: The case of the Bodélé Depression, Chad, *Geophysical Research Letters*, *33*(9), L09401, doi:10.1029/2006GL025827.

Washington, R., C. Bouet, G. Cautenet, E. Mackenzie, I. Ashpole, S. Engelstaedter, G. Lizcano, G. M. Henderson, K. Schepanski, and I. Tegen (2009), Dust as a tipping element : The Bodélé Depression , Chad, *Proceedings of the National Academy of Sciences*, *106*(49), 20564–20571.

Washington, R. (2012) *Fennec: The Saharan Climate System – An Overview*, 4th AMMA International Conference, 2-6 July 2012, Toulouse, France

Webb, N.P., and C.L. Strong (2011) Soil erodibility dynamics and its representations for wind erosion and dust emission models, *Aeolian Research, 3*, 165-179.

Wiggs, G. S. F. (2011), Sediment mobilisation by the wind, in *Arid Zone Geomorphology: Process, Form and Change in Drylands*, edited by D. S. G. Thomas, pp. 455–486, John Wiley & Sons, Ltd., Oxford.

Winckler, G., R. F. Anderson, M. Q. Fleisher, D. McGee, and N. Mahowald (2008), Covariant glacial-interglacial dust fluxes in the equatorial Pacific and Antarctica., *Science, 320*(5872), 93–6, doi:10.1126/science.1150595.

Wolfe, S.A., and Nickling, W.G. (1993), The protective role of sparse vegetation in wind erosion, *Progress in Physical Geography, (17)*, 50–68.

Zender, C. S., D. Newman, and O. Torres (2003), Spatial heterogeneity in aeolian erodibility: Uniform, topographic, geomorphic, and hydrologic hypotheses, *Journal of Geophysical Research*, *108*(D17), 4543, doi:10.1029/2002JD003039.

Zender, C.S., and E. Y. Kwon (2005), Regional contrasts in dust emission responses to climate, *Journal of Geophysical Research, 110*(D13201), doi:10.1029/2004JD005501

Zobeck, T.M. [1991], Soil properties affecting wind erosion, *Journal of Soil Water Conservation, (46)*, 112–118.

Chapter 3

An automated dust detection using SEVIRI: a multi-year climatology of summertime dustiness in the central and western Sahara

Ian Ashpole and Richard Washington

Published in *Journal of Geophysical Research*, *117*,D08202, doi:10.1029/2011JD016845

Abstract

Here we present an automated dust detection scheme using the Infrared (IR) channels of the Spinning Enhanced Visible and Infrared Imager (SEVIRI), carried on board Meteosat Second Generation (MSG) satellites, from which dust scheme images that are now widely used in Saharan dust studies are created. This provides an objective, readily-reproducible and quick way to build up climatologies of dust presence which compares well with subjectively identified dust presence in the daytime hours. At nighttime the automated detection scheme is less reliable due to the strong diurnal cycle of surface temperatures. Our SEVIRI Dust Flag (SDF) is compared to Aerosol Optical Depth (AOD) from the surface and found to successfully and consistently identify moderate-heavy dust outbreaks, although success rate is lower in the early morning and late evening. SDF corresponds to Absorbing Aerosol Index (AAI) from the Ozone Monitoring Instrument (OMI) that is also indicative of moderate-heavy dust outbreaks across the central and western Sahara, but there are differences in the spatial patterns of climatologies created over a number of years that are likely to be due to the different

sensitivities of the detection schemes. Despite these discrepancies, SDF and AAI both place dust hotspots in southern Algeria and across its southern borders with Mali and Niger, and SDF climatologies for June – August 2004 – 2010 reveal that there is a substantial degree of interannual variability in dust presence in the central and western Sahara in the boreal summer.

3.1. Introduction

Mineral dust aerosols are an important part of the climate system [*Forster et al.* 2007]. Dust is known to modify the atmospheric radiation budget directly by reflecting shortwave solar radiation and absorbing longwave terrestrial radiation [e.g. *Miller and Tegen,* 1998], and indirectly by altering cloud properties [e.g. *McFiggans et al.* 2006], with the potential to influence the general circulation of the atmosphere [*Rodwell and Palmer,* 2007]. Dust deposition in a range of environments distant from source region is also known to impact on global ecosystems and processes, providing for example nutrients for oceanic microorganisms and ultimately effecting oceanic biogeochemistry [*Jickells et al.* 2005], and fertilisation for the Amazon rainforest [*Koren et al.* 2006; *Bristow et al.* 2010]. Airborne dust has also been shown to negatively impact air quality and respiratory health in and around source regions [*O'Hara et al.* 2000].

Dust source areas typically occur in data sparse regions requiring specialised field campaigns to recover data [e.g. *Washington et al.* 2006]. As a result, the analysis of satellite derived dust datasets has made a crucial contribution to the identification of persistent source regions [*Prospero et al.* 2002; *Washington et al.* 2003] as well as mechanisms associated with dust emission [e.g. *Washington and Todd*, 2005; *Knippertz and Todd*, 2010].

Until recently, one of the major limitations of satellite products in dust studies has been the relatively coarse temporal resolution (one observation per day) determined by the use of polar orbiting satellites. The very high temporal resolution of the Spinning Enhanced Visible and Infrared Imager (SEVIRI – 15 minutes), carried on board the geostationary Meteosat Second Generation (MSG) satellites makes it a valuable tool for the study of Saharan dust. *Schepanski et al*. [2007; 2009] have used images created from SEVIRI data to map sub-daily scale variability of dust presence over the Sahara. In agreement with previous studies, the central and western Sahara emerges as a strong source region, particularly in the boreal summer months. The reproducibility of these results is constrained both because interpretation of the dust signal in the images is subjective and because the analysis is very time-intensive. There is therefore a need to automate the detection process from SEVIRI in order to ensure the reproducibility of the detection process.

This paper presents a method to objectively detect dust from the central and western Sahara during summer months using SEVIRI, based on the principles of dust detection in infrared that are used to enhance the presence of dust in SEVIRI dust scheme images. We use this to describe summertime dust presence over the central and western Sahara observed by SEVIRI for June – August 2004 – 2010. The remainder of the paper is structured as follows: In section 3.2 we outline dust detection in infrared (IR) wavelengths and explain how dust is enhanced in SEVIRI dust scheme images. Section 3.3 provides an overview of the data and processing methods used. In Section 3.4 our automated detection technique is outlined, developed and compared to subjective identification of dust presence based on analysis of SEVIRI dust scheme imagery. Sections 3.5 and 3.6 compare the detection scheme to surface and satellite measurements that are widely used as indicators of dust presence. Finally, Section 3.7 describes the

patterns of summertime dust presence from June, July and August for 2004 to 2010. The main conclusions are summarised in Section 3.8.

3.2. Dust detection in the IR

3.2.1. Background and theory

Airborne dust over bright desert surfaces during the daytime is detectable in IR wavelengths as a cool anomaly in satellite-observed brightness temperatures (BTs) compared to pristine sky conditions [*Shenk and Curran*, 1974]. This is because it 1) absorbs outgoing terrestrial radiation; and 2) absorbs incoming solar radiation, reducing surface skin temperatures and consequently surface-emitted IR radiance. These effects have been used to create desert dust climatologies [e.g. *Legrand et al*. 2001]. At night, airborne dust causes a warm anomaly over the desert by increasing the downward longwave energy flux and reducing the degree of surface cooling that would occur in pristine sky conditions [*Shenk and Curran*, 1974; *Legrand et al*. 1988]. However, spatial variability in surface emissivity (Figure 3.1), surface skin temperature, atmospheric conditions and the presence of water vapour and clouds all affect the satellite observed brightness temperatures such that it is difficult to deduce the presence of dust using a single IR channel.

Variability in the transmissive and emissive nature of mineral dust aerosols between 8 – 12 μm [e.g. *Ackerman*, 1997] can be exploited to isolate the signature of airborne dust. The distinct maxima in absorption around 10 μm motivates the use of brightness temperature differences (BTDs) with adjacent wavelength channels, a method which has been applied to detect and monitor dust storms in desert regions [e.g. *Ackerman*, 1997; *Zhang et al*. 2006; *Baddock et al*. 2009].

3.2.2. SEVIRI dust scheme

The SEVIRI dust scheme comprises red-green-blue (RGB) composite images created from IR brightness temperatures at 8.7 (BT087), 10.8 (BT108) and 12.0 μm (BT120), which enhance the appearance of dust against the desert background [e.g. *Lensky and Rosenfeld*, 2008]. The RGB bands are defined as follows (Equation 3.1):

Red = BTD (120-108), range = -4 – 2 K

Green = BTD (108-087), range = 0 – 15 K

Blue = BT 108, range = 261 – 289 K

During the day, BT108 decreases in the presence of dust due to the dust absorption maxima around 10 μm [e.g. *Ackerman,* 1997]. For the three SEVIRI channels considered, this is where the thermal emissivity of the desert surface is highest, therefore in pristine sky conditions BT108 is high. BT087 is not as affected by the presence of dust, but is much lower than BT108 under pristine sky conditions. BT120 is similarly less affected by dust presence and lower than BT108 under pristine sky conditions, but not to the same extent as BT087. It follows that, under typical daytime conditions, when dust is present, BTD (120-108) will be more positive than the equivalent for pristine sky conditions, and BTD (108-087) will be lower. Consequently, in the SEVIRI dust scheme, dust over desert is characterised by strong values of red and weak values of green, whereas pristine sky conditions will have weak red and strong green components. The range of BT108 values is restricted so that for typical daytime conditions and dust loadings the blue channel will saturate. This saturation may not occur at nighttime when surface temperatures are low, or in the presence of very heavy dust loadings, whereby satellite-observed BT108 is dominated by emission from the dust layer itself [e.g.

Brindley and Russell, 2009]. In addition, if a near-surface temperature inversion is present, typical of desert at night, the presence of a dust layer may actually cause BTD (120-108) to become more negative relative to pristine conditions. Other atmospheric components such as cirrus clouds and convective cloud tops are much higher and colder, thus generally are characterised by lower values of blue and stronger values of red. Dominated by the red and blue components, airborne dust is represented by vivid magenta colours in the SEVIRI dust scheme images (commonly known as "pink dust") that have been widely used in recent Saharan dust research [e.g. *Schepanski et al*. 2007; 2009].

3.2.3 Limitations

There are a number of limitations to the IR detection of dust that need to be considered. Chiefly, absorption in the IR by water vapour can significantly affect longwave absorption [e.g. *King et al.* 1999; *Chaboureau et al*. 2007; *Schroedter-Homscheidt et al*. 2008]. Recent studies identify problems with the SEVIRI dust scheme over the moist southern parts of west Africa during the summer monsoon season and when the water vapour content on the Saharan fringes is temporarily increased due to monsoon surges or cold pool outflows from meso-scale convective systems [e.g. *Flamant et al.* 2007; *Knippertz and Todd*, 2010].

Mineralogical composition and microphysical characteristics of the dust aerosol, such as particle size distribution and particle shape, are also an important control on its IR radiative signature [e.g. *Wald et al*. 1998; *Hudson et al*. 2008a; 2008b], and as a result of recent field campaigns it has become clear that these controls are highly variable [e.g. *Kandler et al*. 2011]. However, from analysis of several dust storm events from the Lake

Eyre Basin in Australia, *Baddock et al*. [2009] find the BTD technique (MODIS channel 31 (11.03 μm) – 32 (12.02 μm)) to be consistently reliable for dust detection and not significantly affected by dust mineralogy, although they do note that dust/non-dust thresholds vary on a case-by-case basis.

The IR signal of dust is also sensitive to dust layer height [e.g. *Pierangelo et al*. 2004] as well as the density of the dust plume [e.g. *Darmenov and Sokolik*, 2005]. The BTD signal can also be masked by the presence of cirrus clouds [*Chaboureau et al*. 2007], and is sensitive to variability in surface emissivity, which is large in the 8.7 μm band over the desert [*Li et al*. 2007]. Figure 3.1 displays typical surface emissivities for June 2011 across the central and western Sahara, derived from a combination of MODIS observations and laboratory-measured emissivity spectra [*Seemann et al.,* 2008]. Although the wavelength regions do not overlap exactly with those of SEVIRI, we can expect the patterns to be comparable.

3.3. Data and methods

In this study we utilize independent and widely used surface and satellite derived dust datasets to understand the behaviour of individual SEVIRI bands in the presence of dust and against which to compare our automated dust detection scheme.

3.3.1. SEVIRI

SEVIRI data are obtainable from the Eumetsat data centre [archive.eumetsat.int]. For this study, High Rate Level 1.5 image data [*Müller,* 2007] are used. Of 12 spectral channels

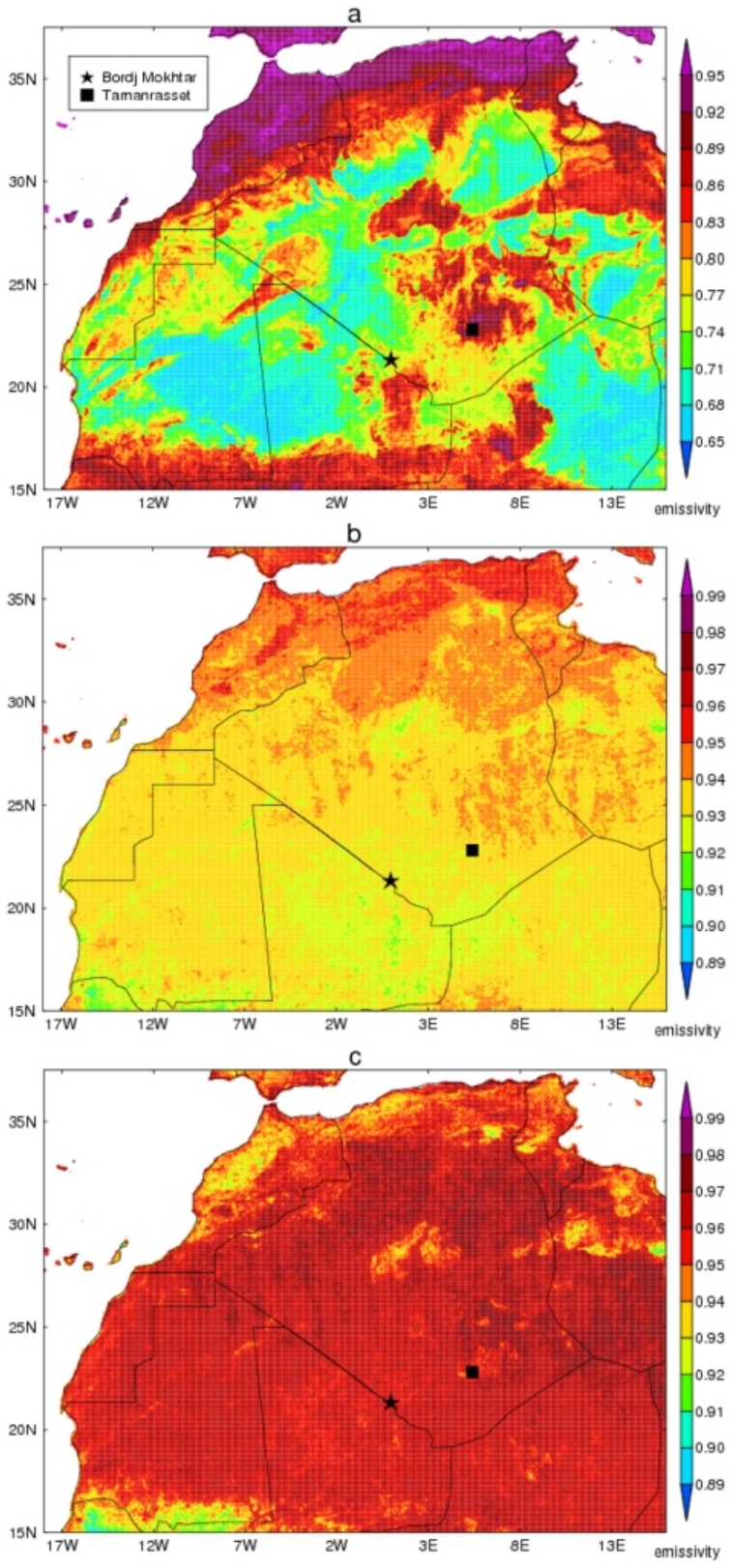

Figure 3.1. Typical surface emissivities across the central and western Sahara for June 2011for **(a)** 8.3 µm. **(b)** 10.8 µm. **(c)** 12.1 µm. See text for details of data used. Note the different scale used for (a) compared to (b) and (c). Symbols correspond to locations from which surface indicators of dustiness are obtained for comparison with SEVIRI data.

that are available, brightness temperatures for channels 7 (IR 8.7 μm), 9 (IR 10.8 μm) and 10 (IR 12.0 μm), with a resolution of 3 km at the sub-satellite point are used. Images were selected and from these the central and western Sahara study area was extracted (18^o W – 16^o E, 15 – 37.5^o N) and interpolated using the nearest neighbour method to a standard latitude/longitude grid of approximately 0.03 x 0.03 degrees resolution. Every 15-minute image available for June – August 2004 – 2010 and June 2011 was obtained. The SEVIRI cloud mask was obtained from Eumetsat for the same period [*Eumetsat,* 2010]. This distinguishes between "clear" and "cloudy" scenes, and is created using data from all SEVIRI channels except for 9.7 μm (ozone absorption) and High Resolution Visible [*Eumetsat,* 2007]. *Derrien and Le Gléau,* [2005] find that the algorithms implemented in the cloud detection scheme perform well when tested against ground observations, however we note from comparison of the cloud mask fields to SEVIRI dust scheme imagery that in some cases the SEVIRI cloud mask incorrectly flags dust as cloud. Consequently, SEVIRI brightness temperature data are not cloud screened prior to dust detection, but instead the cloud mask is applied later in the processing chain (see Section 3.4.4). We assess the degree of erroneous flagging by comparison to ground observations in Sections 3.4.1, 3.4.4 and 3.5.

For comparison with Aerosol Robotic Network (AERONET) station data, SEVIRI data are selected for the 3x3 pixel area centred on the station. In section 3.4.1 where individual SEVIRI bands are considered, the mean value across all these pixels is used; in section 3.5 where dust and cloud flags are considered individually, either must be present in at least one of the pixels for that timestep to be flagged accordingly. For comparison with the Absorbing Aerosol Index (AAI) from the Ozone Monitoring Instrument (OMI) (Section 3.4.1, 3.6), the SEVIRI data are interpolated to a standard 1 x 1 degree grid.

3.3.2. AERONET AOD

Measurements of Aerosol Optical Depth (AOD) are routinely performed and stored by ground-based photometer instruments as part of the AERONET ground network [*Holben et al.* 1998; *Dubovik et al.* 2000]. The only permanent station located within the main dust loading region of the central and western Sahara is Tamanrasset (22.79º N, 5.53º E, altitude 1377m) in the highlands of the Algerian Sahara. Level 1.5 AOD 500 nm data for June, July and August 2006-2010 and June 2011 are used in this study, along with measurements of total column moisture. Level 1.5 data is automatically cloud screened but may not have final calibration applied [*Smirnov et al.* 2000], but is available for an extended time period. We supplement this data with Level 1.5 AOD 500 nm and total column moisture data obtained from Bordj Mokhtar during the Fennec Intensive Observation Period (IOP) in June 2011. Both datasets are binned to a 15-minute timeseries to provide a direct comparison with SEVIRI data (Sections 3.4 and 3.5). Where multiple observations occur within a single 15-minute timestep an average is taken. To screen the data for the effect of non-dust aerosols, only AOD values with an Ångström coefficient value of 0.7 are used. This threshold removes 12 % of values from Tamanrasset and 1.2 % from Bordj Mokhtar.

3.3.3. OMI Absorbing Aerosol Index

The Absorbing Aerosol Index (AAI) from the Ozone Monitoring Instrument (OMI) is a dimensionless index based on measurements in two ultraviolet channels. It has an approximately linear relationship to column AOD for dust and smoke aerosols [*Torres et al.* 2007]. AAI cannot distinguish between dust and other absorbing aerosols. However the former dominates in summer months over the central and western Sahara and AAI

has been used widely as a proxy for dust in past research [e.g. *Engelstaedter and Washington*, 2007]. AAI is sensitive to the vertical distribution of dust, and may not be able to detect dust near the surface below 1.5 km [*Herman and Celarier*, 1997; *Torres et al.* 2002]. This, combined with the early-afternoon sampling time of the instrument, leads to a discrepancy between the source locations identified using OMI AAI and SEVIRI data [*Schepanski et al.* 2007]. Therefore, we only use the 13:30 UTC SEVIRI timeslot, interpolated to the AAI grid, for comparison between AAI and SEVIRI data (Sections 3.4 and 3.6). Daily Level 3 OMI AAI data for June – August 2005 – 2009 at 1 x 1 degree resolution were retrieved from the NASA GIOVANNI website (http://disc.sci.gsfc.nasa.gov/giovanni).

3.4. SEVIRI Dust Flag (SDF): An automated dust detection technique

The development of an automated dust detection scheme proposed as the central aim in this paper followed these steps: 1) Investigation of the relationship between the SEVIRI bands and surface and satellite derived indicators of dustiness; 2) Exploration of the behaviour of individual SEVIRI bands in dust detection for a large Saharan dust outbreak; 3) Sensitivity tests of fixed thresholds of SEVIRI bands to isolate the dust visible in SEVIRI dust scheme images; 4) Filtering of background surface features that are erroneously detected as dust; 5) Evaluation of the performance of the automated detection scheme against subjective classification based on SEVIRI dust scheme images.

3.4.1. Comparison between SEVIRI bands and other indicators of dustiness

The first step in the development of the automated SEVIRI dust detection scheme is the comparison of SEVIRI bands to other widely used indicators of dustiness in order to gain insight into their behaviour. The first of these is AERONET AOD data from Tamanrasset and Bordj Mokhtar, both for June 2011. Data from two different stations are used to reduce the dependency of the results on one specific set of surface conditions. Only Tamanrasset data for June 2011 are presented because we can reasonably assume that atmospheric conditions are similar for this time period at both sites. This should limit the number of factors that could potentially affect the relationship presented between the SEVIRI bands and AOD data at each site, although it is worth noting that there are some small differences, as is shown by the differing total column moisture measurements (see Figure 3.2, left and centre columns). Restricting our analysis to Tamanrasset data from one month also minimises the possibility that the relationship presented for this station is affected by seasonally or annually varying atmospheric and surface conditions here. The results are very similar if all available Tamanrasset data are considered, however (not shown).

Encouragingly the relationship between individual SEVIRI bands and AOD from the two surface sites are completely consistent with what is expected from theory (Section 3.2), with elevated AOD generally corresponding to elevated BTD (120-108) and lower BTD (108-087) (Figure 3.2). The SEVIRI data have not been cloud screened; therefore it is possible that instances of high AOD which correspond to low BT108 are due to cloud contamination, although *Legrand et al.* [2001] do report temperature depressions in daytime IR images of up to 45.6 K during major dust events. Generally the IR dust signal is strongest for high AOD (> 1.5), although at both stations this is not always the case. Figures 3.2(g) and (h) clearly show the difficulty of using a

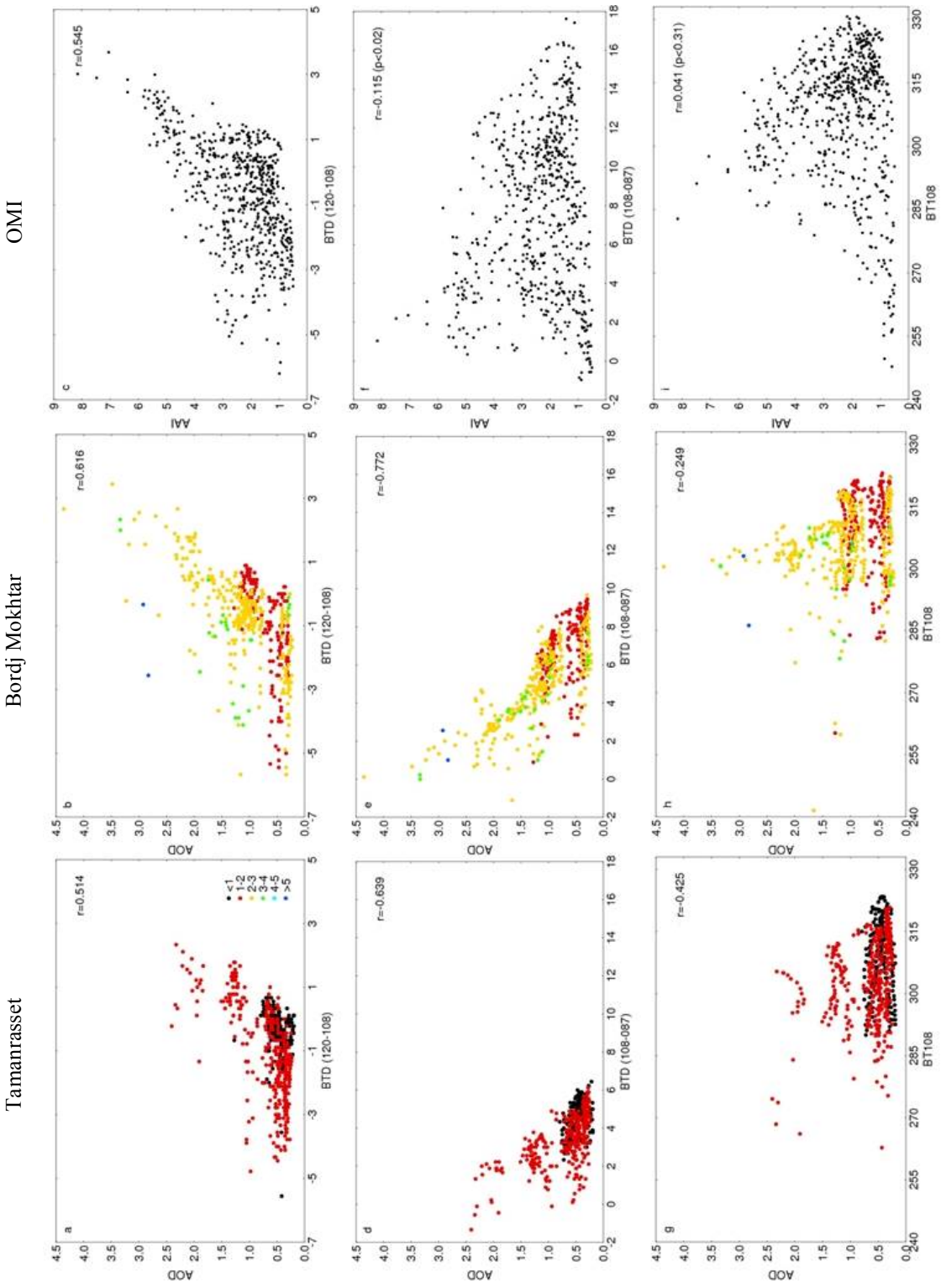

Figure 3.2. Comparison between individual SEVIRI bands and AERONET AOD from Tamanrasset (left column, sample size = 558), AERONET AOD from Bordj Mokhtar (middle column, sample size = 508) and OMI AAI (right column). Top row = BTD (120-108), middle row = BTD (108-087), bottom row = BT108. Shading in comparison with AERONET according to the total column water value (in cm) corresponding to the AOD value used.

single, non-referenced channel to obtain a quantitative measure of dust AOD as the relationship seen with BT108 is much weaker than for the channel differences.

The magnitude of the relationship varies by station, with BTD (120-108) and BTD (108-087) being more strongly correlated with AOD at Bordj Mokhtar than at Tamanrasset. This may be a function of differing surface characteristics, with Tamanrasset being situated in a rocky hamada environment as opposed to Bordj Mokhtar which is located on a sand sheet. To explore this point further we consider surface emissivity for June 2011 (Figure 3.1). Although the wavelength regions are slightly different to those we compare with AOD, we can expect the patterns to be broadly comparable. While the 10.8 and 12.1 μm values are similar at both stations, 8.3 μm is considerably lower at Bordj Mokhtar than at Tamanrasset, due to the silicate reststrahlen band. This emissivity minima weakens as particle size decreases [*Wald et al.,*1998], and consequently we can expect that the BTD (108-087) dust signal will emerge more strongly at Bordj Mokhtar, as is seen in Figure 3.2. Mean AOD is also much higher at Bordj Mokhtar (1.003) than at Tamanrasset (0.610), which may further contribute to the stronger relationship with SEVIRI BTDs as the range of observed AOD values will be higher here.

High values of total column moisture are expected to weaken the IR dust signal (Section 3.2.3), and indeed this is what we see, with the BTD (120-108) signal generally less positive at Bordj Mokhtar for high AOD as total column moisture increases (Figure 3.2b). The total column moisture range is much lower over Tamanrasset, which is likely due both to the altitude of the station (located in the Algerian highlands) and a generally drier climatology (evident in ECMWF reanalyses – not shown).

The second data set for comparison is OMI AAI, which is compared to each SEVIRI channel for a well-defined dust event in the SEVIRI dust scheme images

(2006/06/09 13:30 UTC – Figure 3.2, 3.3a, and 3.3b). It should be noted that due to the sensitivity of the IR method to water vapour, it is possible that the dust scheme image does not represent the full extent of dustiness across the region at this time, especially given the presence of a moist air outbreak from the Intertropical Discontinuity (ITD) around the Algeria-Mali-Niger triple point and in eastern Niger. Qualitatively, the strongest SEVIRI dust signal is associated with AAI above 4. The cloud mask is not applied to the SEVIRI data here because it removes a number of cases of high AOD and AAI due to the erroneous flagging of dust as cloud (see Figure 3.3c).

Despite the different sensitivities of both imagers and the inherent problems with comparing data from two instruments with very different spatial resolutions, there appears to be some correlation between AAI and the SEVIRI channels, with all relationships broadly consistent with those seen from the AERONET sites. However, here we are sampling a much wider range of atmospheric conditions and surface types, and there is a far greater chance of cloud contamination in the measurements, consequently the scatter in the relationships is much larger. Correlation is far lower for BTD (108-087) than with the AERONET sites. This is likely to be because BTD (108-087) has a similar signature in the presence of cloud as dust [*Wald et al.* 1998] and because the land surface emissivity at 8.7 μm is much more variable over desert surfaces than the longer wavelengths considered [*Li et al.* 2007, see also Figure 3.1], which would lead to a much greater degree of variability in BTD (108-087) values across the region.

3.4.2. SEVIRI bands in dusty vs dust free regions

Section 3.4.1 shows that the individual SEVIRI bands do not have a simple linear relationship to other well-known dust data sets. This is because they are influenced by a

range of other variables, including surface emissivity, water vapour and clouds. The aim of this section is to explore how they behave together to produce the distinctive magenta dust signal in dust scheme images.

BTD (108-087) shows a separation between dusty and dust-free areas, as identified in the SEVIRI dust scheme image for 2006/06/09 13:30 UTC (Figure 3.3a), being characterised by lower values in the presence of dust (Figure 3.3d). BTD (120-108) reaches higher values in the dusty area compared to the dust-free area. There is separation based on extreme values but there is also a degree of overlap as the IR dust signal becomes weaker. This is problematic for the application of a fixed threshold on BTD (120-108) to identify dust. BT108 ranges from 295 to 315 K (mean = 306.18 K) in the dusty area compared to 325 – 333 K (mean = 327.78 K) in the dust free area; the blue component of the dust scheme image is therefore saturated for both regions.

It is clear from this case study that of the three components used in SEVIRI dust scheme images, BTD (120-108) and BTD (108-087) show the clearest differences between dusty and dust-free regions in the Sahara. Very high BTD (120-108) and correspondingly low BTD (108-087) are indicative of the presence of dust. There is insufficient information given by BT108 alone to detect the presence of dust. Single band radiances are dependent upon the relative contribution of the ground as well as the overlying atmosphere and are therefore sensitive to a wide range of variables, so additional independent information is required to disentangle the dust signal from the other parameters contributing to the overall signal (see Section 3.2.1).

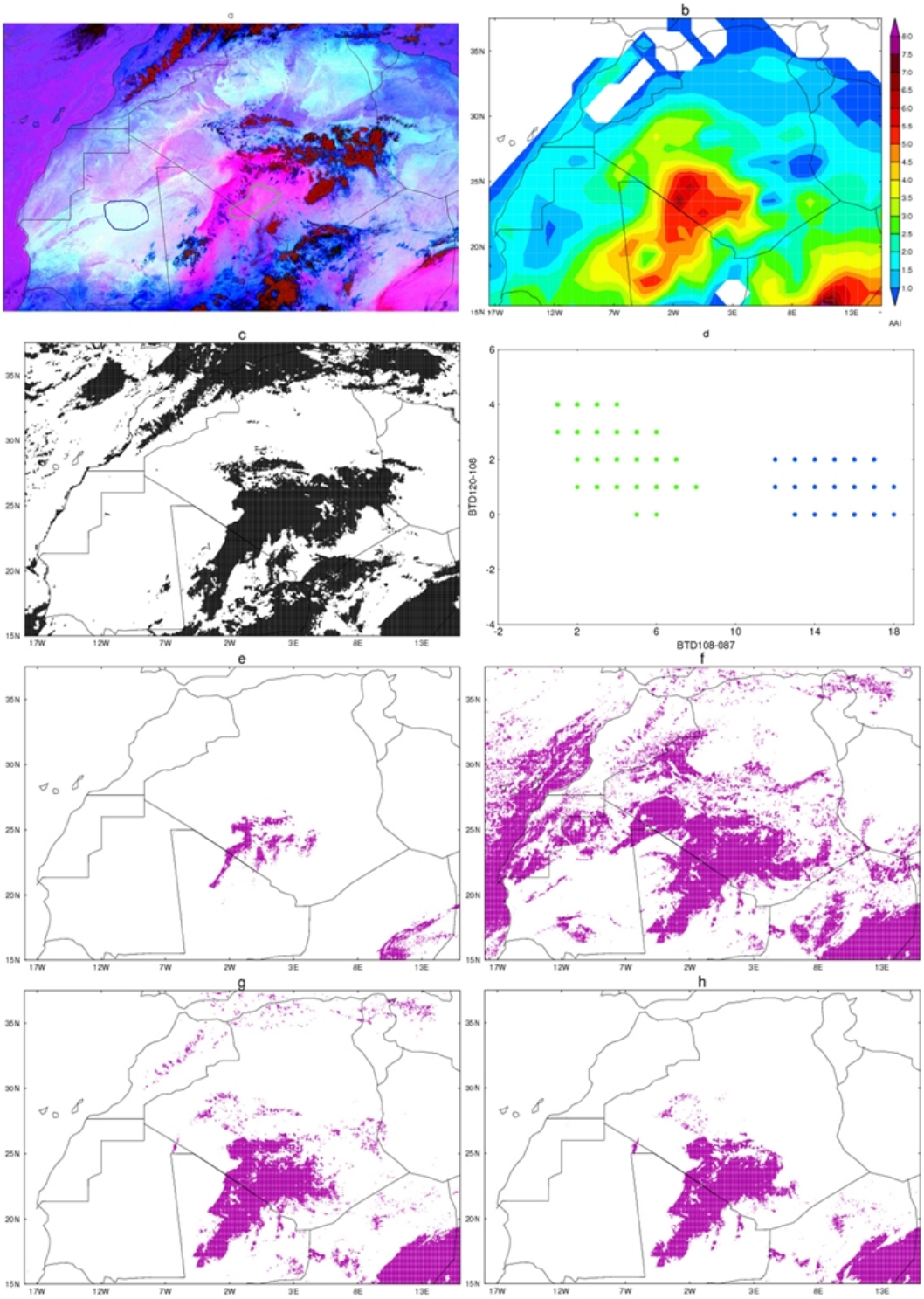

Figure 3.3. (a) SEVIRI dust scheme image for 2006/06/09 13:30 UTC. **(b)** Corresponding OMI AAI field to panel a. **(c)** Corresponding SEVIRI cloud mask field to panel a. **(d)** BTD values for dusty (green) and dust free (blue) pixels in panel a, taken from green and blue outlined regions respectively. **(e)** Distribution of dust detected by applying thresholds of BTD120-108 ≥ 3 and BTD108-087 ≤ 5 to data for panel a. **(f)** As panel d but with thresholds of BTD120-108 ≥ 0 and BTD108-087 ≤ 10. **(g)** As panel e but with additional threshold of $BTD(108\text{-}087)_{anom} \leq -2$ applied. (h) As panel f but with additional threshold of BT108 ≥ 285 applied.

3.4.3 Sensitivity of fixed BTD thresholds

In a comparison of dust detection techniques in the Lake Eyre Basin, using data from the Moderate Resolution Imaging Spectroradiometer (MODIS), *Baddock et al.* [2009] warn that inappropriate thresholds can lead to the foreshortening of dust plumes or the missing of smaller dust outbreaks altogether. This is because the infrared signal of optically thinner dust plumes is dominated by radiation from the surface that is transmitted through the dust layer, whereas for optically thicker plumes emission from the dust layer itself is the main contributor to the signal detected [*Ackerman*, 1997; *Brindley and Russell*, 2009].

The application of restrictive thresholds to BTD (120-108) and BTD (108-087) unambiguously isolates a small proportion of the dust in the dust scheme image, where the dust signal is strongest (Figure 3.3e). However, these thresholds fail to successfully capture the full spatial extent of dust. By applying wider BTD thresholds it is possible to successfully detect a far larger proportion of the dust that is visible in the SEVIRI dust scheme image. However, this also leads to the flagging of surface features and cloud as dust, because their spectral signatures begin to overlap (Figure 3.3f). Section 3.4.4 outlines a strategy to deal with this overlap, which is necessary in order to refine the dust detection process further.

3.4.4. Filtering of background surface features

The surface material of the Sahara is remarkably diverse and includes large sand sheets, rocky hamadas and mountain ranges, all with different surface spectral emissivity signatures. The differences are more pronounced in the 8.7 μm than for the other channels used here [*Li et al.* 2007]. As a result, clear-sky BTD (108-087) is highly

variable spatially, relating to the emissivity of different surface materials (see Figure 3.1). In a study of surface emissivity from the northern Sahara using data obtained from the Advanced Spaceborne Thermal Emission and Reflection Radiometer (ASTER), *Ogawa et al.* [2003] show that emissivities between 8-12 μm from the mountainous areas Hamada de Tinrhert and Tassili-n-Ajjer on the border of Algeria and Libya are higher than those observed from the Grand Erg Oriental in the Saharan lowlands of northeast Algeria. Thus, clear sky BTD (108-087) is lower in areas characterised by rocky surfaces because emissivity at 8.7 μm is not suppressed as it is for sandy surfaces [*Wald et al.* 1998]. It is therefore necessary to distinguish between BTD (108-087) values that have been depressed by the presence of dust and those which are permanently low due to the spectral characteristics of the surface. This poses a problem for the subjective dust detection process of *Schepanski et al.* [2007]. In some cases, the surface appears pinker than surrounding areas, but the pink area is difficult to identify as dust because it is semi-permanently a shade of magenta. It is unclear whether dust is present or not. However, the spectral characteristics are such that without the knowledge that this is a stationary feature, the region would always be interpreted as dust in the automated detection scheme whether dust is present or not. The solution proposed here is the use of a reference image against which a SEVIRI image can be compared. The logic is that the background surface characteristics which cause a region to be generally a pink colour can be controlled for. It is then possible to test whether the area is "anomalously pink".

The reference image is created by calculating the 15-day rolling mean cloud screened BTD (108-087) for each pixel ($\text{BTD (108-087)}_{\text{ref}}$). A 15-day reference period is assumed long enough for each pixel to be dust and cloud free at least once, but short enough that variability in background atmospheric conditions should not significantly affect the surface emissivity signal [*Legrand et al.* 2001]. This assumption is reasonable

for most inland desert areas but may not hold true for desert fringes or coastal areas [*Brindley*, 2007]. The data are cloud screened in this instance because we are interested in the clear-sky BTD signal, and it is therefore necessary to remove the influence of clouds which would serve to decrease the value of BTD $(108\text{-}087)_{ref}$. Because the cloud mask also flags some dust events as cloud, we expect that much of the influence of dust will also be removed. To assess how much dust this removes, we utilise AERONET data from Tamanrasset and Bordj Mokhtar. For both stations we calculate how many observations of a given AOD are removed by application of the SEVIRI cloud mask (Table 3.1). Considering only June 2011, above an AOD of 1.5 every observation is flagged as cloud at both Bordj Mokhtar and Tamanrasset. The percentage of observations of lower AOD removed by cloud screening varies between the two sites, suggesting that the cloud mask is sensitive to surface characteristics up to a certain aerosol loading. Considering all available Tamanrasset data, the proportion of AOD observations above 1.5 removed by cloud screening drops to 87 %. This suggests that the cloud mask may also be sensitive to the specific atmospheric and surface conditions of a given time period considered. Regardless, a proportion of dust below an AOD of 1.5 – 2 is likely to remain following the cloud screening process, and the exact proportion is likely to vary across the study region. This residual dust will serve to lower the value of BTD $(108\text{-}087)_{ref}$.

To calculate the values relative to the reference case, BTD $(108\text{-}087)_{ref}$ is subtracted from BTD(108-087) creating an anomaly field (BTD$(108\text{-}087)_{anom}$). The presence of dust creates a negative anomaly. Adding this test effectively screens out stationary surface features which exhibit "dust-like" spectral behaviour from the SDF. This results in an automated detection scheme that reflects much more closely the full spatial extent of dust in the dust scheme image without any incorrect flagging of surface features (Figure 3.3g).

It is important to note that the technique will be biased towards the detection of larger dust loadings because of the lowering of BTD $(108\text{-}087)_{ref}$ by residual dust that is not removed by the cloud screening process. This means that for a pixel to pass the $BTD(108\text{-}087)_{anom}$ threshold the value of BTD (108-087) must be depressed further than if the reference field did not have dust contamination. Furthermore, it is generally accepted that there is always some level of background dust loading present over the Sahara [*Brooks and Legrand*, 2000; *Brindley and Russell*, 2009], meaning that a certain level of dustiness must be reached before BTD $(108\text{-}087)_{anom}$ is low enough that it can be confidently flagged as dust. It should also be noted that failure of the cloud mask to remove cloud in the creation of the reference image will have the same effect as dust contamination. Assessment of the likelihood of the cloud detection scheme missing cloud is beyond the scope of this study.

3.4.5. Synthesis

The foregoing discussion shows that dust identifiable on analogue SEVIRI images encompasses a mix of RGB values. Apparent extreme and widespread dustiness is readily discernible in the images but uncertainty in identification increases as the infrared dust signal weakens. Following progressive refinement of BTD thresholds from a case study (Sections 3.4.3 and 3.4.4), it is possible to isolate the dust signal in the SEVIRI imagery. However, we note that some cloud features are still left in the resulting dust flag field (Figure 3.3g). Because the blue band of the SEVIRI dust scheme is generally saturated in the presence of dust, BT108 can be used to remove clouds which are higher and colder. This results in a dust flag field which corresponds to the magenta sections of

	Tamanrasset		Tam. (June 2011 only)		Bordj Mokhtar	
AOD Interval	**Total Obs.**	**% removed**	**Total Obs.**	**% removed**	**Total obs.**	**% removed**
< 0.5	6876	9	305	14	144	23
0.5 - 1	2459	31	165	28	132	24
1 - 1.5	517	67	68	99	152	34
1.5 -2	162	87	10	100	87	100
> 2	117	98	10	100	43	100

Table 3.1. Percentage of AOD observations removed by application of the SEVIRI Cloud Mask from Tamanrasset and Bordj Mokhtar.

the dust scheme image, without the erroneous flagging of cloud (Figure 3.3h). We classify dust as being present when:

$BT108 \geq 285$

$BTD\ (120\text{-}108) \geq 0$

$BTD\ (108\text{-}087) \leq 10$

$BTD\ (108\text{-}087)_{anom} \leq -2$

3.4.6. SDF comparison with dust scheme images

The automated dust detection scheme has been developed on the basis of a single case study. In this section the proposed automated SEVIRI dust detection scheme is compared with the subjective interpretation of the SEVIRI imagery by day and night in order to assess the performance and characteristics of the automated scheme over a larger number of cases.

For the June 2010 period, the 03:00 UTC and 12:00 UTC timeslot of each day was visually inspected for the presence of dust. Where dust was present in an image, the areal extent of the dominant plume was manually digitised and all pixels within this outline were flagged as dust. Individual plots could then be compared, and a mean dust presence field for that timestep created from all of the images. Because this is a highly subjective task, this process was completed by two individuals, both with experience of studying SEVIRI dust scheme imagery, and both sets of results are considered.

3.4.6.1. Daytime

Over the course of June 2010, dust was identified in 19 out of 30 dust scheme images for the 12:00 UTC timeslot. For these 19 cases, the level of agreement between both sets of manual dust flags is high at 77%, and in these cases the dust signal is strong, being characterised by low average BTD (108-087) and BT108 and high average BTD (120-108) (Table 3.2 – compare values to Figure 3.2). Disagreement between manual dust flag fields is restricted to the boundaries of dust plumes where the dust signal is less clear and the surface begins to dominate observed radiances, causing difficulty in judging whether dust is present or absent – this is reflected by much higher average BTD (108-087) and BT108 and lower average BTD (120-108) in these areas. SDF is present 79% of the time that a manual dust flag is present, and is therefore about as reliable as another human observer. When both manual dust flags are present the level of agreement with SDF increases to 87%. SDF is present in areas where the magenta colour is weaker and the land surface is visible beneath, which were not manually flagged as dust (Figure 3.4a). 22% of total SDFs in this analysis are without a corresponding manual dust flag, and in these cases BTD120-108 and BTD108-087 are much lower and higher respectively than when both manual dust flags are present.

There is very good agreement between the location of maximum mean dust presence in SDF and both manually detected dust presence maps (Figure 3.5, top row). The overall spatial extent of dust presence is also in good agreement between both methods. There is an isolated area of dust presence on the Atlantic coastline in southern Morocco close to the border with Western Sahara that is only visible in the SDF map. From inspection of dust scheme imagery, this appears to be stratus cloud of marine origin.

	Time (UTC)	Manual Agreement	Manual Disagreement	Manual no SDF	SDF no Manual	SDF & Manual agree
BTD (120-108)	12:00	2.21	0.76	0.98	0.61	2.17
	03:00	1.9	0.87	0.97	0.38	1.76
BTD (108-087)	12:00	2.86	5.73	5.03	5.29	2.84
	03:00	1.43	2.88	3.12	3.19	1.31

Table 3.2. SEVIRI band statistics for different categories of the automated/manual dust flag comparison for all case studies in the 12:00UTC and 03:00UTC timeslots. Values (in K) correspond to the mean BTD/BT averaged across all pixels when: The two manual observers agree; the two manual observers disagree; there is a manual dust flag which is not matched by SDF; there is a SDF which is not matched by a manual dust flag; both manual dust flags and SDF are present.

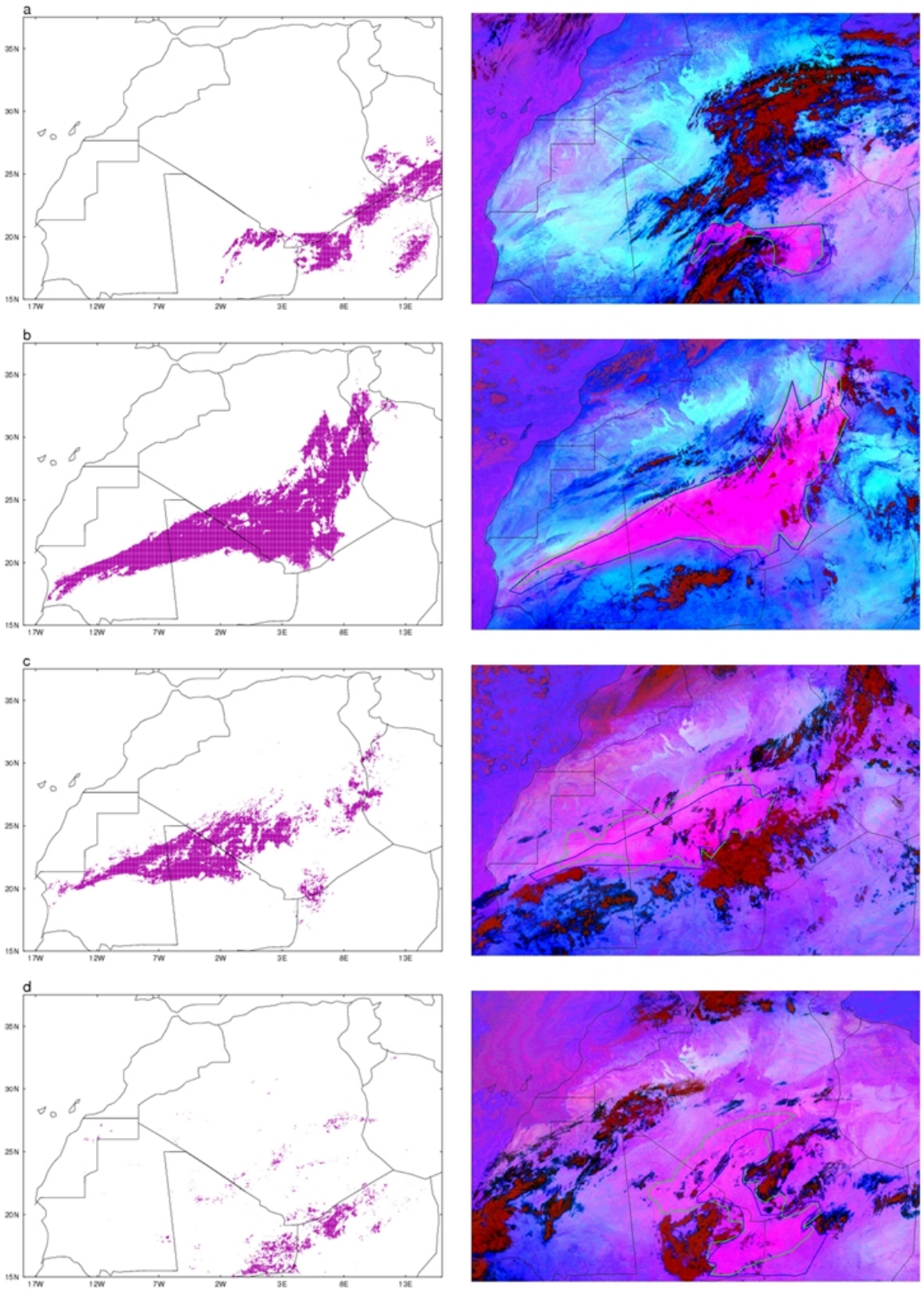

Figure 3.4. Agreement between manual dust flags (blue and green polygons on dust scheme image) and SDF for: **(a)** 2010/06/04 12:00 UTC; **(b)** 2010/06/11 12:00 UTC; **(c)** 2010/06/12 03:00 UTC; **(d)** 2010/06/29 03:00 UTC. Any obvious cloud captured in the manual dust flag field is removed by manual digitisation in the same way that the dust is manually digitised.

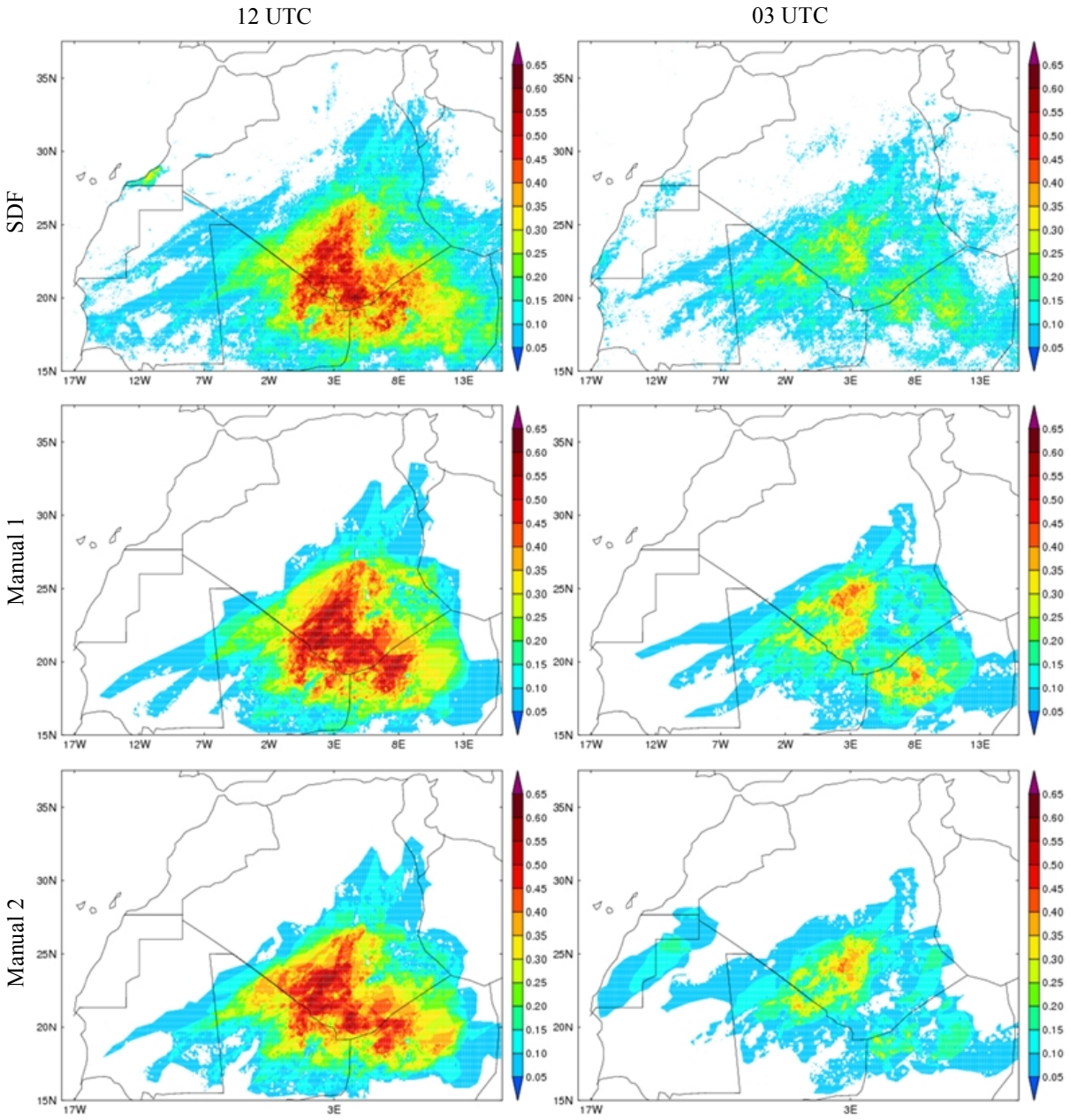

Figure 3.5. Mean dust presence at 12:00 UTC (left column) and 03:00 UTC (right column) in June 2010 according to SDF (top row) and manual detection (centre and bottom rows). Scale is probability of dust flag occurrence across all case studies, whereby 0 corresponds to no dust flag in any case and 1 corresponds to dust flag present in every case.

3.4.6.2. Nighttime

In comparison to the 12:00 UTC timeslot, it is much more difficult to detect dust against the desert background at 03:00 UTC (Figure 3.4c,d). Consequently, only 52% of total manual dust flags are in agreement with each other, and it is clear from Table 3.2 that generally when the manual dust flags are in agreement the dust signal is stronger than when they are in disagreement. In some cases the location of dust presence was completely different in the manual dust flag datasets. SDF and manual dust flags were collocated 55% of the time, so as with the 12:00 UTC timeslot SDF is about as reliable as another human observer. Where both manual dust flags are present, agreement with SDF increases to 73%. SDF occurs without a corresponding manual dust flag 31% of the time, and as with the 12:00 UTC timeslot the dust signal is far weaker in these cases. It is noticeable from Table 3.2 that the magnitude of the dust impact on the SEVIRI bands is lower at 03:00 UTC than 12:00 UTC. This is discussed in Section 3.4.6.3.

As with the daytime analysis, there is an encouraging degree of similarity in location of maximum mean dust presence and the spatial extent of dust presence between both detection methods (Figure 3.5, bottom row). However, SDF seems to underestimate dust presence, compared to when it is detected manually, although this could be a result of the manual detections incorrectly flagging dust. Dust presence is detected on the border between northern Mauritania and Western Sahara in one of the manual detection fields, which is not reflected in SDF nor the other manual field. From the visual inspection of sequences of dust scheme imagery around the periods in question, it is unclear whether the signal here is due to the presence of dust or is a function of surface emissivities. Either way, the signal is relatively weak compared to the more obvious dust plumes detected elsewhere, not satisfying the criteria for SDF.

3.4.6.3. Diurnal cycle

It is clear that there is more uncertainty about the presence of dust at 03:00 UTC than at 12:00 UTC. SDF has some success in identifying the presence of dust at 03:00 UTC, but in some cases the field is not as spatially extensive or coherent as dust scheme images suggest it should be (e.g. Figure 3.4d). Although the thresholds are tuned using a daytime case study, the detection scheme cannot be improved by applying less restrictive thresholds without increased flagging of areas in which it is unclear whether dust is present or not (Figure 3.6). Instead, the uncertainty is because much of the surface tends towards magenta in nighttime dust scheme imagery. Under pristine sky conditions, BTD (120-108) is higher and BTD (108-087) is lower at nighttime than during daytime hours (Figure 3.7). Nighttime pristine sky spectral characteristics are therefore similar to dust spectral characteristics. Furthermore, dust effects on brightness temperatures are reduced at nighttime due to a combination of factors, such as subsidence of the dust layer induced by surface cooling and a lower lapse rate (both of which cause a decrease in thermal contrast with the surface) [e.g. *Legrand et al.* 1988; *King et al.* 1999; *Klüser and Schepanski,* 2009]. Therefore, in general, over a desert surface, daytime surface temperatures and lapse rates combine to allow easier detection of a dust layer, assuming the dust layer characteristics themselves remain unchanged (i.e. optical thickness, height, and mineralogy), compared to the situation at night. Thus it is likely that SDF will only be reliable at nighttime in the presence of dust with a strong IR signal, otherwise the BTD $(108\text{-}087)_{anom}$ threshold may not be exceeded and the pixel may not be flagged as dust (compare Figure 3.4c and d).

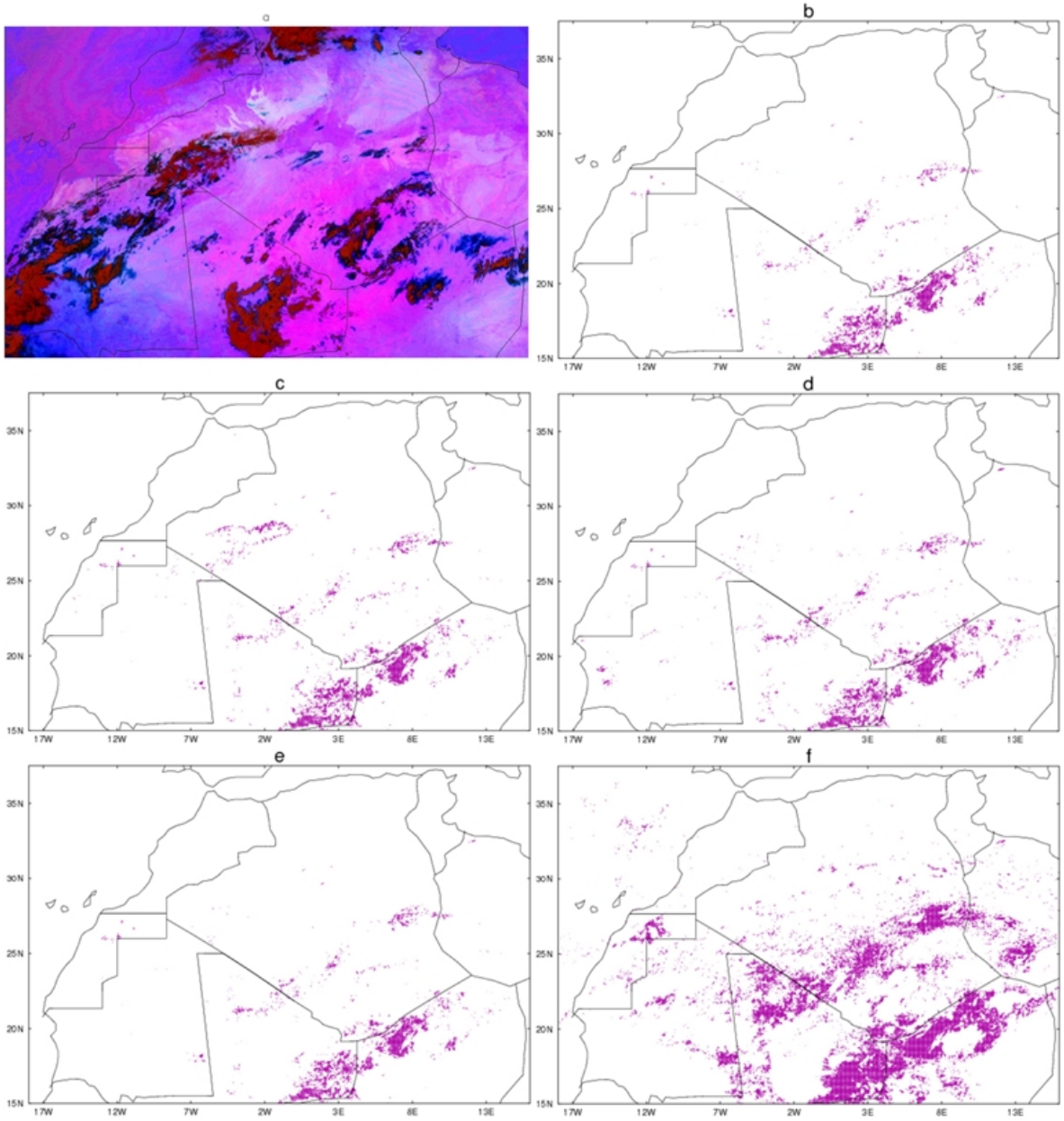

Figure 3.6. (a) SEVIRI dust scheme image for 2010/06/29 03:00 UTC. **(b)** Corresponding SDF field to panel a. **(c)** As panel b but with BT108 threshold relaxed to BT108 ≥ 270. **(d)** As panel b but with BTD120-108 threshold relaxed to BTD120-108 ≥ -1 **(e)** As panel b but with BTD108-087 threshold relaxed to BTD108-087 ≤ 15 **(f)** As panel b but with $BTD(108\text{-}087)_{anom}$ threshold relaxed to $BTD(108\text{-}087)_{anom} \leq -1$

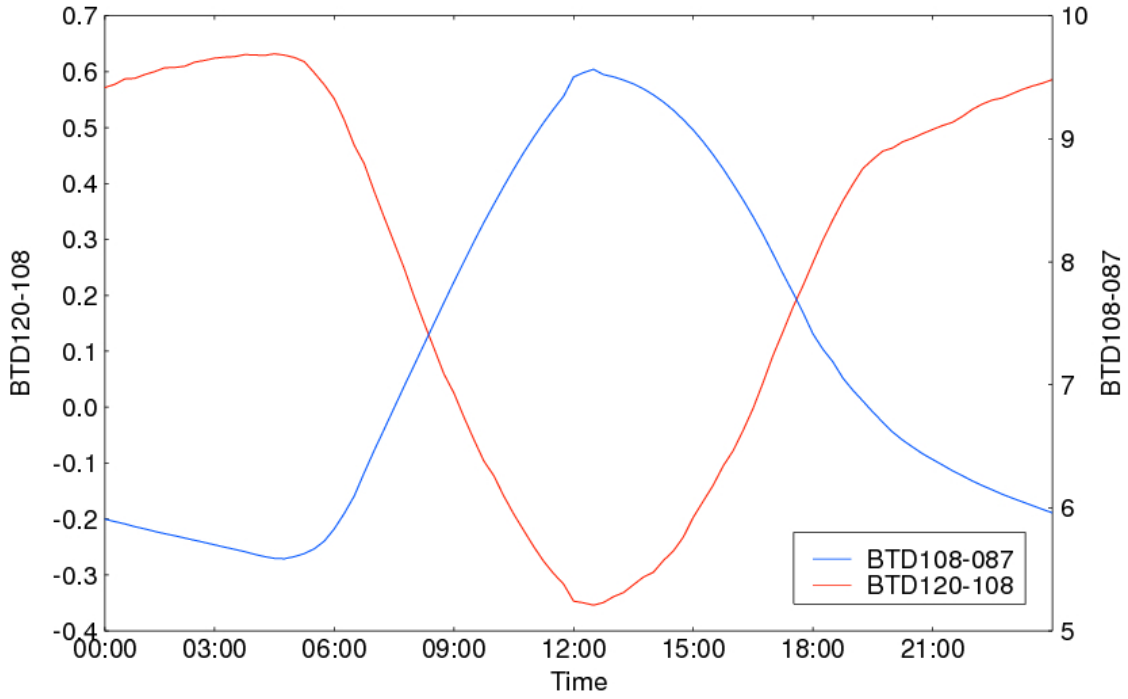

Figure 3.7. Diurnal cycle of clear sky SEVIRI BTD bands averaged over all land pixels for the 15-day period 02 – 16 June 2006. Note that these values may contain some dust contamination – see discussion in Section 3.4.4.

3.5. SDF comparison with AERONET AOD

SDF and Cloud Flag data are taken for every timestep between 05:00 UTC and 18:00 UTC and compared to every AERONET AOD value from Tamanrasset for June – August 2006 – 2010 and June 2011, and Bordj Mokhtar for June 2011. AOD is plotted for the following categories of SDF: clear – where neither a SDF or cloud flag are present; cloud present – where a cloud flag is present; and SDF present (Figure 3.8). Note that SDF takes precedence over the cloud flag in situations where both are present, because the cloud flag erroneously flags cases of dustiness as cloud. At Tamanrasset, 85 % of observations in which SDF is present are also flagged as cloudy by the cloud flag and this corresponds to 89 % at Bordj Mokhtar. Of all available AOD observations from Tamanrasset (Bordj Mokhtar), 16 % (39 %) have a corresponding cloud flag. As detailed in Section 4.4, the cloud flag more consistently flags a scene as dusty as AOD increases. A more detailed breakdown of these statistics can be seen in Table 3.3.

It is clear that SDF is successful at capturing dust loadings of high AOD at both sites. When cloud is present dust is undetectable, but SDF also fails to detect elevated AOD if cloud is present in preceding or following timesteps. This is to be expected given that SDF is a threshold-based detection scheme, since the dust signal in the infrared is strongly affected by the presence of atmospheric moisture [e.g. *Chaboureau et al.* 2007]. Mean AOD when SDF is present is 1.52 at Tamanrasset (1.77 at Bordj Mokhtar), compared to 0.63 (0.87) when flagged as cloudy and 0.36 (0.74) for clear sky conditions. The difference of these means is statistically significant based on Mann-Whitney U test ($p < 0.01$). SDF is biased towards dust loadings of higher AOD, with the quartile range at Tamanrasset being between AOD of 1.1 and 1.9 (1.2 and 2.1 at Bordj Mokhtar) when

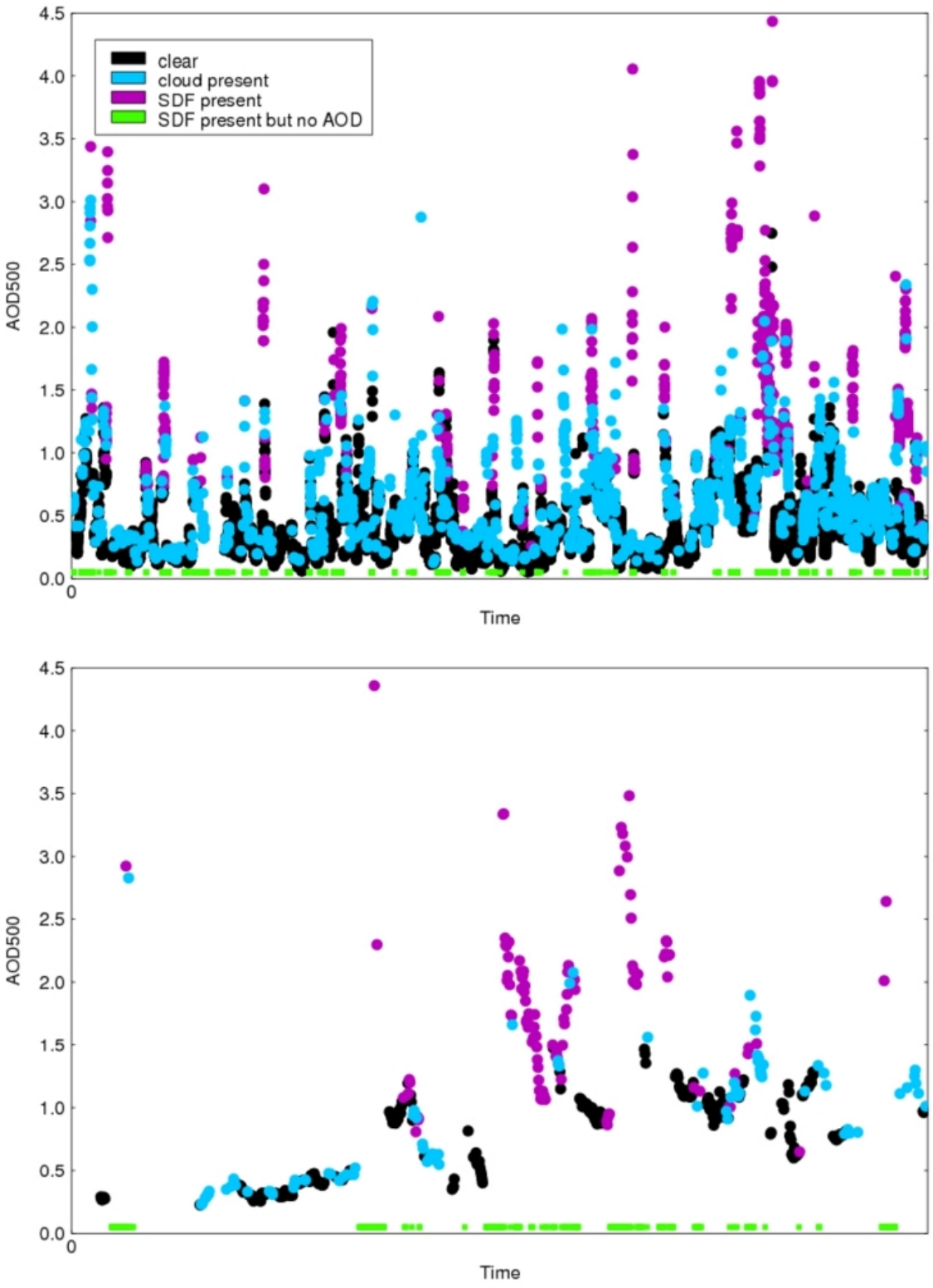

Figure 3.8. AERONET AOD at 500 nm when clear, flagged as cloud, and flagged as dust, for Tamanrasset during June-August 2006-2010 and June 2011 (top) and Bordj Mokhtar during Fennec IOP in June 2011 (bottom). Where SDF is present but there is no corresponding AOD value due to gaps in the AERONET data a false value of 0.05 is given so that this can be visually compared to the AOD values in the surrounding timeseries without giving the impression of a successfully flagged value.

dust is present compared to 0.2 and 0.5 (0.4 – 1) for clear conditions (Figure 3.9). SDF does infrequently capture lower dust loadings however, to an AOD below 0.4. Over 75% of Tamanrasset AOD values classed as clear by SEVIRI are below 0.5 (35 % at Bordj Mokhtar), and only around 2% (30%) of them are greater than 1 (Figure 3.10a). SDF is present at least 75% (85%) of the time that AOD exceeds 1.5, with almost all of the remaining occurrences obscured by the presence of cloud (Figure 3.10b).

These results are promising, especially when it is considered that scale differences between ground-based point measurements and lower-resolution top of atmosphere satellite observations could lead to discrepancies in scene classification [*Brindley and Russell,* 2009]. There are some differences between the statistics obtained for the two stations however. Tamanrasset is not in a core dust producing region as the surrounding surface type is mainly rocky Hamada, whereas Bordj Mokhtar is almost the perfect location to evaluate the peak in SEVIRI dust occurrence in the central and western Sahara. Consequently mean AOD is much higher at Bordj Mokhtar (0.994) than at Tamanrasset (0.464), and SDF is present for far more of the observations (27.6 % compared to 5.2 % respectively). Note that this value for Tamanrasset increases to 16 % if only June 2011 is considered (mean AOD 0.61), therefore it is likely that the values obtained for Bordj Mokhtar correspond to a month of above average levels of dustiness compared to a reference period of 2006-2010. While there is a degree of overlap between observations being flagged as clear or dusty by SEVIRI for an AOD of between 0.5 and 1.5, SDF is extremely reliable at both sites in flagging AOD above 1.5 when cloud is not present. This bias towards events of moderate-heavy dust loading is to be expected for a detection scheme based on fixed thresholds [*Brindley*, 2007].

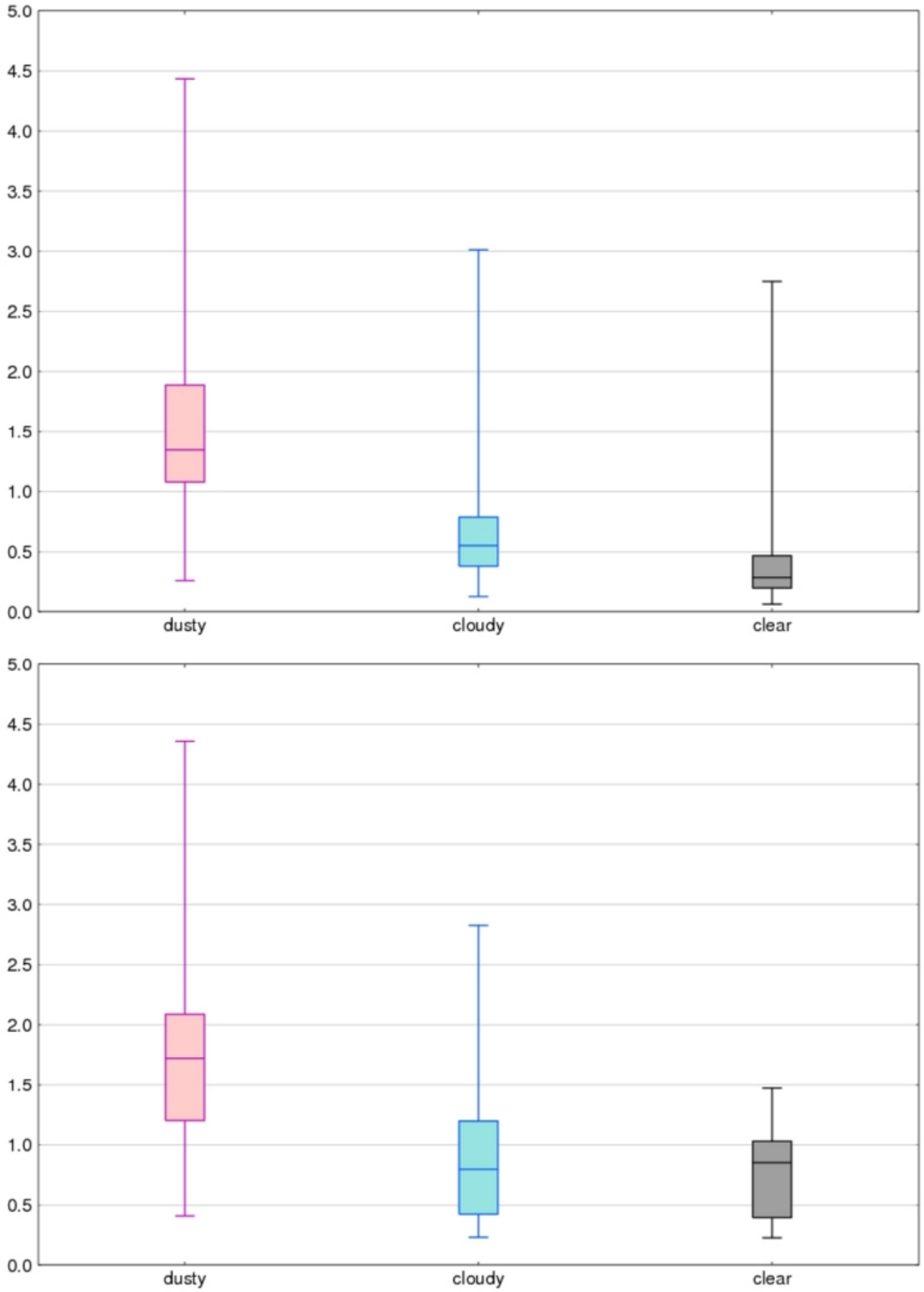

Figure 3.9. Distribution of AERONET AOD values according to category for whole time period at Tamanrasset (top) and Bordj Mokhtar (bottom) Sample sizes are different for each category: dusty = 306 at Tamanrasset (116 at Bordj Mokhtar) values, cloudy = 1115 (93) values, clear = 7127 (299) values.

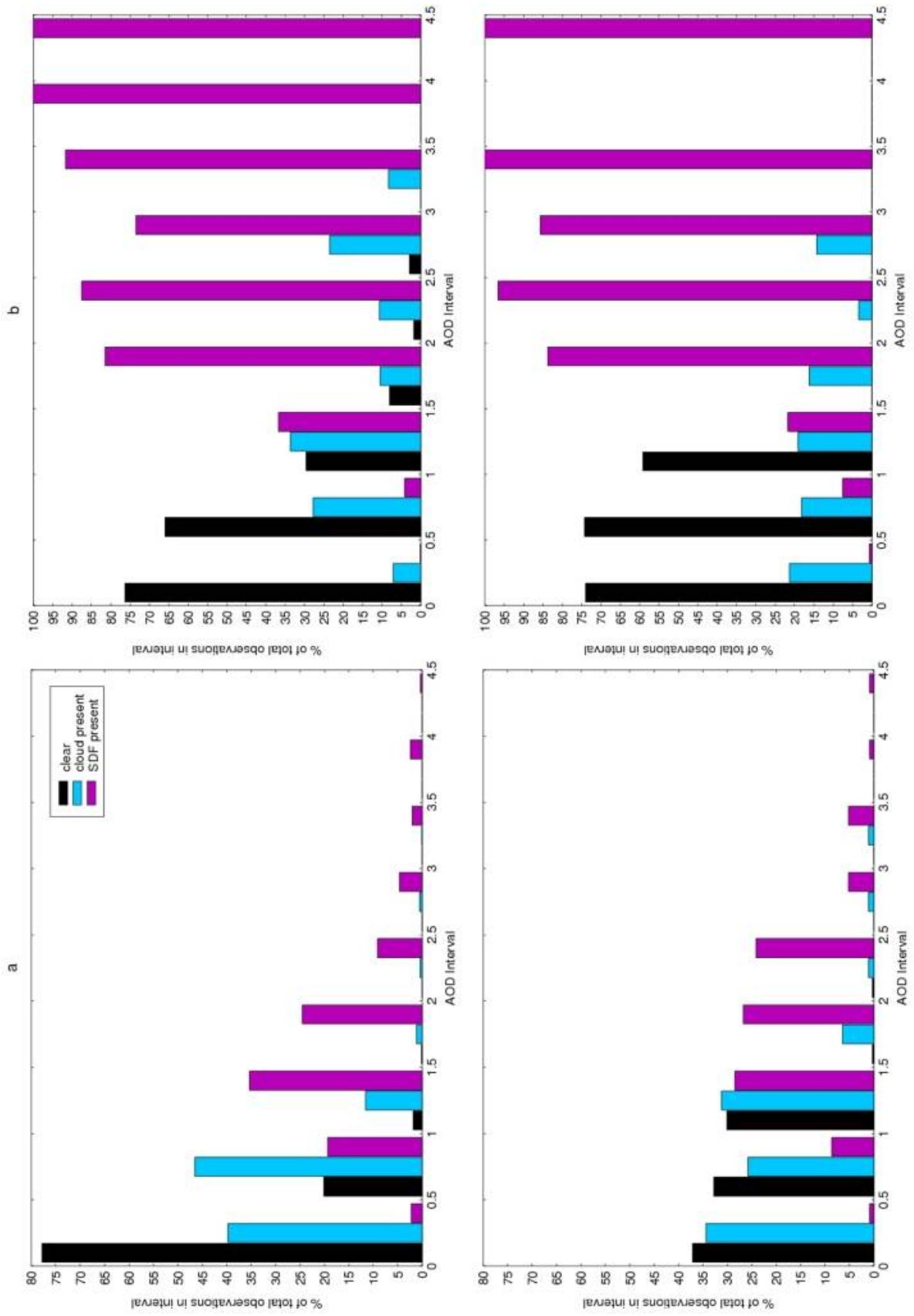

Figure 3.10. (a) Percentage of total observations for each category between different AOD intervals for Tamanrasset (top) and Bordj Mokhtar (bottom). **(b)** Percentage of total observations at different AOD intervals represented by each different category.

Table 3.3 highlights that there is also a temporal aspect to the likelihood of SDF being present for an increased AOD observation. First we focus on Tamanrasset (Table 3.3a): in the early morning hours, SDF is only consistently present for the highest AOD values, but as the surface heats up into the day it is more likely to be present for lower AOD. For example, only 50 % of AOD observations greater than 1 are detected by SDF between 06:00 and 07:00, whereas 93 % are detected between 12:00 – 13:00. By contrast only 2 AOD values greater than 2 are missed over the whole time period. Assuming that nothing else changes through the day with a similar cycle to surface temperature and lapse rate, these results are consistent with the notion that a decreased thermal contrast between the surface and dust layer aloft results in SDF being less reliable in early morning hours before the desert surface has been sufficiently heated. This is unless the dust layer is optically thick (and therefore has a stronger thermal signal), in which case it may still be detected. Consequently, the success rate of SDF declines slightly into the evening hours. These trends hold for Bordj Mokhtar also (Table 3.3b), although it is worth noting that the SDF success rate is lower here for morning hours but does not decline into the evening hours. This may be due to the differing thermal inertia of surface materials surrounding the stations – sand takes longer to heat up in the morning than rock, and cools less slowly into the evening. It is also interesting to note that the likelihood of the cloud mask flagging an event as dusty, or indeed cloudy, displays similar temporal characteristics to SDF at both stations.

a

Time (UTC)	AOD > 0.5				AOD > 1				AOD > 1.5				AOD > 2				AOD > 2.5			
	total	SDF	cloud	both	total	SDF	cloud	both	total	SDF	cloud	both	total	SDF	cloud	both	total	SDF	cloud	both
05:00-06:00	36	4	36	100	1	0	100	0												
06:00-07:00	347	11	33	67	66	50	62	68	18	85	78	82	5	100	100	100				
07:00-08:00	343	17	30	85	95	57	61	91	43	85	84	97	13	92	92	100				
08:00-09:00	405	20	30	81	99	66	63	88	45	93	91	97	18	94	94	100	11	90	91	100
09:00-10:00	431	20	31	78	113	64	65	90	40	91	88	94	26	100	100	100	14	100	100	100
10:00-11:00	393	17	31	85	95	61	69	98	28	96	96	100	17	100	100	100	14	100	100	100
11:00-12:00	315	28	48	88	77	83	86	95	26	100	100	100	9	100	100	100	7	100	100	100
12:00-13:00	281	35	58	98	76	93	95	100	26	100	100	100	9	100	100	100	6	100	100	100
13:00-14:00	243	32	59	93	59	93	95	100	25	100	100	100	7	100	100	100	2	100	100	100
14:00-15:00	190	33	62	100	47	97	98	100	14	100	100	100	7	100	100	100	3	100	100	100
15:00-16:00	114	37	58	76	31	87	84	90	13	100	85	78	5	100	100	100	4	100	100	100
16:00-17:00	111	37	70	89	29	75	86	100	1	100	100	100	1	100	100	100				
17:00-18:00	46	37	72	86	8	75	88	100												

b

Time (UTC)	AOD > 0.5				AOD > 1				AOD > 1.5				AOD > 2			
	total	SDF	cloud	both	total	SDF	cloud	both	total	SDF	cloud	both	total	SDF	cloud	both
05:00-06:00	0															
06:00-07:00	23	27	61	67	14	0	14									
07:00-08:00	27	4	15	100	18	6	17	100	1	100	100	100	1	100	100	100
08:00-09:00	34	16	18	80	23	23	22	80	5	100	100	100	3	100	100	100
09:00-10:00	33	25	27	100	18	44	44	100	5	100	100	100	2	100	100	100
10:00-11:00	38	30	42	89	26	41	46	89	7	100	100	100	2	100	100	100
11:00-12:00	27	32	37	71	15	47	33	71	4	100	100	100	1	100	100	100
12:00-13:00	23	37	48	100	15	54	60	100	8	100	100	100	2	100	100	100
13:00-14:00	40	59	60	84	32	73	69	84	16	100	100	100	8	100	100	100
14:00-15:00	38	60	66	94	27	90	89	94	13	100	100	100	12	100	100	100
15:00-16:00	42	60	64	83	26	100	88	83	14	100	100	100	9	100	100	100
16:00-17:00	24	62	58	85	11	100	100	100	7	100	100	100	3	100	100	100
17:00-18:00	15	91	93	100	7	100	100	100								

Table 3.3. Classification of AOD values according to SEVIRI schemes applied, by hour, at Tamanrasset **(a)** and Bordj Mokhtar **(b)**. Total: number of AOD values above selected threshold; SDF: percentage of cloud-free observations flagged as dust by SDF. Cloud-free observations are total observations *minus* number of observations flagged as cloudy by the cloud mask *plus* those observations flagged as cloudy that have a corresponding SDF; cloud: percentage of total observations flagged as cloudy by the cloud mask; both: percentage of observations flagged as dust by SDF which are also flagged as cloudy by the cloud mask.

3.6. SDF comparison with OMI AAI

We have shown that SDF performs reasonably well at identifying dustiness over two point locations in the central and western Sahara, especially for moderate-heavy outbreaks. The final step in the assessment of the SEVIRI dust automation scheme is to compare the spatial distribution of SDF with that of OMI AAI across the whole of the central and western Sahara for all available data (JJA 2005 – 2009).

3.6.1. Quantification of relationship between AAI and SDF

AAI values are classified according to whether SDF is present or absent for each gridbox. There is clear separation between AAI values when SDF is present or absent (Figure 3.11). The majority of AAI values when SDF is not present are below 2-3, and at AAI of above 2-3 SDF is more frequently present than not. SDF has a success rate in excess of 50% above an AAI of 3 and is present over 80% of the time when AAI exceeds 4 (Table 3.4). The mean AAI in the presence of SDF is 2.89 compared to 1.7 in its absence, and this difference is statistically significant based on the T-test ($p < 0.01$). 75 % of AAI values when SDF is not present fall below 2.25, while almost 75 % in its presence are above this value (Figure 3.12). Different sensitivities of the IR and UV dust detection schemes are likely responsible for SDF missing some occurrences of elevated AAI, and this is discussed in detail in the next section.

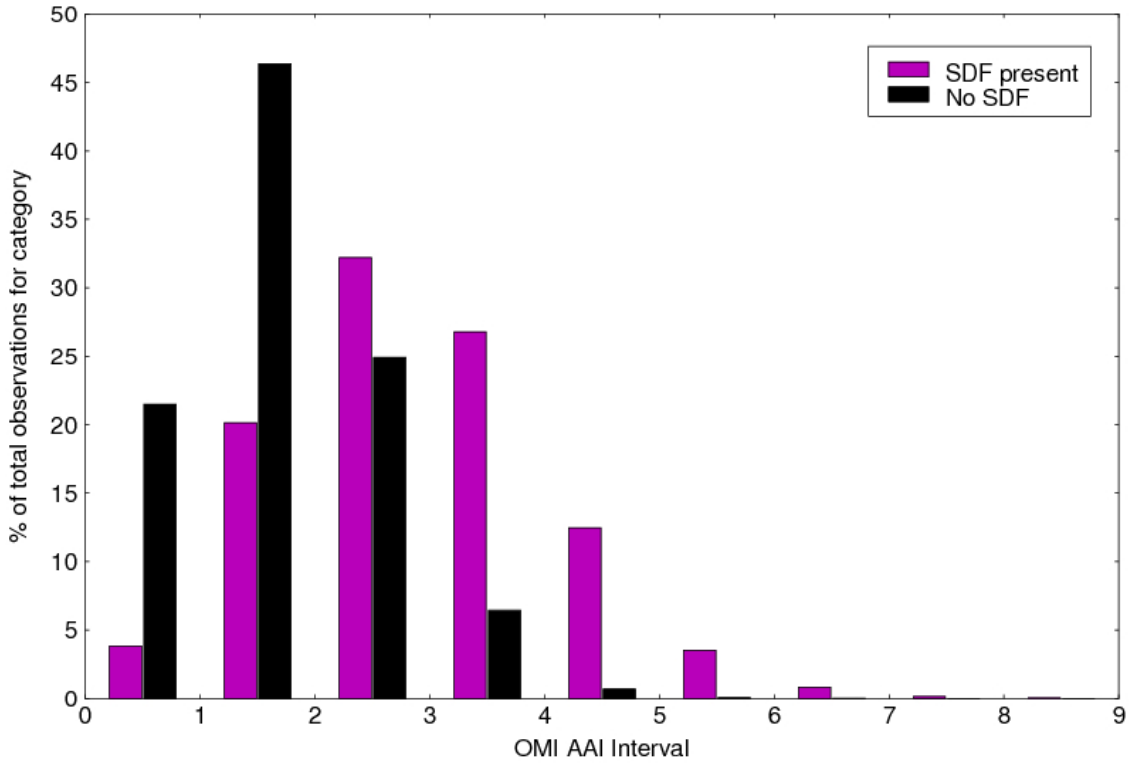

Figure 3.11. Distribution of AAI values in the presence and absence of SDF. Values represent % of AAI values for each category falling within the interval. Sample size = 63542 when SDF is present and 247202 when it is absent.

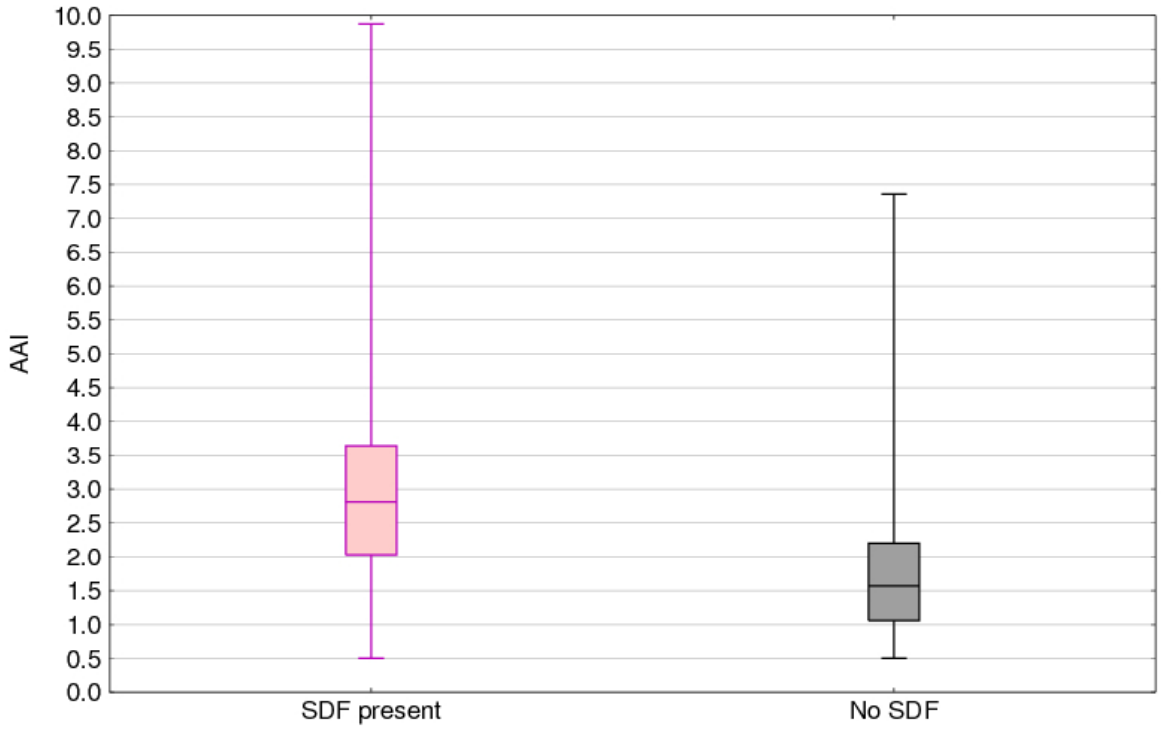

Figure 3.12. Distribution of AAI values in the presence and absence of SDF. Sample size = 63542 when SDF is present and 247202 when it is absent.

AAI Interval	SDF presence (%)
< 1	4
1-2	10
2-3	25
3-4	52
4-5	82
5-6	94
6-7	97
7-8	99
> 8	100

Table 3.4. Percentage of occurrences of AAI that correspond to SDF presence.

3.6.2. Spatial comparison between AAI and SDF

Both OMI AAI and SDF datasets agree that dust is frequently present in southern Algeria along the borders with Mali and Niger, and this is where the highest mean AAI is placed (Figure 3.13). Here, two separate loading centres are present in both datasets: close to the Algeria-Mali-Niger triple point and midway along the Algeria-Mali border. However, the precise locations of these differ between the two datasets, being slightly to the southwest in the AAI data compared to SDF. AAI extends the centre of activity into and across Northern Mali and into Eastern central Mauritania for events between an AAI of 3 and 4 (more pronounced for frequency of AAI > 3 than AAI > 4); this is a pattern that is not replicated by SDF. Generally it would seem that SDF is less successful at matching high AAI in the south of the region towards central Mali, and into Mauritania. As a higher threshold is placed on AAI, spatial agreement with SDF improves.

The spatial distribution of dustiness according to OMI AAI presented here is consistent with previous work using long-term mean TOMS AAI that place a centre of activity on the Mali-Mauritania border (see, for example, Figure 3 of *Engelstaedter et al.* [2006]). *Schepanski et al.* [2007] recognise this discrepancy when comparing mean OMI AAI and dust source activation frequency from SEVIRI for July 2006, and suggest that this is due to the early afternoon sampling time of OMI and its potential height sensitivity, not detecting dust in lower 1.5km of boundary layer which is where freshly emitted dust is likely to lie. However, our analysis uses only the 13:30 UTC SEVIRI timestep and still identifies this discrepancy. A possible explanation could be that, in contrast to ultraviolet AAI, the IR signal is highly sensitive to the presence of water vapour, which could well create problems for dust detection over moister southern parts of the region or where moist oceanic air masses are advected inland

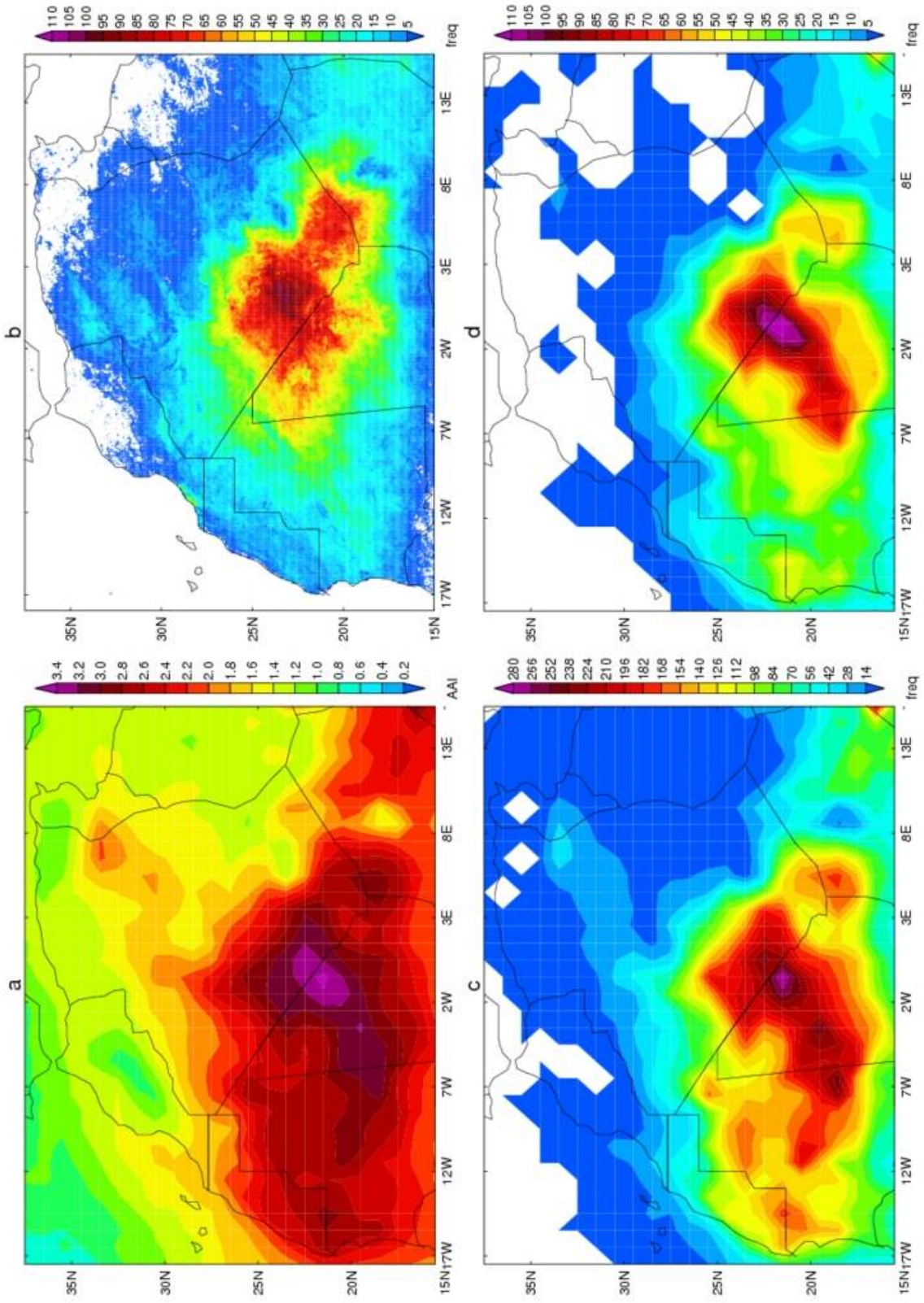

Figure 3.13. (a) Mean AAI. **(b)** Frequency of SDF (from 13:30 UTC timeslot only). **(c)** Frequency of AAI values above 3 **(d)** Frequency of AAI values above 4. All for JJA2005-2009. Total observations for b – d = 460. White areas correspond to no observations in the category.

[e.g. *Legrand et al.* 2001; *Chaboureau et al.* 2007]. Both techniques also have different sensitivities to clouds which will add a further degree of uncertainty to the interpretation of the results. *Pierangelo et al.* [2004] observe a decrease in infrared dust signal with distance from source compared to that at shorter wavelengths (from which AAI is derived), and attribute this to the settling out of coarser mode particles to which the IR method is more sensitive. Combined with the height sensitivity of AAI, we can speculate then that the observed spatial discrepancy may also be, in part, due to the different techniques detecting dust at different stages of transport, especially given the increased agreement as higher thresholds are placed on AAI. It should be noted that the IR method itself may not be able to detect dust that is close to the surface, however.

3.7. Summertime central and western Sahara dustiness

For all available data, SDF is calculated and where present the value of 1 is given. Daily SDF frequency is calculated for each pixel, giving a daily total SDF frequency between 0 (no dust) and 96 (dust present at every timestep). This is converted to a percentage of total timesteps with SDF present. Mean daily SDF frequency is then calculated for every year from 2004 to 2010 (Figure 3.14), and for June, July and August across for 2005 – 2009 for comparison with AAI (Figure 3.15). Because dust cannot be detected when cloud is present, the SEVIRI cloud mask is treated in the same way to aid interpretation of mean SDF frequency fields and inform as to whether patterns are real or a function of increased cloudiness obscuring the presence of dust. Due to the cloud mask flagging some dust loads as cloud, the cloud mask is first screened such that where SDF is present cloud cannot be.

SDF is most frequently present in southern Algeria, spreading along and across the borders with Mali and Niger. This is a consistent pattern that occurs every year. There are two main "hotspots": one centred slightly northeast of the Algeria-Mali-Niger triple point, and one midway along the Algeria-Mali border, centred in southern Algeria on 0^{o} E, 22^{o} N. In 2004 – 2006 and to a lesser degree 2009 and 2010, the area of most frequent SDF presence extends south into northern Mali and is reasonably frequent to the west, stretching into central Mauritania. In 2007 – 2009 the southern Algeria hotspot is much narrower, being more focussed along the Mali border. There is clear inter-annual variability in the intensity of these hotspots, with SDF being less frequently present in 2007 and 2008, and a distinct northward shift in the activity centre occurs through the summer, with northern Mali becoming quieter after June and the southern Algerian loading centre contracting to the east in August. This general trend is reflected in frequency of AAI > 4 and AAI > 3, although AAI > 3 clearly favours a westward expansion of the main dust loading region into Mauritania in July. There is good agreement on a retraction of the overall burden of dust into Southern Algeria for August (Figure 3.15). Encouragingly, increased cloud presence over the region does not appear to relate with reduced SDF frequency; in fact, 2007, the least dusty year appears also to be the year with least cloud extending north into Algeria.

The spatial distribution of SDF is in good agreement with the results of *Schepanski et al.* [2007], although it is important to note SDF is only an indicator of dust *presence*, which incorporates both an emission and transport aspect, whereas they focussed only on dust source activation. Importantly however, previously the frequency of occurrence of elevated TOMS AAI has been used to infer the location of dust source regions [*Prospero et al.* 2002; *Goudie and Middleton,* 2001], so it is reasonable to

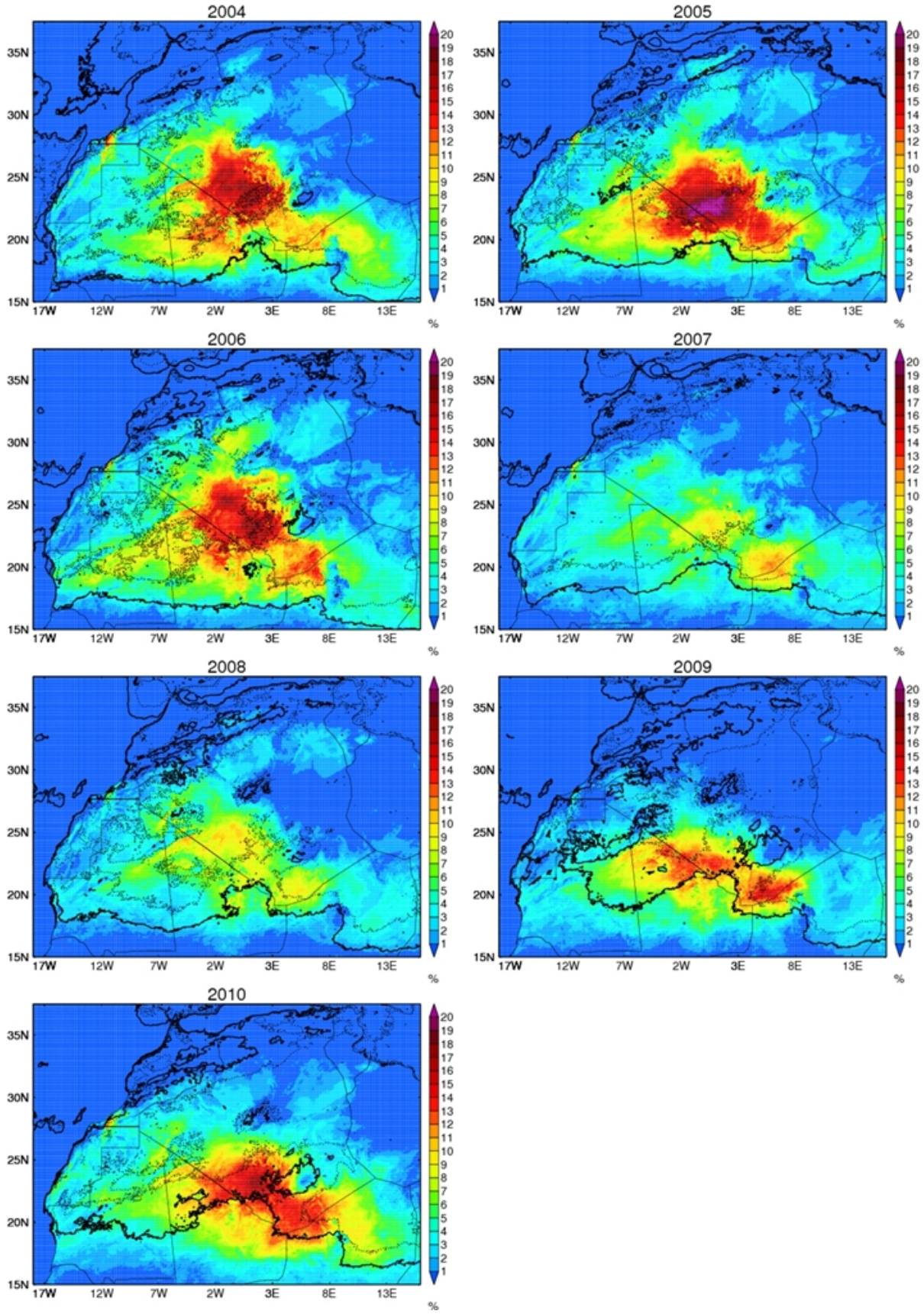

Figure 3.14. Mean summertime daily SDF frequency (shading) and cloud (contours: solid thick contour = 30%, light dotted contour = 20%) frequency, by year.

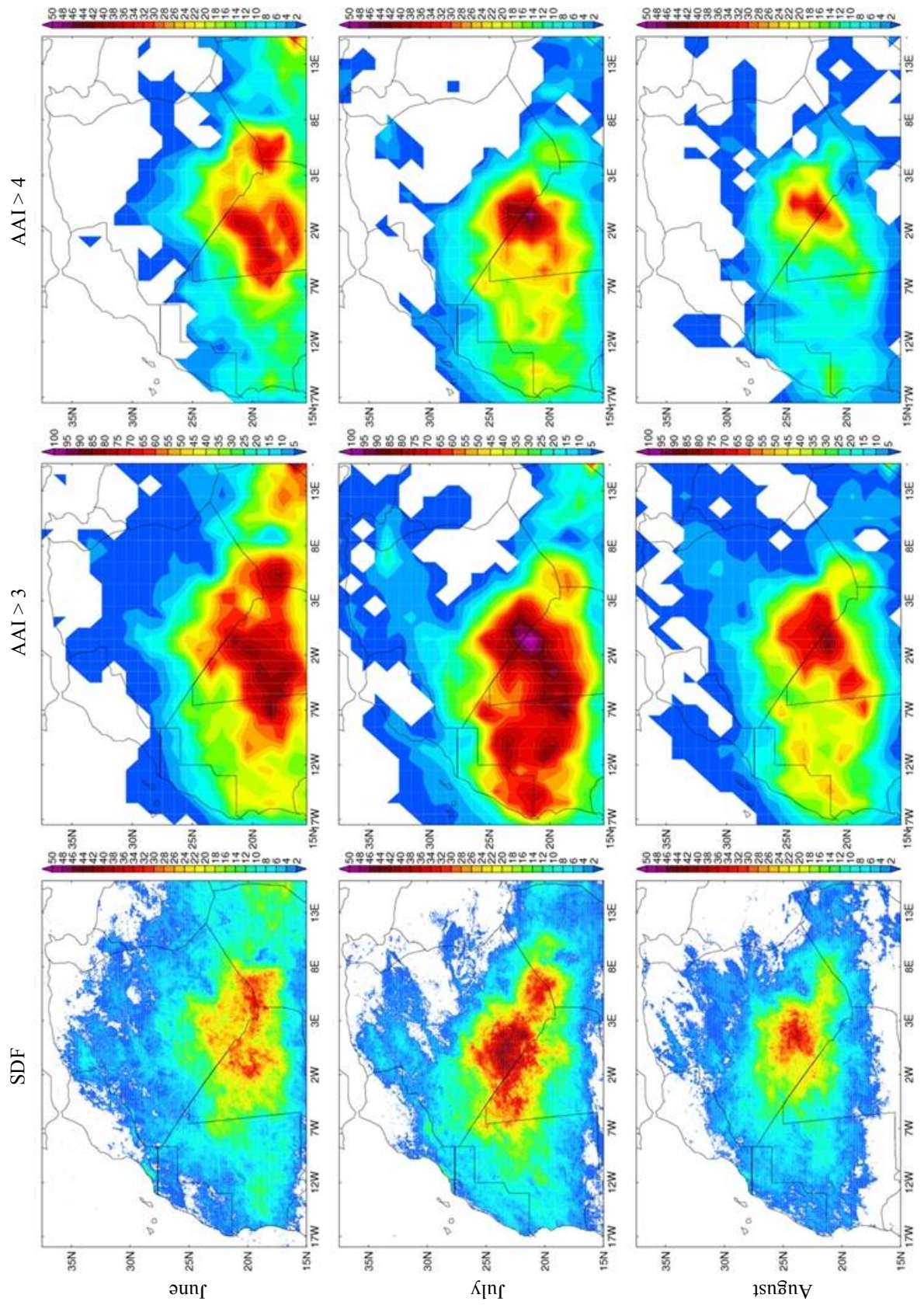

Figure 3.15. Frequency of SDF (left), AAI > 3 (middle), and AAI > 4 (right) for June (top), July (middle), and August (bottom) 2005-2009.

suggest that the most frequently active dust source regions in the central and western Sahara are located in the hotspots identified by mean daily SDF frequency.

3.8. Summary

In this paper we have described a method to automatically detect the presence of dust in SEVIRI imagery. This is based on analysis of how the individual components of SEVIRI dust scheme images behave compared to different dust products. Apparent extreme and widespread dustiness is readily discernible but uncertainty in identification increases as the IR dust signal weakens. Thresholds are placed on the individual components to maximise detection success, and a method has been developed to minimise the misidentification of dust. SDF agrees very well with the subjective detection of dust during daytime hours. At nighttime and in the early morning, however, confidence in SDF is far lower due to a decrease in the spectral contrast between cooler surfaces and the dust layer aloft. We would advise against uncritical application during these hours. However, in the absence of another objective dust product available across the whole of the central and western Sahara at nighttime it may still provide valuable information about the nocturnal dynamics of dust.

SDF is successful at identifying moderate-heavy dust loadings as indicated by Tamanrasset and Bordj Mokhtar AERONET AOD in the absence of clouds, and corresponds well to high OMI AAI. Due to different sensitivities of satellite indicators of dust, there is disagreement between the spatial extent and locations of dust loading centres as indicated by SDF and AAI. Encouragingly, both agree that dust hotspots are located in southern Algeria along its borders with Mali and Niger. Mean SDF frequency shows a distinct monthly cycle through June – August which is evident in the AAI

dataset and agrees with previous studies on Saharan dustiness [e.g. *Engelstaedter and Washington,* 2007]. The identified hotspots demonstrate substantial interannual variability in this region in the summer months, however, and this is the focus of research that is currently underway.

Acknowledgements

We would like to thank Gil Lizcano and Sebastian Engelstaedter for their help in managing and reprojecting the raw SEVIRI data, and Helen Brindley for her useful comments on dust detection. We would also like to thank two anonymous reviewers, whose constructive comments helped to improve an earlier version of the paper.

3.9. References

Ackerman, S. A. (1997), Remote sensing aerosols using satellite infrared observations, *Journal of Geophysical Research, 102*(D14), 17069-17079

Baddock, M. C., J. E. Bullard, and R. G. Bryant (2009), Dust source identification using MODIS: A comparison of techniques applied to the Lake Eyre Basin, Australia, *Remote Sensing of Environment, 113,* 1511-1528, doi:10.1016/j.rse.2009.03.002

Brindley, H. E. (2007), Estimating the top-of-atmosphere longwave radiative forcing due to Saharan dust from satellite observations over a west African surface site, *Atmospheric Science Letters, 8,* 74-79, doi:10.1002/asl.155

Brindley, H. E., and J. E. Russell (2009), An assessment of Saharan dust loading and the corresponding cloud-free longwave direct radiative effect from geostationary satellite observations, *Journal of Geophysical Research, 114,* D23201, doi:10.1029/2008JD011635

Bristow, C. S., K. A. Hudson-Edwards, and A. Chappell (2010), Fertilizing the Amazon and equatorial Atlantic with West African dust, *Geophysical Research Letters, 37*, L14807, doi:10.1029/2010GL043486

Brooks, N., and M. Legrand (2000), Dust variability over northern Africa and rainfall in the Sahel, in McLaren, S. J., and D. Kniverton (eds.), *Linking land surface change to climate change,* Kluwer Academic Publishers, Dordrecht, 1-25

Chaboureau, J.-P., P. Tulet, and C. Mari (2007), Diurnal cycle of dust and cirrus over

West Africa as seen from Meteosat Second Generation satellite and a regional forecast model, *Geophysical Research Letters, 34,* L02822, doi:10.1029/2006GL027771

Darmenov, A., and I. N. Sokolik (2005), Identifying the regional thermal-IR radiative signature of mineral dust with MODIS, *Geophysical Research Letters, 32*, L16803, doi:10.1029/2005GL023092.

Derrien, M. and H. Le Gléau (2005), MSG/SEVIRI cloud mask and type from SAFNWC, *International Journal of Remote Sensing, 21*(10), 4707-4732

Dubovik, O., A. Smirnov, B. N. Holben, M. D. King, Y. J. Kaufman, T. F. Eck, I. Slutsker (2000), Accuracy assessments of aerosol optical properties retrieved from Aerosol Robotic Network (AERONET) Sun and sky radiance measurements, *Journal of Geophysical Research, 105*(D8), 9791-9806, doi:10.1029/2000JD900040

Engelstaedter, S., I. Tegen, and R. Washington (2006), North African dust emissions and transport, *Earth Science Reviews, 79*, 73-100, doi: 10.1016/j.earscirev.2006.06.004

Engelsatedter, S., and R. Washington (2007), Atmospheric controls on the annual cycle of North African dust, *Journal of Geophysical Research, 112,* D03103, doi:10.1029/2006JD007195

Eumetsat (2007), *Cloud detection for MSG – algorithm theoretical basis document,* Darmstadt, Doc. no: EUM/MET/REP/07/0132

Eumetsat (2010), *Cloud mask factsheet,* Darmstadt, Doc. No: EUM/OPS/DOC/09/5164

Flamant, C., J.-P. Chaboureau, D. Parker, C. Taylor, J.-P. Cammas, O. Bock, F. Timouk, and J. Pelon (2007), Airborne observations of the impact of a convective system on the planetary boundary layer thermodynamics and aerosol distribution in the inter-tropical discontinuity region of the West African Monsoon, *Quarterly Journal of the Royal Meteorological Society*, *133*, 1175–1189.

Forster, P., V. Ramaswamy, P. Artaxo, T. Bernsten, R. Betts, D. W. Fahey, J. Haywood, J. Lean, D. C. Lowe, G. Myhre, J. Nganga, G. Prinn, M. Schulz, and R. Van Dorland (2007), Changes in Atmospheric Constituents and in Radiative Forcing, in Solomon, S., D. Qin, Z. Chen, M. Marquis, K. B. Averyt, M. Tignor, and H. L. Miller (eds.), *Climate Change 2007: The Physical Science Basis. Contribution of Working Group 1 to the Fourth Assessment Report of the Intergovernmental Panel on Climate Change,* Cambridge University Press, Cambridge.

Goudie, A. S., and N. J. Middleton (2001), Saharan dust storms: nature and consequences, *Earth Science Reviews, 56,* 179-204

Herman, J. R., and E. A. Celarier (1997), Earth surface reflectivity climatology at 340 – 380 nm from TOMS data, *Journal of Geophysical Research, 102*(D23), 28003-28011

Holben, B. N., T. F. Eck, I. Slutsker, D. Tanré, J. P. Buis, A. Setzer, E. Vermote, J. A. Reagan, Y. J. Kaufman, T. Nakajima, F. Lavenu, I. Janowiak, and A. Smirnov (1998), AERONET – A federated instrument network and data archive for aerosol characterization, *Remote Sensing of Environment, 66,* 1-16, doi:10.1016/S0034-4257(98)00031-5

Hudson, P. K., M. A. Young, P. D. Kleiber, and V. H. Grassian (2008a), Coupled infrared extinction spectra and size distribution measurements for several non-clay components of mineral dust aerosol (quartz, calcite, dolomite), *Atmospheric Environment, 42,* 5991-5999

Hudson, P. K., E. R. Gibson, M. A. Young, P. D. Kleiber, and V. H. Grassian (2008b), Coupled infrared extinction and size distribution measurements for several clay components of mineral dust aerosol, *Journal of Geophysical Research, 113,* D01201, doi:10.1029/2007JD008791

Jickells, T. D., Z. S. An, K. K. Andersen, A. R. Baker, G. Bergametti, N. Brooks, J. J. Cao, P. W. Boyd, R. A. Duce, K. A. Hunter, H. Kawahata, N. Kubilay, J. laRoche, P. S. Liss, N. Mahowald, J. M. Prospero, A. J. Ridgwell, I. Tegen, R. Torres (2005), Global iron connections between desert dust, ocean biogeochemistry, and climate, *Science*, *308*(5718), 67-71, doi:10.1126/science.1105959

Kandler, K., L. Schütz, S. Jäckel, K. Lieke, C. Emmel, D. Müller-Ebert, M. Ebert, D. Scheuvens, A. Schladitz, and B. Šegvić (2011), Ground-based off-line aerosol measurements at Praia, Cape Verde, during the Saharan Mineral Dust Experiment: microphysical properties and mineralogy, *Tellus, 63B*, 459-474

King, M. D., Y. J. Kaufman, D. Tanré, and T. Nakajima (1999), Remote sensing of tropospheric aerosols from space: Past, present, and future, *Bulletins of the American Meteorological Society, 80*(11), 2229-2259

Klüser, L., and K. Schepanski (2009), Remote sensing of mineral dust over land with MSG infrared channels: A new Bitemporal Mineral Dust index, *Remote Sensing of Environment, 113*, 1853-1867

Knippertz, P., and M. C. Todd (2010), The central west Saharan dust hotspot and its relation to African easterly waves and extratropical disturbances, *Journal of Geophysical Research, 115,* doi: 10.1029/2009JD012819

Koren, I., Y. J. Kaufman, R. Washington, M. C. Todd, Y. Rudich, J. V. Martins, and D. Rosenfeld (2006), The Bodélé depression: a single spot in the Sahara that provides most of the mineral dust to the Amazon forest, *Environmental Research Letters, 1,* doi:10.1088/1748-9326/1/1/014005

Legrand, M., M. Desbois, and K. Vovor (1988), Satellite detection of Saharan dust: Optimized imaging during nighttime, *Journal of Climate, 1*, 256-264

Legrand, M., A. Plana-Fattori, and C. N'doumé (2001), Satellite detection of dust using the IR imagery of Meteosat 1. Infrared difference dust index, *Journal of Geophysical Research, 106*(D16), 18251-18274

Lensky, I. M., and D. Rosenfeld (2008), Clouds-aerosols-precipitation satellite analysis tool (CAPSAT), *Atmospheric Chemistry and Physics, 8,* 6739-6753

Li, J., P. Zhang, T. J., Schmit, J. Schmetz, and W. P. Menzel (2007), Quantitative monitoring of a Saharan dust event with SEVIRI on Meteosat-8, *International Journal of Remote Sensing, 28*(10), 2181-2186

McFiggans, G., P. Artaxo, U. Baltensperger, H. Coe, M. C. Facchini, G. Feinold, S. Fuzzi, M. Gysel, A. Laaksonen, U. Lohmann, T. F. Mentel, D. M. Murphy, C. D. O'Dowd, J. R. Snider, and E. Weingartner (2006), The effect of physical and chemical aerosol properties on warm cloud droplet activation, *Atmospheric Chemistry and Physics, 6,* 2593-2649

Miller, R. L., and I. Tegen (1998), Climate response to soil dust aerosols, *Journal of Climate, 11,* 3247-3267, doi: 10.1175/1520-0442(1998)011<3247:CRTSDA>2.0.CO;2

Müller, J. (2007), *MSG Level 1.5 image data format description*, EUMETSAT, Darmstadt, Doc. No: EUM/MSG/ICD/105

Ogawa, K., T. Schmugge, and F. Jacob (2003), estimation of land surface window (8 – 12 μm) emissivity from multi-spectral thermal infrared remote sensing – A case study in part of Sahara Desert, *Geophysical Research Letters, 30*(2), 1067, doi:10.1029/2002GL016354

O'Hara, S. L., G. F. S. Wiggs, B. Mamedov, G. Davidson, and R. B. Hubbard (2000), Exposure to airborne dust contaminated with pesticides in the Aral Sea region, *The Lancet, 355*, 627-628

Pierangelo, C., A. Chédin, S. Heilliette, N. Jacquinet-Husson, and R. Armante (2004), Dust altitude and infrared optical depth from AIRS, *Atmospheric Chemistry and Physics Discussions, 4,* 3333-3358

Prospero, J. M., P. Ginoux, O. Torres, S. E. Nicholson, and T. E. Gill (2002), Environmental characterisation of global dust sources of atmospheric soil dust identified with the Nimbus 7 Total Ozone Mapping Spectrometer (TOMS) absorbing aerosol product, *Reviews of Geophysics, 40*(1), 1002, doi:10.1029/2000RG000095

Pye, K. (1987), *Aeolian dust and dust deposits*, Academic Press, London

Rodwell, M. J., and T. N. Palmer (2007), Using numerical weather prediction to assess climate models, *Quarterly Journal of the Royal Meteorological Society, 133,* 129-146, doi:10.1002/qj.23

Schepanski, K., I. Tegen, B. Laurent, B. Heinold, and A. Macke (2007), A new Saharan dust source activation frequency map derived from MSG-SEVIRI IR-channels, *Geophysical Research Letters, 34,* L18803, doi: 10.1029/2007GL030168

Schepanski, K., I. Tegen, M. C. Todd, B. Heinold, G. Bönisch, B. Laurent, and A. Macke (2009), Meteorological processes forcing Saharan dust emission from MSG-SEVIRI observations of subdaily dust source activation and numerical models, *Journal of Geophysical Research, 114,* D10201, doi:10.1029/2008JD010325

Schroedter-Homscheidt, M., A. Drews, and S. Heise (2008), Total water vapour column retrieval from MSG-SEVIRI split window measurements exploiting the daily cycle of land surface temperatures, *Remote Sensing of Environment, 112*, 249-258

Seemann, S., E. Borbas, R. Knuteson, G. Stephenson, and H.-L. Huang (2008), Development of a global land surface emissivity database for application to clear sky sounding retrievals from multi-spectral satellite radiance measurements, *Journal of Applied Meteorology and Climatology,47*, 108–123, 2008.

Shenk, W. E., and Curran, R.J. (1974), The detection of dust storms over land and water with satellite visible and infrared measurements, *Monthly Weather Reviews*, *102*, 830-837

Smirnov, A., B. Holben, T. Eck, O. Dubovik, and I. Slutsker (2000), Cloud screening and quality control algorithms for the AERONET database, *Remote Sensing of Environment, 73,* 337-349, doi.10/1016/S0034-4275(00)00109-7

Sokolik, I. N., O. B. Toon, and R. W. Bergstrom (1998), Modelling the radiative characteristics of airborne mineral aerosols at infrared wavelengths, *Journal of Geophysical Research, 103,* 8813-8826

Torres, O., P. K. Bhartia, J. R. Herman, A. Sinyuk, P. Ginoux and B. Holben (2002), A long-term record of aerosol optical depth from TOMS observations and comparison to AERONET measurements, *Journal of Atmospheric Science, 59*(3), 398-413

Torres, O., A. Tanskanen, B. Veihelmann, C. Ahn, R. Braak, and P. K. Bhartia (2007), Aerosols and surface UV products from Ozone Monitoring Instrument observations: An overview, *Journal of Geophysical Research, 112,* doi:10.1029/2007JD008809

Wald, A. E., Y. J. Kaufman, D. Tanré, and B.-C. Gao (1998), Daytime and nighttime detection of mineral dust over desert using infrared spectral contrast, *Journal of Geophysical Research, 103*(D24), 32307-32313

Washington, R., M. C. Todd, N. J. Middleton, and A. S. Goudie (2003), Dust-storm source areas determined by the Total Ozone Monitoring Spectrometer and surface observations, *Annals of the Association of American Geographers, 93*(2), 297-313

Washington, R., and M.C. Todd (2005), Atmospheric controls on mineral dust emission from the Bodélé Depression, Chad: The role of the low level jet, *Geophysical Research Letters,32,* L17701, doi:10.1029/2005GL023597

Washington, R., M. C. Todd, S. Engelstaedter, S. Mbainayel, and F. Mitchell (2006), Dust and the low-level circulation over the Bodélé Depression, Chad: Observations from BoDEx 2005, *Journal of Geophysical Research*, *111*, D03201, doi:10.1029/2005JD006502

Zhang, P., N-m. Lu, X-q. Hu, C-h. Dong (2006), Identification and physical retrieval of dust storm using three MODIS thermal IR channels, *Global Planet. Change, 52*, 197-206

Chapter 4

A new high-resolution central and western Saharan summer time dust source map from automated satellite dust plume tracking

Ian Ashpole and Richard Washington

Published in *Journal of Geophysical Research*, doi: 10.1002/jgrd.50554

Abstract

In this paper we outline a new objective dust source detection method for the central and western Sahara (CWS), based on the automated tracking of individual dust plumes in data from the Spinning Enhanced Visible and Infrared Imager (SEVIRI), available every 15 minutes at ~0.03^{o} spatial resolution. The method is used to map the origin of summertime dust storms in the CWS for June to August 2004 – 2010. It reveals the sources of these events in unprecedented detail, allowing for the identification of specific, highly active source areas. The study of collocated surface features reveals that many of the dominant sources are likely associated with palaeo-lakes and outwash plains, many in close proximity to the Saharan mountains. Extensive non-source areas are associated with low albedo and elevated terrain, pointing to the mountainous regions of the Sahara. Additionally, sand seas are not identified as important source areas, but their margins sometimes are. The automated tracking method also facilitates analysis of the transport direction of dust plumes from key source regions, and the inference of emission mechanisms. It is found that there are two broad domains within the CWS: one in

southwest Algeria and northwest Mali, characterised primarily by transport towards the southwest and very likely dominated by low-level jets embedded in the northeasterly Harmattan winds; and a second in southern Algeria, northwest Niger and northeast Mali where there is no preferred transport direction and a strong potential association between dust events and deep convection, pointing towards cold pool outflows as the likely deflation mechanism.

4.1. Introduction

Mineral dust is an important component of the Earth system with a wide range of effects on weather and climate [*Klüser and Holzer-Popp*, 2010; *Rodwell and Palmer*, 2007; *Tompkins et al.*, 2005], biogeochemical cycles [*Mahowald et al.*, 2010] and human health [*Kellogg et al.*, 2004]. Knowledge of the specific sources of dust is central to improving the representation of dust in numerical models of weather and climate [*Cakmur et al.*, 2006]. Spatial offsets between model and real dust sources lead to potential errors in dust transport and atmospheric dust loadings. These errors then progress to large radiative and associated dynamical errors [*Rodwell and Palmer*, 2007]. Moreover, the myriad impacts of dust within the Earth system have a strong dependence on particle characteristics such is mineralogy, size and shape [*Durant et al.*, 2009], which, although subject to modification during transport [*Carslaw et al.*, 2010], are a function of the source from which they are derived [*Shao et al.*, 2011].

Satellite data have often been used to identify dust sources due to the unparalleled spatial coverage they offer. The specification of global dust sources estimated from satellite derived datasets such as the Total Ozone Mapping Spectrometer (TOMS) Aerosol Index (AI) [*Prospero et al*., 2002; *Washington et al*., 2003; *Engelstaedter and*

Washington, 2007a] has made demonstrable improvements to modelled dust distributions globally [*Ginoux et al.*, 2001; *Tegen et al.*, 2002]. Source areas derived from Moderate Resolution Imaging Spectroradiometer (MODIS) data have helped to assess the potential anthropogenic footprint of emissions [*Ginoux et al*., 2012], while satellite data has been used in conjunction with a range of other data types (i.e. field surveys) to create a land-surface classification scheme that has enhanced knowledge of preferred sources of dust [*Bullard et al.*, 2011]. Much therefore depends on the fidelity of the identified source regions.

There are constraints to identifying dust sources from satellite data however. Chief among these is that datasets derived from polar orbiting satellites are limited to one observation per satellite per day. These data introduce a spatial bias in source detection in regions where prime dust emissions occur nocturnally or in the early morning, because dust tends to be transported away from the true source by the time it is observed. This is highlighted in a detailed comparison of Saharan dust sources detected from different satellite products [*Schepanski et al.*, 2012], which concludes that high temporal resolution (i.e. multiple observations per day) is key to precisely identifying dust source areas since it can enable the identification of dust close to source before a significant amount of transport can occur. This is especially important in the summertime CWS where at least 50 % of dust emissions are nocturnal, as demonstrated by analysis of field observations [*Marsham et al.*, 2013] and high-resolution model studies [*Heinold et al.*, 2013]. The precision of remotely-sensed dust sources also depends upon the dust detection scheme employed, each with different sensitivities to, among others, dust mineralogy, surface reflectance [*Baddock et al.*, 2009], and atmospheric conditions [*Brindley et al.*, 2012].

Schepanski et al. [2007; 2009; 2012 – herein *Schepanski et al.*] has derived dust source area maps for the Sahara by manual (i.e. by eye) backtracking of dust identified in high-temporal resolution (15-minutes) Spinning Enhanced Visible and Infrared Imager (SEVIRI) dust scheme imagery. The temporal distribution of sources has, in turn, been used to infer dust emission mechanisms across the central Sahara such as low-level jets (LLJs). Incorporation of these maps into emission models as source masks yields improved simulation of dust emission and distribution for case study events [*Cavazos et al.*, 2009], and they have also been used to evaluate modelled dust emissions where source masks are not incorporated [*Johnson et al.*, 2011].

The central aim of this paper builds on the work of *Schepanski et al.* by developing a method to detect automatically and track coherent dust plumes in the SEVIRI data and objectively identify their source regions, utilising as close to possible the full spatial resolution of SEVIRI data of approximately 0.03^{o} x 0.03^{o} (see Section 2). We use this scheme to derive a new, high spatial resolution dust source map for the central and western Sahara (CWS) in the boreal summer, which dominates the Saharan dust burden at this time of the year [*Engelstaedter et al.*, 2006; *Washington et al.*, 2003; *Prospero et al.*, 2002; *Brooks and Legrand*, 2000], for the years 2004-2010. Development of a dust source map for the summertime Saharan dust source is a key aim of the Fennec programme on central Saharan climate (http://fennec.ouce.ox.ac.uk). We argue that this new map is a potential improvement on existing SEVIRI derived dust source maps, which have a 1^{o} x 1^{o} latitude-longitude resolution [*Schepanski et al.*, 2007; 2009; 2012]. A successful automated technique also has the advantage of seamless and reproducible processing of the continual provision of newly derived data from SEVIRI. Adjustments to the scheme can likewise be made retrospectively with relative ease compared with manual processing. We go on to identify potential atmospheric features

associated with dust uplift from key source regions, such as cold pool outflows from deep convection which is known to be important in parts of the CWS [*Marsham et al.*, 2013], based on analysis of the transport direction of dust plumes that originate at these sources and the presence or absence of deep convection close to the source around the first time step of dust plume detection.

The paper is structured as follows: data utilised in the study are described in Section 4.2; in Section 4.3 the dust plume tracking scheme is outlined along with explanations for how source areas, transport direction and potential association with deep convection are derived for tracked dust plumes; Section 4.4 provides detailed case studies of the scheme performance for two different dust events that are representative of the broader population that are tracked; in Section 4.5 the objective source map is presented and compared to a range of ancillary data, including the manual source map of *Schepanski et al.*, in order to verify the patterns presented and to offer clarification of the surface types associated with frequent and infrequently detected source areas, and the intraseasonal cycle in source areas is described; in Section 4.6 we present results concerning the transport pathways and potential association with deep convection of events to originate in key CWS source areas; finally, Section 4.7 contains a summary and conclusions.

4.2. Data

We use the SEVIRI Dust Flag (SDF) dataset [*Ashpole and Washington*, 2012] to provide information on the presence or absence of dust over the central and western Sahara. These data are currently available every 15-minutes, 24 hours a day for June – August 2004 – 2010 on a standard latitude/longitude grid of approximately 0.03 x 0.03 degrees

resolution for the broad CWS domain, which we define in this study as the region encompassing 18° W – 16 ° E, 15 ° – 37.5 ° N. SDF stems from the SEVIRI dust scheme (see e.g. *Lensky and Rosenfeld* [2008] for a description), which is also the basis for the *Schepanski et al.* dust source mapping. SEVIRI has been widely used to provide qualitative information on the location of dust plumes in recent Saharan dust research.

There are several known limitations with the SEVIRI dust scheme that are in turn passed to the SDF data. *Brindley et al.* [2012] demonstrates that even for high values of aerosol optical depth (AOD), this scheme is sensitive to the presence of atmospheric water vapour, the altitude of the dust layer, and the lower-tropospheric lapse rate. Dust detection at nighttime is also difficult due to similarities in the infrared signal of the desert background and dust (see *Ashpole and Washington* [2012] for further details). In areas of weakened dust signal resulting from these limitations, the resulting SDF field contains spatial and temporal inconsistencies and these will then affect the performance of the tracking scheme presented in this paper. Where possible, the algorithm attempts to compensate for these known issues but to do so in all cases is not possible. Dust can also not be detected beneath cloud using SEVIRI. Despite these limitations, SDF is the only such dataset available to fulfil the objectives of this paper due to its 24-hour coverage. Potential consequences of these limitations for source detection are discussed in Section 4.3.2.

A known issue with SDF is the erroneous flagging of dust presence along parts of the coastline of Morocco/Western Sahara, especially at nighttime. This appears to be stratus cloud of marine origin rather than dust, leading to spurious and frequent detection of dust sources in this region when the algorithm described in Section 4.3 is applied. We therefore apply a mask over parts of Western Sahara and the southwest Moroccan coastline to prevent spurious sources from being detected here (the masked area is clearly

highlighted in all relevant Figures). Based on the source regions reported in *Schepanski et al.* [2012] from a range of different satellite indicators of dustiness and source detection methods, this should not affect the results presented in this paper, since the masked region has not previously been considered to be a notable source area. This is verified by comparison with the manual source map of *Schepanski et al.* in Section 4.5.2, to which the mask is not applied. Note that we do not mask out the northeastern part of Western Sahara, the foothills of which are expected to be a source region [*Schepanski et al.*, 2012].

In addition to SDF, we employ the SEVIRI Brightness Temperature at 10.8 μm (BT108) for the detection of deep convection. Data specification and availability is as for SDF. For information on surface elevation and albedo, we use the Shuttle Radar Topography Mission (SRTM) 30 arc-second version 4 digital elevation dataset [*Jarvis et al.*, 2008; *Reuter et al.*, 2007] and the 1-second Moderate Resolution Imaging Spectroradiometer (MODIS) Filled Land Surface Albedo Product [*Moody et al.*, 2005] respectively, both interpolated to the SDF grid.

4.3. Methods

This section outlines the algorithm that has been developed to track dust plumes and how this is used to detect dust sources, determine the transport trajectory of dust plumes, and identify a potential link between their initiation and deep convection.

4.3.1. Automated dust plume tracking algorithm

The dust plume tracking algorithm developed here draws on techniques that have been successfully applied to the tracking of mesoscale convective systems (MCSs) using high temporal resolution satellite data [e.g. *Morel and Senesi*, 2002; *Mathon and Laurent*, 2001; *Williams and Houze*, 1987].

The first step is the detection of discrete dust plumes at each time step (t), which are contiguous SEVIRI dust flags (SDFs) that represent dust plumes. This is achieved by identifying clusters of connected SDFs that exceed an area threshold (*Ath*), which is set as 250 spatially connected SDFs (~ 0.48 x 0.48 degrees). Area thresholding is necessary for two reasons: First, in order for a dust plume to be linked between one time step and the next (15 minutes), its areal propagation must be small compared to its size otherwise it becomes difficult to connect the same dust plume between time steps using the areal overlap method employed here (see below). Second, an inherent problem with temperature thresholding in IR satellite data as applied in creating the SDF dataset, is that incoherent and disconnected shapes readily result when the dust signal is weak (for example, as a result of increased atmospheric water vapour or at nighttime, as explained in Section 4.2) and a set of SDFs are just below the threshold. Without a threshold area, many very small clusters are detected, some of which may only last for a single time step, and most of which are impossible to definitively identify as actual dust plumes by eye in the analogue SEVIRI images. The assumption bound up in the *Ath* application is that larger, more coherent clusters of SDFs will correspond to better-developed dust plumes. The value of *Ath* is somewhat arbitrary but a drawback to the filtering of minor dust plumes is that the lifetime of a tracked dust event is reduced as the SDF cluster ceases to be defined as a dust plume when it reaches the *Ath* limit. This then effectively determines the precision with which the source of any one tracked dust event can be detected (see

section 4.3.2). It also determines a potential error in pinpointing sources, particularly in the case of small source regions as the dust plume may only assume a threshold areal value once downwind of the source. A series of iterative tests demonstrated that the dust source map does not differ notably whether a smaller (100 SDFs) or larger (500 SDFs) *Ath* value is applied. The same dominant source areas appear in each case.

With dust plumes defined using *Ath*, dust plumes in consecutive time steps are then linked using an areal overlap method, which assumes that dust plumes at a later time step correspond to those at an earlier time step given at least a partial overlap in their positions. For a given dust plume at *t+1*, there are several possible cases:

1. The dust plume at *t+1* corresponds with only one dust plume at *t* and is therefore automatically linked across the time steps. This is possible because at *t+1* the position of the dust plume partially overlaps with its previous position at *t*. This is depicted in Figure 4.1. In this case, two dust plumes are identified at each time step but because they remain spatially separated they are easily tracked as discrete events.
2. The dust plume at *t+1* corresponds to multiple independent dust plumes at time *t*. This represents the merging of independent dust plumes into a single, larger dust plume across two time steps. The problem here is identifying from the larger dust plume the smaller contributing dust plumes at earlier time steps. The dust plume at *t+1* is linked to the dust plume at *t* with which there is the greatest degree of spatial overlap. If the greatest degree of spatial overlap is with more than one dust plume at *t*, then the link is created with the largest of these dust plumes. Where a merging of dust plumes occurs, only one dust plume continues to exist at subsequent time steps; the others end. This is depicted in Figure 4.2. In this case it is possible to determine that the green dust plume at *t+5* is the result of the

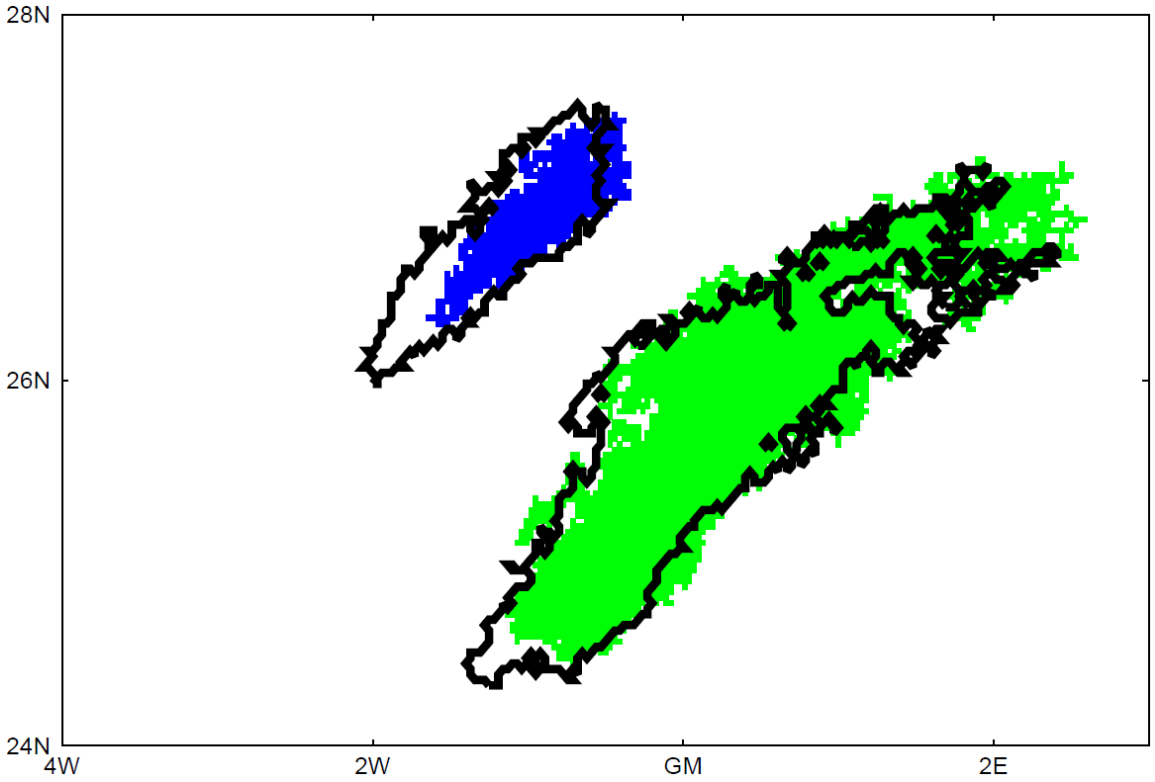

Figure 4.1. Example of a simple tracking case over the partial CWS domain showing two separate dust plumes at two successive time steps. Dust plumes at timestep *t+1* are defined by black contours and dust plumes at timestep *t* by shaded areas.

merging of 4 previously separate dust plumes. Another dust plume is also evident from *t+4* (purple shading) but this is considered independently as it does not merge with the green plume at any of the time steps considered.

3. The dust plume at *t+1* corresponds to no dust plume at *t.* Where this is the case, the algorithm attempts to establish a link between the dust plume and any dust plumes detected at *t–1, t–2,* and *t–3*, according to case 1 or 2 above. This is because analysis of the tracked output revealed a sensitivity of the number of tracked plumes to the value of *Ath.* This can result in the sporadic on/off switching of dust plumes consisting of members close to this value (probably due to the SDF thresholding). Thus, a great degree of overlap may exist between a dust plume at *t+1* and *t–1* but not at *t*. If there is overlap existing between a dust plume at *t+1* and a dust plume/dust plumes in any of *t–1, t–2,* or *t–3*, the link is made according to 1 or 2 above. If there is still no overlap, this is considered to be a new dust plume.

When multiple independent dust plumes at *t+1* overlap with a single dust plume at *t*, all are linked according to condition 1 above. This represents the splitting of the dust plume at *t*. As with merging, this can also occur due to spatial inconsistencies in the SDF field, and it is often the case that a dust plume may temporarily break into multiple smaller plumes before reforming at a later time step. Linking the multiple independently detected dust plumes at *t+1* to the 'parent' dust plume at *t* ensures that they are not considered to be new dust plumes, preventing the erroneous detection of dust sources (see Section 4.3.2). Occasionally a dust plume may break into multiple independent bodies which each follow different transport trajectories. This will have implications for transport trajectory calculations if it is assumed that the dust plume consists only of one independent unit, and is addressed later on in Section 4.6.1.

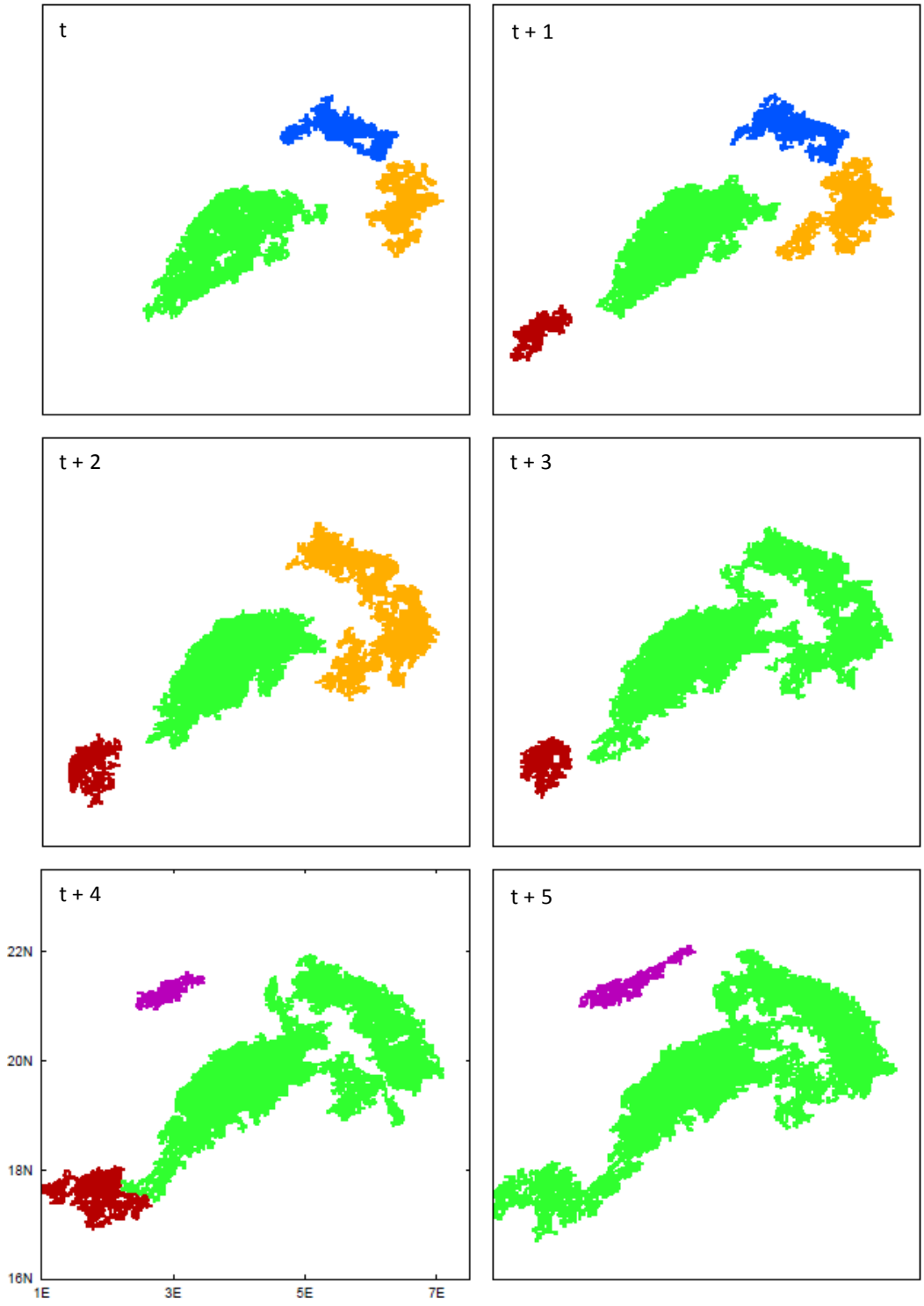

Figure 4.2. Example of dust plumes merging together at successive time steps across the partial CWS domain. Top row: time *t* (left), time *t+1* (right), middle row: time *t+2* (left), time *t+3* (right), bottom row: *t+4* (left), *t+5* (right). Independent dust plumes at a given timestep are represented by unique colours. The same colours link the same dust plumes through the time steps.

The algorithm defined here is applied to the whole SDF data set, with individual years between 2004 and 2010 dealt with independently so that tracking stops at the end of August each year. A sequence of dust plumes through time is termed a 'tracked dust event'. For each tracked dust event we calculate the following: The first time step of detection (*t1*); the centre of gravity (centroid) of the dust plume at every time step, which yields the dust plume position as latitude and longitude; the event duration. The transport trajectory of a tracked dust event is calculated as the angular difference between the centroid of the dust plume at *t1* and at a later time step. The trajectory is assumed to be predominantly a function of the wind direction, although it is possible that topography may impact on dust plume shape, which may affect the centroid location and therefore the calculated transport trajectory.

4.3.2. Source detection

The area covered by a dust plume at *t1* is defined as its source. There are several caveats behind this method of dust source detection. First, it is possible that some dust transport has occurred before the dust satisfies both the SDF and tracking thresholds. Second, visual inspection shows that each tracked dust event does not necessarily correspond to a single, independent dust event, for reasons previously mentioned. Third, dust sources cannot be detected beneath clouds. The implication of these caveats is that the location of a dust plume at *t1* does not necessarily always correspond to a real dust source at the surface. In some cases, the detected source may be downwind of the actual source. All of these constraints are true also of the subjective, manual tracking method of *Schepanski et al*. One potential advantage of the manual tracking is that judgement can be used in the case of uncertainty in interpretation of the dust signal. Despite these limitations, it is

expected that the areas more frequently detected as sources using the scheme presented herein will be more likely to correspond to real source areas at the surface – hence our focus on the source 'hotspots' in Section 4.5.1. Additionally, while *Ath* defines that the maximum precision with which the source of any one tracked dust event can be specified is ~0.48^{o} x 0.48^{o} (compared to 1^{o} x 1^{o} of *Schepanski et al.*), greater detail up to a best achievable resolution of ~0.03^{o} x 0.03^{o} degrees is gleaned by the frequent overlapping of areas detected as a source within this for different tracked dust events. It is assumed that such areas will likely correspond to stationary surface features, while the rest of the area covered by dust plumes at *t1* is more likely to be a result of the spreading of dust by the wind that is driving emission. Both of these assumptions are verified by comparison with detailed information about the surface (see Section 4.5).

It should be borne in mind that a limitation of both the automated method developed here, the subjective method of *Schepanski et al.* and indeed any dust source detection method based on satellite-derived data is that deflation of dust may occur both at the origin of the dust plume as well as along the corridor of the dust plume transport. This can create a bias towards upwind dust sources, since sources that contribute dust to an already developed dust plume will be missed, as also noted by others [e.g. *Bullard et al.,* 2011; *Baddock et al.*, 2009; *Lee et al.*, 2009].

4.3.3. Linking tracked dust event initiation to deep convection

The area proximate to the source of tracked dust events is searched for the presence of deep convection at *t1* and in the preceding two hours. For each tracked dust event, the maximum and minimum longitude and latitude values of the source are expanded by 1^{o} to create a search box surrounding the source. The presence of deep convection in this

area is then detected using the SEVIRI BT108. Deep convection presence is flagged for all SEVIRI pixels with a value below 270^{o} K following *Lavaysse et al.* [2009] and an association is made with the dust event if, as with dust plume detection, contiguous deep convection flags exceeding an *Ath* of 250 flags (~0.48^{o} x 0.48^{o}) is present at *t1* or in the preceding two hours. The close proximity of deep convection at, or shortly prior to *t1* of a tracked dust event does not necessarily imply causality, but it provides evidence that there may be a link, especially when considered with the transport trajectory of the dust plume (Section 4.6.2).

4.4. Demonstration of tracking performance

In this section we assess the ability of the tracking scheme outlined in Section 4.3 to a) adequately track individual dust plumes; b) detect the source of tracked dust events; and c) provide information about the transport direction of the dust plume and its potential association with deep convection. We consider a low-level jet (LLJ) event and a haboob event, which are characteristic of the larger population of tracked dust events included in this study, and evaluate each of the tests set above. In the case studies, images are provided at time steps that best illustrate the performance of the tracking scheme rather than the 15-minute intervals that comprise the actual tracking. This is simply to economise on figures. In addition to this Section, the fidelity of the tracking and source detection scheme is assessed by comparing the automated source map with the manually-derived source map of *Schepanski et al.* and also by evaluation of the surface characteristics of the source regions (both covered in Section 4.5).

4.4.1. Low-Level Jet event

Northeasterly near-surface winds (not shown) lead to dust deflation in central Algeria on the morning of 8th July 2010 (Figure 4.3). The early morning timing and clear sky conditions strongly implicate the LLJ mechanism in driving emission [e.g. *Schepanski et al.*, 2009]. At 05:45 no dust plumes are detected. At 07:45, a coherent dust plume is detected for the first time, centred on 2° E, 27° N (green shading, Figure 4.3). Small clusters of SDFs (pink shading) are also evident around this dust plume, but they are not connected to this and do not pass the tracking thresholds at this time step (i.e. they consist of less than 250 contiguous SDFs). The dust plume is identifiable in all subsequent time steps shown in Figure 4.3 and is therefore adequately tracked by the algorithm as a discrete dust plume.

The area covered by the green dust plume in its first time step of detection (i.e. when it first exceeds 250 SDFs – in this case at 07:45) is considered to be its source. The transport direction of the dust plume is computed as the direction of successive centroids of the plume at each 15-minute timestep (shown as 'X' in Figure 4.3). In this way the dust plume direction can be explicitly calculated rather than inferred from winds such as those of the reanalyses datasets, which may not resolve the mesoscale circulations responsible for the dust emission. The centroid clearly shows a displacement towards the southwest between 07:45 and 13:45, which will yield a transport trajectory in this direction for the dust event. Timestep two of Figure 4.3 shows a 1° x 1° box surrounding the source of the dust plume. Within this box a search is made for deep convection at this time step and in the preceding 2 hours (see Section 4.3.3). In this example no deep convection is detected and deep convection is therefore not thought to be associated with the initiation of the tracked dust event.

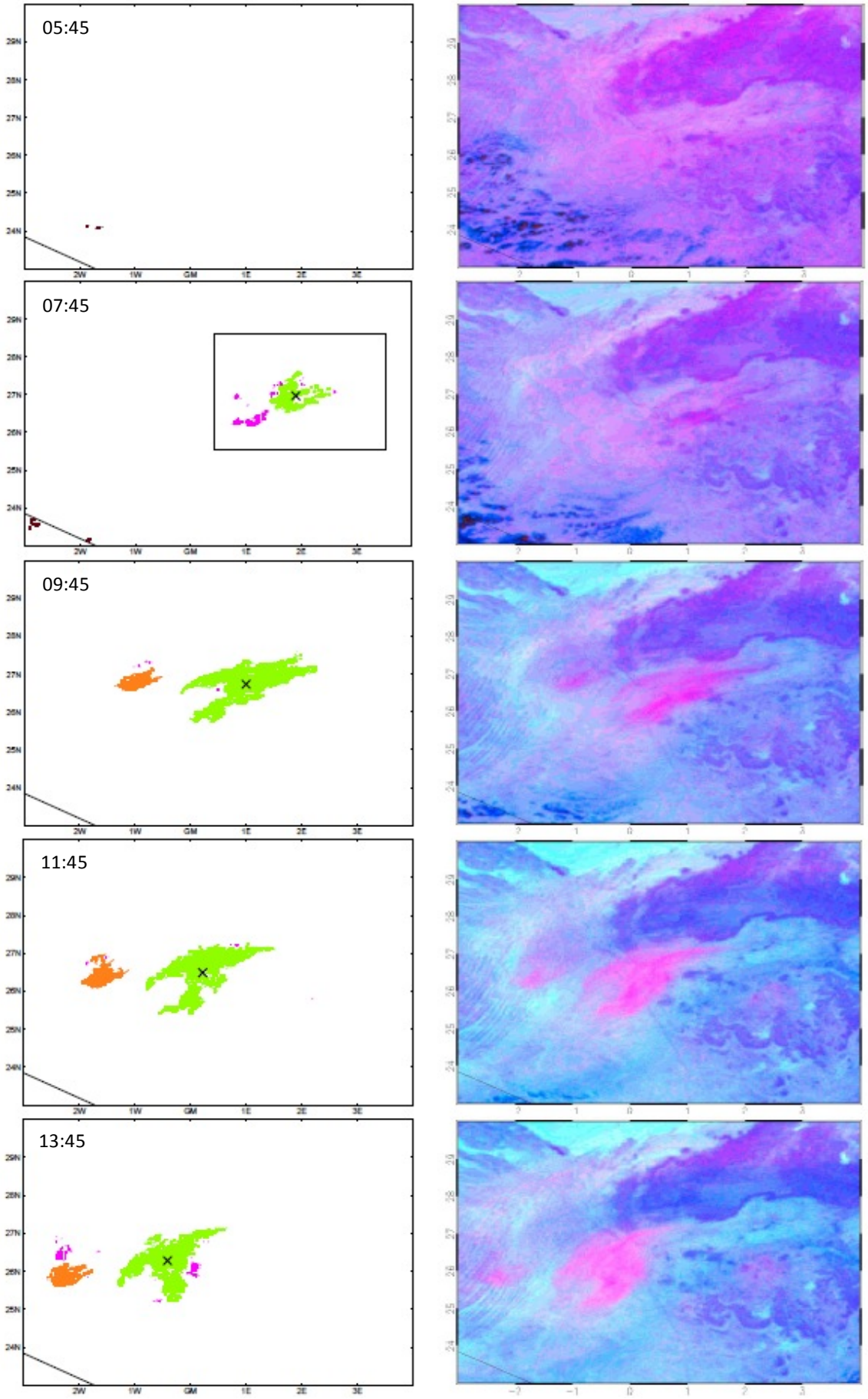
05:45
07:45
09:45
11:45
13:45

Figure 4.3. (previous page) Source detection and tracking example for LLJ case on 8th July 2010, originating in central Algeria. **Top row** = 05:45, **2nd row** = 07:45 (first timestep of detection), **3rd row** = 09:45, **4th row** = 11:45, **5th row** = 13:45 (times in UTC). **Left column:** green = case study dust plume, orange = other tracked dust plumes, magenta = SDFs that do not pass tracking criteria, red/brown = deep convection, 'X' = the centroid of the case study dust plume at each time step, outlined region at 07:45 corresponds to area searched for presence of deep convection (see text for details). **Right column:** SEVIRI dust scheme imagery – dust appears pink, deep convective cloud red, highly moist air dark blue, and the desert background can be light blue to purple depending on time of day and surface emissivity.

In Figure 4.3, additional dust plumes are also identifiable. From 09:45 onwards an additional plume (orange shading) is treated as an independent dust event by the tracking algorithm for all subsequent time steps. A new source will therefore be detected. It is also clear that there are some small clusters of SDFs in all time steps that are not defined as dust plumes because they fail to reach the threshold value of 250 SDFs. Some of these clusters merge with the green dust plume as it grows and is transported in successive time steps. It is unclear by comparison with the SEVIRI dust scheme imagery whether these SDFs correspond to independent dust plumes (i.e. represent independent emission events) or are part of the green dust plume that are not connected as a result of spatial inconsistencies in the SDF field from the thresholding process in dust detection (causes for this have previously been outlined). If these are independent dust plumes, their sources will not be detected in the objective tracking algorithm since they do not pass the tracking thresholds for dust plume definition. The sensitivity of the dust source map to this threshold is discussed in Section 4.3.

4.4.2. Haboob event

The haboob event occurred on 11 June 2007 in the Ifoghas Mountains of northeast Mali (Figure 4.4). Cold pool outflow from convective complexes here leads to dust deflation. No dust plumes are detected at 17:30, but at 19:30 a coherent dust plume is detected for the first time (green shading) within the convective outflow. This dust plume is adequately tracked as it propagates towards the northwest with the convective outflow over following hours, this transport direction being reflected by the change in centroid location.

The green area at 19:30 is considered to be the source of the dust plume. Deep convection is clearly flagged (brown shading) and is spatially located within a 1^{o} x 1^{o} box surrounding the source. A link is therefore made between deep convection and the initiation of the tracked dust event. A potential limitation to the detection of dust sources in this case and all haboob cases is that any dust presence beneath the parent deep convection will not be detected. There is currently no high temporal resolution satellite product with the capability to detect dust beneath cloud. It is thus impossible to determine whether the actual source of the dust is beneath the cloud or not.

Dust presence is detected within the convective outflow at 17:30, before the tracking scheme identifies the source. This is because the detected cluster of SDFs does not pass the size threshold to be tracked at this time. When the source is detected at 19:30, there is an additional cluster of untracked SDFs slightly to the northeast, which also appears to be within the convective outflow. 15 minutes later (19:45) this cluster passes the tracking threshold and is detected as a new dust plume (orange shading) that is independent of the green plume because they are not connected. A new source is therefore detected. Incidentally, deep convection will also be detected within a 1^{o} x 1^{o} box surrounding this new source. By 21:30 the new dust plume has merged with the

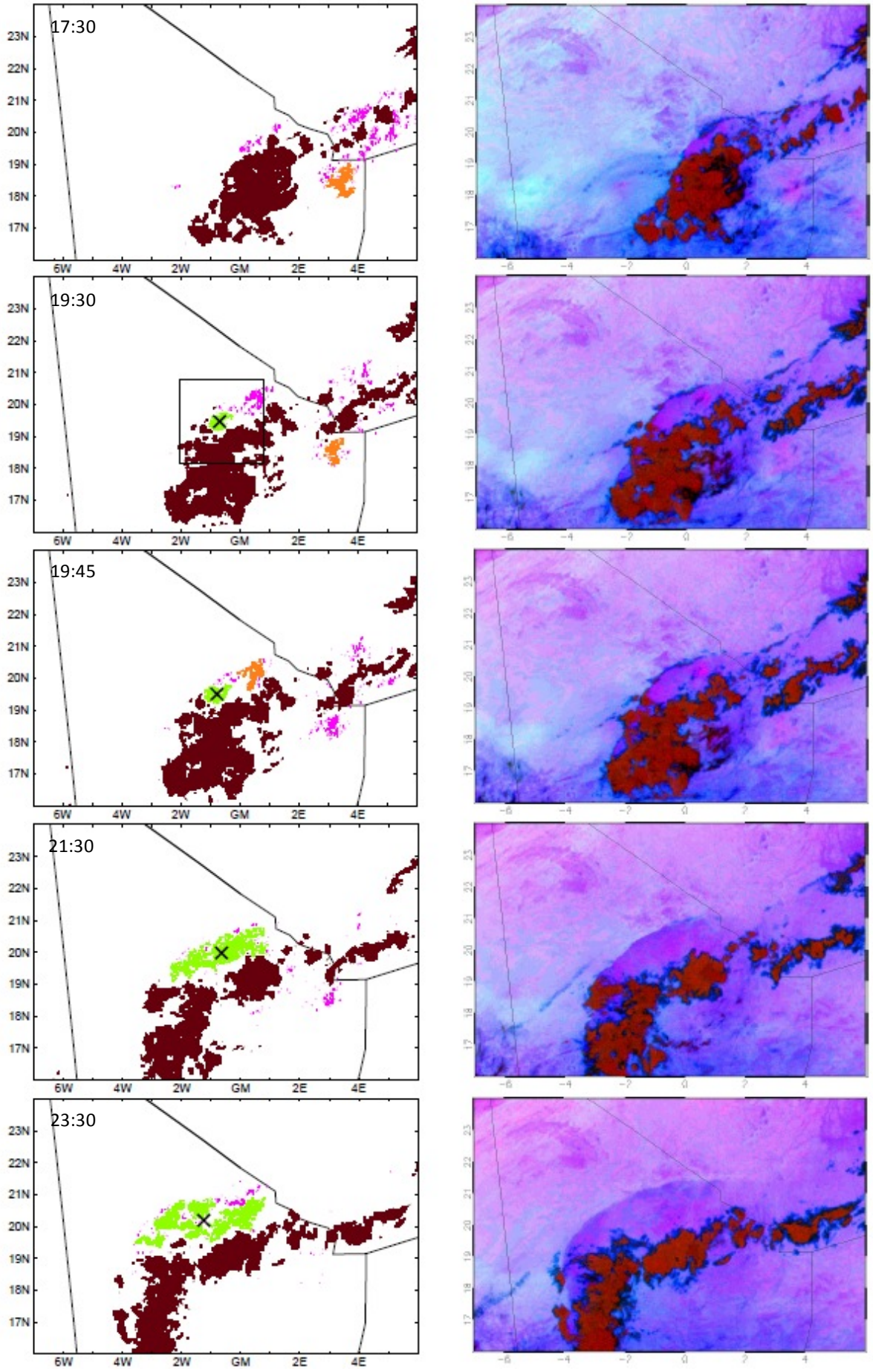
17:30
19:30
19:45
21:30
23:30
23N
22N
21N
20N
19N
18N
17N
6W
4W
2W
GM
2E
4E

4.5. An automated, objective dust source map

To map the CWS dust sources for the June – August period 2004 – 2010 we sum the frequency with which each 0.03^{o} x 0.03^{o} pixel is detected as a dust source (or, more precisely, falls within the area detected as a dust source).

4.5.1. Description and features

The map of dust source frequency is shown in Figure 4.5 at a spatial resolution of 0.03^{o} x 0.03^{o}. The CWS summer time dust sources are evident in unprecedented detail. Given this level of precision, identification of the specific source areas at the surface and their co-location with likely erodibility features is possible for the first time.

The largest concentration of frequently active sources is in southern Algeria, northern Mali and northwest Niger. Overall there are some 15-20 clusters of very active dust sources (>30 frequency count in Figure 4.5), all of which consist of multiple individual sources. Of these, the highest concentration of sources spans the Algeria/Mali border of the Majabat al Koubra ('Big Void'). This part of the CWS features a relatively flat and completely uninhabited sand sheet interspersed with small palaeolakes such as those 30 km west-south-west of Bordj Badji Mokhtar (‘H’ on Figure 4.5). Table 4.1 summarises the most coherent sources and the erodibility features with which they are likely to be associated as inferred from Google Earth and from the IGN 1:200,000 maps of the Sahara. Of these sources, the majority (ten) feature palaeolakes or dry lakes and five feature outwash plains. In the case of three, there is no readily discernible erodibility feature other than featureless reg. Apart from the highlighted sources in Table 4.1, it is also striking that extensive regions of the CWS serve, albeit infrequently, as sources of dust storms. Winds in excess of the thresholds needed to start sediment movement are

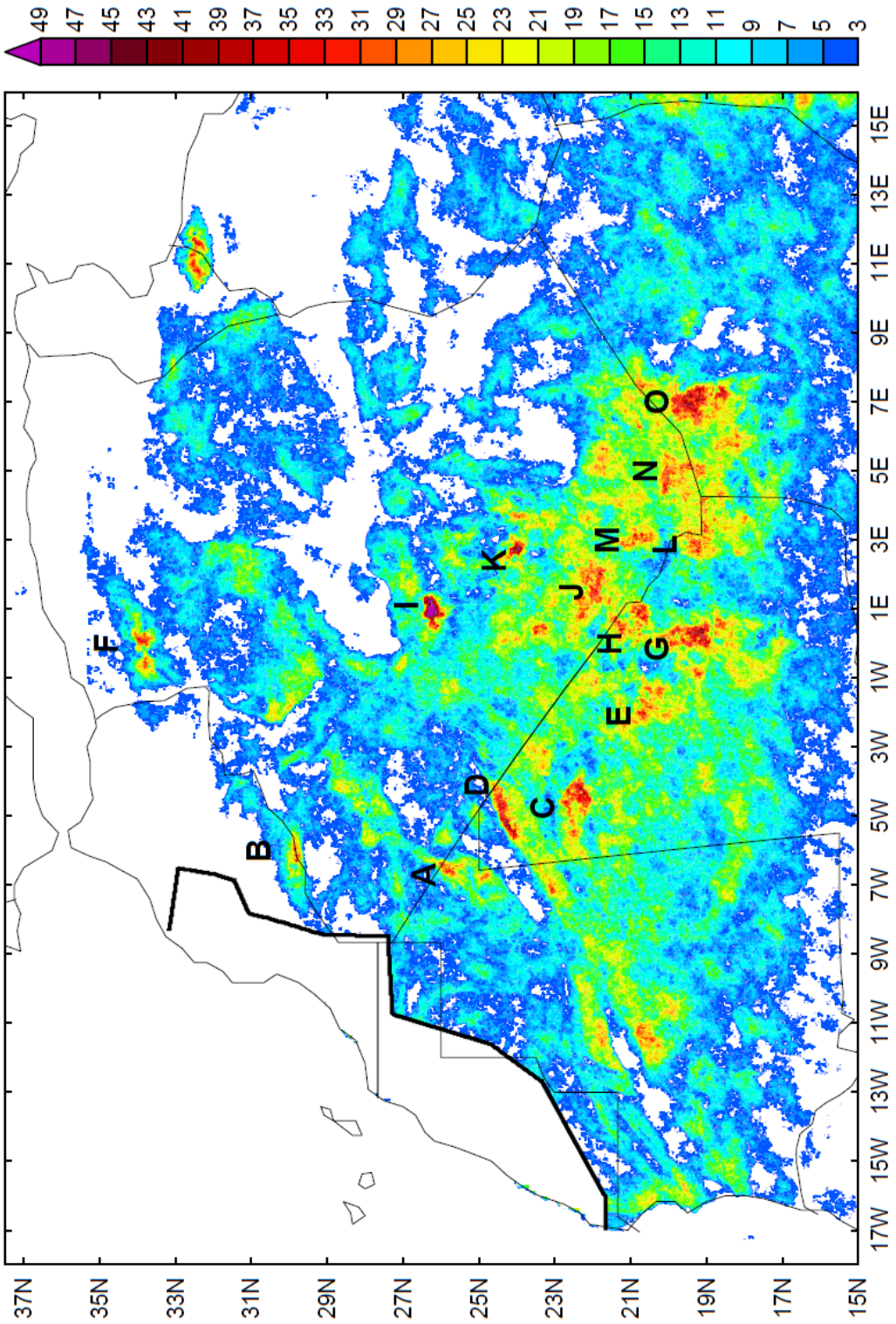

Figure 4.5. Frequency of occurrence of automatically detected dust sources produced from automated tracking 2004 – 2010 June – August inclusive. White regions correspond to count < 5. Black contour highlights the masked region where source detection is set to zero (see Section 4.2). Labels correspond to sources discussed in Table 4.1.

Label on Figure 5 and Position	Named features or position description	Erodibility feature	Boundary coordinates for analysis in Section 4.6 (if included)
A: 25.5 – 26° N, 6.5° W	Southern most end of Erg Iguidi, Mauritania – Algeria border	Numerous small (200m long) lake deposits in interdune corridors	
B: 29.5 – 30° N, 6° W	Lake Iriki, Morocco	Salt lake fed by River Draa	
C: 22 – 23° N, 4 – 5° W (also 5.5° W)	Southern edge of Erg Chech, Mali	Small diffuse palaeo lakes in the interdune corridors of Erg Chech, each typically a few hundred meters in diameter	21.5 – 23° N, 3.5 – 6° W
D: 24 – 24.5° N, 4 – 5.5° W	North of Erg Chech, Mali	Palaeo lakes aligned ENE to WSW Longest > 23Km.	23 – 25° N, 3.5 – 6° W
E: 20 – 21° N, 1 – 2.25° W	West of Djebel Timitrine, Mali	Numerous diffuse palaeo lakes in outwash from Djebel Timitrine to the East	19.5 – 22° N, 1 – 3° W
F: 34° N, 0° E	Chott Ech Chergui, south of Atlas mountains, NW Algeria	Endorheic salt lake	
G: 19 – 20° N, 0 – 0.5° E	Djebel Timitrine, Mali	No obvious erodibility feature	18 – 20.5° N, 1.5° W – 1.5° E
H: 20.5 – 21.5° N, 0 – 1° E	30 km west-south-west of Bordj Badji Mokhtar, in northern Mali close to Algeria border	Palaeo lakes	20.4 – 23° N, 0.5° W – 2.5° E*
I: 26 – 26.5° N, 0.5 – 1.5° E	Tidihelt Depression, south-central Algeria	Palaeo lakes	25 – 28.5° N, 0.5° W – 3° E
J: 21.5 – 22.5° N, 1 – 2° E	Tanezrouft, Algeria, ~ 100 km N/NW of Bordj Badji Mokhtar	Palaeo lakes, largest 2.5km across in outwash of Oued Itaferh	20.4 – 23° N, 0.5° W – 2.5° E*
K: 24° N, 2.5 – 3° E	Plains south of the Adrar n Ahnet, Algeria	Outwash plains	23 – 25° N, 1.5 – 4° E
L: 19 – 19.5° N, 3° E	100 km south of Tin Zaouatine, Algeria/Mali border	No obvious erodibility feature	17.5 – 20° N, 2.2 – 4° E
M: 20.5 – 21° N, 3° E	40 km North of Tin Zaouatine, Algeria	Outwash plain along edge of 100m high ridge	20 – 21.5° N, 2.5 – 4° E
N: 19 – 20° N, 4.5 – 5° E	Tassili Oua-N-Ahaggar dessert, south of Ahaggar mountains	No obvious erodibility feature	18.5 – 20.5° N, 4 – 6° E
O: 19 – 20° N, 6.5 – 7.5° E	West of Aïr mountains, Niger	Outwash plain and dry lakes (largest 4km across)	18 – 20.5° N, 6 – 8° E

Table 4.1. (previous page) Key CWS dust sources as determined from automated tracking (see Figure 4.5). Approximate location of source in latitude and longitude and label on Figure 5 (column 1), nearby named places or description of location (column 2), collocated erodibility features (column 3) and broader source area from which events selected for analysis in Section 4.6 originate (column 4).
* denotes these two sources considered together for analysis in Section 4.6.

---

presumably exceeded in these areas but these threshold winds do not evidently occur frequently. The single most frequently active summertime CWS source is the Tidihelt Depression in central/southern Algeria ('I' on Figure 4.5), which includes Sebkha Azzel Matti, Sebkha Mekerrhane and numerous chotts which are fed by drainage from the nearby Adrar Ahnet to the south and the Tademait Plateau to the north.

The dust source map is remarkable also for the extent of CWS regions that are flagged as dust sources less than 5 times across the seven summers of analysis. These regions include almost all of Morocco (where the mask is not applied), extensive parts of Algeria and Niger and most of Tunisia and western Libya. A simple explanation for the relative lack of dust emission from these areas lies in the lack of erodibility of the surface material. While there are no complete ground-based observational data sets to demonstrate this directly (the major source regions in Table 4.1, except for Lake Iriki in Morocco, have received little or no scientific study), there is persuasive proxy evidence from albedo and terrain heights (Figure 4.6) as to the erodibility explanation. For every 0.03^{o} x 0.03^{o} degree pixel in the domain, we compare the source count with height and albedo, which offer clarification of surface type. For areas detected as a source less than 3 times over seven years, the mean albedo is 0.311 (n=198,148) while for all areas detected more than 3 times, the mean albedo is considerably higher at 0.385 (n=430,722). The distinction between non-source and source areas for terrain heights demonstrates

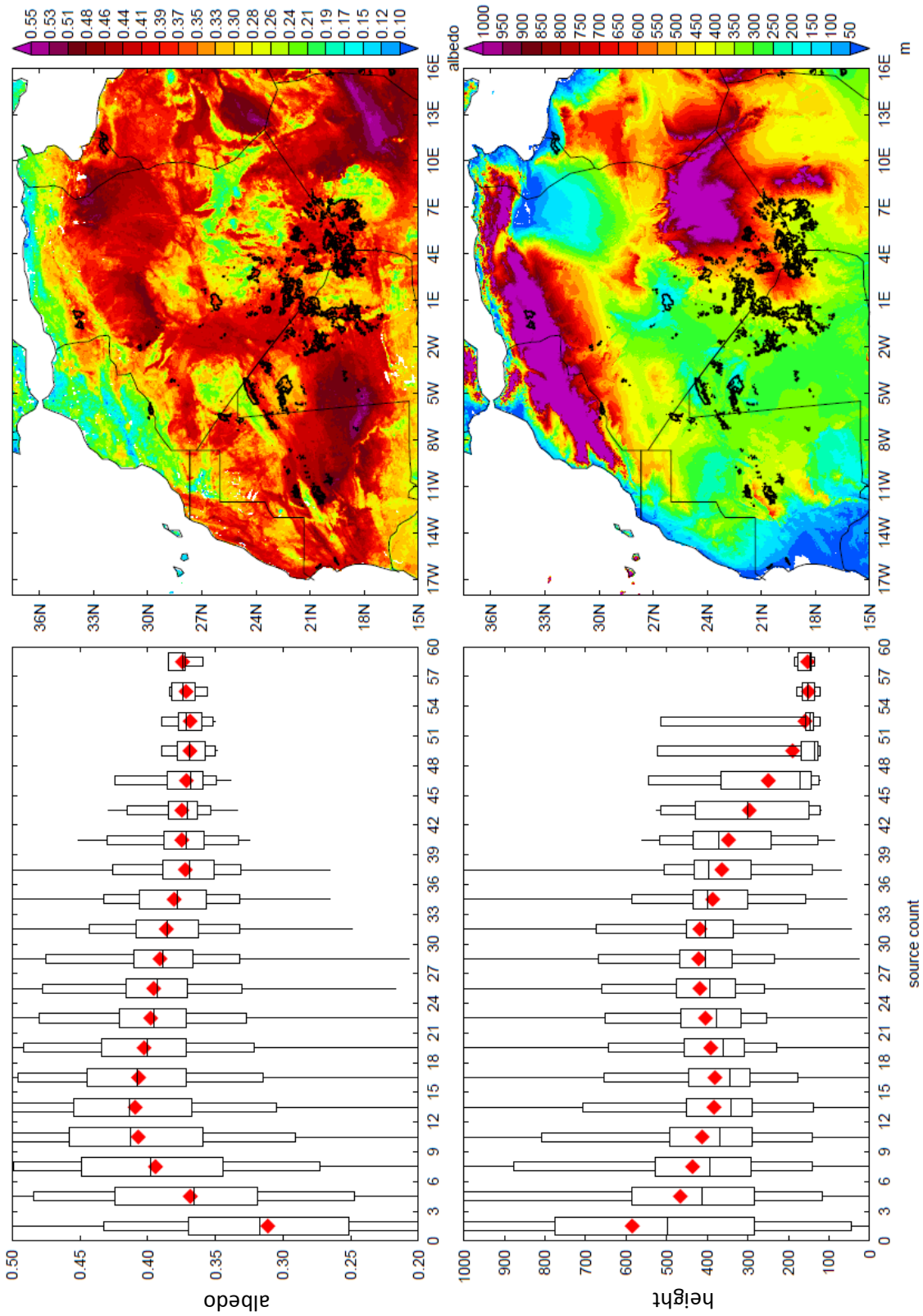
albedo
m
36N
33N
30N
27N
24N
21N
18N
15N
17W
14W
11W
8W
5W
2W
1E
4E
7E
10E
13E
16E
albedo
height
source count

Figure 4.6. (previous page) **Left column =** Box and whisker plots for categories of dust source frequency (horizontal axis) and corresponding albedo (top) and terrain height (m) (bottom). Mean (red diamond), median (horizontal dividing line of large box, 25-75th percentile (large box), 5-95th percentile (small box), minimum and maximum (whisker). **Right column =** Albedo (top) and terrain height (bottom) maps. Black contours correspond to dust source frequency > 25.

---

similar clarity. Mean terrain height for regions detected as a source less than 3 times is 583 m while the mean for all source areas detected more than 3 times is over 200 m lower at 346 m. It is striking that the mean terrain height for the three most frequently active source categories (>=51 events) lies below the 5th percentile of most other categories. Active dust source regions are generally of high albedo and they are low lying. It is clear from Figure 4.6 that the majority of the most active sources tend to be situated in the low-lying, high albedo regions immediately to the south/west of the Saharan mountains. Their proximity to the mountains, as opposed to being scattered across all areas of low-lying terrain and high albedo, supports the hypothesis that drainage from the highlands under past, wetter climates was crucial in supplying sediment suitable for deflation [e.g. *Prospero et al.*, 2002] and episodic flow events in these normally dry rivers may also serve to replenish sediment. Regions rarely detected as sources are of lower albedo and are not in depressions. The combination of lower albedo and high terrain for such areas points to the mountainous regions in the Sahara as the major non-erodible source areas. The boundary between non-source and source areas (white to blue areas in Figure 4.5) frequently corresponds to the limit of escarpments, particularly in southern Algeria. Here the edge of the Tassili escarpment, which comprises Nubian sandstone, coincides with the edge of the active dust storm source regions very closely, as do the igneous mountains of Assekrem near Tamanrasset in

southern Algeria and the Tademait plateau north of In Salah in central Algeria. The central interior of major sand seas such as the Grand Erg Oriental, the Grand Erg Occidental and Erg Chech are also not frequently the origin of dust events, but some of their edges, as noted in Table 4.1 and evident in Figure 4.6, are.

4.5.2. Comparison with the source map of *Schepanski et al.*

In this section, the automated dust source map is compared with the manually and subjectively generated map of *Schepanski et al*., which has a resolution of 1^o x 1^o (Figure 4.7). The automated dust source map was therefore degraded to a resolution of 1^o x 1^o (i.e. the 1^o x 1^o box in which the source would lie were this the original tracking resolution used) to enable direct comparison. The manual source detection method of *Schepanski et al.* only allows each 1^o x 1^o grid box to be detected as a source once per day. We have therefore also placed this constraint on the automated source map. This does not alter the overall patterns discussed in the previous section, but it does decrease the frequency of source detection in some areas, especially southern Algeria and northern Mali. The maps cover the same period for this comparison, namely June – August 2006 – 2009. Note, the mask over parts of Western Sahara and Morocco is not applied to the map of *Schepanski et al.* and it is clear from this comparison that sources are rarely detected in this region using the manual tracking method.

There are some strong similarities between the maps. Both place the most active source areas in the Tidihelt Depression, northern Mali and northwest Niger to the southeast of the border triple-point with Algeria and Mali. Both maps show low to zero activity in Morocco, Tunisia, northwest Libya and northern Algeria and low activity over the mountainous areas such as the Tassili escarpment in Algeria. There are also several

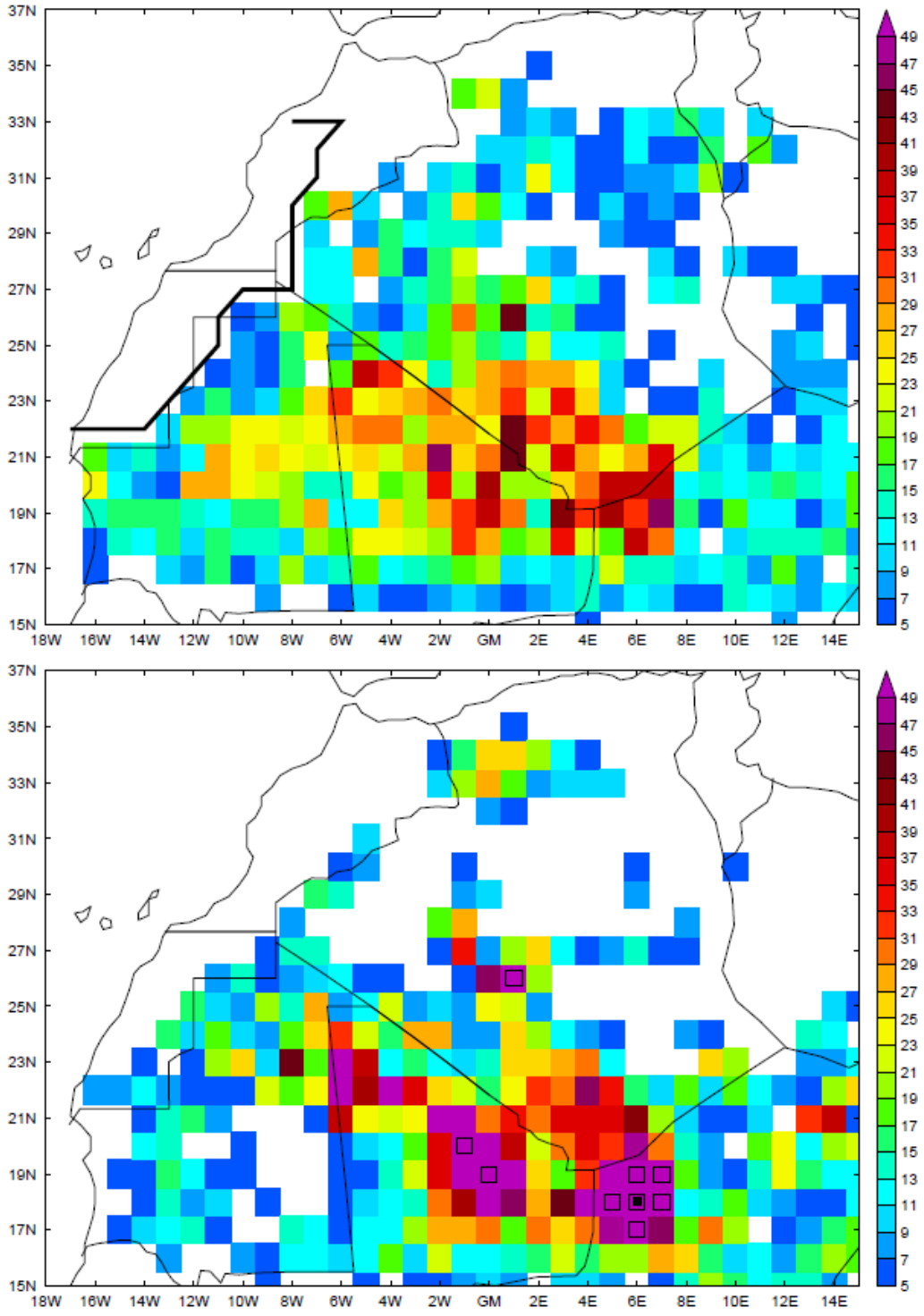

Figure 4.7. Automated dust source map degraded to 1 x 1 degree resolution (top), and manually derived source map of *Schepanski et al.*, bottom. Scale is frequency of occurrence as detection as a dust source in both cases. White regions on both panels correspond to count < 5 and black outlined (filled) boxes on bottom panel correspond to count ≥ 60 (90). Black outline on top panel highlights the masked region where source detection is set to zero (see Section 4.2; no masking applied to bottom panel). Both maps cover the period 2006 – 2009 June – August inclusive.

key differences. Most clearly, source detection frequency is higher using the manual method, especially in the main hotspot areas which are broader and have a greater maximum source count, which gets close to double that of the automated method in northwest Niger (black filled square, Figure 4.7 bottom panel). This could be due to the missing of minor events by the automated technique due to the various thresholds applied for both the detection of dust and tracking of dust plumes. Another obvious difference is the absence of source areas in central/eastern Mauritania and lack of detection hot spots (relative to detection frequency in other hotspots) in central southern Algeria to the border with Mali in the map of *Schepanski et al*. A potential reason for this may be that source regions partially obscured by cloud are not recorded in the manual tracking of *Schepanski et al*. This is supported, at least for the central southern Algeria/Mali border region, by the results in Section 4.6. In addition, the presence of clouds may contribute to some of the smaller differences in structure of the detection frequency field within the broader hotspot regions. A consequence of the relatively coarse spatial resolution, evident when comparing Figure 4.7 (top) with Figure 4.5, is that it does not enable the identification of surface features noted in Table 4.1. Source regions in the 1^{o} x 1^{o} resolution map merge in to large, coherent areas that obscure the small palaeolakes that are central to most emission sources.

4.5.3. Intraseasonal evolution

We present the intraseasonal evolution of CWS dust sources through the summer in Figure 4.8 with mean wind vectors overlaid for the same period. In addition we plot the mean 2-meter dewpoint temperature contour of 14^{o}C. This is widely used as an indicator

of the Intertropical Discontinuity (ITD), which marks the leading edge of the moist West African Monsoon (WAM) flow. Climate data are from the ERA Interim reanalysis [*Dee et al.*, 2011].

It is clear that there is a general northwards progression in the activity centre from predominantly northern Mali in June towards northernmost/northwest Mali and southern Algeria in July and August. Dust source activity appears to decline in August, with a similar source distribution to July apparent. The Tidihelt Depression peaks in July and is more active in August than in June.

Since the surface (erodibility) conditions remain largely unchanged through the hyper-arid CWS, changes in the location of the most active sources through the summer season point essentially to changes in wind (erosivity) controls on deflation. One simple explanation could be in the fact that the northwards progression of the sources is matched by a northwards shift of the ITD from June to July, as observed by *Engelstaedter and Washington* [2007b]. This marks the onset of the WAM, which typically occurs in late June [*Sultan and Janicot*, 2003]. Cold pool outflows from convective complexes are known to be important to dust emission in this region [e.g. *Marsham et al.* 2013]. With the onset of the WAM, deep convection can occur further north into the Saharan interior, resulting in cold pool activation of sources further north, although it is worth noting that the WAM influence can occasionally be detected as far north as Bordj Badji Mokhtar (approx. 21.38^{o} N, 0.92^{o} E) prior to the WAM onset [*Marsham et al.* 2013]. In addition to the shift in ITD location, the northeasterly Harmattan flow strengthens through central Algeria into northwest Mali from June to July. This may be linked to increased dust storm activity in the Tidihelt depression and the northwest tip of Mali. The fact that changes in location of source regions as the summer season progresses are well matched

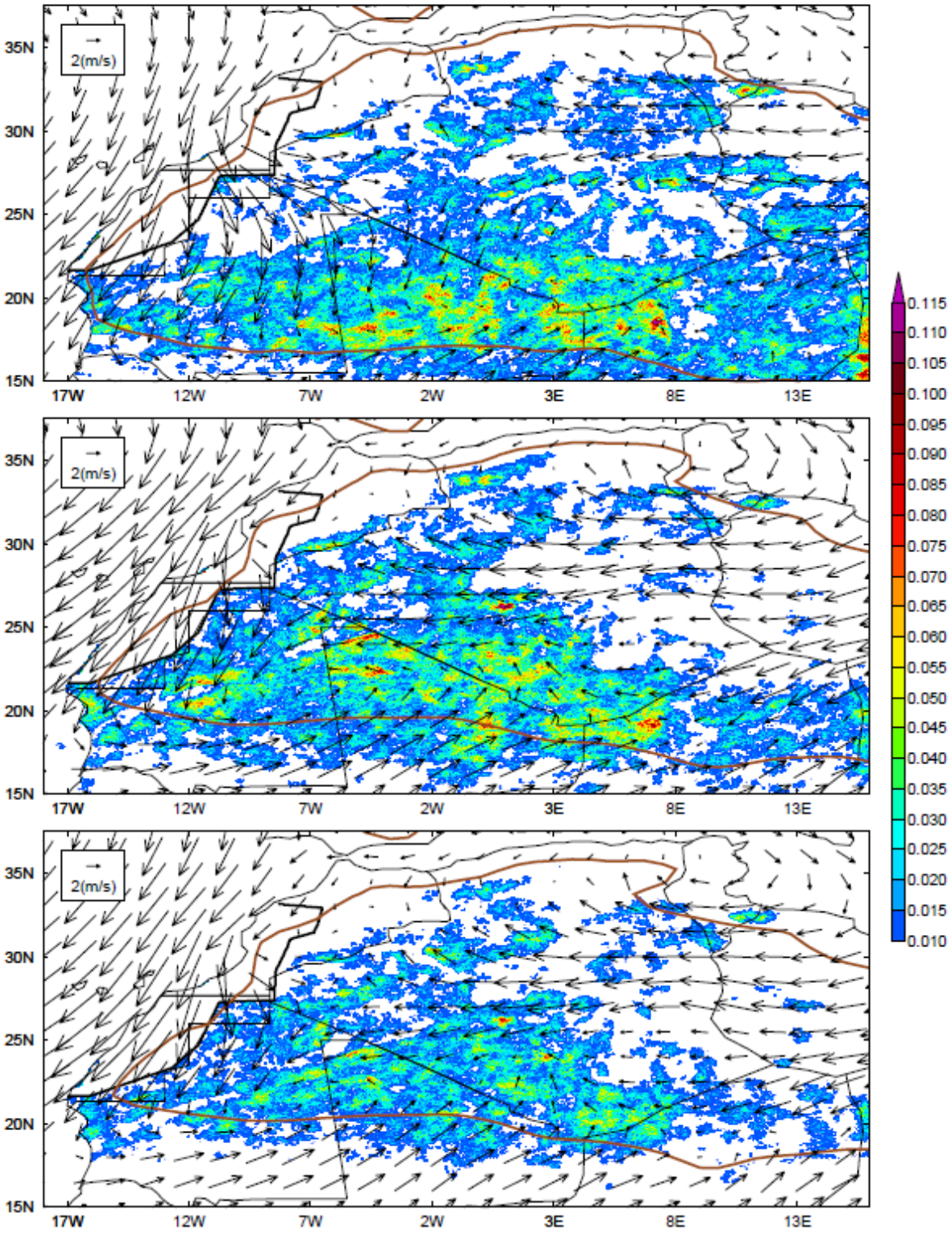

Figure 4.8. Frequency of occurrence of automatically detected dust sources produced from automated tracking over 2004-2010 for: (top) June; (middle) July; (bottom) August. Scale is mean activations per day. White regions correspond to < 0.01 activations per day. Mean 925 hPa wind vectors and 2-meter dewpoint temperature contour of 14^{o}C overlaid for same period (from ERA Interim reanalysis). Black outline highlights the masked region where source detection is set to zero in the automated map (see Section 4.2).

by changes in mean climatology supports the notion that deflation is essentially controlled in this region by erosivity factors.

4.6. Characteristics of dust events originating from key sources in the CWS

We now focus on the dominant source areas in the CWS in an attempt to establish the typical characteristics of dust plume transport from which the wind regimes associated with deflation may be inferred. Additionally, the temporal association of dust source detection with deep convection is assessed as cold pool outflows are known to be important for dust initiation in this region [*Marsham et al*., 2013].

4.6.1. Event selection and transport trajectory calculation

All tracked dust events originating from within a broader area centred on the dominant CWS sources were initially selected for study (see Table 4.1, column 4 for boundary definitions). Dust events originating only partly inside one of the areas are included if more than 50 % of the detected source lies within the defined region. Events that last for at least 6 hours (24 time steps) are included in the analysis although conclusions are insensitive to the use of shorter (3 hours) or longer (9 hours) time thresholds. Events that fall below this time threshold are considered either to be minor and of little importance to the overall dust burden, or will have merged with larger events which do pass the time threshold. In the latter case, the results should therefore provide some indication of the characteristics of the shorter-lived events before merging, as it is likely that they will have been under the influence of the same wind regime.

We calculate the transport trajectory of selected tracked dust events based on the change in dust plume centroid location at *t1* and 6 hours later (*t24*). One potential limitation is the effect on centroid location of the splitting/merging of dust plumes. Of the events selected for this analysis, over 60 % feature a split or merge in their first 6 hours. Large changes (> 1 degree) in centroid location are infrequent compared to small changes (Figure 4.9), so we are confident that the trajectory results presented here largely represent the behaviour of tracked dust events in response to the wind regime at the time of detection and in the following 6 hours and are generally unaffected by the effects of dust plume splits/merges. Conclusions are very similar however if only events that do not feature a change in centroid location of greater (less) than 1 degree (-1 degree) between any two time steps in their first 6 hours are retained for the analysis. It is also possible that the inferred dust plume transport direction may be influenced by topographic features, although this is not expected to influence the broad-scale conclusions that are drawn in the following section.

4.6.2. Dust plume transport trajectory and association with deep convection

Dust plume transport trajectory and association with deep convection divides the CWS into two broad regions (Figure 4.10): 1) central Algeria/NW Mali; and 2) northeast Mali, southern Algeria and northwest Niger.

Central Algeria and NW Mali are characterised by a clear modal transport of dust towards the west-southwest and a generally low association of dust events with deep convection. We interpret this to point to the role of LLJs in the northeasterly Harmattan near surface winds. In this part of the CWS the mean near surface wind direction is

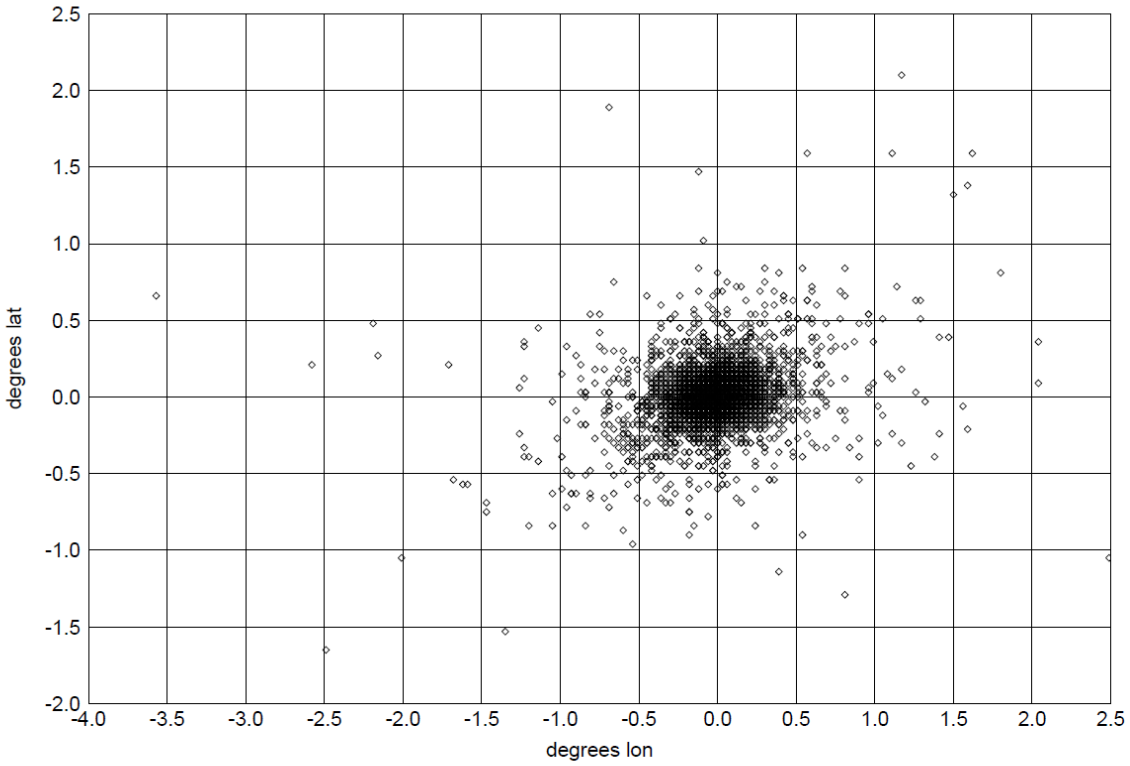

Figure 4.9. Change in location of centroid between two consecutive time steps for all time steps of all tracked dust events lasting for longer than 6 hours included in the analysis in Section 4.6.

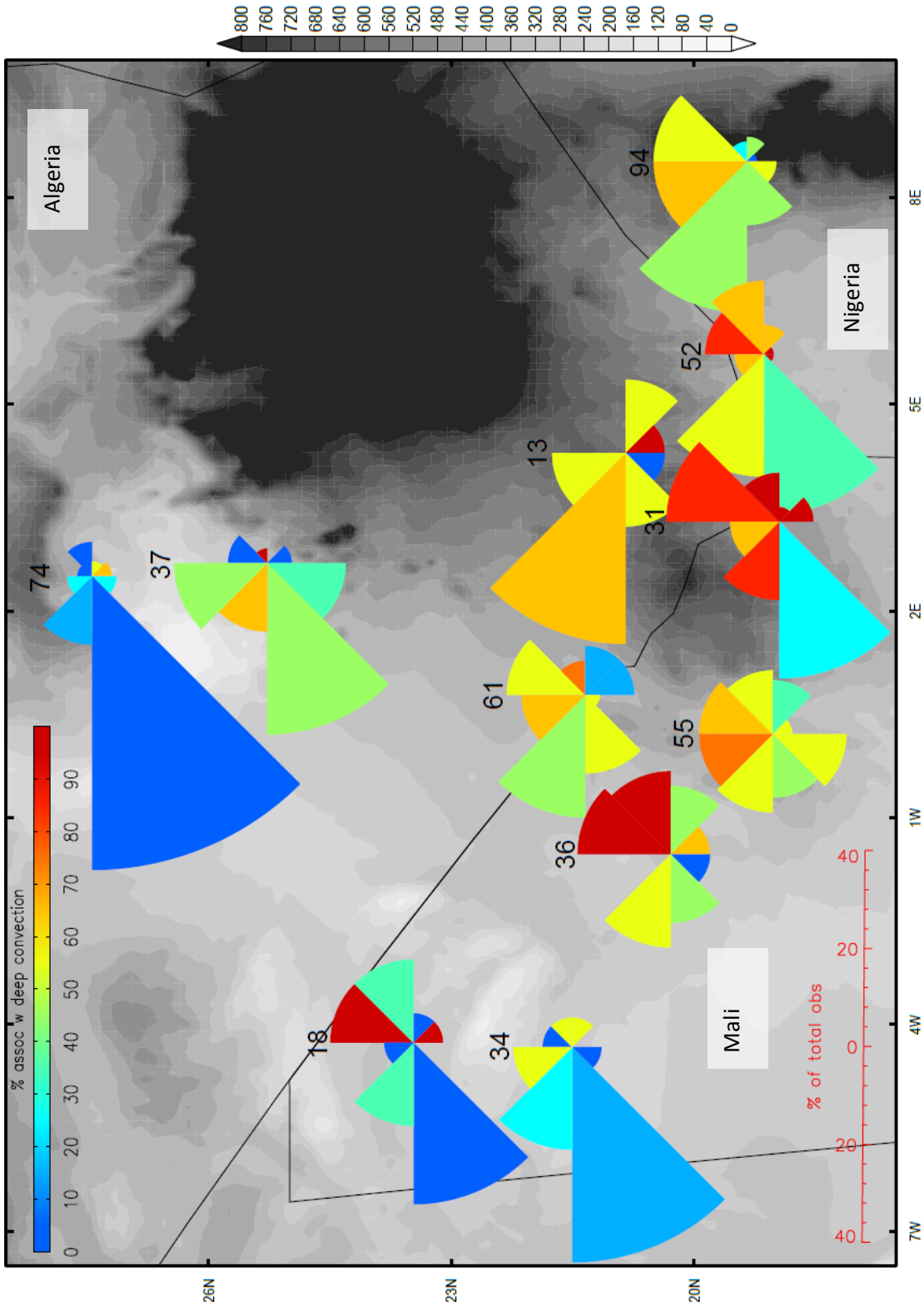
800
760
720
680
640
600
560
520
480
440
400
360
320
280
240
200
160
120
80
40
0
Algeria
Nigeria
Mali
74
37
18
34
61
36
55
13
31
52
94
% assoc w deep convection
0
10
20
30
40
50
60
70
80
90
% of total obs
40
20
0
20
40
26N
23N
20N
7W
4W
1W
2E
5E
8E

Figure 4.10. (previous page) Characteristics of dust events to originate from the dominant CWS dust sources. Each dust source shows transport direction of dust events in their first 6 hours following first detection (i.e. away from the centre of the wind rose) and proportion of events to originate at that source area travelling in each segment direction (length of segments). Colours of each segment indicate % of events travelling in that direction associated with deep convection. Number above each source area corresponds to number of events included in the analysis. Greyscale shading on background map represents topography in m.

---

northeasterly (see Figure 4.8) and LLJs have previously been invoked as an explanation for source activation across the region (*Schepanski et al.*, 2009).

Dust events in the second zone near the borders of Mali, Niger and Algeria, have a far greater association with deep convection (several sources > 60% of all analysed events) and the transport is much less dominated by one directional sector, as might be expected from cold pool outflows from convective systems, which are not necessarily directional when compared with the steady trade winds. Cold pool outflows are therefore likely to be responsible for generating high wind speeds that drive dust emission from these sources. The activation of these sources is thus tied to the dynamics of the WAM, which clearly influences the southern part of the CWS during the boreal summer (Figure 4.8). Tracked dust events from these sources that follow a trajectory towards the north, into central Algeria, show an especially strong association with deep convection.

4.7. Summary and Conclusions

This paper presents an automated, objective method for detecting the sources of dust events in the central and western Sahara (CWS) during the northern hemisphere summer

season using an algorithm applied to SEVIRI dust flags (SDFs). The method delivers a reproducible CWS dust source map for the boreal summer season of unprecedented detail, which allows for the identification of specific, highly active source areas. Most highly active sources are in southern Algeria, northwest Niger and northern Mali. Many (10/15) are likely to be associated with palaeo-lakes. The most active source is the Tidihelt Depression in central-southern Algeria and the most active regions are characterised by low terrain heights and high albedo, close to the Saharan mountains. Non-source areas are extensive and are associated with low albedo and high terrain heights – pointing to the mountainous areas of the Sahara. The centres of sand-seas are not important source areas but their margins are – particularly where sand seas provide material for saltation onto palaeolakes fed by drainage from the Saharan mountains. These results are therefore in disagreement with those of *Crouvi et al.* [2012], which argues for the importance of sand dunes as dust sources in the Sahara and that dry lake beds only rarely act as sources. On the other hand, the results are in better agreement with those of *Bullard et al.* [2011], which from limited consideration of Saharan sources suggests that palaeolakes and palaeorivers make up 70 % of these with less than 2 % classified as sand dunes, and *Prospero et al.* [2002] which points towards the importance of dry lakes and fluvial systems in this region. Compared with the Bodélé Depression, the sources in the CWS are roughly an order of magnitude smaller. They are also diffuse across the broad desert region, leading to a complicated collection of quite specific sources.

Based on inferred dust generating mechanisms, there are two key areas of dust production. One in southwest Algeria and northwest Mali is dominated by transport to the southwest, very likely driven by low-level jets embedded in the northeasterly Harmattan winds. These source regions have a low percentage association with deep convection – especially in events transported towards the southwest. The other area is in

southern Algeria, northwest Niger and northeast Mali where there is no preferred transport direction and the association between dust events and deep convection is very high, particularly events that travel northwards towards Algeria. Cold pool outflows are very likely the mechanism for deflation in these cases. Within this region are sources with no obvious erodibility surface feature. It may be the case that outflow from convection is sufficiently strong to exceed emission thresholds in these areas whereas elsewhere across very similar surfaces, the wind speed does not reach such high values due to the lack of a driving meteorological mechanism. It is striking that the preferred regions of convection in the Hoggar (Aïr) Mountains in southeastern Algeria (Niger) and Djebel Timitrine in Mali [*Birch et al.*, 2012] are proximate to these sources. Adequately representing the strong winds associated with cold pool outflows requires regional models of very high spatial resolution [e.g. *Marsham et al.*, 2011], which is computationally expensive and likely not feasible for climate prediction. This poses significant problems for the prospect of satisfactorily modelling dust emissions from these source regions in the southern CWS.

Model simulations incorporating dust emission modules are being run over the North African and the Saharan domain at ever-higher resolution (e.g. 4 km, *Heinold et al.*, 2013). The dust schemes in such models can depend on erodibility data sets that specify the surface properties such as particle size distribution and clay fraction that are crucial controls on dust emission [e.g. *Darmenova et al.,* 2009], but which have no ground-truthing. An alternative approach to dust emission modelling is to specify preferred dust source areas derived from satellite data, which can improve the spatial and temporal structure of simulated emission and transport [e.g. *Cavazos et al.*, 2009]. The high spatial resolution source map presented here, which points to specific key sources from which dust emission in the CWS occurs during the boreal summer, has potential application to

models run at high spatial resolution which require specification of preferred source areas at a matching resolution. The source map also helps to identify source areas deserving of focused field observations. The method outlined in this paper to objectively detect dust source regions using SEVIRI data could likely be expanded spatially to include the rest of the Sahara and other areas covered by SEVIRI data where dust storms occur, and temporally to consider all seasons, although modification of the dust detection algorithm outlined in *Ashpole and Washington* [2012] might be necessary to cope with alternative atmospheric and surface conditions. The automated approach also enables the creation of extended timeseries' of dust source activation with the continued provision of new SEVIRI observations, which will be useful for understanding variability in CWS source strength on longer timescales.

4.8. References

Ashpole, I., and R. Washington (2012), An automated dust detection using SEVIRI: A multiyear climatology of summertime dustiness in the central and western Sahara, *Journal of Geophysical Research*, *117*, D08202, doi:10.1029/2011JD016845

Baddock, M. C., J. E. Bullard, and R. G. Bryant (2009), Dust source identification using MODIS: A comparison of techniques applied to the Lake Eyre Basin, Australia, *Remote Sensing of Environment, 113,* 1511-1528, doi:10.1016/j.rse.2009.03.002

Birch, C. E., Parker, D. J., Marsham, J. H., and Devine, G. M. (2012), The effect of orography and surface albedo on stratification in the summertime Saharan boundary layer: Dynamics and implications for dust transport, *Journal of Geophysical Research, 117*(D5), D05105. doi:10.1029/2011JD015965

Brindley, H., P. Knippertz, C. Ryder, and I. Ashpole (2012), A critical evaluation of the ability of the Spinning Enhanced Visible and Infrared Imager (SEVIRI) thermal infrared red-green-blue rendering to identify dust events: Theoretical analysis, *Journal of Geophysical Research*, *117*, D07201, doi:10.1029/2011JD017326

Brooks, N., and M. Legrand (2000), Dust variability over northern Africa and rainfall in the Sahel, in McLaren, S. J., and D. Kniverton (eds.), *Linking land surface change to climate change,* Kluwer Academic Publishers, Dordrecht, 1-25

Bullard, J. E., Harrison, S. P., Baddock, M. C., Drake, N., Gill, T. E., McTainsh, G., and Sun, Y. (2011), Preferential dust sources: A geomorphological classification designed

for use in global dust-cycle models, *Journal of Geophysical Research,116*(F4), F04034. doi:10.1029/2011JF002061

Cakmur, R. V., Miller, R. L., Perlwitz, J., Geogdzhayev, I. V., Ginoux, P., Koch, D., Kohfeld, K. E., Tegen, I., and Zender, C. S. (2006), Constraining the magnitude of the global dust cycle by minimizing the difference between a model and observations, *Journal of Geophysical Research*, *111*(D6), D06207. doi:10.1029/2005JD005791

Carslaw, K. S., Boucher, O., Spracklen, D. V., Mann, G. W., Rae, J. G. L., Woodward, S., and Kulmala, M. (2010), A review of natural aerosol interactions and feedbacks within the Earth system, *Atmospheric Chemistry and Physics, 10*(4), 1701–1737. doi:10.5194/acp-10-1701-2010

Cavazos, C., Todd, M. C., & Schepanski, K. (2009), Numerical model simulation of the Saharan dust event of 6–11 March 2006 using the Regional Climate Model version 3 (RegCM3). *Journal of Geophysical Research, 114*, D12109, doi: 10.1029/2008JD011078

Crouvi, O., Schepanski, K., Amit, R., Gillespie, A.R., and Enzel, Y. (2012), Multiple dust sources in the Sahara Desert: The importance of sand dunes, *Geophysical Research Letters, 39*(13), n/a–n/a. doi:10.1029/2012GL052145

Darmenova, K., Sokolik, I. N., Shao, Y., Marticorena, B., and Bergametti, G. (2009), Development of a physically based dust emission module within the Weather Research and Forecasting (WRF) model: Assessment of dust emission parameterizations and input parameters for source regions in Central and East Asia, *Journal of Geophysical Research, 114*(D14), D14201. doi:10.1029/2008JD011236

Dee, D. P., S. M. Uppala, A. J. Simmons, P. Berrisford, P. Poli, S. Kobayashi, U. Andrae, M. A. Balmaseda, G. Balsamo, P. Bauer, P. Bechtold, A. C. M. Beljaars, L. van de Berg, J. Bidlot, N. Bormann, C. Delsol, R. dragani, M. Fuentes, A. J. Geer, L. Haimberger, S. B. Healy, H. Hersbach, E. V. Holm, L. Isaksen, P. Kallberg, M. Kohler, M. Marticardi, A. P. McNally, B. M. Monge-Sanz, J.-J. Morcrette, B.-K. Park, C. Peubey, P. de Rosnay, C. Tavolato, J.-N. Thepaut, and F. Vitart (2011), The ERA-Interim reanalysis: configuration and performance of the data assimilation system, *Quarterly Journal of the Royal Meteorological Society*, *137*(656), 553–597, doi:10.1002/qj.828.

Durant, A. J., Harrison, S. P., Watson, I. M., and Balkanski, Y. (2009), Sensitivity of direct radiative forcing by mineral dust to particle characteristics, *Progress in Physical Geography*, *33*(1), 80–102. doi:10.1177/0309133309105034

Engelstaedter, S., I. Tegen, and R. Washington (2006), North African dust emissions and transport, *Earth Science Reviews, 79*, 73-100, doi:10.1016/j.earscirev.2006.06.004

Engelsatedter, S., and R. Washington (2007a), Atmospheric controls on the annual cycle of North African dust, *Journal of Geophysical Research, 112,* D03103, doi:10.1029/2006JD007195

Engelstaedter, S., and Washington, R. (2007b), Temporal controls on global dust emissions: The role of surface gustiness, *Geophysical Research Letters, 34*(15), L15805. doi:10.1029/2007GL029971

Ginoux, P., Chin, M., Tegen, I., Prospero, J.M., Holben, B., Dubovik, O., and Lin, S-J. (2001) Sources and distributions of dust aerosols simulated with the GOCART model,

Journal of Geophysical Research, 106(D17), 20255-20273

Ginoux, P., Prospero, J. M., Gill, T. E., Hsu, N. C., and Zhao, M. (2012), Global-scale attribution of anthropogenic and natureal dust sources and their emission rates based on MODIS Deep Blue aerosol products, *Reviews of Geophysics*, *50*(RG3005). doi:10.1029/2012RG000388

Heinold, B., Knippertz, P., Marsham, J.H., Fiedler, S., Dixon, N. S., Schepanski, K., Laurent, B., and Tegen, I. (2013), The Role of Deep Convection and Nocturnal Low-Level Jets for Dust Emission in Summertime West Africa – Estimates from Convection-Permitting, *Journal of Geophysical Research*

Herman, J. R., and E. A. Celarier (1997), Earth surface reflectivity climatology at 340 – 380 nm from TOMS data, *Journal of Geophysical Research, 102*(D23), 28003-28011

Jarvis A., Reuter, H.I., Nelson, A., and Guevara, E. (2008), Hole-filled seamless SRTM data V4, *International Centre for Tropical Agriculture (CIAT)*, available from http://srtm.csi.cgiar.org

Johnson, B. T., Brooks, M. E., Walters, D., Woodward, S., Christopher, S., and Schepanski, K. (2011), Assessment of the Met Office dust forecast model using observations from the GERBLIS campaign. *Quarterly Journal of the Royal Meteorological Society*, *137*(658), 1131–1148, doi:10.1002/qj.736.

Kellogg, C. A., Griffin, D. W., Garrison, V. H., Peak, K. K., Royall, N., Smith, R. R., and Shinn, E. A. (2004), Characterization of aerosolized bacteria and fungi from desert dust events in Mali, West Africa, *Aerobiologia, 20*, 99–110

Klüser, L., and Holzer-Popp, T. (2010), Relationships between mineral dust and cloud properties in the West African Sahel, *Atmospheric Chemistry and Physics, 10*(14), 6901–6915. doi:10.5194/acp-10-6901-2010

Lavaysse, C., C. Flamant, S. Janicot, D.J. Parker, J-P. Lafore, B. Sultan, and J. Pelon (2009), Seasonal evolution of the West African heat low: a climatological perspective, *Climate Dynamics, 33,* 313-330

Lee, J. A., Gill, T. E., Mulligan, K. R., Dominguez Acosta, M., and Perez, A. E. (2009), Land use/land cover and point sources of the 15 December 2003 dust storm in southwestern North America, *Geomorphology, 105*(1-2), 18–27. doi:10.1016/j.geomorph.2007.12.016

Lensky, I. M., and D. Rosenfeld (2008), Clouds-aerosols-precipitation satellite analysis tool (CAPSAT), *Atmospheric Chemistry and Physics, 8,* 6739-6753

Mahowald, N. M., Kloster, S., Engelstaedter, S., Moore, J. K., Mukhopadhyay, S., McConnell, J. R., Albani, S., Doney, S. C., Bhattacharya, A., Curran, M. A. J., Flanner, M.G., Hoffman, F. M., Lawrence, D. M., Lindsay, K., Mayewski, P.A., Neff, J., Rothenberg, D., Thomas, E., Thornton, P. E., Zender, C. S. (2010), Observed 20th century desert dust variability: impact on climate and biogeochemistry, *Atmospheric Chemistry and Physics, 10*(22), 10875–10893. doi:10.5194/acp-10-10875-2010

Marsham, J. H., D. J. Parker, C. M. Grams, C. M. Taylor, and J. M. Haywood (2008), Uplift of Saharan dust south of the intertropical discontinuity, *Journal of Geophysical Research, 113*, D21102

Marsham, J. H., P. Knippertz, N. S. Dixon, D. J. Parker, and G. M. S. Lister (2011), The importance of the representation of deep convection for modeled dust-generating

winds over West Africa during summer, *Geophysical Research Letters, 38*(16), L16803

Marsham, J.H., Hobby, M., Allen, C.J.T., Banks, J.R., Bart, M., Brooks, B.J., Cavazos-Guerra, C., Engelstaedter, S., Gascoyne, M., Lima, A.R., Martins, J.V., McQuaid, J.B., O'Leary, A., Ouchene, B., Ouladichir, A., Parker, D.J., Saci, A., Salah-Ferroudj, R. (2013), Meteorology and dust in the central Sahara: Observations from Fennec supersite-1 during the June 2011 Intensive Observation Period, *Journal of Geophysical Research,* doi:10.1002/jgrd.50211

Mathon, V. and H. Laurent (2001), Life cycle of the Sahelian mesoscale convective cloud systems, *Quarterly Journal of the Royal Meteorological Society, 127*, 377–406

Moody, E. G., King, M. D., Member, S., Platnick, S., and Schaaf, C. B. (2005), Spatially Complete Global Spectral Surface Albedos : Value-Added Datasets Derived From Terra MODIS Land Products, *IEEE Transactions on Geoscience and Remote Sensing, 43*(1), 144–158.

Morel, C. and S. Senesi (2002), A climatology of mesoscale convective systems over Europe using satellite infrared imagery. 1: Methodology, *Quarterly Journal of the Royal Meteorological Society, 128*, 1953-1971

Prospero, J. M., P. Ginoux, O. Torres, S. E. Nicholson, and T. E. Gill (2002), Environmental characterisation of global dust sources of atmospheric soil dust identified with the Nimbus 7 Total Ozone Mapping Spectrometer (TOMS) absorbing aerosol product, *Reviews of Geophysics, 40*(1), 1002, doi:10.1029/2000RG000095

Reuter, H.I, Nelson, A., Jarvis, A. (2007), An evaluation of void filling interpolation methods for SRTM data, *International Journal of Geographical Information Science, 21*(9), 983-1008

Rodwell, M. J., and Palmer, T. N. (2007), Using numerical weather prediction to assess climate models, *Quarterly Journal Royal Meteorological. Society, 146*, 129–146. doi:10.1002/qj

Schepanski, K., I. Tegen, B. Laurent, B. Heinold, and A. Macke (2007), A new Saharan dust source activation frequency map derived from MSG-SEVIRI IR-channels, *Geophysical. Research. Letters, 34,* L18803, doi: 10.1029/2007GL030168

Schepanski, K., I. Tegen, M. C. Todd, B. Heinold, G. Bönisch, B. Laurent, and A. Macke (2009), Meteorological processes forcing Saharan dust emission from MSG-SEVIRI observations of subdaily dust source activation and numerical models, *Journal of Geophysical Research, 114,* D10201, doi:10.1029/2008JD010325

Schepanski, K., I. Tegen, and A. Macke (2012), Comparison of satellite based observations of Saharan dust source areas, *Remote Sensing of Environment, 123*, 90-97

Shao, Y., Wyrwoll, K.-H., Chappell, A., Huang, J., Lin, Z., McTainsh, G. H., Mikami, M., et al. (2011), Dust cycle: An emerging core theme in Earth system science, *Aeolian Research, 2*(4), 181–204. doi:10.1016/j.aeolia.2011.02.001

Sultan, B., and S. Janicot (2003), The West African monsoon dynamics. Part II: The "preonset" and "onset" of the summer monsoon, *Journal of Climate*, *16*(21), 3407-3427

Tegen, I., Harrison, S. P., Kohfeld, K. E., Prentice, C., Coe, M., and Heimann, M. (2002),

Impact of vegetation and preferential source areas on global dust aerosol: Results from a model study, *Journal of Geophysical Research, 107*(D21), 4576. doi:10.1029/2001JD000963

Tompkins, A. M., Cardinali, C., Morcrette, J.-J., and Rodwell, M. (2005), Influence of aerosol climatology on forecasts of the African Easterly Jet. *Geophysical Research Letters, 32*(10), L10801. doi:10.1029/2004GL022189

Washington, R., M. C. Todd, N. J. Middleton, and A. S. Goudie (2003), Dust-storm source areas determined by the Total Ozone Monitoring Spectrometer and surface observations, *Annals of the Association American Geographers, 93*(2), 297-313

Williams, M. and R.A. Houze Jr. (1987), Satellite-observed characteristics of winter monsoon cloud clusters, *Monthly Weather Reviews, 115*, 505–519

Chapter 5

Intraseasonal variability and atmospheric controls on daily dust occurrence frequency over the central and western Sahara during the boreal summer

Ian Ashpole and Richard Washington

Under review in *Journal of Geophysical Research*, #2013JD020267

Abstract

We classify maps of daily dust occurrence frequency over the Central and Western Sahara (CWS) during the boreal summer in order to identify typical patterns using the neural network based system of Self Organised Maps (SOMs). Resulting dust states vary in terms of the frequency of dust occurrence and its location. The most commonly occurring dust states are those of relatively low dust detection frequency. On days with relatively high dust occurrence, dust tends to favour either a location close to the Algeria-Mali-Niger border triple point (TP), or further to the northwest across the western half of the Mali-Algeria border (MAB). States in which dust is detected at both locations simultaneously are rare. There is a distinct intraseasonal progression in preferred dust location from the TP in the early season to the MAB later in the season. The evolution of dust states reveals a one-way transition from dust at the TP to dust at the MAB and then to reduced dustiness. There is a distinct degree of interannual variability in the occurrence frequency of the different states, dominated by the extremes of high and low dust detection frequency. Analysis of climatological composites demonstrates that

monsoon surges into the Saharan heat low are associated with days of high dust detection frequency, while a strong Harmattan into the CWS is linked to days with less frequent dust presence. The CWS atmospheric dust budget is thus strongly linked to the dynamics of the West African Monsoon.

5.1. Introduction

The Central and Western Sahara (CWS) is the dustiest place on Earth in the boreal summer [*Prospero et al*., 2002; *Washington et al.*, 2003]. Through its effects on the radiation budget [e.g. *Haywood et al.*, 2005] and impacts on cloud properties [e.g. *McFiggans et al.,* 2006], mineral dust has the potential to modify the general circulation of the atmosphere [e.g. *Rodwell and Jung*, 2008] as well as regional weather systems [e.g. *Lavaysse et al.*, 2011] and extreme weather events [e.g. *Dunion and Velden*, 2004]. It also plays an important role in global biogeochemical cycles [e.g. *Mahowald et al.,* 2010] and can be a hazard to human health and transport both close to and far from source regions. Quantifying the effects of dust and its accurate model representation depends upon a thorough understanding of the processes related to dust emission and transport in key dust hotspots such as the CWS. Analysis of temporal variability in dustiness at these locations can yield valuable insights into these processes [e.g. *Schepanski et al.*, 2009; *Engelstaedter and Washington*, 2007].

Dust Sources in the CWS are dispersed over a wide area and mainly related to past fluvial environments [*Ashpole and Washington,* in press]. High wind speeds responsible for dust emission are driven primarily by low-level jets (LLJs) embedded in both the northeasterly Harmattan flow and the southwesterly west African monsoon

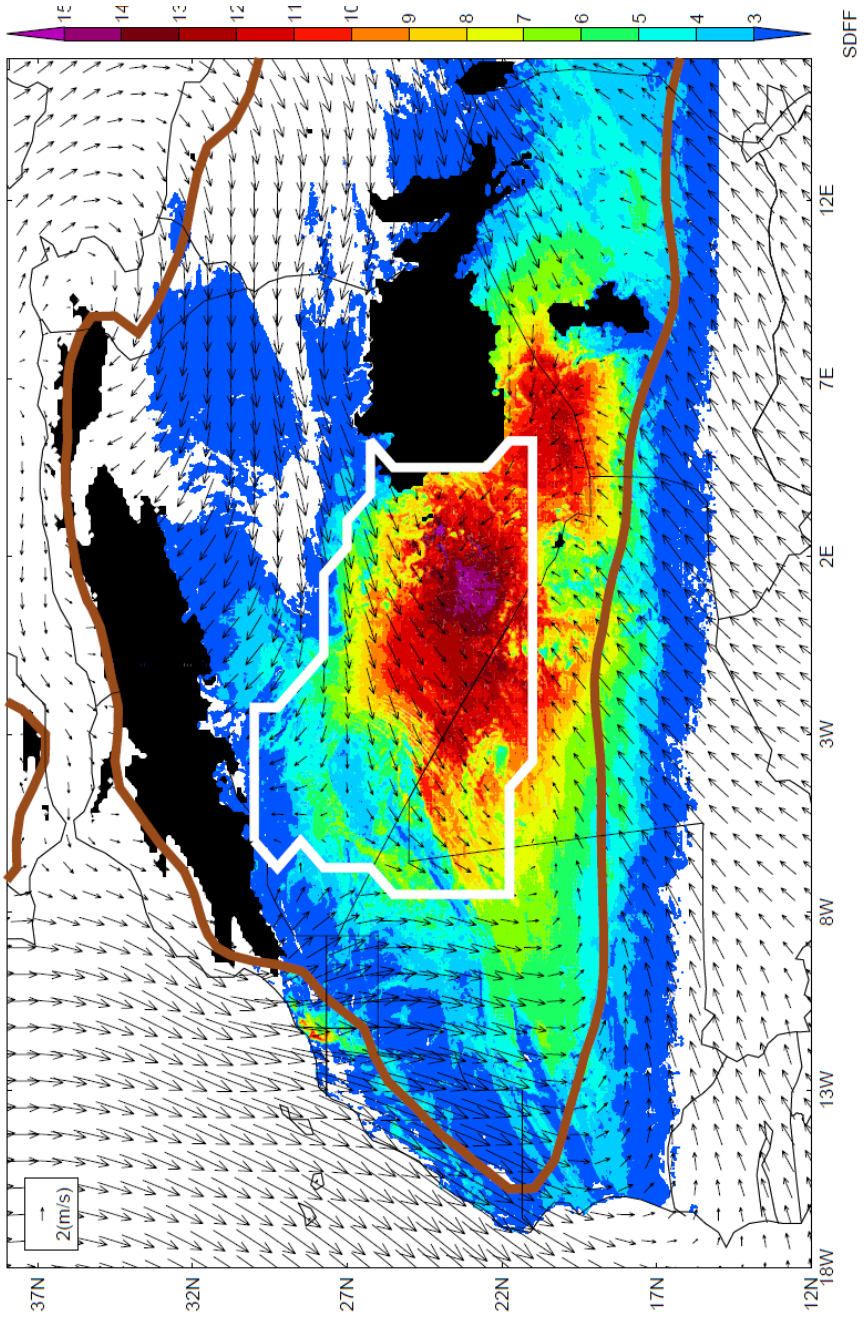

Figure 5.1. Mean central and western Sahara summer climate for JJA 2004-2010. Shading = % of all timesteps that dust is present (indicated by SEVIRI dust flag – see Section 5.2); vectors = 925 hPa winds; brown contour = ITD, defined as 2-metre dewpoint temperature contour of 14°C; white contour = mean location of SHL, calculated using objective criteria of *Lavaysse et al.* [2009]; black regions = topography in excess of 750 metres.

(WAM) flow (Figure 5.1), and by cold pool outflows from convective complexes that are sometimes present over the southern Sahara (see *Marsham et al.*, [2013] and references therein). Given the hyper-aridity of the CWS, surface erodibility is assumed to be broadly invariant; therefore temporal variability in the presence of atmospheric dust over the CWS is likely controlled by temporal variability in the occurrence of these emission mechanisms over the source areas. This is ultimately constrained by regional atmospheric dynamics, as demonstrated by *Knippertz and Todd* [2010], which links intensity of the CWS dust hotspot to the passage of African Easterly Waves (AEWs), suggesting that these synoptic features organise both dust emission and subsequent transport.

The climate of the CWS during the boreal summer is dominated by the Saharan Heat Low (SHL), which occupies a climatological location between the Hoggar Massif of southeast Algeria and the Atlas Mountains to the northwest [*Lavaysse et al.*, 2009]. The convergence of regional winds into this thermal low (Figure 5.1) is associated with dust emission, and also to the transport of emitted dust into the dry convective zone where it is mixed vertically to heights of around 6 km [*Cuesta et al.*, 2009]. The Intertropical Discontinuity (ITD – also referred to as the 'monsoon trough'), typically located at the southern edge of the SHL, marks the boundary of the dry Saharan and the moist monsoon air masses and is at its northernmost extent during the boreal summer when the WAM is well developed. This has been linked to the timing of the CWS dust peak [*Engelstaedter and Washington*, 2007], which may be due to the greater availability of energy for convective downdrafts (which fuel cold pool outflows) over the southern CWS at this time of year [*Marsham et al.*, 2008].

This mean climatological context is highly variable during the summer season however. The WAM is characterised by the succession of active phases and pauses on a range of intraseasonal timescales [*Janicot et al.*, 2011]. On synoptic timescales,

variability over West Africa is dominated by westward propagating African Easterly Waves (AEWs – e.g. *Kiladis et al.*, [2006]), which have been strongly implicated in organising convective activity [*Fink and Reiner*, 2003]. Their influence is often increased by interactions with midlatitude depressions [*Lavaysse et al.*, 2010a]. Additionally, successive northwards excursions of the WAM flow are evident on the 3-5 day timescale [*Couvreux et al.*, 2010], often coupled with enhanced moist convection. These 'monsoon surges' are driven by SHL intensification, and many interact with AEWs, especially once the WAM is well established. On longer intraseasonal timescales, robust modes of variability in WAM activity have been identified, characterised by significant modulations of convective activity and atmospheric circulation across the West African domain [*Mounier et al.*, 2008; *Sultan et al.*, 2003; *Janicot et al.*, 2010; *Matthews*, 2004]. The SHL also shows strong fluctuations in intensity and location on intraseasonal timescales, controlled primarily by interactions with AEWs and midlatitude circulations and with notable impacts on the WAM system [*Lavaysse et al.*, 2010a,b; *Chauvin et al*, 2010; *Vizy and Cook*, 2009]. All of these identified modes of variability are associated with significant circulation anomalies and increased/decreased deep convection. This has consequences for the temporal and spatial distribution of the atmospheric mechanisms known to be responsible for dust emission in the CWS, as well as for the transport of dust once it is emitted. It is reasonable therefore to assume that CWS dust presence will display similar variability throughout the summer season. That is the focus of this paper.

Owing to the remoteness and inhospitality of the CWS, our understanding of dust processes here relies to a large extent on the analysis of satellite data. Data obtained from the Spinning Enhanced Visible and Infrared Imager (SEVIRI) enables the monitoring of dust plumes at 15-minute intervals throughout the day. Until recently, these data have only been utilised to provide qualitative information on the location of dust on a case

study basis. However, *Ashpole and Washington* [2012] outlines a method to automatically detect dust across the CWS during the boreal summer with SEVIRI, facilitating for the first time the detailed quantitative analysis of dust presence here at high temporal resolution. The method employed in this paper to detect intraseasonal variability in summer time CWS dust presence is therefore to classify the preferred patterns of daily dust detection frequency; identify variability in the occurrence frequency of these patterns on intraseasonal to interannual timescales; identify preferred sequences of change among these patterns from one day to the next; and finally, to link these patterns to specific atmospheric conditions. This develops on the work of *Knippertz and Todd* [2010], which was based on an area averaged dust index at daily resolution, by adding a spatial dimension to the analysis and considering the persistence of dust presence each day, an as-yet unexplored component of CWS dust processes but likely of much importance to the atmospheric radiative budget. In Section 5.2 we outline data and methods used; Section 5.3 details the main dust states over the CWS, variability in their occurrence at a range of timescales, and commonly occurring sequences of change between these; Section 5.4 outlines the atmospheric characteristics coincident with the different dust states; the results are discussed in Section 5.5; and Section 5.6 contains a summary and conclusions.

5.2. Data and methods

5.2.1. Data

We use the SEVIRI Dust Flag (SDF) dataset [*Ashpole and Washington*, 2012] to provide information on the presence or absence of dust over the central Sahara. These data cover every available 15-minute SEVIRI observation for June – August 2004 – 2010 and are

available on a standard latitude/longitude grid of approximately 0.03 x 0.03 degrees resolution over the CWS domain of 15 ^{o} – 37.5 ^{o} N, 18^{o} W – 16 ^{o} E. We analyse the daily total SDF frequency of occurrence (SDFF) at each of the pixels within the domain over June-August, 2004-2010, which yields 643 days (1 day is missing). Maximum potential SDFF at a point for a single day is 96, and minimum is 0.

SDF stems from the SEVIRI dust scheme (see e.g. *Lensky and Rosenfeld* [2008] for a description) that has been widely used to provide qualitative information on the presence of dust in recent Saharan dust research [e.g. *Schepanski et al.*, 2009], but for which there are several known limitations including a sensitivity to the presence of atmospheric water vapour, the altitude of the dust layer, and the lower-tropospheric lapse rate, even for optically very thick dust clouds [*Brindley et al.,* 2012]. These limitations are in turn passed to the SDF data. *Ashpole and Washington* [2012] also note issues in dust detection at nighttime due to similarities in the infrared signal of the desert background and dust.

In addition to SDF, we utilise the SEVIRI brightness temperature at 10.8 μm (BT108) for the detection of deep convection (Section 5.4). Data specification and availability is as for SDF. We flag deep convection presence when brightness temperature falls below 270 K following *Lavaysse et al.* [2009]. Information on the atmospheric circulation is derived from the European Centre for Medium Range Weather Forecasts (ECMWF) ERA Interim (ERA-I) reanalysis, horizontal resolution 0.75 x 0.75 degrees [*Dee et al.*, 2011]. We employ the Saharan Heat Low (SHL) detection scheme outlined in *Lavaysse et al.* [2009].

5.2.2. Classification of daily dust distribution

We classify maps of daily dust frequency occurrence over the central Sahara using the neural network based system of Self Organised Maps (SOMs). SOMs have been successfully applied to numerous meteorological and climatological problems including analysis of climate change [*Hewitson and Crane*, 2002], the spatial/temporal characteristics of the NAO [*Reusch et al.*, 2007] and the downscaling of precipitation data [*Hewitson and Crane,* 2005].

SOM analysis uses artificial neural networks to objectively characterise variability within a dataset [*Kohonen*, 2001]. SOMs are a powerful form of data reduction that summarise the key features of the dataset in a user-specified (usually small) number of patterns. The output from SOM analysis is akin to that of a clustering exercise whereby similar data samples are placed into separate groups and each group is then represented by a single idealised pattern which best represents the shared characteristics of all its members.

Trained patterns from the SOM analysis are presented in a regular grid or 'map', with similar patterns positioned close to each other and the most extreme patterns located in the corners. The number of patterns (i.e. size of the grid) dictates the degree of generalisation that occurs in the analysis, with a higher number of patterns enabling greater between-pattern differentiation. However, irrespective of the SOM grid size, the underlying structure will remain the same, i.e. the same main patterns will emerge from training [*Hewitson and Crane,* 2006]. Each timestep of the input dataset most closely matches one of the trained SOM patterns. This therefore provides an objective means to classify the dust frequency distribution of each day and explore, for example, occurrence frequencies of particular patterns and associated temporal variability, and preferred sequences of change.

Results presented here were created using the SOM_PAK software (Version 3.1 – see *Kohonen*, [1995]). In this study we focus on results using a 4x3 grid which provides a concise summary of the dominant recurring patterns in the daily SDFF dataset. Conclusions are relatively insensitive to the use of larger grids (results have also been compared with 5x4 and 7x5 grids) but the greater degree of between-pattern differentiation makes the salient results less clear. For computational efficiency in SOM training, we reduce the resolution of the SDFF data to 0.25 x 0.25 degrees.

5.3. Results

In this section we describe results from the SOM-based classification of the daily dust detection frequency in the summer time CWS.

5.3.1. Generalised daily dust detection frequency patterns

Two main daily dust coverage conditions are classified in a 4x3 SOM (Figure 5.2): states with high daily dust occurrence (HIGHDUST), positioned on the left of the plot (columns 1 and 2, with the exception of 2,2) with a peak SDFF of up to 40% (i.e. dust is present at a given location for 40 % of time steps, 9-10 hours); and states with comparatively much lower daily dust occurrence (LOWDUST), positioned on the right (columns 3 and 4). Patterns 2,2, 3,1 and 3,3 represent a midpoint along a continuum of HIGHDUST to LOWDUST, with a peak SDFF of around 20% (4-5 hours). Within these main states are two further classifications: a) dust near the Mali-Algeria-Niger border triple-point (TP – bottom row); and b) dust across the Mali-Algeria border (MAB – top row). These are most clearly represented by the 4 corners of the SOM (TP-HIGHDUST

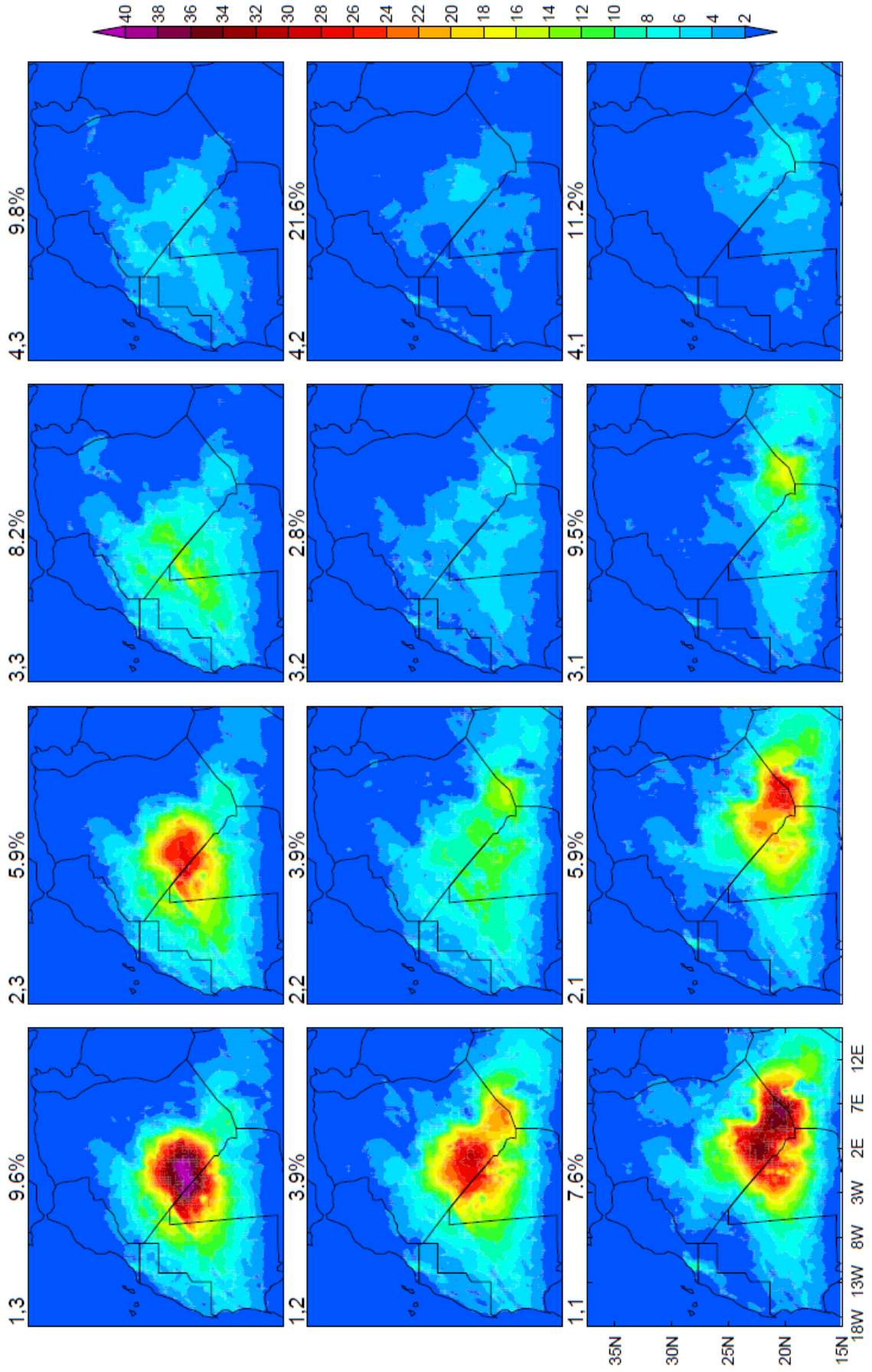
40
38
36
34
32
30
28
26
24
22
20
18
16
14
12
10
8
6
4
2
1,3
9.6%
1,2
3.9%
1,1
7.6%
2,3
5.9%
2,2
3.9%
2,1
5.9%
3,3
8.2%
3,2
2.8%
3,1
9.5%
4,3
9.8%
4,2
21.6%
4,1
11.2%
35N
30N
25N
20N
15N
18W
13W
8W
3W
2E
7E
12E

Figure 5.2. (previous page) Patterns of daily dust frequency. X,Y value in top left corner of each state corresponds to state reference, value in centre above each state corresponds to frequency of occurrence as a percentage of total input fields (n=643). Shading corresponds to daily SDFF, minimum possible value = 0, maximum possible value = 96.

= 1,1; TP-LOWDUST = 4,1; MAB-HIGHDUST = 1,3; MAB-LOWDUST = 4,3). Between these extremes of the SOM there are a variety of intermediate states.

One pattern in the LOWDUST state (4,2) occurs over 21% of the time, which is far more frequently than any of the others. Both other column 4 states occur more frequently than any other state on the SOM. Thus, while the CWS is the dustiest part of the planet in the boreal summer, the most frequently occurring states are LOWDUST. Since the analysis is based on daily dust detection frequency, this suggests that dust outbreaks are not long lived when considering the season as a whole. MAB-HIGHDUST and state 3,1, which depicts moderate dust occurrence, also occur relatively frequently. With the exception of 4,2, the row 2 states occur less frequently than those of rows 1and 3. Row 2 is characterised by a more widely spread dust burden, encompassing both the TP and MAB regions. This suggests that on any given day, dust is more likely to occur at one of these locations than at both.

5.3.2. Monthly evolution in dust frequency distribution

The distribution of CWS dust states follows a discernible evolution during the summer (Figure 5.3). TP patterns occur far more frequently in June than do the other patterns and

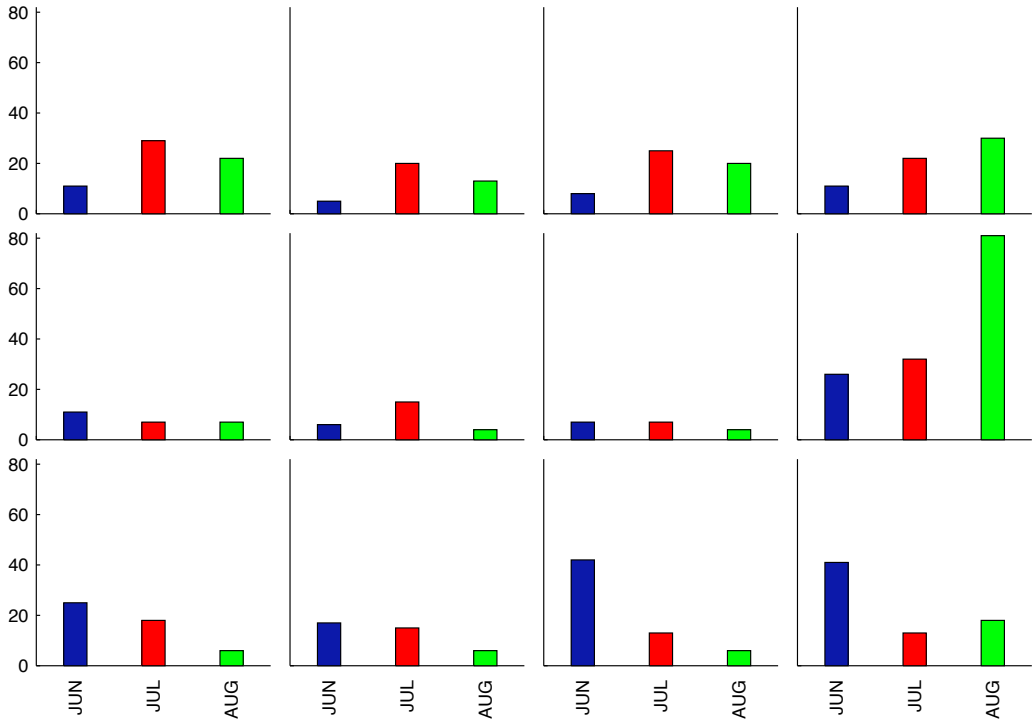

Figure 5.3. Monthly occurrence frequency of each dust state. Blue bar = June, red bar = July, green bar = August. Y axis value = raw count. Value in centre above each state corresponds to occurrence frequency as a raw count of total input timesteps (n=643).

are less frequent in July and August. MAB patterns are more typical of July and August. The preferred location for the occurrence of atmospheric dust therefore migrates towards the MAB position from TP as the summer progresses.

State 4,2 (the least dusty state in the classification) occurs relatively frequently in comparison to the other states through all months and, in August, is by far the modal occurrence of any pattern by month. It occurs more frequently in August than any other state occurs across the whole summer. 37% of all August time steps are classified as this state, and this accounts for 30% of all LOWDUST classifications across all months.

5.3.3. Interannual variability of dust states

There is considerable interannual variability in the occurrence frequency of the dust states (Figure 5.4). Whereas the years 2004-2006 were generally characterised by high occurrences of HIGHDUST states relative to 2007-2010, the opposite is true of the LOWDUST states, where the years 2004-2006 feature low occurrence. Implicitly this switch between the extremes in the daily dust classification indicates that the intermediate states between LOWDUST and HIGHDUST do not tend to dominate in any one year. Within the HIGHDUST years, there are also important spatial differences in the location of the dust. Whereas in the generally dust free year of 2008 there were no occurrences of dust near TP, in the generally dusty year of 2005 there were 13 such days. The year 2005 also featured peak occurrence of dust at MAB.

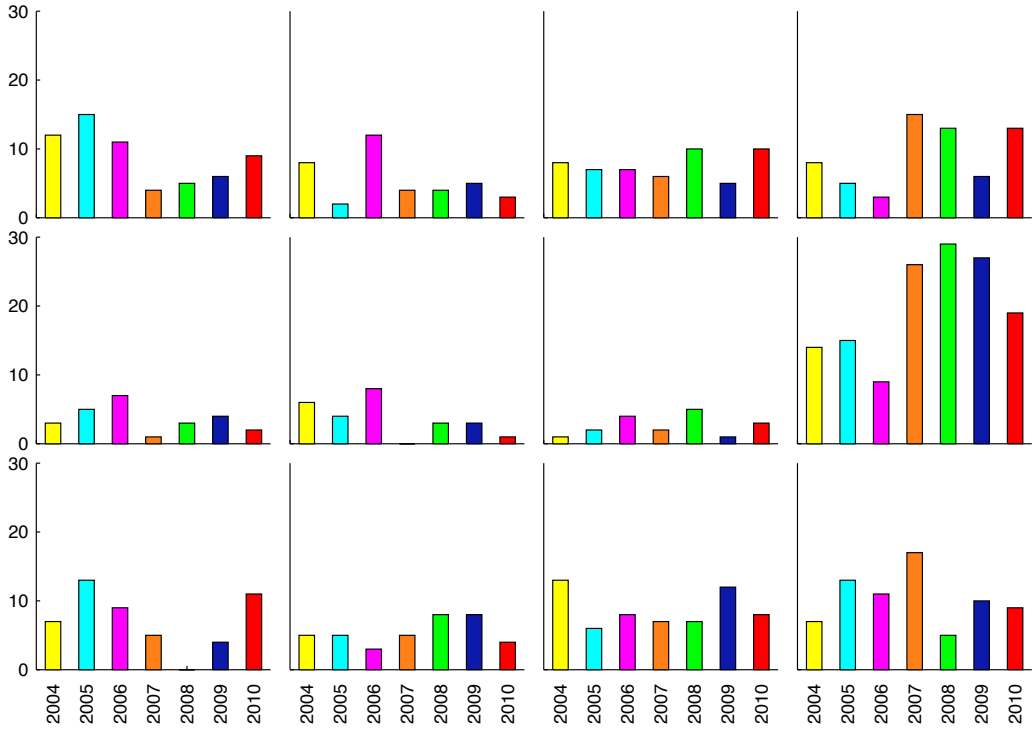

Figure 5.4. Annual occurrence frequency of each dust state. 2004 – 2010 left – right. Y axis value = raw count, value in centre above each state corresponds to occurrence frequency as a raw count of total input timesteps (n=643).

5.3.4. Preferred sequences of change

SOM analysis provides information on the time-wise change between states, thereby enabling the identification of preferred evolution between dust states on a day-to-day basis. Figure 5.5 presents the preferred sequences of change across the daily SDFF dataset. We focus on two different types of sequence: persistence and transition. For example, across the whole of the JJA period, the TP-HIGHDUST state occurs on successive days (persistence) for 43% of the total days classified as TP-HIGHDUST (n=21 days). When a transition to another state from one day to the next occurred, TP-HIGHDUST had a preferred transition to the neighbouring state 1,2 36% of the time.

5.3.4.1. Persistence

Over the whole summer season (JJA), the most persistent state is the least dusty state in the classification (4,2). This is followed by TP-HIGHDUST and MAB-HIGHDUST. Persistence is lower than 20% in 4 of the 6 intermediate states. Persistence is more common than transition to another state for 3 of the 4 extreme states of the SOM matrix (the exception being MAB-LOWDUST) so that once an extreme state occurs, the characteristics of the dust distribution tend to remain in that state for several days. In general, the LOWDUST states tend to persist for more consecutive days than HIGHDUST states. HIGHDUST persistence decreases sharply from July to August (45% to 23% for MAB and 44% to <20% for TP). Fewer states favour persistence over transition in August compared with preceding months. An exception is state 4,2, the least dusty state in the classification, which reaches a peak of 56% persistence in August with one year in which the state persisted for 11 consecutive days, thus corresponding to a prolonged period of relatively dust-free conditions. In contrast, TP-HIGHDUST shows a


(a)
HIGHDUST
LOWDUST
MAB
TP
36%
21%
43%
24%
50%
31%
(b)
HIGHDUST
LOWDUST
MAB
TP
36%
25%
48%
27%
39%
32%
24%
26%
(c)
HIGHDUST
LOWDUST
MAB
TP
45%
20%
44%
24%
23%
47%
23%
23%
(d)
HIGHDUST
LOWDUST
MAB
TP
23%
24%
56%
33%
33%
33%

Figure 5.5. (previous page) Preferred sequences of change of each dust state. Value in box at centre of each state corresponds to frequency of persistence as a percentage of total occurrences of that state, arrows correspond to preferred transitions, value at the end of the arrow is the percentage days state A transfers to state B when a transition occurs. Where either of these values is less than 20%, or is only based on a single occurrence, it is ignored. Yellow shading corresponds to the most common pattern(s) of change for each state. **a.** JJA combined; **b.** June; **c.** July; **d.** August.

---

string of 6 consecutive days in June, which is indicative of prolonged widespread dust occurrence at this location.

5.3.4.2. Transitions

Next we consider preferred transition pathways between states. There are several preferred transition directions across JJA as a whole. LOWDUST states tend to favour transitions between one another, with just under half (49%) of all transitions from a LOWDUST state being to another LOWDUST state. Combined with the persistence noted above, LOWDUST on day n is followed by LOWDUST on day n+1 69 % of the time. This suggests that sustained periods characterised by relatively low daily SDFF are common. When LOWDUST does transition to another type of state, it tends to favour TP states (50 % of all transitions away from LOWDUST are to a TP state). Intermediate TP states (3,1 and 2,1) then most commonly transition to another TP state (68 %), favouring a switch to a state representing lower dust occurrence. When TP-HIGHDUST does occur, it is usually preceded by another TP state (74 % of all occurrences). TP-HIGHDUST favours transitions towards the other HIGHDUST states, switching to one of these on 68 % of occasions, and MAB-HIGHDUST then prefers transitions to other

MAB states (68 %) as opposed to TP states. Therefore, on the whole, there is a preferred clockwise transition around the SOM matrix with TP-HIGHDUST transiting to MAB-HIGHDUST and thereafter towards LOWDUST, with TP states most likely to eventually follow.

The patterns above are evident each month, although certain sequences are more/less strong depending on the month being considered. Additional preferred transitions are sometimes evident, but the general direction of the overall evolution between states remains unchanged. It is interesting to note that row 2 states tend to favour transitions towards TP states in June as opposed to MAB states in July and August. The intermediate TP states also break from their strong tendency towards other TP states in July, instead having a higher proportion of transitions towards row 2 and MAB-HIGHDUST (although they revert to favouring other TP states in August).

5.4. Atmospheric controls

We create composites of 925 hPa winds and location of the SHL in order to identify potential atmospheric circulation controls on the patterns that the SOM-based classification has revealed (Figure 5.6). From these we seek to answer two questions: 1) what is the difference in atmospheric circulation between days classified as HIGHDUST and days classified as LOWDUST? 2) What is the difference between days with a TP classification and those with a MAB classification?

An important difference between HIGHDUST and LOWDUST composites is the presence of strengthened monsoon inflow along the Algeria/Mali border in the case of HIGHDUST composites. Monsoon inflow extends up to about 5^{o} further north compared to LOWDUST composites. Likely associated with the strengthened monsoon inflow is an

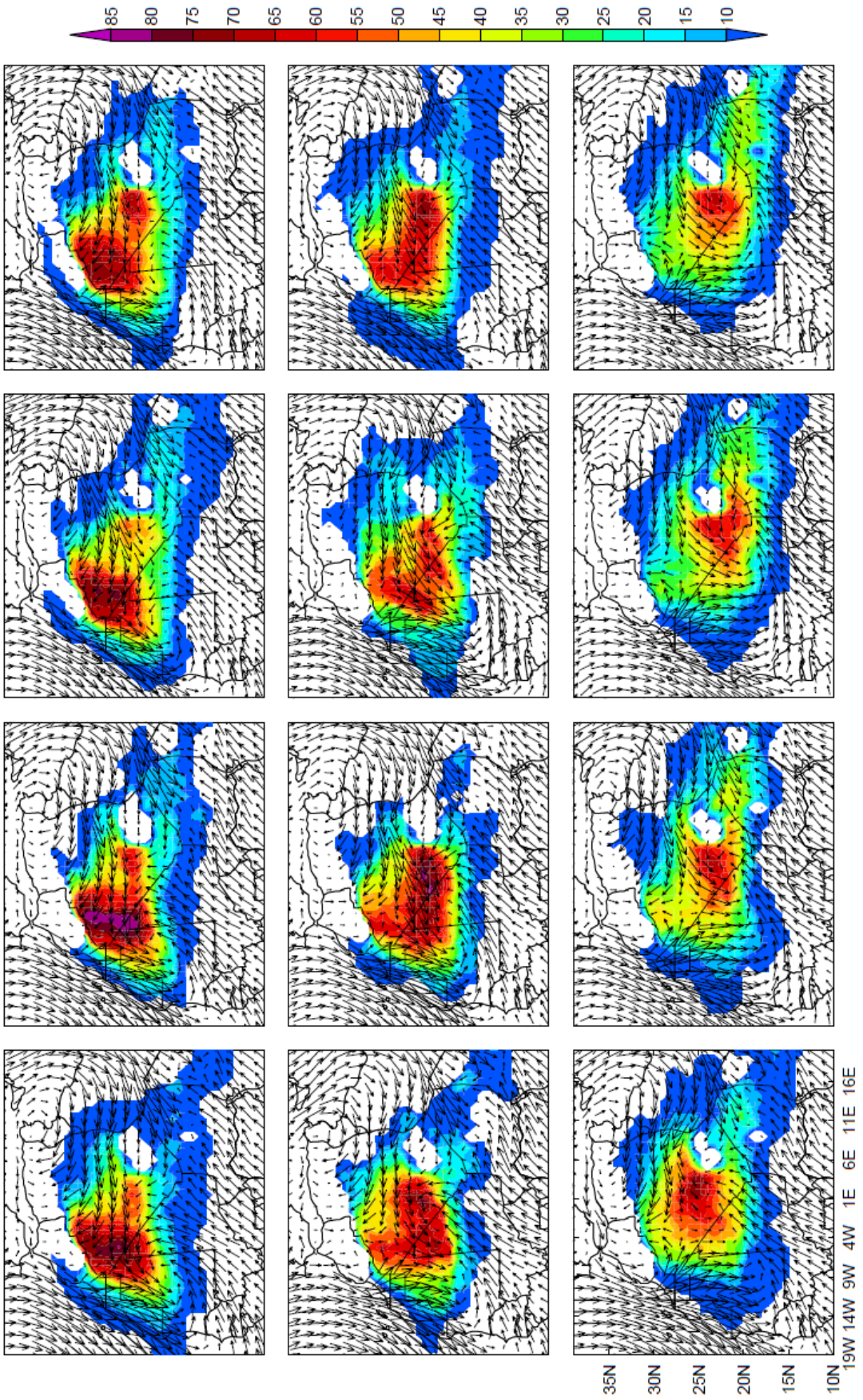

Figure 5.6. Climatological composites for each dust state. Vectors = 925hPa winds, shading = detection frequency of heat low core (as percentage of total timesteps).

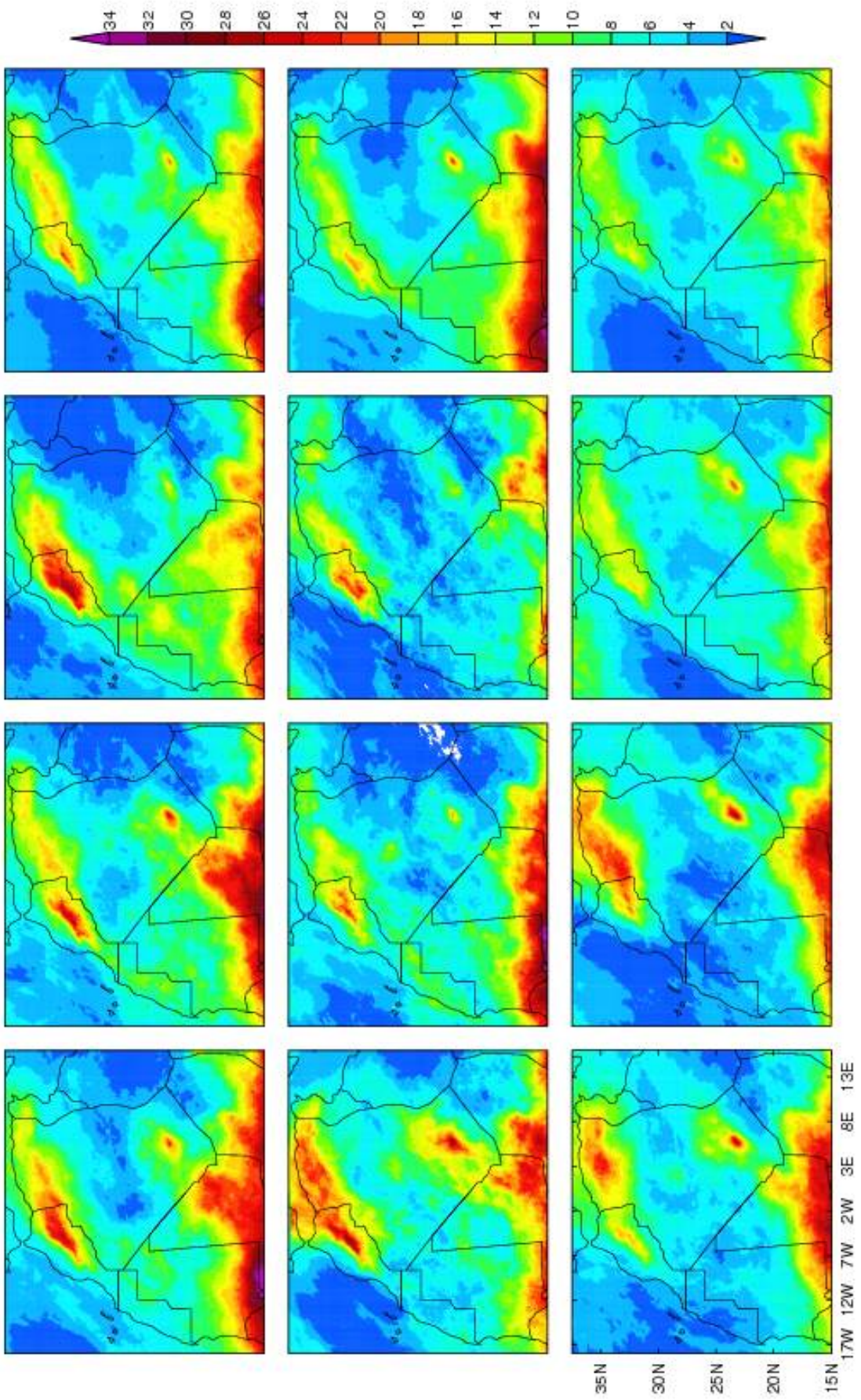

Figure 5.7. As Figure 5.6, but for detection of deep convection. Shading = percentage of total timesteps.

increase in deep convection in northern Mali and parts of northern Niger and southern Algeria in the HIGHDUST states compared with LOWDUST (Figure 5.7). In addition to this, there are marked differences in the northeasterly Harmattan between HIGHDUST and LOWDUST composites (and also most of the intermediate states). The northeasterly flow dominates Algeria, extending into northwest Mali in LOWDUST states, whereas on HIGHDUST days it is noticeably retracted and weaker across central and southern Algeria. Finally, the overall spread of locations in which the heat low core is detected is noticeably broader for LOWDUST composites compared to HIGHDUST, especially towards the east.

The composites also reveal differences in climatology between preferential dust location at TP and MAB. When dust occurs near the TP, the heat low tends to favour a location in central/southern Algeria and the monsoon flows across northeast Mali and western Niger, reaching well into southern Algeria just to the west of the Hoggar at its most northerly extent. When dust occurs in the MAB region, the heat low favours a location in western-most Algeria, northwest Mali and northern Mauritania. Similarly, the most northerly extent of the monsoon flow is now located several degrees further west, through northwest Mali, and these winds have a distinct cyclonic tendency, which is not evident when dust occurs near the TP. In addition, the northwards excursion of deep convection is better developed when dust occurs at the MAB, with high occurrence frequencies well north of 20^{o}N and several degrees further west compared with TP.

5.5. Discussion

The classification of daily summer dust distribution in the central and western Sahara identifies four typical states arranged along axes of high to low dust presence and dust

located near the triple point of Algeria, Mali and Niger versus distribution further west along the Mali-Algerian border. There is marked intraseasonal and interannual variability in the occurrence frequency of the classified states and preferential sequences of change among the states from one day to the next. Analysis of circulation characteristics contemporaneous with each dust state in the classification points to clear atmospheric controls on the location of dust and frequency with which it is detected.

LOWDUST and intermediate states are generally coincident with a Harmattan-dominated CWS, while HIGHDUST states occur when the northeasterlies are weaker and the southerly WAM winds instead are well advanced into the core of the Sahara. Monsoon surges are a common phenomenon in West Africa [*Couvreux et al.*, 2010]. These are related to dust emission in two ways. First, the low level monsoon winds are at times strong enough to cause deflation [*Marsham et al.*, 2013]. Second, moisture advection into the southern Sahara facilitates deep convection and consequently the occurrence of cold pool outflows from convective complexes, which have been identified as an important driver of dust emission in observational [*Marsham et al.* 2013] and modelling studies [*Marsham et al.*, 2011]. Emitted dust is then transported into Algeria in the monsoon surge, which flows towards the heat low, the major driver of these moist air penetrations [*Couvreux et al.*, 2010]. In June HIGHDUST occurs more frequently at TP than MAB. This reverses in August consistent with the heat low which is found closer to the Atlas Mountains in late summer than the Hoggar around the monsoon onset [*Lavaysse et al.*, 2009].

Monsoon surges can last for several days, which may explain the observed persistence in HIGHDUST patterns. Their dynamics may also explain the existence of a preferred, one-way transition from TP-HIGHDUST towards MAB-HIGHDUST. Specifically, *Couvreux et al.* [2010] notes that a preferred surge location is to the

southwest of the Hoggar, coincident with the TP location, due both to monsoon flow acceleration by cyclonic circulation associated with the heat low; and potentially due to the modulation of the circulation by the mountains themselves. On following days the surge then spreads towards the west. Additionally, *Couvreux et al.* [2010] notes that around half of the monsoon surges interact with AEWs and therefore migrate from east to west. A link between AEWs and both dust emission and transport has already been established based on the statistical analysis of daily satellite observations [*Knippertz and Todd*, 2010]. It is possible that the increased occurrence of MAB states in July and August may therefore also be linked to increased AEW activity later in the season [*Thorncroft and Hodges*, 2001], which would favour the increased transport of dust away from the TP region.

In addition to a high degree of intraseasonal variability, the WAM is highly variable on interannual timescales (see *Rodriquez-Fonseca et al.* [2011] for an overview). This may explain the interannual variability evident in the occurrence frequency of HIGHDUST states, given their link to WAM dynamics. AEW activity has been found to vary markedly on interannual timescales [*Thorncroft and Hodges*, 2001], suggesting that the WAM flow does not influence the southern Sahara to the same degree each year. A greater (lesser) WAM influence in this region will lead to more (less) days classified as HIGHDUST in a given year, necessarily implying less (more) LOWDUST days.

The presence of a stronger Harmattan across the CWS on LOWDUST (and intermediate state) days points towards the role of Low Level Jets (LLJs). The relatively much lower daily SDFF suggests that these a) are not associated with such widespread dust emission; and/or b) they efficiently transport dust away from the CWS towards the southwest. The persistence of the LOWDUST states and their preferred transitions among each other

suggests that Harmattan-dominated conditions are more characteristic of the CWS, interspersed occasionally by monsoon surges that bring periods of sustained dustiness.

5.6. Summary and concluding remarks

High temporal resolution satellite derived dust data is used to provide insights into intra-seasonal variability of summer time dust distribution in the central and western Sahara. A neural network based classification of daily dust distribution provides the framework for evaluating the seasonal cycle, intra-seasonal transition, and interannual variability of characteristic dust states. Two specific regions are favoured locations for the frequent occurrence of dust, namely the triple point of Algeria, Mali and Niger (TP) and the border between Mali and Algeria (MAB). There is a distinct seasonal progression from dust at TP early in the season to dust at MAB later in the season, and on daily timescales there is a one-way transition from dust at the TP to dust at the MAB and then to reduced dust presence. While the Sahara is the location of the planet's largest dust loadings in the boreal summer, the dominant dust state is one of low dust occurrence, which occurs over 21 % of the time between JJA 2004-2010. Combined with the other 2 lowest dust states, this figure raises to over 42 %. Years of greater dustiness (2004-2006) occur consecutively, as do years of relatively low dust occurrence.

The dust states produced by the classification scheme map on closely to features of the broad scale circulation known to drive dust emission. Monsoon surges into the Saharan heat low constitute the ingredients for widespread and long-lived events. Circulation dominated by strong Harmattan winds on the other hand corresponds to relatively less dusty conditions. The frequency with which dust is detected over the

CWS, and the location of the dust, is thus highly sensitive to variability in the West African Monsoon, of which there are several known modes on intraseasonal to interannual timescales with a range of different controls [*Janicot et al.*, 2011; *Rodriquez-Fonseca et al.*, 2011; *Rowell,* 2003].

5.7. References

Ashpole, I., and R. Washington (2012), An automated dust detection using SEVIRI: A multiyear climatology of summertime dustiness in the central and western Sahara, *Journal of Geophysical Research*, *117*(D8), D08202, doi:10.1029/2011JD016845.

Ashpole, I., Washington, R. (in press), A new high-resolution central and western Saharan summer time dust source map from automated satellite dust plume tracking, *Journal of Geophysical Research*, doi:2012JD019355.

Brindley, H., P. Knippertz, C. Ryder, and I. Ashpole (2012), A critical evaluation of the ability of the Spinning Enhanced Visible and Infrared Imager (SEVIRI) thermal infrared red-green-blue rendering to identify dust events: Theoretical analysis, *Journal of Geophysical Research*, *117*(D7), D07201, doi:10.1029/2011JD017326.

Chauvin, F., R. Roehrig, and J.-P. Lafore (2010), Intraseasonal Variability of the Saharan Heat Low and Its Link with Midlatitudes, *Journal of Climate*, *23*(10), 2544–2561, doi:10.1175/2010JCLI3093.1.

Couvreux, F., F. Guichard, O. Bock, B. Campistron, J.-P. Lafore, and J.-L. Redelsperger (2010), Synoptic variability of the monsoon flux over West Africa prior to the onset, *Quarterly Journal of the Royal Meteorological Society*, *136*(S1), 159–173, doi:10.1002/qj.473.

Cuesta, J., J. H. Marsham, D. J. Parker, and C. Flamant (2009), Dynamical mechanisms controlling the vertical redistribution of dust and the thermodynamic structure of the West Saharan atmospheric boundary layer during summer, *Atmospheric Science Letters*, doi:10.1002/asl.

Dee, D. P., S. M. Uppala, A. J. Simmons, P. Berrisford, P. Poli, S. Kobayashi, U. Andrae, M. A. Balmaseda, G. Balsamo, P. Bauer, P. Bechtold, A. C. M. Beljaars, L. van de Berg, J. Bidlot, N. Bormann, C. Delsol, R. dragani, M. Fuentes, A. J. Geer, L. Haimberger, S. B. Healy, H. Hersbach, E. V. Holm, L. Isaksen, P. Kallberg, M. Kohler, M. Marticardi, A. P. McNally, B. M. Monge-Sanz, J.-J. Morcrette, B.-K. Park, C. Peubey, P. de Rosnay, C. Tavolato, J.-N. Thepaut, and F. Vitart (2011), The ERA-Interim reanalysis: configuration and performance of the data assimilation system, *Quarterly Journal of the Royal Meteorological Society*, *137*(656), 553–597, doi:10.1002/qj.828.

Dunion, J. P., and C. S. Velden (2004), The Impact of the Saharan Air Layer on Atlantic Tropical Cyclone Activity, *Bulletin of the American Meteorological Society*, *85*(3), 353–365, doi:10.1175/BAMS-85-3-353.

Engelstaedter, S., and R. Washington (2007), Atmospheric controls on the annual cycle of North African dust, *Journal of Geophysical Research*, *112*(D3), D03103, doi:10.1029/2006JD007195.

Fink, A. H., and A. Reiner (2003), Spatiotemporal variability of the relation between African Easterly Waves and West African Squall Lines in 1998 and 1999, *Journal of Geophysical Research*, *108*(D11), 4332, doi:10.1029/2002JD002816.

Haywood, J. M., R. P. Allan, I. Culverwell, T. Slingo, S. Milton, J. Edwards, and N. Clerbaux (2005), Can desert dust explain the outgoing longwave radiation anomaly over the Sahara during July 2003?, *Journal of Geophysical Research*, *110*(D5), D05105, doi:10.1029/2004JD005232.

Hewitson, B. C., and R. G. Crane (2002), Self-organizing maps : applications to synoptic climatology, *Climate Research*, *22*, 13–26.

Hewitson, B. C., and R. G. Crane (2006), Consensus between GCM climate change projections with empirical downscaling: precipitation downscaling over South Africa, *International Journal of Climatology*, *26*(10), 1315–1337, doi:10.1002/joc.1314.

Janicot, S., F. Mounier, S. Gervois, B. Sultan, and G. N. Kiladis (2010), The Dynamics of the West African Monsoon. Part V: The Detection and Role of the Dominant Modes of Convectively Coupled Equatorial Rossby Waves, *Journal of Climate*, *23*(14), 4005–4024, doi:10.1175/2010JCLI3221.1.

Janicot, S. G. Caniaux, F. Chauvin, G. de Coetlogon, B. Fontaine, N. Hall, G. Kiladis, J.-P. Lafore, C. Lavaysse, S. L. Lavender, S. Leroux, R. Marteau, F. Mounier, N. Philippon, R. Roehrig, B. Sultan and C.M.Taylor (2011), Intraseasonal variability of the West African monsoon, *Atmospheric Science Letters*, *12*(1), 58–66, doi:10.1002/asl.280.

Kiladis, G. N., C. D. Thorncroft, and N. M. J. Hall (2006), Three-Dimensional Structure and Dynamics of African Easterly Waves. Part I: Observations, *Journal of the Atmospheric Sciences*, *63*(9), 2212–2230, doi:10.1175/JAS3741.1.

Knippertz, P., and M. C. Todd (2010), The central west Saharan dust hot spot and its relation to African easterly waves and extratropical disturbances, *Journal of Geophysical Research*, *115*(D12), D12117, doi:10.1029/2009JD012819.

Kohonen, T. (2001), *Self-Organizing Maps*, 3rd ed., Springer, Berlin.

Kohonen, T., Hynninen, J., Kangas, J., Laaksonen, J. (1995), *SOM_PAK, The self-organizing map program package, version 3.1*.

Lavaysse, C., C. Flamant, S. Janicot, D. J. Parker, J.-P. Lafore, B. Sultan, and J. Pelon (2009), Seasonal evolution of the West African heat low: a climatological perspective, *Climate Dynamics*, *33*(2-3), 313–330, doi:10.1007/s00382-009-0553-4.

Lavaysse, C., C. Flamant, S. Janicot, and P. Knippertz (2010a), Links between African easterly waves, midlatitude circulation and intraseasonal pulsations of the West African heat low, *Quarterly Journal of the Royal Meteorological Society*, *136*(S1), 141–158, doi:10.1002/qj.555.

Lavaysse, C., C. Flamant, and S. Janicot (2010b), Regional-scale convection patterns during strong and weak phases of the Saharan heat low, *Atmospheric Science Letters*, *11*(4), 255–264, doi:10.1002/asl.284.

Lavaysse, C., J.-P. Chaboureau, and C. Flamant (2011), Dust impact on the West African heat low in summertime, *Quarterly Journal of the Royal Meteorological Society*, *137*(658), 1227–1240, doi:10.1002/qj.844.

Lensky, I. M., and D. Rosenfeld (2008), and Physics Clouds-Aerosols-Precipitation Satellite Analysis Tool (CAPSAT), *Atmos. Chem. Phys.*, (1998), 6739–6753.

Mahowald, N. M., S. Kloster, S. Engelstaedter, J. K. Moore, S. Mukhopadhyay, J. R. McConnell, S. Albani, S. C. Doney, A. Bhattacharya, M. A. J. Curran, M. G. Flanner, F. M. Hoffman, D. M. Lawrence, K. Lindsay, P. A. Mayewski, J. Neff, D. Rothenberg, E. Thomas, P. E. Thornton, and C. S. Zender (2010), Observed 20th

century desert dust variability: impact on climate and biogeochemistry, *Atmosphere, Chemistry and Physics*, *10*(22), 10875–10893, doi:10.5194/acp-10-10875-2010.

Marsham, J. H., D. J. Parker, C. M. Grams, C. M. Taylor, and J. M. Haywood (2008), Uplift of Saharan dust south of the intertropical discontinuity, *Journal of Geophysical Research*, *113*(D21), D21102, doi:10.1029/2008JD009844.

Marsham, J. H., P. Knippertz, N. S. Dixon, D. J. Parker, and G. M. S. Lister (2011), The importance of the representation of deep convection for modeled dust-generating winds over West Africa during summer, *Geophysical Research Letters*, *38*(16), L16803, doi:10.1029/2011GL048368.

Marsham, J.H., Hobby, M., Allen, C.J.T., Banks, J.R., Bart, M., Brooks, B.J., Cavazos-Guerra, C., Engelstaedter, S., Gascoyne, M., Lima, A.R., Martins, J.V., McQuaid, J.B., O'Leary, A., Ouchene, B., Ouladichir, A., Parker, D.J., Saci, A., Salah-Ferroudj, R. (2013), Meteorology and dust in the central Sahara: Observations from Fennec supersite-1 during the June 2011 Intensive Observation Period, *Journal of Geophysical Research*, doi:10.1002/jgrd.50211.

Matthews, A. J. (2004), Intraseasonal Variability over Tropical Africa during Northern Summer, *Journal of Climate*, *17*, 2427–2440.

Mcfiggans, G., P. Artaxo, U. Baltensperger, H. Coe, M. C. Facchini, G. Feingold, S. Fuzzi, M. Gysel, A. Laaksonen, U. Lohmann, T. F. Mentel, D. M. Murphy, C. D. O'Dowd, J. R. Snider, and E. Weingartner (2006), The effect of physical and chemical aerosol properties on warm cloud droplet activation, *Atmophere, Chemistry and Physics.*, *6*, 2593–2649.

Mounier, F., S. Janicot, and G. N. Kiladis (2008), The West African Monsoon Dynamics. Part III: The Quasi-Biweekly Zonal Dipole, *Journal of Climate*, *21*(9), 1911–1928, doi:10.1175/2007JCLI1706.1.

Prospero, J.M., Ginoux, P., Torres, O., Nicholson, S.E., Gill, T. E. (2002), Environmental characterization of global sources of atmospheric soil dust identified with the NIMBUS 7 Total Ozone Mapping Spectrometer (TOMS) absorbing aerosol product, *Reviews of Geophysics*, *40*(1), 1002, doi:10.1029/2000RG000095.

Reusch, D. B., and R. B. Alley (2007), Antarctic sea ice: a self-organizing map-based perspective, *Annals of Glaciology*, *46*(1), 391–396, doi:10.3189/172756407782871549.

Rodríguez-Fonseca, B., S. Janicot, E. Mohino, T. Losada, J. Bader,C. Caminade, F. Chauvin, B. Fontaine, J. Garcıa-Serrano, S. Gervois, M. Joly, I. Polo, P. Ruti, P. Roucou, and A. Voldoire (2011), Interannual and decadal SST-forced responses of the West African monsoon, *Atmospheric Science Letters*, *12*(1), 67–74, doi:10.1002/asl.308.

Rodwell, M. J., and T. Jung (2008), Understanding the local and global impacts of model physics changes : An aerosol example, *Quarterly Journal of the Royal Meteorological Society*, *134*, 1479–1497, doi:10.1002/qj.

Rowell, D. P. (2003), The Impact of Mediterranean SSTs on the Sahelian Rainfall Season, *Journal of Climate*, *16*, 849–862.

Schepanski, K., I. Tegen, M. C. Todd, B. Heinold, G. Bönisch, B. Laurent, and A. Macke (2009), Meteorological processes forcing Saharan dust emission inferred from MSG-SEVIRI observations of subdaily dust source activation and numerical models, *Journal of Geophysical Research*, *114*(D10201), doi:10.1029/2008JD010325.

Sultan, B., S. Janicot, and A. Diedhiou (2003), The West African Monsoon Dynamics . Part I : Documentation of Intraseasonal Variability, *Journal of Climate*, *16*(21), 3389–3406.

Thorncroft, C., and K. Hodges (2000), African Easterly Wave Variability and Its Relationship to Atlantic Tropical Cyclone Activity, *Journal of Climate*, *14*, 1166–1179.

Vizy, E. K., and K. H. Cook (2009), A mechanism for African monsoon breaks: Mediterranean cold air surges, *Journal of Geophysical Research*, *114*(D1), D01104, doi:10.1029/2008JD010654.

Washington, R., M. Todd, N. J. Middleton, and A. S. Goudie (2003), Dust-Storm Source Areas Determined by the Total Ozone Monitoring Spectrometer and Surface Observations, *Annals of the Association of American Geographers*, *93*(2), 297–313.

Chapter 6

Circulation controls on interannual variability in central and western Saharan summertime dust presence

Ian Ashpole and Richard Washington

Submitted to *Climate Dynamics*

Abstract

We use high temporal resolution (15-minute) satellite observations of dust presence over the central and western Sahara (CWS) for the period June-August 2004-2010 to identify reasons for interannual variability in dust coverage. The dustiest year (2005) is characterised by an increase in dust presence of almost 10 days compared to the least dusty year (2008). A considerable proportion of the difference between the two years is due to a series of 3 exceptionally large peaks in dust presence in 2005, that each last for several days. Using detailed case studies, we compare these 3 periods of prolonged dustiness in 2005 to the 3 dustiest periods in 2008 and identify the midtropospheric (700hPa) circulation as a key control on the residence time of dust in the atmosphere over the CWS. When this flow is northeasterly, it acts to transport dust that is mixed vertically through the atmosphere following emission towards the south/southwest and away from the Sahara. When calm winds or weak easterlies/southerlies overly the CWS, dust is able to remain in suspension above the region for much longer, often several days, until northeasterly flow is re-established. The nature of the midtropospheric flow is dictated by the strength and location of the anticyclone present at these levels, which

shows strong interactions with the midlatitudes. We therefore argue that the midtropospheric circulation is an important control on the atmospheric dust budget of the CWS that needs consideration, in addition to emission controls, when identifying reasons for variability in dustiness over the Sahara.

6.1. Introduction

Vast quantities of mineral dust are transported from the world's arid regions, with important consequences for terrestrial [*Koren et al.,* 2006] and oceanic ecosystems when deposited [*Jickells et al.,* 2005] and air quality when present in the human realm [*Prospero*, 1999]. In the atmosphere, dust aerosol interacts directly with solar and terrestrial radiation [*Miller and Tegen*, 1998], modifying the radiation budget [*Haywood et al.*, 2005] and ultimately influencing atmospheric dynamics via radiative heating and decreasing both land and sea surface temperatures [*Haywood et al.*, 2003; 2005]. Atmospheric dust also modifies cloud properties, with consequent indirect impacts on the radiation budget [*McFiggans et al.,* 2006]. Through these effects, dust can have important consequences for regional weather systems both close to and far from source [*Lavaysse et al.*, 2011; *Dunion and Velden*, 2004] and the global atmospheric circulation [*Rodwell and Jung*, 2008]. Research into processes occurring in dust source regions has therefore burgeoned over the past decade.

During the boreal summer, the global dust burden is dominated by the central and western Sahara (CWS) [*Engelstaedter et al.*, 2006; *Washington et al.,* 2003; *Prospero et al.,* 2002]. Dust emission is driven predominantly by low-level jets (LLJs) occurring in both the dry northeasterly Harmattan flow and the moist southwesterlies of the West African Monsoon (WAM); and by episodic cold pool outflow from convective

complexes, particularly in the south of the region (see *Marsham et al.* [2013], *Allen et al.* [2013], and references therein for an overview). Once airborne, dust is mixed vertically through the deep Saharan boundary layer [*Cuesta et al.*, 2009] and is usually transported westward over the Atlantic within the Saharan Air Layer, often reaching the Americas.

It is important to understand how and why atmospheric dust loadings vary on a range of timescales in order to better constrain simulations of the future dust burden, given its demonstrable climatic importance [*Mahowald et al.* 2006; 2010]. Interannual variability in CWS dustiness has received little attention to date. Sahelian rainfall and the North Atlantic Oscillation are thought to play a role [e.g. *Prospero and Lamb*, 2003; *Chiapello et al.*, 2005], but a reliance on data collected distant from source (i.e. at Barbados in the case of *Prospero and Lamb* [2003]) or time-averaged once-daily satellite observations has possibly prevented a thorough analysis of the processes occurring close to source.

The 15-minute temporal resolution of the Spinning Enhanced Visible and Infrared Imager (SEVIRI), carried onboard geostationary Meteosat Second Generation satellites, makes it ideally suited to monitoring CWS dust dynamics. Crucially, it enables differentiation between dust that is freshly emitted and dust that has been present in the atmosphere for several hours or days [*Ashpole and Washington*, 2013], a distinction that is not possible using data derived from polar-orbitting satellites that offer, at most, 2 observations per day. This offers a new dimension to the analysis of the mechanisms that create this summertime dust hotspot. The presence – or absence – of atmospheric dust over the CWS is a function of both the surface winds responsible for its emission and the circulation higher up in the Saharan atmosphere that is responsible for its transport away from the region. While much research has focussed on the former, the latter has received little attention. It has recently been demonstrated that years experiencing a greater

number of dust source activations are not necessarily dustier than those with less individual dust events [*Tegen et al.*, 2013]. Processes influencing the transport of dust away from source regions therefore deserve attention, since they can clearly impact time-averaged measures of dustiness.

Ashpole and Washington [2012] outlines a method to detect objectively the presence of dust in SEVIRI data, and demonstrates that the frequency with which dust is detected over the CWS varies substantially on an interannual basis between the summers of 2004 and 2010 inclusive. In this paper, we compare the summers with highest (2005) and lowest (2008) dust detection frequency and demonstrate that the key difference is the occurrence of several multi-day periods in 2005 that are characterised by the prolonged presence of atmospheric dust over the CWS following large emission events. We link this persistent dust presence to features of the large-scale atmospheric circulation by comparison with periods in 2008 that evolve in a similar manner but in which the dust does not remain in suspension over the CWS for as long. The layout of this paper is as follows: In Section 6.2, the data and methods used are presented; Section 6.3 addresses interannual variability in CWS dust presence frequency and demonstrates that the key difference between extreme years is the occurrence of 3 multi-day periods characterised by frequent dust coverage; Section 6.4 contains case studies of the exceptional events of 2005 and the largest events of 2008 and identifies atmospheric controls on dust duration; Section 6.5 discusses the results; and Section 6 6 summarises and concludes the study.

6.2. Data and methods

In this study we utilise high temporal resolution satellite observations of dust and cloud presence provided by SEVIRI, and combine them with information on the state of the

atmosphere provided by reanalysis data in order to identify potential climatological mechanisms that modulate atmospheric dust presence.

6.2.1. Satellite observations

Information on the presence of dust is provided by the SEVIRI Dust Flag (SDF) dataset [*Ashpole and Washington,* 2012]. These data are available every 15-minutes for June – August 2004 – 2010 on a standard latitude/longitude grid of approximately 0.03 x 0.03 degrees resolution for the broad CWS domain encompassing 18^{o} W – 16 ^{o} E, 15 ^{o} – 37.5 ^{o} N. SDF stems from the SEVIRI dust scheme imagery (see e.g. *Lensky and Rosenfeld* [2008] for a description), which has been widely used to provide qualitative information on the location of dust plumes in recent Saharan dust research. There are several known limitations with the SEVIRI dust scheme that are in turn passed to the SDF data. *Brindley et al.* [2012] demonstrates that even for high values of AOD, this scheme is sensitive to the presence of atmospheric water vapour, the altitude of the dust layer, and the lower-tropospheric lapse rate. Dust detection at nighttime is also difficult owing to similarities in the infrared signal of the desert background and dust (see *Ashpole and Washington* [2012] for further details).

In addition to the detection of dust, we also use SEVIRI data to detect the presence of convective complexes in the study region. These appear as deep red features in the SEVIRI dust scheme. Deep convection is detected by application of a brightness temperature (BT) threshold of ≤ 270 K to the 10.8 μm channel, as applied in previous studies to identify the presence of deep convection [e.g. *Ashpole and Washington*, 2013; *Lavaysse et al.,* 2009].

We also employ daily Level 3 Ozone Mapping Instrument (OMI) Absorbing Aerosol Index (AAI) data for June – August 2005 – 2009 at 1 x 1 degree resolution for

verification of the degree of interannual variability in dust presence. We only consider AAI > 4, which provides the closest match to SDF [*Ashpole and Washington*, 2012].

6.2.2. Reanalysis data

Information on the state of the atmosphere is obtained from the European Centre for Medium Range Weather Forecasts (ECMWF) ERA Interim (ERA-I) reanalysis, horizontal resolution 0.75 x 0.75 degrees [*Dee et al.*, 2011].

We employ the heat low detection scheme detailed by *Lavaysse et al.* [2009] in order to monitor the location of the Saharan Heat Low (SHL). This is based on measurements of low-level atmospheric thickness (LLAT) – the difference between the geopotential heights at 700 and 925 hPa – which reflects the dilation of the lower atmospheric levels induced by heating. *Lavaysse et al.* [2009] defines grid points with the 10 % highest LLAT values over the broad West African area [20 W–30 E, 0–40 N] as the heat low. In this study we employ a slightly stricter threshold of the top 5 % of the cumulative distribution of LLAT values, which enables the detection of well-defined heat low areas, but we note that results are largely insensitive to the threshold applied.

6.3. Interannual variability in summertime dust presence

There is a considerable degree of interannual variability in SDF frequency (SDFF) over the CWS during the period June-august 2004-2010 (Figure 6.1). This signal is clearly not a result of increased deep convective coverage over the dust hotspot region of southern Algeria-northern Mali during the less dusty years, since it would be expected that less frequent dust coverage here would be matched by more frequent cloud coverage – which is not the case.

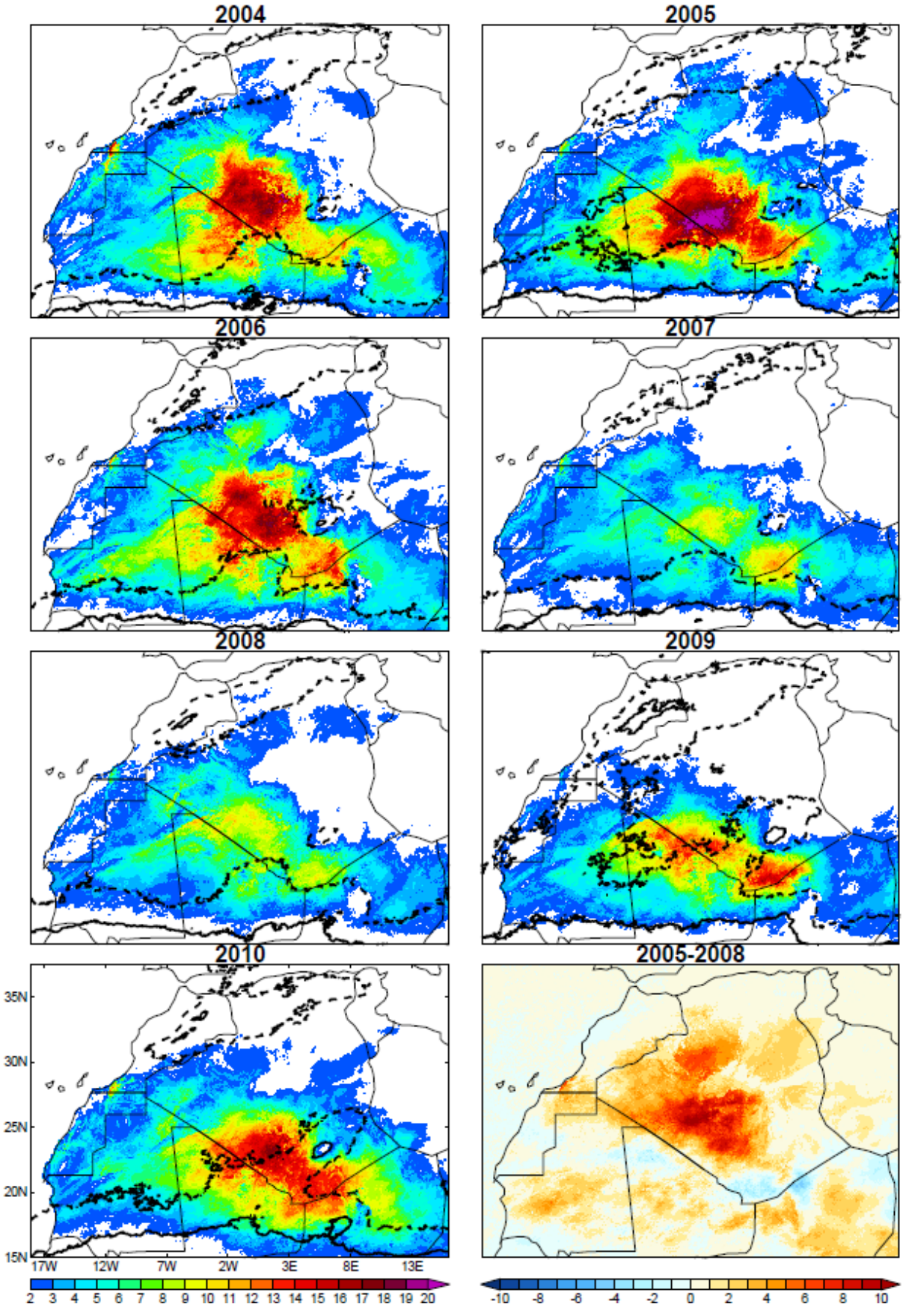
2004
2005
2006
2007
2008
2009
2010
2005-2008
35N
30N
25N
20N
15N
17W
12W
7W
2W
3E
8E
13E
2 3 4 5 6 7 8 9 10 11 12 13 14 15 16 17 18 19 20
-10 -8 -6 -4 -2 0 2 4 6 8 10

Figure 6.1. (previous page) SDFF as % of total SEVIRI time steps for June – August period for each year from 2004 – 2010. White areas correspond to < 2 %. Solid black line (dotted black line) = 20 % (10 %) frequency of occurrence of deep convection contour for same period and same time steps. Bottom right panel = SDFF 2005 – SDFF 2008, shading corresponds to days.

Maximum SDFF in the dust hotspot area of southern Algeria/northern Mali peaks at 23.2 % in 2005 (i.e. dust is detected in this location on almost a quarter of all available SEVIRI timesteps between June and August), and is at a minima of 12.5 % in 2008. This corresponds to an increase in dust presence of almost 10 days during the summer of 2005 compared to the summer of 2008 (Figure 6.1, bottom right). To check for the sensor-dependence of this result, we compare the detection frequency of OMI AAI > 4 over this region for these 2 years and find a similar degree of difference (a maximum frequency of 31 in 2005 vs 19 in 2008; note that OMI only provides one observation per day, in the early afternoon, so we would not necessarily expect the overall magnitude of these values to be the same as SDFF). This is therefore a robust pattern, and we chose to compare these 2 extreme years in order to identify reasons for the large difference in dustiness.

The majority of the difference in dust presence between 2005 and 2008 is down to a series of 3 exceptionally large and long-lived (for the period in consideration) peaks in daily SDFF in 2005, occurring in late June – mid July (Figure 6.2). The mean daily percentage of potential SDFs flagged as dust in 2005 is almost 60 % greater than that of 2008 (3.96 % vs 2.48 %), while this drops to 28 % if the 3 anomalous peaks are removed from the 2005 timeseries (3.18 % vs 2.48 %). These 3 peaks thus explain over half of the difference between the two extreme years and account for over 35 % of total mean daily SDFs present in 2005. Had they been of similar magnitude to the rest of the peaks in dust

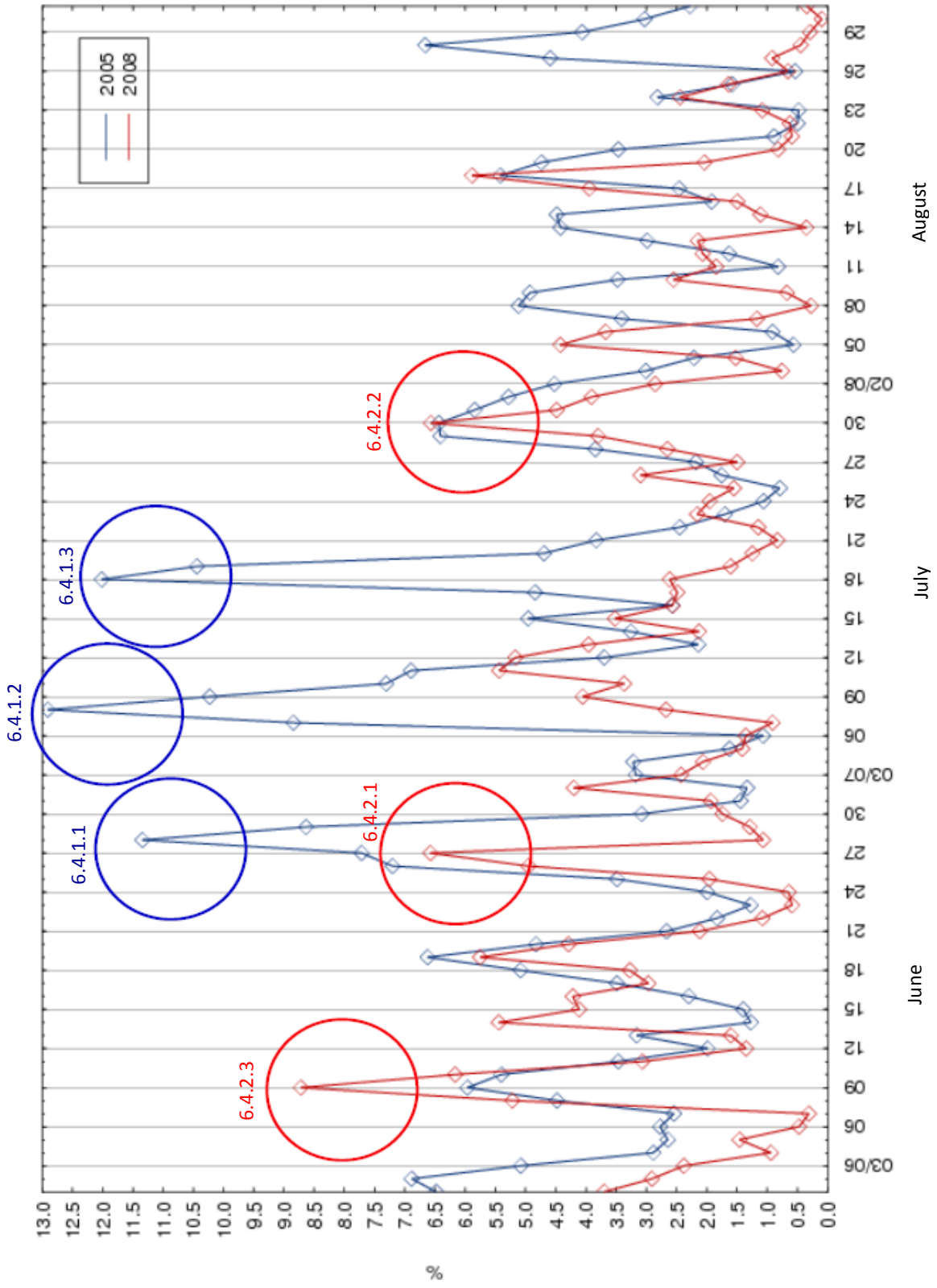

Figure 6.2. Daily dust presence timeseries'. Scale = mean daily percentage of potential SDFs flagged as dust, blue line = 2005, red line = 2008. Case study periods of Section 6.4 circled in blue (red) for 2005 (2008).

presence, 2005 would not have been a standout summer (although it would still have been dustier than 2008).

6.4. Case studies

In the following section we examine the three anomalously large dust peaks of 2005 and compare them to the three largest to occur in 2008 in order to establish why those of 2005 were so much larger (the peaks that are studied are circled on Figure 6.2). We use daily fields of SDFF and deep convection flag frequency to highlight the location and persistence of dust and convective complexes respectively. Mid-tropospheric (700hPa) geopotential height and wind fields are used to identify potential circulation controls on the transport of dust once it is mixed vertically by dry convection in the Saharan atmosphere.

6.4.1. Anomalous dust events from the dustiest year

6.4.1.1. 26 – 29th June 2005

On the 26th June a near permanent blanket of dust is present along the Algeria-Mali border west of around 2^{o} E and in central Mauritania (Figure 6.3a). The dust is the result of large-scale convectively-driven emission early on the 25th (overnight from the 25th-26th) from the Algeria-Mali-Niger border triple point region (the Algeria-Mali border) that is slowly spread to the west. Some dust is recirculated east late in the day towards central southern Algeria, where the SHL is consistently detected throughout this period. Further emission overnight from the 26th – 27th from southern Algeria and northern Mali,

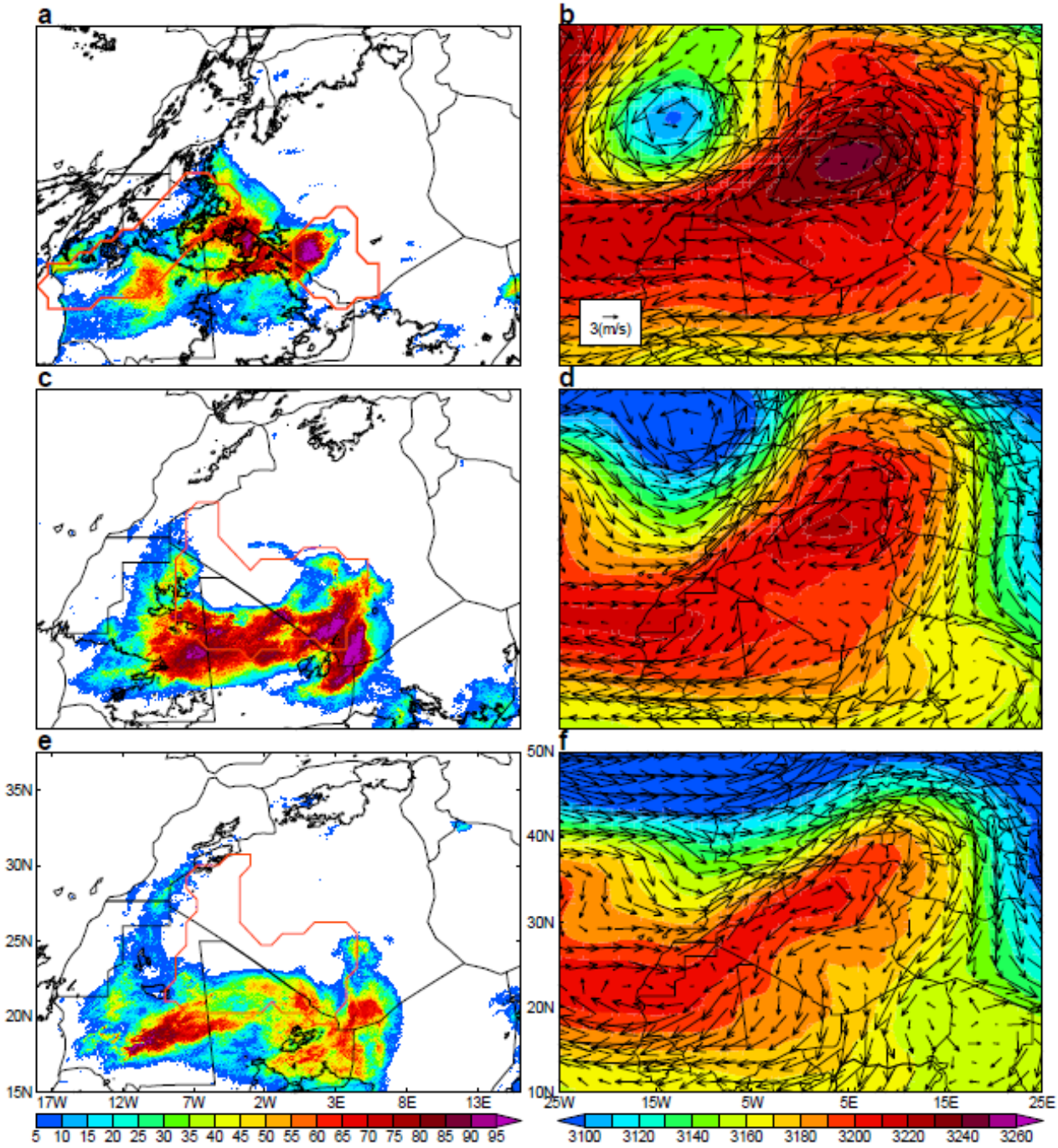

Figure 6.3. Distribution of dust and deep convection and circulation features for 26th June 2005 (**a,b)**, 28th June 2005 (**c,d)** and 29th June 2005 **(e,f)**. **a, c, e:** Daily SDFF (shading) as % of total time steps (96), white areas correspond to < 5 %; 20 % frequency of occurrence of deep convection contour (solid black line); SHL location (orange line). **b, d, f:** 700 hPa geopotential height in m (shading) and winds (vectors).

again linked to deep convection, contributes additional dust to the already dust laden CWS atmosphere. On the 27th and 28th, a large, relatively stationary body of dust remains suspended over southern Algeria and northern Mali, coincident with the southern part of the SHL (Figure 6.3c). The dust plume persists until the 29th but is slowly tending towards the south/southwest (Figure 6.3e), and by the 30th the CWS atmosphere is relatively clear of dust.

It is notable that the prolonged dust presence during this period is concurrent with a period of quite calm low to mid-tropospheric flow across central and southern Algeria and northern Mali, which is broadly in agreement with the transport characteristics of the dust plume (Figure 6.3b,d,e). This is because a strong anticyclone develops over the Mediterranean coast of Algeria, associated with ridging across the western Mediterranean into Europe, which acts to draw midtropospheric flow away from the dusty region to the south (Figure 6.3b,d). The anticyclone has shifted to this location from a position over westernmost Algeria, southern Morocco and Western Sahara on previous days when SDFF was lower. Related to a weakening of this anticyclone on the 28th and its retraction towards its previous location on the 29th-30th, north/northeasterly flow gains control of the region (Figure 6.3f), coincident with the southward retreat of the dust plume and declining SDFF.

6.4.1.2. 7 – 10th July 2005

In this case the dust results from a single large-scale emission event occurring during the night of 6th – 7th July, again in association with large-scale deep convection around the Algeria-Mali-Niger border triple point. The dust is transported west into central southern Algeria on the 7th (Figure 6.4a) and slowly spreads towards the north on subsequent days

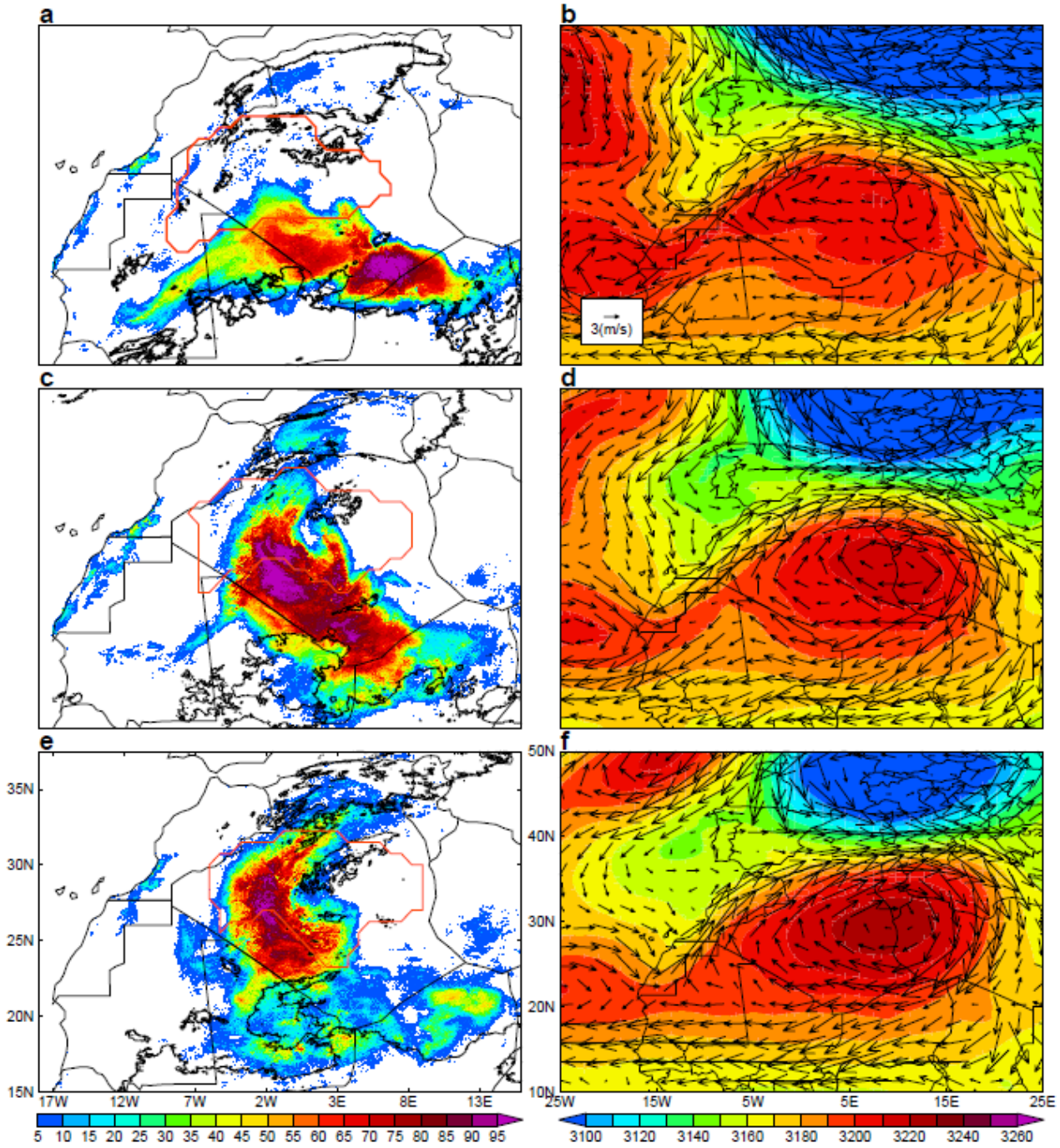

Figure 6.4. As Figure 6.3 but for 7th July 2005 **(a,b)**, 8th July 2005 **(c,d)** and 9th July 2005 **(e,f)**.

across the western half of Algeria (Figure 6.4c,e). It is interesting to note that deep convection is detected north of its preferred climatological location throughout this period and is fairly stationary, in contrast to its normal westward-transport. No further dust emission linked to this is evident, however. The SHL is located predominantly in central and northern Algeria throughout the course of this event.

The prolonged presence of dust over much of Algeria and its slow transport towards the west (north) during this event coincides with weak midtropospheric easterlies (southeasterlies) (Figure 6.4b,d,f). Controlling this flow is the development of the Saharan anticyclone on the Algeria/Libya border, its intensification marking the change from easterly towards southerly flow. As in Case 6.4.1.1, this has migrated away from a location extending from westernmost Algeria across the Atlantic coast of southern Morocco and Western Sahara on previous days, when predominantly northerly flow overlies the CWS. Other important components of the circulation coincident with the change in location and intensification of the Saharan anticyclone include extensive ridging across the north Atlantic that stretches towards the UK (associated with a northwards extension of the Azores high) and a deep trough over central Europe, extending towards the Mediterranean coast of North Africa, which begins to fill as the Saharan anticyclone intensifies.

6.4.1.3. 17 – 20th July 2005

Reasonably widespread dust emission occurs on the morning of the 17th in very strong northeasterly flow across central and southwest Algeria (Figure 6.5a). The dust plume is relatively quickly transported towards the southwest (hence lower overall SDFF on this day compared to previous cases) reaching central Mauritania on the 18th.

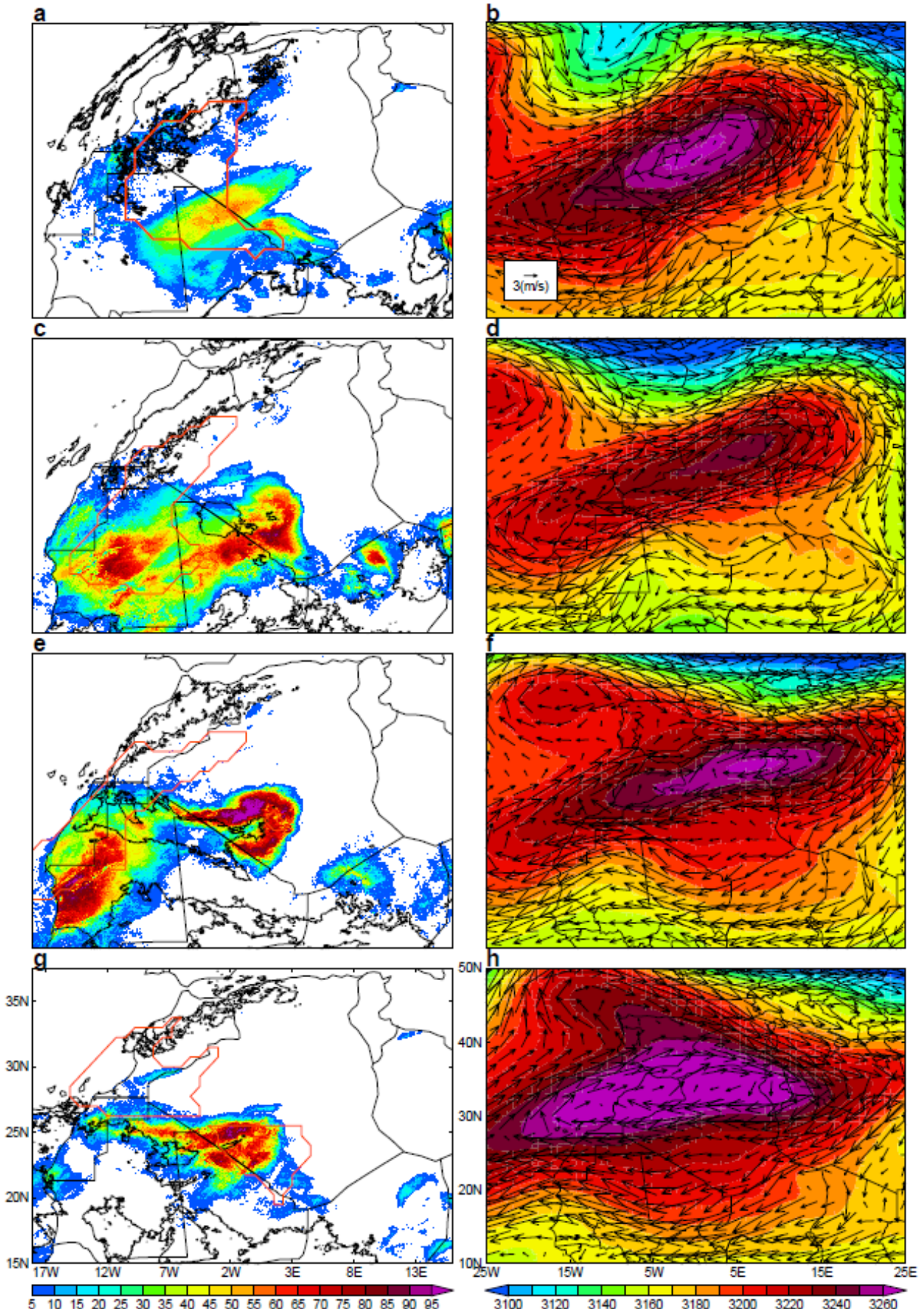
a
b
3(m/s)
c
d
e
f
g
h
35N
30N
25N
20N
15N
17W
12W
7W
2W
3E
8E
13E
5 10 15 20 25 30 35 40 45 50 55 60 65 70 75 80 85 90 95
50N
40N
30N
20N
10N
25W
15W
5W
5E
15E
25E
3100 3120 3140 3160 3180 3200 3220 3240 3260

Figure 6.5. (previous page) As Figure 6.3 but for 17th July 2005 **(a,b)**, 18th July 2005 **(c,d)**, 19th July 2005 **(e,f)** and 20th July 2005 (**g,h)**.

The northeasterlies appear to be reinforced by a Mediterranean Cold Surge [*Vizy and Cook*, 2009] at this time, which serves to ventilate the CWS and drive the SHL towards the west (Figure 6.5a,c,e). Further dust emission occurs overnight from the 17th-18th in association with deep convection drawn across northern Mali behind this cold surge. The dust is carried into southern Algeria and spread west across southern Algeria/northern Mali on the 18th (Figure 6.5c). Some of this dust is advected towards the southwest into Mauritania, where it is mixed with dust emitted the previous day and slowly transported west over the Atlantic on subsequent days, while some remains relatively stationary in south/southwest Algeria where it persists on the 19th-20th before also being transported towards the west/southwest late on 20th and into the 21st (Figure 6.5e,g).

Midtropospheric northeasterlies around an intense anticyclonic centre over northwest Algeria/Morocco dominate the CWS at the start of this event (Figure 6.5b), which are responsible for transporting much of the dust across northwest Mali and into Mauritania. From the 18th-19th the anticyclone retracts towards Tunisia, the axis of the northeasterlies is drawn north, and flow overlying south/southwest Algeria weakens and takes on a weak southerly component, coincident with the stationary part of the dust plume (Figure 6.5d,f). By the 20th the anticyclone has broadened and spread back towards the west, and relatively strong east/northeasterly flow has regained control of southern Algeria, advecting the dust towards the west/southwest (Figure 6.5h).

6.4.2. Dust events from the least dusty year

6.4.2.1. 25 – 28th June 2008

Dust emission occurs in northern Mali/southern Algeria during the evening of the 25th, driven by cold pool outflow from deep convection that develops over the area. The dust is spread west across southern Algeria on the 26th with a well-developed band of deep convection that persists well north of its preferred location (Figure 6.6a). On the 27th both the dust and the cloud are rapidly transported towards the south, with maximum SDFF values much lower, and the area of peak SDFF becoming far more fragmented, than any of the cases in 2005 (Figure 6.6c). By the 28th this dust has been removed from the CWS and the atmosphere is relatively clean (Figure 6.6e). The SHL is located far to the west of the region throughout this event, away from the climatological dust hotspot location.

There are marked differences in the midtropospheric conditions in this case compared to the 2005 cases. Of most significance to the overall dust presence, the flow is characterised by strong northeasterlies that extend across central and southern Algeria and into northern Mali throughout the course of the event (Figure 6.6b,d,f). Suspended dust is therefore relatively quickly transported towards the southwest and out of the CWS, as opposed to remaining in suspension over the region for several days. Unlike any of the anomalous cases of 2005, the Saharan anticyclone is permanently located over northwest Algeria and Morocco during this period, linked to riding over the Atlantic around the Azores region (Figure 6.6d). Central and southern Algeria is therefore coincident with the easterly flank of this circulation which brings strong northeasterly flow and efficient removal of atmospheric dust, thus limiting SDFF for the period. It is notable that, in concordance with cool northeasterly ventilation of central Algeria, the SHL favours a location towards northern Mauritania.

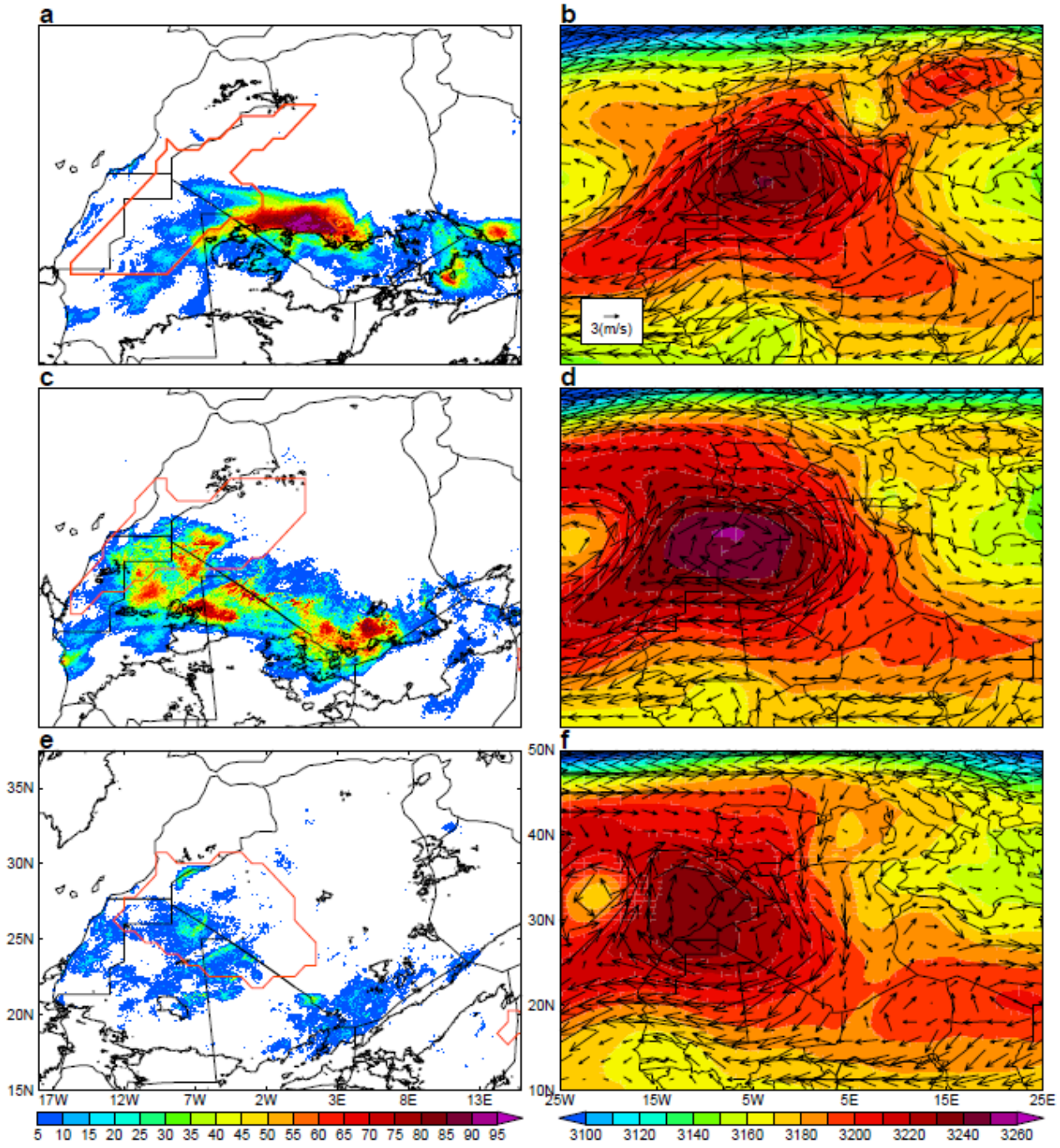

Figure 6.6. As Figure 6.3 but for 26th June 2008 **(a,b)**, 27th June 2008 **(c,d)** and 28th June 2008 **(e,f)**.

6.4.2.2. 28 – 31st July 2008

High SDFF results from convectively-driven emission occurring overnight on the 27th-28th from the Algeria-Mali-Niger border triple point region. The dust is slowly spread to the west on subsequent days, closely tied to its parent convective cells, which are present to the east of the dust plume on the 29th but have diminished by the 30th (Figure 6.7a,c). Dust presence peaks on 30th over southwest Algeria, coincident with the SHL, but declines by the 31st as the majority of the dust is either transported southwest towards Mauritania or west into Morocco (Figure 6.7e). Additional dust is emitted from central Algeria, southern Algeria and northwest Mali on the mornings of the 30th and 31st respectively, in association with a strengthening Harmattan, but this is not widespread and it is directed quickly towards the southwest.

At the beginning of this event the mid-tropospheric flow over the CWS is relatively weak and predominantly easterly around the weak anticyclone situated in northwest Algeria (Figure 6.7b). This likely explains the steady westward spreading of the dust plume following emission. On the 30th the anticyclone intensifies and on the 31st it spreads west into Morocco, associated with ridging through the Atlantic to the northwest of Africa (Figure 6.7d,f). Strong northeasterlies are therefore installed over Algeria and across northwest Mali, leading to the export of dust from the CWS atmosphere. The end of this event resembles a Mediterranean Cold Surge, but unlike the case of 6.4.1.3 the anticyclone migrates southwest through Morocco and across the Atlantic coast (in Case 6.4.1.3 it initially retracts towards Tunisia), thus maintaining strong northeasterly flow across southern Algeria and northern Mali.

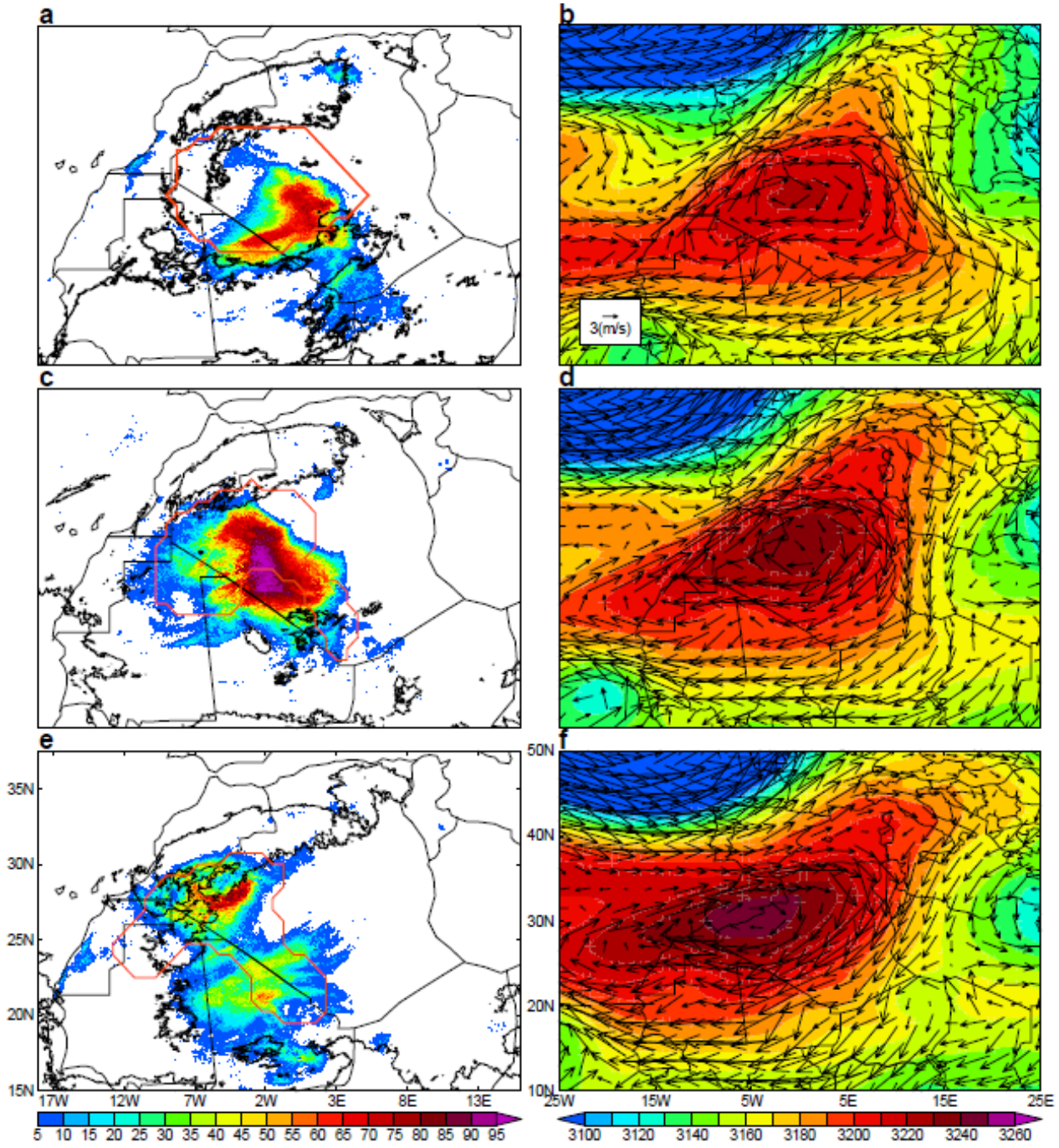

Figure 6.7. As Figure 6.3 but for 29th July 2008 **(a,b)**, 30th July 2008 **(c,d)** and 31st July 2008 **(e,f)**.

6.4.2.3. 8 – 11th June 2008

Despite being the largest dust peak of 2008, this event partly occurs beyond the eastward limit of SEVIRI data available for this study. Nonetheless, it is clear that high SDFF over eastern Niger/Chad is collocated with weak southwesterly tending midtropospheric flow, as a result of the Saharan anticyclone locating over southeastern Libya, which acts to spread dust north towards Libya on the 8th and 9th (Figure 6.8a,b). Dust is then transported west from the 10th and SDFF begins to decline, which occurs along with the arrival of strong east/northeasterlies in the dusty region as the Saharan anticyclone intensifies and migrates west into Algeria (Figure 6.8c,d). In addition to activity in the east, dust outbreaks are evident over the CWS domain on the mornings of the 9th and 10th, driven by strong westerly surface flow in western, central and northern Algeria towards the eastward-located SHL (Figure 6.8a). This is however small-scale and short lived in comparison to events to the east, and likely makes only a small contribution to the peak in SDFF evident in Figure 6.2.

6.5. Discussion

The above case studies have highlighted the midtropospheric circulation as an important control on the residence time of atmospheric dust over CWS, with implications for interannual variability in overall summer time dust presence. The midtroposphere is the key difference between the anomalous cases of 2005 (and also potentially case 6.4.2.3, as is discussed below) and the cases of 2008, with all events considered effectively evolving in the same manner – that is, dust provided to the atmosphere primarily by cold pool outflow from deep convection driving emission from sources located in the southern CWS. When the flow overlying the CWS is predominantly northeasterly, dust is

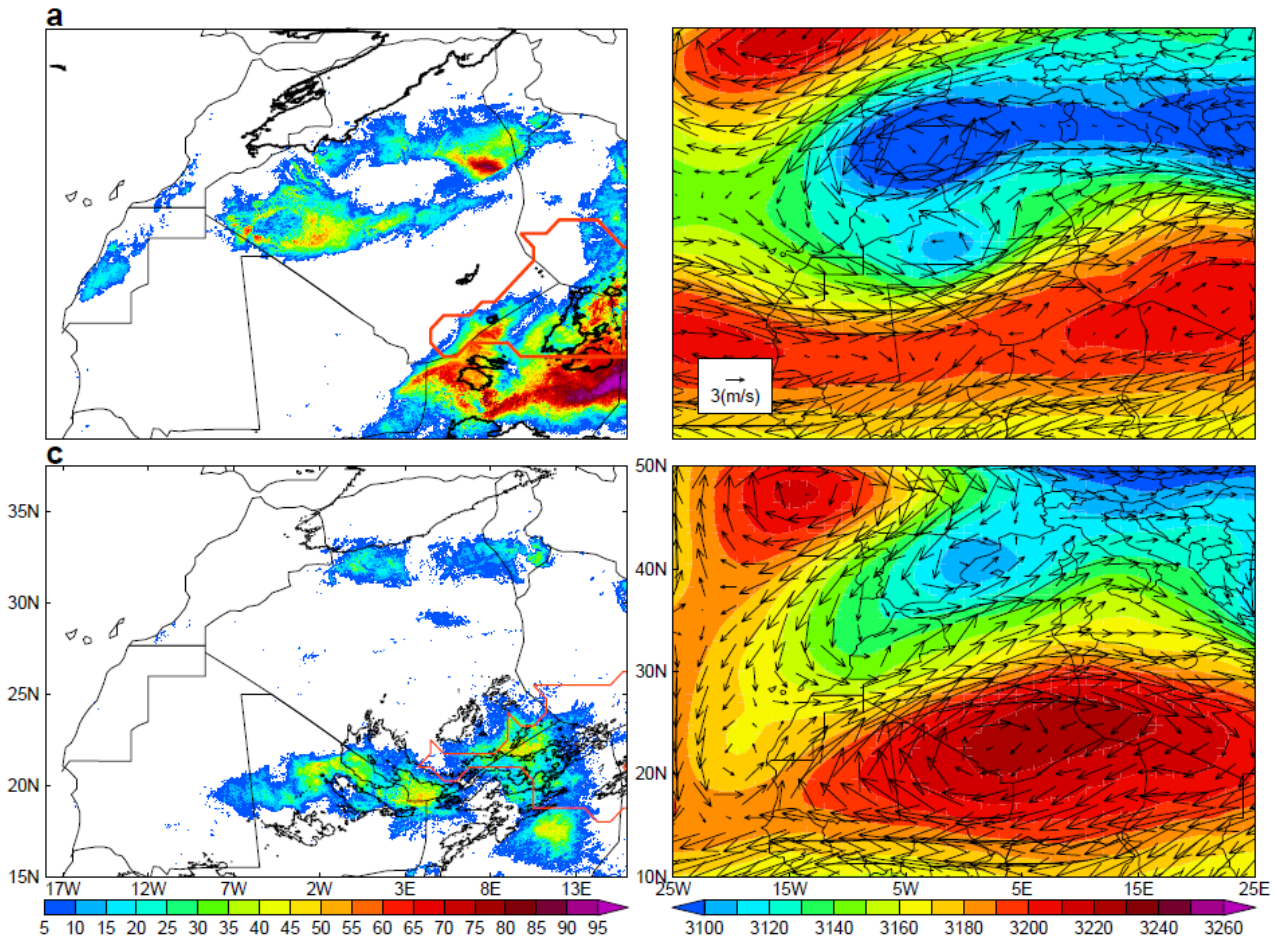

Figure 6.8. As Figure 6.3 but for 9th June 2008 **(a,b)** and 11th June 2008 **(d,e)**.

efficiently transported towards the south/southwest. When the northeasterly flow is replaced either by calm conditions or weak easterly/southerly tending flow, as in the anomalously dusty cases of 2005, the residence time of dust in the atmosphere over the CWS is prolonged, since, in lieu of efficient removal towards the southwest, it can remain in suspension here for several days until the northeasterly flow returns (Figure 6.9). These episodes of persistent dust presence explain over half of the difference in dust detection frequency between the summers of 2005 and 2008, and are responsible for making 2005 the standout summer in terms of overall dustiness for the period 2004-2010.

Northeasterly midtropospheric flow corresponds to the eastern flank of the anticyclone present over the northern Sahara. The location and intensity of this anticyclone ultimately dictates whether northeasterlies will overly the CWS or not. The climatological position of the anticyclone is over northwestern Algeria/Morocco (Figure 6.10). Consequently, midtropospheric northeasterlies are typically in place to work against the prolonged presence of dust in the CWS atmosphere by transporting it towards the southwest. In the anomalous cases the anticyclone is centred to the extreme north of Algeria or further east into Tunisia/Libya. Strong northeasterly flow is thus absent and prolonged dust presence is possible.

The question arises as to why similar events to those of 2005 did not occur in 2008. An explanation is not immediately apparent from comparison of mean summer climatologies. The dominant difference in the midtroposphere is in the midlatitudes, with strong positive geopotential anomalies stretching from the Strait of Gibraltar across western Europe and the Atlantic towards the UK, and a northwards shift of the storm tracks (Figure 6.11a). The impact that this has on midtropospheric flow over North Africa is not clear, although strong interactions between the Saharan anticyclone and the midlatitudes are evident in the case studies of Section 4. Midlatitude atmospheric

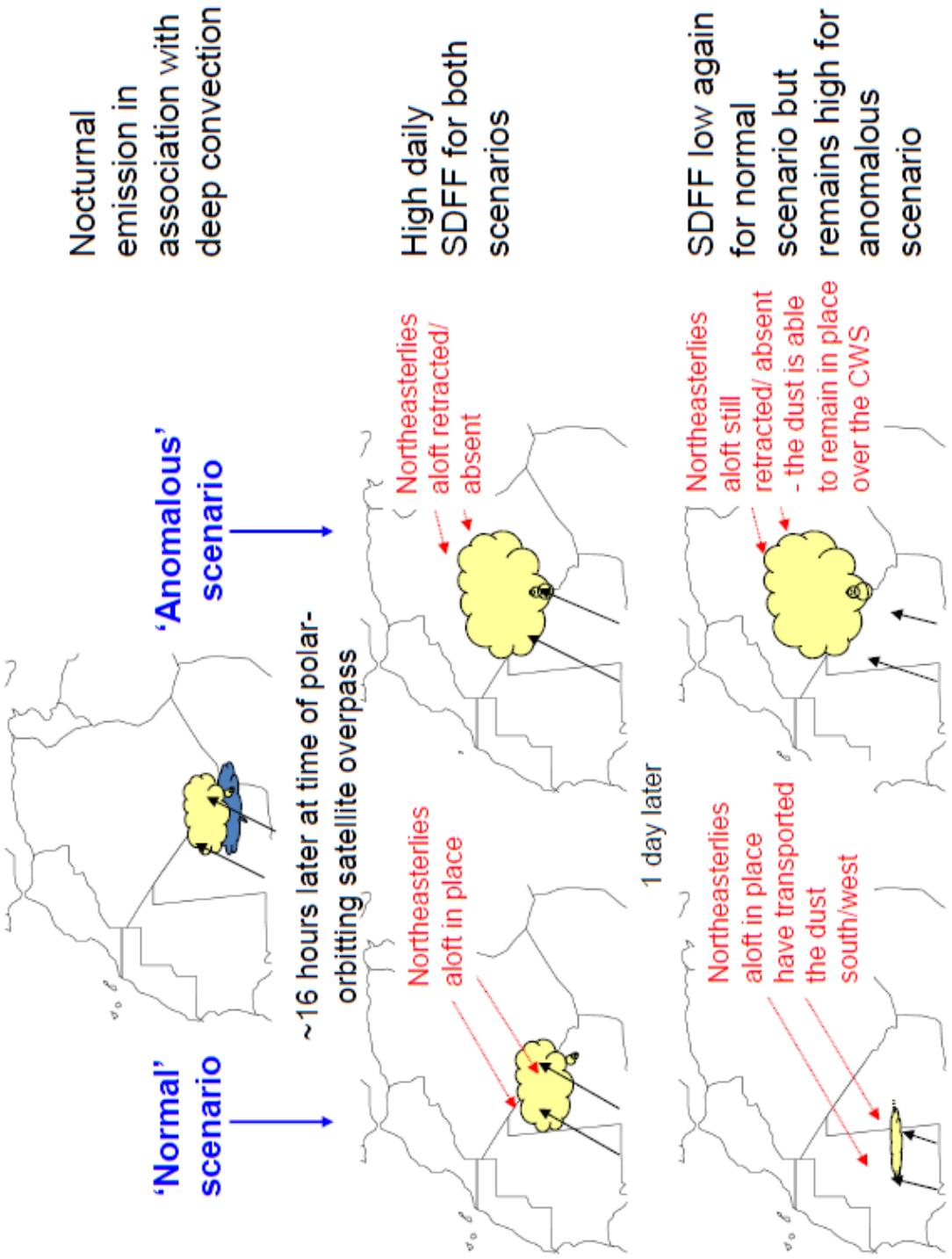

Figure 6.9. Schematic representation of midtropospheric control on the temporal evolution of CWS dust presence. Light yellow shading = dust, blue shading = deep convection, red arrows = midtropospheric winds, black arrows = monsoon flow.

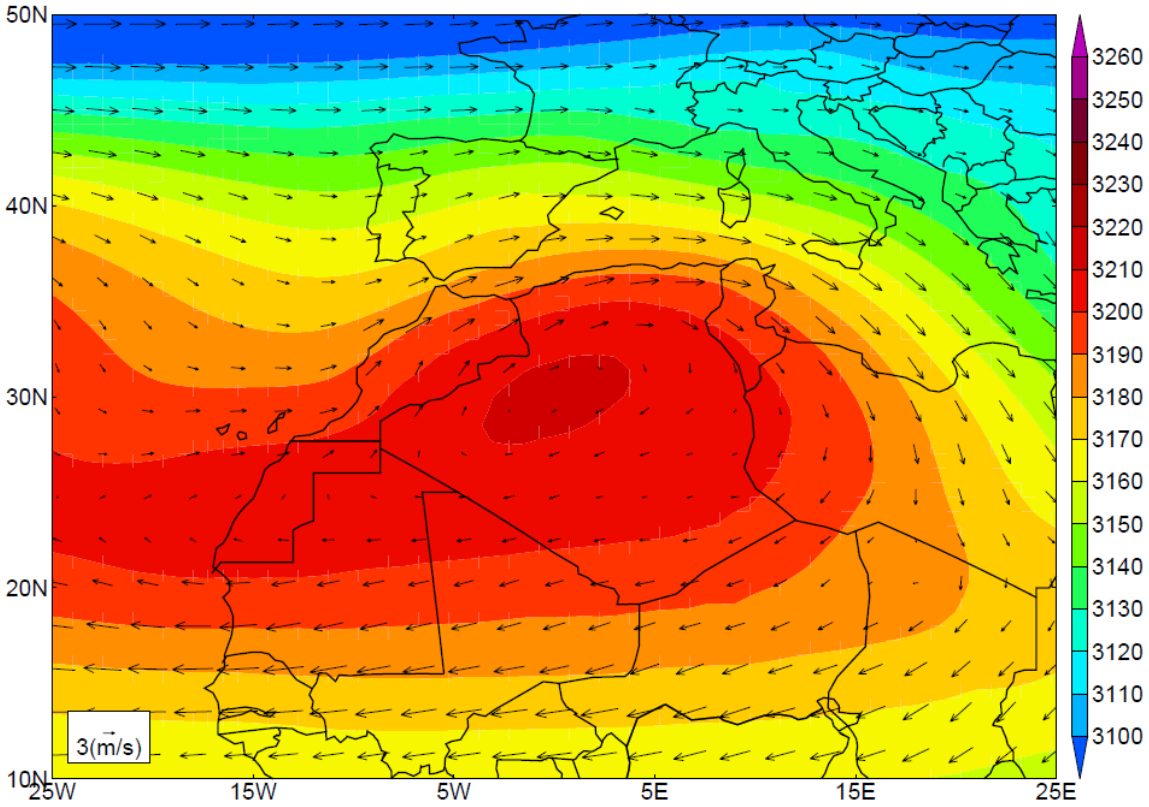

Figure 6.10. Mean 700hPa geopotential height in m (shading) and winds (vectors) for June – August 2004 – 2010.

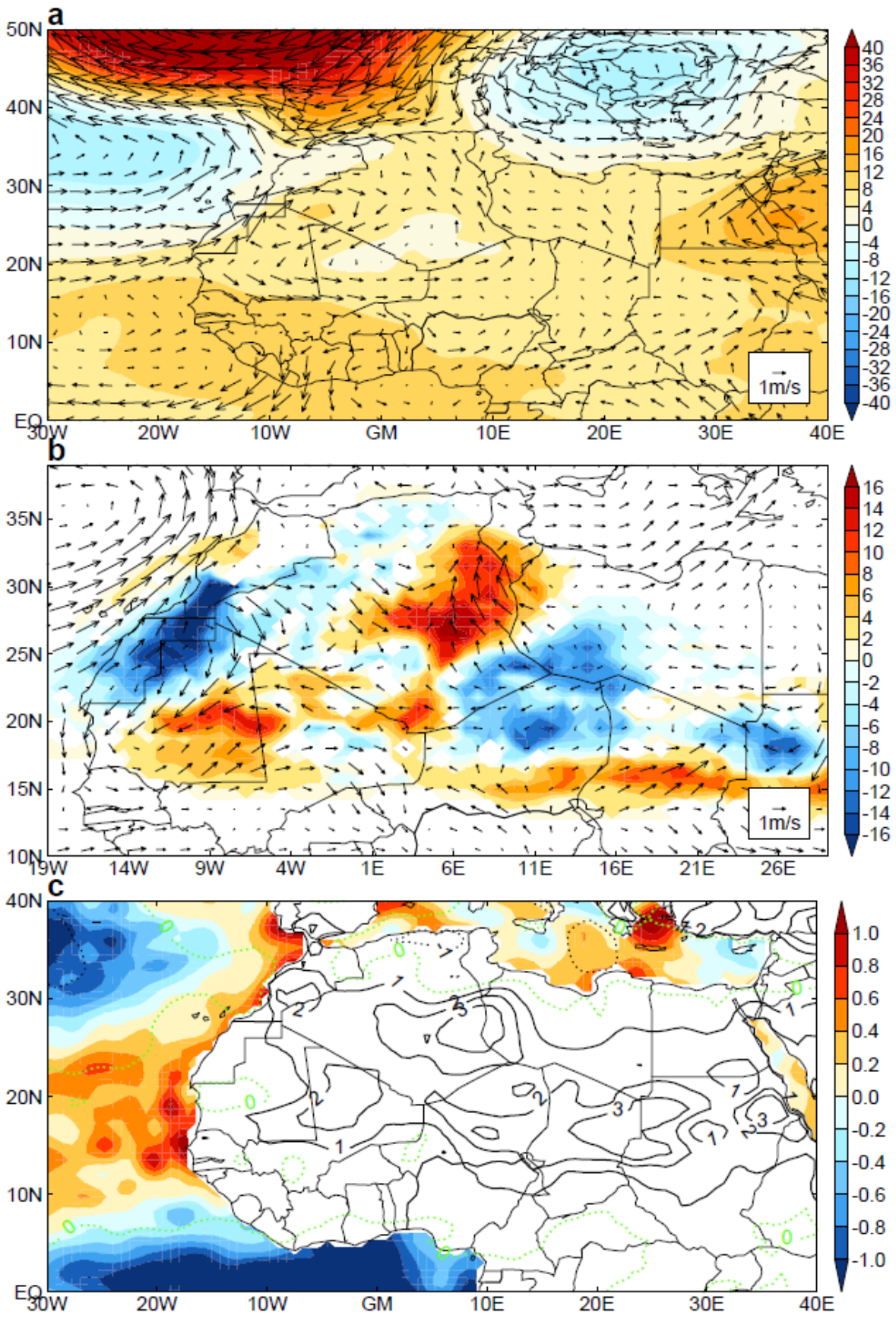
a
50N
40N
30N
20N
10N
EQ
30W
20W
10W
GM
10E
20E
30E
40E
1m/s
40
36
32
28
24
20
16
12
8
4
0
-4
-8
-12
-16
-20
-24
-28
-32
-36
-40
b
35N
30N
25N
20N
15N
10N
19W
14W
9W
4W
1E
6E
11E
16E
21E
26E
1m/s
16
14
12
10
8
6
4
2
0
-2
-4
-6
-8
-10
-12
-14
-16
c
40N
30N
20N
10N
EQ
30W
20W
10W
GM
10E
20E
30E
40E
1.0
0.8
0.6
0.4
0.2
0.0
-0.2
-0.4
-0.6
-0.8
-1.0

Figure 6.11. (previous page) Mean difference JJA2005-JJA2008 **a.** 700hPa geopotential height in m (shading) and winds (vectors); **b.** SHL detection frequency as % of days (shading) and 925 hPa winds (vectors); **c.** SST in degrees (shading) and 2-m dewpoint temperature in degrees, solid contours = 2005 higher, dotted contours = 2008 higher, green dotted contour = no difference.

---

processes are known to significantly modulate both the location and strength of the SHL via modification to the circulations that ventilate the Sahara from the Atlantic and Mediterranean sectors [*Chauvin et al.*, 2010; *Lavaysse et al.*, 2010]. It is therefore logical that this will have consequences for dust presence too, given a dependence of both emission and transport on regional wind patterns. The locational sensitivity of the SHL to northeasterly ventilation was evident in all case studies presented in Section 6.4, favouring a location in central/southern Algeria in the absence of this flow and the west of the region when it was strong. Across the whole summer period, the SHL was detected much more frequently in central Algeria in 2005 than in 2008 (Figure 6.11b), indicative of a decrease in northeasterlies over the dust hotspot region and a greater potential for prolonged dust presence. The increased detection frequency to the west in 2008 on the other hand is indicative of more persistent northeasterlies in this area and a decreased likelihood of long-lived dust plumes.

In addition, there is strong evidence for enhanced WAM activity in 2005 in Atlantic and Mediterranean sea surface temperatures [*Rodríguez-Fonseca et al.*, 2011; *Rowell*, 2003] and increased 2-m dewpoint temperatures, which indicate greater atmospheric moisture, over the whole of North Africa (Figure 6.11c). A link has been established between high daily dust detection frequency over the CWS and WAM surges, which favour the occurrence of deep convection over the southern Sahara where strong

outflows can initiate large-scale dust emission [*Ashpole and Washington*, submitted]. A stronger WAM in 2005 may therefore make anomalous, prolonged dust events more likely to occur than in 2008 by increasing the potential for days of high dust presence, which may then persist for several days if midtropospheric conditions are conducive. Ultimately, episodes of prolonged CWS dust presence thus depend upon the co-occurrence of a quite specific set of independent events relating to the emission of dust and its transport.

Note that actually, a similarly prolonged event to those of 2005 did appear to occur in 2008 – Case 6.4.2.3 – but as this was so early in the summer season that it did not occur over the core CWS dust region. This is because the SHL, which controls the location of monsoon surges [*Couvreux et al.*, 2010], typically does not become fully established in the CWS until late June, favouring a location further east until then [*Lavaysse et al.*, 2009].

The results of this paper show that time-averaged indicators of dustiness are influenced by more than just dust emission: the circulation of the dust following emission can also have a significant impact. This suggests that caution must be applied when using observations of increased dustiness over a period to imply more emission. In fact, there is evidence to suggest that actually more individual dust emission events may have occurred in 2008 than in 2005. We have manually counted the number of LLJ events to occur in the two summers – identifiable as dust streaks that originate in the morning hours under clear sky conditions – and find that 2008 experienced almost double that of 2005 (250 vs 131). Of these, the greatest difference is in the number of events driven by the northeasterly Harmattan flow, originating in central, eastern and southern Algeria, northern Niger and northern Mali. Although manual counting of individual dust events is subjective and subject to the limitations of the SEVIRI dust scheme as outlined by

Brindley et al. [2012], a southerly anomaly across much of eastern Algeria in 925hPa wind fields is indicative of weakened Harmattan flow towards the CWS dust peak region in 2005 compared with 2008 (Figure 6.11b), which supports these results.

6.6. Summary and concluding remarks

In this paper we have identified controls on interannual variability in summertime dust presence over the CWS between 2004 and 2010 inclusive by focussing on the two most extreme years in this period: 2005, the dustiest summer, and 2008, the least dusty. Much of the difference is due to 3 multi-day periods of prolonged dust presence that occur in 2005. We compare these periods to the 3 largest to occur in 2008 and highlight that the key reason for the difference in dust duration time over the CWS is the nature of the midtropospheric flow. When this flow is northeasterly, it acts quickly to transport emitted dust towards the south/southwest and away from the region. When this flow is replaced by calm winds or weak easterlies/southerlies, the dust is able to remain in suspension above the CWS for much longer, often several days, until either the northeasterly flow is re-established or the dust is advected away from the region along an alternative pathway. The nature of the midtropospheric flow is dictated by the strength and location of the anticyclone present at these levels, which shows strong interactions with the midlatitudes. In identifying the control of the midtropospheric flow on dust residence time over the CWS we have demonstrated that variability in atmospheric dustiness is not simply a function of surface conditions and meteorology. The midtroposphere appears to be an active player in modulating atmospheric dust levels and not simply a passive recipient of dust. The veracity of model representations of individual dust events and longer-term

climatologies will depend upon the accurate simulation of the circulation at this level, which is shown to be highly variable.

6.7. References

Allen, C. J. T., R. Washington, and S. Engelstaedter (2013), Dust emission and transport mechanisms in the central Sahara: Fennec ground-based observations from Bordj Badji Mokhtar, June 2011, *Journal of Geophysical Research: Atmospheres* (in press), doi:10.1002/jgrd.50534.

Ashpole, I., and R. Washington (2012), An automated dust detection using SEVIRI: A multiyear climatology of summertime dustiness in the central and western Sahara, *Journal of Geophysical Research*, *117*(D8), D08202, doi:10.1029/2011JD016845.

Ashpole, I., and R. Washington (2013), A new high-resolution central and western Saharan summer time dust source map from automated satellite dust plume tracking, *Journal of Geophysical Research: Atmospheres*, doi:10.1002/jgrd.50554.

Ashpole, I., and R. Washington (submitted), Intraseasonal variability and atmospheric controls on daily dust occurrence over the central and western Sahara, *Journal of Geophysical Research*, doi:2013JD020267.

Brindley, H., P. Knippertz, C. Ryder, and I. Ashpole (2012), A critical evaluation of the ability of the Spinning Enhanced Visible and Infrared Imager (SEVIRI) thermal infrared red-green-blue rendering to identify dust events: Theoretical analysis, *Journal of Geophysical Research*, *117*(D7), D07201, doi:10.1029/2011JD017326.

Chauvin, F., R. Roehrig, and J.-P. Lafore (2010), Intraseasonal Variability of the Saharan Heat Low and Its Link with Midlatitudes, *Journal of Climate*, *23*(10), 2544–2561, doi:10.1175/2010JCLI3093.1.

Chiapello, I., C. Moulin, and J. M. Prospero (2005), Understanding the long-term variability of African dust transport across the Atlantic as recorded in both Barbados surface concentrations and large-scale Total Ozone Mapping Spectrometer (TOMS) optical thickness, *Journal of Geophysical Research*, *110*(D18), D18S10, doi:10.1029/2004JD005132.

Couvreux, F., F. Guichard, O. Bock, B. Campistron, J.-P. Lafore, and J.-L. Redelsperger (2010), Synoptic variability of the monsoon flux over West Africa prior to the onset, *Quarterly Journal of the Royal Meteorological Society*, *136*(S1), 159–173, doi:10.1002/qj.473.

Cuesta, J., J. H. Marsham, D. J. Parker, and C. Flamant (2009), Dynamical mechanisms controlling the vertical redistribution of dust and the thermodynamic structure of the West Saharan atmospheric boundary layer during summer, *Atmospheric Science Letters*, doi:10.1002/asl.

Dee, D. P., S. M. Uppala, A. J. Simmons, P. Berrisford, P. Poli, S. Kobayashi, U. Andrae, M. A. Balmaseda, G. Balsamo, P. Bauer, P. Bechtold, A. C. M. Beljaars, L. van de Berg, J. Bidlot, N. Bormann, C. Delsol, R. dragani, M. Fuentes, A. J. Geer, L. Haimberger, S. B. Healy, H. Hersbach, E. V. Holm, L. Isaksen, P. Kallberg, M. Kohler, M. Marticardi, A. P. McNally, B. M. Monge-Sanz, J.-J. Morcrette, B.-K. Park, C. Peubey, P. de Rosnay, C. Tavolato, J.-N. Thepaut, and F. Vitart (2011), The ERA-Interim reanalysis: configuration and performance of the data assimilation system,

Quarterly Journal of the Royal Meteorological Society, *137*(656), 553–597, doi:10.1002/qj.828.

Dunion, J. P., and C. S. Velden (2004), The Impact of the Saharan Air Layer on Atlantic Tropical Cyclone Activity, *Bulletin of the American Meteorological Society*, *85*(3), 353–365, doi:10.1175/BAMS-85-3-353.

Engelstaedter, S., I. Tegen, and R. Washington (2006), North African dust emissions and transport, *Earth-Science Reviews*, *79*(1-2), 73–100, doi:10.1016/j.earscirev.2006.06.004.

Haywood, J., P. Francis, S. Osborne, M. Glew, N. Loeb, E. J. Highwood, D. Tanré, G. Myhre, P. Formenti, and E. Hirst (2003), Radiative properties and direct radiative effect of Saharan dust measured by the C-130 aircraft during SHADE: 1. Solar spectrum, *Journal of Geophysical Research*, *108*(D18), 8577, doi:10.1029/2002JD002687.

Haywood, J. M., R. P. Allan, I. Culverwell, T. Slingo, S. Milton, J. Edwards, and N. Clerbaux (2005), Can desert dust explain the outgoing longwave radiation anomaly over the Sahara during July 2003?, *Journal of Geophysical Research*, *110*(D5), D05105, doi:10.1029/2004JD005232.

Jickells, T. D., Z. S. An, K. K. Andersen, A. R. Baker, G. Bergametti, N. Brooks, J. J. Cao, P. W. Boyd, R. A. Duce, K. A. Hunter, H. Kawahata, N. Kubilay, J. laRoche, P. S. Liss, N. Mahowald, J. M. Prospero, A. J. Ridgwell, I. Tegen, and R. Torres (2005), Global iron connections between desert dust, ocean biogeochemistry, and climate., *Science (New York, N.Y.)*, *308*(5718), 67–71, doi:10.1126/science.1105959.

Koren, I., Y. J. Kaufman, R. Washington, M. C. Todd, Y. Rudich, J. V. Martins, and D. Rosenfeld (2006), The Bodélé depression: a single spot in the Sahara that provides most of the mineral dust to the Amazon forest, *Environmental Research Letters*, *1*(1), 014005, doi:10.1088/1748-9326/1/1/014005.

Lavaysse, C., C. Flamant, S. Janicot, D. J. Parker, J.-P. Lafore, B. Sultan, and J. Pelon (2009), Seasonal evolution of the West African heat low: a climatological perspective, *Climate Dynamics*, *33*(2-3), 313–330, doi:10.1007/s00382-009-0553-4.

Lavaysse, C., C. Flamant, S. Janicot, and P. Knippertz (2010), Links between African easterly waves, midlatitude circulation and intraseasonal pulsations of the West African heat low, *Quarterly Journal of the Royal Meteorological Society*, *136*(S1), 141–158, doi:10.1002/qj.555.

Lavaysse, C., J.-P. Chaboureau, and C. Flamant (2011), Dust impact on the West African heat low in summertime, *Quarterly Journal of the Royal Meteorological Society*, *137*(658), 1227–1240, doi:10.1002/qj.844.

Lensky, I. M., and D. Rosenfeld (2008), and Physics Clouds-Aerosols-Precipitation Satellite Analysis Tool (CAPSAT), *Atmos. Chem. Phys.*, (1998), 6739–6753.

Mahowald, N. M., M. Yoshioka, W. D. Collins, A. J. Conley, D. W. Fillmore, and D. B. Coleman (2006), Climate response and radiative forcing from mineral aerosols during the last glacial maximum, pre-industrial, current and doubled-carbon dioxide climates, *Geophysical Research Letters*, *33*(20), L20705, doi:10.1029/2006GL026126.

Mahowald, N. M., S. Kloster, S. Engelstaedter, J, K, Moore, S. Mukhopadhyay, J. R. McConnell, S. Albani, S. C. Doney, A. Bhattacharya, M. A. J. Curran, M. G. Flanner, F. M. Hoffman, D. M. Lawrence, K. Lindsay, P. A. Mayewski, J. Neff, D. Rothenberg, E. Thomas, P. E. Thornton, and C. S. Zender (2010), Observed 20th century desert dust variability: impact on climate and biogeochemistry, *Atmos. Chem. Phys.*, *10*(22), 10875–10893, doi:10.5194/acp-10-10875-2010.

Marsham, J.H., Hobby, M., Allen, C.J.T., Banks, J.R., Bart, M., Brooks, B.J., Cavazos-Guerra, C., Engelstaedter, S., Gascoyne, M., Lima, A.R., Martins, J.V., McQuaid, J.B.,

O'Leary, A., Ouchene, B., Ouladichir, A., Parker, D.J., Saci, A., Salah-Ferroudj, , R. (2013), Meteorology and dust in the central Sahara: Observations from Fennec supersite-1 during the June 2011 Intensive Observation Period, *Journal of Geophysical Research*, doi:10.1002/jgrd.50211.

Mcfiggans, G., P. Artaxo, U. Baltensperger, H. Coe, M. C. Facchini, G. Feingold, S. Fuzzi, M. Gysel, A. Laaksonen, U. Lohmann, T. F. Mentel, D. M. Murphy, C. D. O'Dowd, J. R. Snider, and E. Weingartner (2006), The effect of physical and chemical aerosol properties on warm cloud droplet activation, *Atmos. Chem. Phys.*, *6*, 2593–2649.

Miller, R.L., Tegen, I. (1998), Climate Response to Soil Dust Aerosols, *Journal of Climate*, *11*, 3247–3267.

Prospero, J. M. (1999), Assessing the Impact of Advected African Dust on Air Quality and Health in the Eastern United States, *Human and Ecological Risk Assessment*, *5*(3), 471–479, doi:10.1080/108070399.1999.10518872.

Prospero, J. M., and P. J. Lamb (2003), African droughts and dust transport to the Caribbean: climate change implications., *Science (New York, N.Y.)*, *302*(5647), 1024–7, doi:10.1126/science.1089915.

Prospero, J.M., Ginoux, P., Torres, O., Nicholson, S.E., Gill, T. E. (2002), Environmental characterization of global sources of atmospheric soil dust identified with the NIMBUS 7 Total Ozone Mapping Spectrometer (TOMS) absorbing aerosol product, *Reviews of Geophysics*, *40*(1), 1002, doi:10.1029/2000RG000095.

Rodríguez-Fonseca, B., S. Janicot, E. Mohino, T. Losada, J. Bader, C. Caminade, F. Chauvin, B. Fontaine, J. Garcia-Serrano, S. Gervois, M. Joly, I. Polo, P. Ruti, P. Roucou, and A. Voldoire (2011), Interannual and decadal SST-forced responses of the West African monsoon, *Atmospheric Science Letters*, *12*(1), 67–74, doi:10.1002/asl.308.

Rodwell, M. J., and T. Jung (2008), Understanding the local and global impacts of model physics changes : An aerosol example, *Quarterly Journal of the Royal Meteorological Society*, *134*, 1479–1497, doi:10.1002/qj.

Rowell, D. P. (2003), The Impact of Mediterranean SSTs on the Sahelian Rainfall Season, *Journal of Climate*, *16*, 849–862.

Tegen, I., K. Schepanski, and B. Heinold (2013), Comparing two years of Saharan dust source activation obtained by regional modelling and satellite observations, *Atmos. Chem. Phys.*, *13*(5), 2381–2390, doi:10.5194/acp-13-2381-2013.

Vizy, E. K., and K. H. Cook (2009), A mechanism for African monsoon breaks: Mediterranean cold air surges, *Journal of Geophysical Research*, *114*(D1), D01104, doi:10.1029/2008JD010654.

Washington, R., M. Todd, N. J. Middleton, and A. S. Goudie (2003), Dust-Storm Source Areas Determined by the Total Ozone Monitoring Spectrometer and Surface Observations, *Annals of the Association of American Geographers*, *93*(2), 297–313.

Chapter 7

Conclusions

7.1. Overview

The CWS is the dustiest place on Earth during the boreal summer. Knowledge of the processes that create this hotspot, quite aside from satisfying the Geographer's desire to understand how nature conspires to fashion the patterns that we see in the world today, is essential if we are to better predict its behaviour in the future and fully appreciate and quantify its role in the Earth System. This is important for a range of reasons that have only been touched on in this thesis. While a dearth of observations from the CWS dictates that our understanding of the region relies to a great extent on the analysis of remotely sensed data, the broad spatial coverage and extremely high temporal sampling of SEVIRI makes it well suited to the job. By unlocking the potential of SEVIRI to closely monitor the presence of dust across the CWS this thesis has highlighted distinct patterns of spatial and temporal variability therein and linked these to known emission mechanisms and features of the larger-scale atmospheric circulation.

The scope of the work was as follows:

- Automation of dust detection using SEVIRI and evaluation against other satellite and surface derived indicators of dust presence;
- Creation of an objective map of CWS dust sources based on the automated tracking of individual dust plumes in SEVIRI data, and identification of the

climatological transport pathways and potential emission mechanisms associated with dust events to originate from the dominant source regions that emerge;

- Classification of dominant patterns of intraseasonal variability in summertime daily dust coverage over the CWS, analysis of their frequency of occurrence throughout the summer and each year, and identification of atmospheric controls on these patterns;
- Identification of atmospheric controls on interannual variability in the frequency of summertime dust presence over the CWS.

This concluding chapter summarises the results presented in the preceding research chapters, focusing specifically on how these address each of the research aims proposed in Section 1.2. These results are then drawn together to form broader conclusions in the context of the existing work in this area. Caveats and limitations to the analyses are discussed, before finally outlining the logical steps to take in the future progression of this work.

7.2. Summary of results

1) *Automate the detection of dust over the CWS during the boreal summer using data from SEVIRI.*
    - *Evaluate against other widely used indicators of dustiness.*

Dust detection is automated based on the widely used SEVIRI dust scheme imagery. This results in a detection that typically identifies moderate-heavy dust loadings, as indicated by comparison of SDF with surface AOD and OMI AAI. The detection of dust is more

difficult at night because of the strong diurnal cycle of surface temperatures, which results in the convergence of nighttime pristine sky spectral characteristics and dust spectral characteristics. Due to different sensitivities of the IR and UV dust signals, there are differences in the overall climatologies of dust presence created by SDF and OMI AAI. This is likely due to the water vapour sensitivity of SDF (as discussed in *Brindley et al.* [2012]). Both agree that dust is frequently present in the southern Algeria/northern Mali region, however.

2) *Derive an objective map of summertime dust sources in the CWS that utilises the native resolution of SEVIRI.*
    - *What are the climatological transport pathways associated with the most frequently active sources?*
    - *What is the spatial association with deep convection?*

An objective map of summertime dust sources in the CWS that utilises the native resolution of SEVIRI is created based upon the automated tracking of individual dust plumes. This reveals the location of persistent sources in unprecedented detail, highlighting the importance of palaeolakes and outwash plains, many in close proximity to the Saharan mountains, and suggests that sand seas are not frequent sources of dust in the CWS. The CWS is clearly divided into two broad domains in terms of transport pathways and association with deep convection: one in central and southwest Algeria and northwest Mali, characterised primarily by transport towards the southwest and very likely dominated by low-level jets embedded in the northeasterly Harmattan winds given a lack of potential association with deep convection; and a second in southern Algeria, northeast Mali and northwest Niger where there is no preferred transport direction and a

strong potential association between dust events and deep convection, pointing towards cold pool outflows as the likely deflation mechanism.

3) *What are the dominant patterns of intraseasonal variability in daily dust coverage over the CWS during the boreal summer?*
    - *Do they occur with the same frequency throughout the summer and every year?*
    - *What are the atmospheric controls on these?*

Intraseasonal variability in daily dust coverage varies in terms of the frequency of dust occurrence and its location. The most commonly occurring dust states are those of relatively low dust detection frequency. On days with relatively high dust occurrence, dust tends to favour either a location close to the Algeria-Mali-Niger border triple point (TP), or further to the northwest across the western half of the Mali-Algeria border (MAB). States in which dust is detected at both locations simultaneously are rare. There is a distinct seasonal progression in preferred dust location from the TP in the early season to the MAB later in the season and a distinct degree of interannual variability in the occurrence frequency of the different states, dominated by the extremes of high and low dust detection frequency.

High daily dust detection frequency is associated with Monsoon surges into the Saharan heat low, while days with less frequent dust presence are characterised by a strong Harmattan through the CWS. This suggests that ultimately the CWS dust hotspot and its intraseasonal progression is a result of WAM dynamics and its day-to-day variability is governed by the interplay between the WAM and Harmattan flows.

4) *What role does the atmospheric circulation play in generating substantial interannual variability in the frequency of summertime dust presence over the CWS?*

There is a substantial degree of interannual variability in summertime CWS dustiness between 2004 and 2010. The dustiest year (2005) is characterised by an increase in dust presence of almost 10 days compared to the least dusty year (2008). A considerable proportion of the difference between the two years is due to a series of three exceptionally large peaks in dust presence in 2005, that each last for several days. This prolonged dust presence is a result of the midtropospheric (700hPa) circulation overlying the CWS. Northeasterly flow acts to transport dust emitted into the CWS atmosphere towards the south/southwest and away from the Sahara. When calm winds or weak easterlies/southerlies overly the CWS, dust is able to remain in suspension above the region for much longer, often several days, until northeasterly flow is re-established. The nature of the midtropospheric flow is dictated by the strength and location of the anticyclone present at these levels. Specifically, it corresponds to its eastern flank. When the anticyclone is focussed on the western side of the continent northeasterly flow overlies the CWS. When it is situated to the north or to the east, the northeasterlies are absent. The anticyclone appears to be strongly influenced by the midlatitudes. Much of the difference in dust coverage between the most and least dusty years is therefore due to differences in the circulation of dust following emission, not due to differences in emission itself, with evidence suggesting that actually more emission events occurred in the least dusty year. The midtropospheric circulation thus appears to be an important control on the atmospheric dust budget of the CWS that needs consideration, in addition to emission controls, when identifying reasons for variability in dustiness over the region.

7.3. Overall conclusions

The CWS dust hotspot is the result of emission from numerous disperse sources driven by multiple processes, but the contribution that each of these makes in terms of the overall presence of dust is spatially variable. The "Harmattan corridor" sources, while some of the most active in the region, are generally not associated with long lived dust over the CWS, since it is transported away from the hotspot area and towards the south/southwest comparatively quickly by the northeasterly flow that very likely initiates emission. The sources from the southern CWS, on the other hand, are generally associated with more sustained dust presence over the CWS, since dust from these regions is carried towards the hotspot area in the southerly WAM flow, where it remains until it is transported away by the overlying flow (usually to the south/southwest), which can sometimes take several days.

The atmosphere into which dust is emitted is not simply a passive recipient of the dust; rather it plays an active role in controlling its residence time over the CWS, which can impose itself on interannual variability in hotspot intensity. This is an aspect of the hotspot that has not previously been explored, since it is not possible with once-daily satellite observations to determine whether detected dust has been freshly emitted or suspended over the desert for several days. The results of this thesis therefore suggest that assumptions about variability in CWS dust emissions cannot be made based on observations of variability in atmospheric CWS dust concentrations.

Given the different transport directions and residence time in the CWS atmosphere of dust from the two broad source regions described, it is reasonable to suggest that the range of impacts within the Earth System will vary too. Dust from the southern Sahara will have a greater impact on the radiative budget of the CWS than dust from the Harmattan corridor, and it is possible that this dust may occasionally follow

alternative large-scale transport pathways if the overlying northeasterlies are absent or may settle back over the CWS due to increased potential for dry deposition here (simply by virtue of greater residence time). Dust from the Harmattan corridor on the other hand may make a more consistent contribution to transatlantic transport due to its more direct route into the AEJ region, which is responsible for the westwards transport of Saharan dust.

The results of this thesis are in broad agreement with the growing scientific consensus on the importance of deep convection in the West African Monsoon flow to summertime CWS dustiness. Recent results from Bordj Badji Mokhtar (BBM) on the Algeria-Mali border (very close to 'H' on Figure 4.5) during the Intensive Observation Period of the Fennec campaign (2011) highlight that cold pool outflows contribute substantial amounts (around 45 - 54 % depending on the method used) to observed local dust uplift [*Allen et al*., 2013; *Marsham et al.*, 2013a, respectively] and suggest that a further 27 % of dust observed at this time is the result of cold pool advection (i.e. emission driven by cold pools elsewhere and then transported to BBM) [*Allen et al.*, 2013]. The foregoing work has highlighted that these results are representative of a longer time period and a broader region, and uniquely highlight that this dust can persist over the Sahara for several days, contributing significantly to the broad dust hotspot detected here during the summer months. All of this reinforces the hypothesis of *Marsham et al.* [2008] that haboobs are key to explaining the summertime dust peak over the CWS. Interestingly, the area dominated by cold pool-driven emission appears to be shielded from the Harmattan flow that governs emission elsewhere by the Hoggar Mountains of south/southeast Algeria. In addition to being preferred sources of deep convection [*Birch et al.*, 2012], they are thought to play a role in dictating the location of monsoon surges, creating a favoured surge location to their southwest [*Couvreux et al.*,

2010]. The distribution of persistent dust sources around the mountain range evident in Figure 4.6 implies that drainage from the highlands under wetter climatic regimes in the past may be crucial in supplying sediment suitable for deflation today. It is an intriguing possibility therefore that the CWS summertime dust hotspot is a somewhat inevitable consequence of the geology and climate history of North Africa.

7.4. Caveats/limitations

Below the significance of data problems and methodological approaches to the overall results and conclusions of this thesis are considered. It should be borne in mind that uncovering and qualifying many of the limitations to SEVIRI dust detection that are outlined was facilitated by the development of SDF for this thesis, which was applied in the *Brindley et al.* [2012] paper to determine whether the dust signal would be detectable in the dust scheme imagery or not.

Many of the caveats/limitations outlined in this section revolve around a lack of observational data from the CWS region. It is work like that presented in this thesis that is essential to building the case for addressing this situation.

7.4.1. SEVIRI

SEVIRI provides a unique view of dust over the CWS, which has shed valuable insights on patterns and causes of spatial and temporal variability therein. It is however only one view, and limitations to the dust detection scheme need to be borne in mind when considering the results and conclusions of this thesis. We consider conditional limitations, the effects of which are variable and ultimately constrain where and when

dust will be detected; and absolute limitations, which dictate that dust detection will fail under all circumstances. The effects of conditional limitations are tested for throughout this thesis, and their implications for the results are considered below. Addressing the absolute limitations is beyond the scope of this thesis. The significance of all limitations discussed can only be properly ascertained by detailed comparison with different dust detection products utilising surface/airborne observations of the 'true' distribution of atmospheric dust.

7.4.1.1. Conditional limitations

First and foremost, dust detection beneath clouds is not possible. In the infrared, this is because the measured IR signal is typically dominated by their cold upper-levels. Clouds are problematic for all dust detection methods based on satellite data, however. Secondly, the widely-used SEVIRI dust scheme, upon which SDF is based, is highly sensitive to the presence of atmospheric water vapour, the lower-tropospheric lapse rate, and the altitude of the dust layer [*Brindley et al.,* 2012]. As in the cloud limitation, this ultimately dictates that under certain atmospheric conditions, dust detection with SEVIRI will fail. Conditional limitations have implications for the following:

1. *Dust source detection*

If dust emission occurs beneath clouds, the source of this emission will be missed. Thus, the designation of regions on cloud boundaries where clusters of SDFs are first detected as dust sources (Section 4.3.2 – see Figure 4.4) is potentially erroneous, since the actual source may be upwind of this location, beneath the parent convective cell. The

downwind bias may be confounded by the water vapour limitation of SEVIRI dust detection, given that cold pools are known to transporting moisture into the Saharan region [*Marsham et al.*, 2013b]. This may contribute to some of the differences in the southern part of the region evident between the automated and manually derived SEVIRI dust source maps (Figure 4.7), since the manual tracking ignores dust events when source detection is complicated by the presence of cloud [*Schepanski et al.*, 2007]. However, the persistent detection of certain source areas in the automated scheme, the collocated surface features and characteristics, and the fact that not all source detections in those areas are associated with deep convection, supports that these are actual source locations. Moreover, given the fact that dust plumes associated with cold pool outflow from deep convection often take the form of elongated fronts that can spread for hundreds of kilometres, it is likely that multiple source areas are activated as opposed to one single point source. The sensitivity of the dust signal to the dust layer altitude may also lead to a downwind offset in source detection, since by the time dust reaches an altitude at which it can be detected it may have been transported some distance away from the source. This would also be a problem for the manual detection method. The benefit of the objective source detection method developed in this thesis is that the effect of any differences made by modifications to the scheme can be quantified and, moreover, a new version of the source map can be quickly computed.

2. *Intraseasonal variability in most frequently active dust sources and the location of the SDF hotspot*

The presence of clouds and high water vapour ultimately constrains where dust can be detected. The ITD, which marks the boundary between moist monsoon and dry Saharan

air, moves north as the summer progresses implying a northwards migration of the southern-most latitudes at which SEVIRI can detect dust, on average (although in reality this is never a smooth boundary transition and this limit will be characterised by a series of northwards and southwards excursions throughout the summer). This may contribute to the observed northwards shift of the most active dust source regions and the SDF hotspot as the summer progresses. There are however plausible climatological explanations for these trends, however: the demonstrated importance of northwards surges of the WAM flow in generating high daily dust presence; and a strengthening of the Harmattan through the CWS, which dominates the central Algerian dust source areas, from June into July and August (Figure 4.8). The northwards contraction of the dust hotspot from June to August is well matched by OMI AAI (Figure 3.15), so is not simply a result of the limitations of SEVIRI dust detection. Additional data are required to determine whether dust (or at least the moderate-heavy dust loadings that typically correspond to SDF) is actually present south of the late-season hotspot and is just obscured by cloud and/or large amounts of atmospheric water vapour.

3. *Intraseasonal and interannual variability in hotspot intensity*

Given that SDFF fields highlight the frequency of detection of dust for a given time period, it is plausible that conditional limitations to the dust detection scheme may at least contribute to patterns of high and low SDFF. Reassuringly, the climatological and deep convection frequency composites that correspond to the HIGHDUST and LOWDUST states in Chapter 5 (Figure 5.7) suggest that states of more frequent dust presence are characterised by greater cloud coverage over the dust hotspot region and an advanced WAM. The opposite would be expected if the dust states were simply a result

of cloud and water vapour limitations to the dust detection scheme. Similarly, while it is possible that these limitations have some bearing on overall SDFF on interannual timescales, they certainly did not appear significant for the case study analysis of Chapter 6 and are therefore are not the dominant difference between extreme years of dust presence.

7.4.1.2. Absolute limitations

As demonstrated in Chapter 3, SDF corresponds to moderate-heavy dust loadings when compared to surface-derived AOD and AAI from the spaceborne OMI. Dust events/source regions that only contribute small quantities of dust to the atmosphere may therefore be missed. Additionally, the IR dust signal used in SEVIRI dust detection is sensitive to dust optical properties, primarily constrained by the composition of the dust, and the underlying surface emissivity [*Brindley et al.*, 2012]. This implies that even under perfect atmospheric conditions SEVIRI still fails in some cases to detect dust and therefore may provide an incomplete picture of CWS dust dynamics and sources.

These absolute limitations are ultimately not expected to have a bearing on the patterns of spatial and temporal variability discussed in this thesis, as the characteristics of dust that is/is not detectable and the locations over which SEVIRI can/cannot detect dust are likely uniform across the whole study period. Moreover, any variability therein is much harder to deduce than variability in cloud coverage, for example.

Some of the limitations discussed above result in a modification to the overall 'strength' of the dust signal in the SEVIRI brightness temperature channels. This is particularly problematic for the fixed thresholds of the SDF detection scheme. It may be possible to

reduce their overall impact on dust detection (i.e. to reduce the likelihood of a missed detection) by modifying this scheme. This is considered in Section 7.5.

7.4.2. ERA Interim

In addition to caveats and limitations concerning SEVIRI dust detection, it should be borne in mind that ERA Interim data are assumed to provide a reliable representation of the atmospheric situation over North Africa during the period of study. This is hard to qualify given the lack of observational data against which to assess them. Many falsely believe that reanalyses represent 'observed' data. While they do incorporate more observations than would have been available at the time of the original analysis, they are nonetheless model data. Especially where there is a lack of observational data to assimilate, their reliability decreases. Moreover, the data will not represent atmospheric features known to affect atmospheric dynamics. These include dust, the importance of which on weather and climate modelling has been emphasised throughout this thesis; and cold pool outflows from deep convection, the resolution of which requires spatial resolution significantly above that of the ERA Interim model but which recent observations suggest are of importance to the overall Saharan climate [*Garcia-Carreras et al.*, 2013].

Despite these limitations, reanalysis data are widely used in all aspects of Saharan climate research in lieu of spatially and temporally dense observations, and ERA Interim is common throughout the literature. The data are used in this thesis to address quite large-scale components of the Saharan Climate system as opposed to small features in which the detail is important where model shortcomings are likely to be more of a

problem. A comparison with an alternative reanalysis dataset would help qualify this assumption, however.

7.5. Future work

An obvious next step for this work would be to quantify the relative importance of each source area identified in Chapter 4 to the overall CWS dust hotspot. One approach would be to simply 'switch off' the sources by suppressing the tracked dust events known to originate from them and then recalculating SDFF fields. The effect of switching off different sources on overall CWS dust coverage could then be calculated. A similar method could be used with events associated with deep convection, for example. An alternative approach would be to utilise SEVIRI Aerosol Optical Depth (AOD) retrievals described by *Banks and Brindley* [2013] to quantify how much dust these different source areas actually emit. It may be that the most frequently activated source areas are associated with events of relatively much lower AOD than less persistent source regions. Again, events linked to deep convection and those initiated under clear sky conditions could be compared. An obstacle to overcome would be the temporal limitation of AOD to the 6 am-4 pm period, however. This should not be too problematic given that the tracked SDF events are linked through time.

Utilising a similar method, SEVIRI AOD could be utilised in combination with the tracked SDF events to determine how the AOD of an event varies over its lifetime. The assumption is that AOD will be highest close to source and that this will gradually decrease as the dust is advected away – but is this actually the case? One currently intractable problem is whether dust emission occurs along the corridor of dust transport.

An increase in AOD away from the source of the event would imply that additional, obscured sources are being activated.

The results presented in this thesis would benefit from any improvements to the dust detection scheme. *Murray et al.* [2013], demonstrates that weak dust signals in SEVIRI over the key southern African source regions can be enhanced by comparison of brightness temperatures at multiple wavelengths (not just at 10.8μm as in the SDF algorithm) to corresponding clear-sky composites. A similar approach might reduce SDF limitations concerning dust loadings, surface emissivity, and dust composition. Part of the problem with SDF is the fixed threshold method. A fruitful course of action might be to relax these thresholds in the time period and area surrounding dust that is already detected using SDF. In particular this could help to further improve the precision of source detection, since it has been demonstrated in sensitivity studies elsewhere that restrictive thresholding can foreshorten dust plumes and result in a downwind bias to source detection [*Baddock et al.*, 2009]. Regarding sensitivity of the dust detection to atmospheric moisture, alternative brightness temperature thresholds might improve detection, since it is possible by manual inspection of SEVIRI dust scheme imagery to infer that the atmosphere contains a mixture of dust and water vapour by the presence of purple shading, as opposed to magenta that is typical of dust. This is often common in cold pool outflow regions, with the purple eventually tending towards pink.

The relationship between increased CWS dust presence and monsoon surges could be used to explore how the hotspot intensity may change under different climate change scenarios. A necessary first step however would be to identify whether every monsoon surge is associated with a dust outbreak over the CWS. If not, what are the differences between those that are and those that aren't? Similarly, any changes in the midtropospheric circulation will have consequences for hotspot intensity.

Beyond the CWS, work is already ongoing to expand the temporal coverage of the automated dust and source detection schemes to consider all seasons of the year. While the boreal summer is the peak dust season for the CWS, Harmattan transport of dust from here occurs throughout the year, affecting millions of people in the Sahel, especially during the boreal winter when the Inter Tropical Convergence Zone (ITCZ) is at its southern-most location and northeasterlies dominate the whole of West Africa, resulting in ubiquitous dust presence at Sahelian latitudes [*Engelstaedter and Washington*, 2007; *N'tchayi Mbourou et al.*, 1997]. It is therefore important to understand controls on variability in this transport. Similarly, the dust and source detection schemes outlined in this thesis will be expanded spatially to cover the whole of North Africa and the Middle East. While the CWS and Bodélé Depression have received much research attention, the dust dynamics of the rest of the East African and Middle East region remain to be well understood. Of particular interest are areas in Sudan that peak in the boreal spring – summer period [*Ginoux et al.*, 2012; *Schepanski et al.*, 2007] and Saudi Arabia and Iran that peak around the same time [*Ginoux et al.*, 2012].

A personal ambition is to conduct fieldwork at the source areas identified in Chapter 4. We have no description of the geomorphological and sedimentological characteristics of these sites and these are a crucial control on dust emission through their influence on surface erodibility and the actual processes responsible for the production of dust that is then uplifted into the atmosphere, such as sand blasting, aggregate disintegration or aerodynamic entrainment. The reliability of the soil and land-surface parameters that provide these details in model simulations are known to be a key limitation on dust emission modelling [*Shao et al.*, 2011]. Observations from source regions in projects such as BoDEx (the Bodélé Depression) and DO4 Models (southern Africa) have provided valuable new insights about the surface characteristics and

production of dust at the surface that can help evaluate model simulations of dust [e.g. *Todd et al.*, 2008; *Haustein et al.*, 2013; *King et al.*, 2013]. Some of the sources in the CWS area are unfortunately out of reach due to political instability and war in the region (especially those of northern Mali), but the central Algerian sources represent possible sites to target for field campaigns in the future.

7.6. References

Allen, C. J. T., R. Washington, and S. Engelstaedter (2013), Dust emission and transport mechanisms in the central Sahara: Fennec ground-based observations from Bordj Badji Mokhtar, June 2011, *Journal of Geophysical Research: Atmospheres*, doi:10.1002/jgrd.50534.

Baddock, M. C., J. E. Bullard, and R. G. Bryant (2009), Dust source identification using MODIS: A comparison of techniques applied to the Lake Eyre Basin, Australia, *Remote Sensing of Environment*, *113*(7), 1511–1528, doi:10.1016/j.rse.2009.03.002.

Banks, J. R., and H. E. Brindley (2013), Evaluation of MSG-SEVIRI mineral dust retrieval products over North Africa and the Middle East, *Remote Sensing of Environment*, *128*, 58–73, doi:10.1016/j.rse.2012.07.017.

Birch, C. E., D. J. Parker, J. H. Marsham, and G. M. Devine (2012), The effect of orography and surface albedo on stratification in the summertime Saharan boundary layer: Dynamics and implications for dust transport, *Journal of Geophysical Research*, *117*(D5), D05105, doi:10.1029/2011JD015965.

Brindley, H., P. Knippertz, C. Ryder, and I. Ashpole (2012), A critical evaluation of the ability of the Spinning Enhanced Visible and Infrared Imager (SEVIRI) thermal infrared red-green-blue rendering to identify dust events: Theoretical analysis, *Journal of Geophysical Research*, *117*(D7), D07201, doi:10.1029/2011JD017326.

Bullard, J. E., S. P. Harrison, M. C. Baddock, N. Drake, T. E. Gill, G. McTainsh, and Y. Sun (2011), Preferential dust sources: A geomorphological classification designed for use in global dust-cycle models, *Journal of Geophysical Research*, *116*(F4), F04034, doi:10.1029/2011JF002061.

Couvreux, F., F. Guichard, O. Bock, B. Campistron, J.-P. Lafore, and J.-L. Redelsperger (2010), Synoptic variability of the monsoon flux over West Africa prior to the onset, *Quarterly Journal of the Royal Meteorological Society*, *136*(S1), 159–173, doi:10.1002/qj.473.

Engelstaedter, S., and R. Washington (2007b), Atmospheric controls on the annual cycle of North African dust, *Journal of Geophysical Research*, *112*(D3), D03103, doi:10.1029/2006JD007195.

Garcia-Carreras, L., J. H. Marsham, D. J. Parker, C. L. Bain, S. Milton, a. Saci, M. Salah-Ferroudj, B. Ouchene, and R. Washington (2013), The impact of convective cold pool outflows on model biases in the Sahara, *Geophysical Research Letters*, *40*(8), 1647–1652, doi:10.1002/grl.50239.

Ginoux, P., J. M. Prospero, T. E. Gill, N. C. Hsu, and M. Zhao (2012), Global-scale attribution of anthropogenic and natureal dust sources and their emission rates based on MODIS Deep Blue aerosol products, *Reviews of Geophysics*, *50*(RG3005), doi:10.1029/2012RG000388.

Haustein, K., J. King, G. Wiggs, and R. Washington (2013), Do4Models : Performance of current climate model dust emission schemes from a 1D box model perspective using field campaign data to constrain the simulated dust emission flux, in *European Geosciences Union General Assembly 2013*, vol. 15, EGU2013-11641

King, J., K. Haustein, G. F. S. Wiggs, F. Eckardt, D. S. G. Thomas, and R. Washington (2013), The role of roughness in predicting transport thresholds on desert surfaces : temporal and spatial variability, in *European Geosciences Union General Assembly 2013*, vol. 15, EGU2013-13760

Marsham, J. H., D. J. Parker, C. M. Grams, C. M. Taylor, and J. M. Haywood (2008), Uplift of Saharan dust south of the intertropical discontinuity, *Journal of Geophysical Research*, *113*(D21), D21102, doi:10.1029/2008JD009844.

Marsham, J.H., Hobby, M., Allen, C.J.T., Banks, J.R., Bart, M., Brooks, B.J., Cavazos-Guerra, C., Engelstaedter, S., Gascoyne, M., Lima, A.R., Martins, J.V., McQuaid, J.B., O'Leary, A., Ouchene, B., Ouladichir, A., Parker, D.J., Saci, A., Salah-Ferroudj, R. (2013a), Meteorology and dust in the central Sahara: Observations from Fennec supersite-1 during the June 2011 Intensive Observation Period, *Journal of Geophysical Research*, doi:10.1002/jgrd.50211.

Marsham, J. H., N. S. Dixon, L. Garcia-Carreras, G. M. S. Lister, D. J. Parker, P. Knippertz, and C. E. Birch (2013b), The role of moist convection in the West African monsoon system: Insights from continental-scale convection-permitting simulations, *Geophysical Research Letters*, doi:10.1002/grl.50347.

Murray, J. E., H. E. Brindley, R. G. Bryant, J. E. Russell, and K. F. Jenkins (2013), Enhancing weak transient signals in SEVIRI false colour imagery : application to dust source detection in southern Africa, in *European Geosciences Union General Assembly 2013*, vol. 15, EGU2013–5363.

N'tchayi Mbourou, G. N., J. J. Bertrand, and S. E. Nicholson (1997), The diurnal and seasonal cycles of wind-borne dust over Africa north of the equator, *Journal of Applied Meteorology, 36*(7), 868–882.

Schepanski, K., I. Tegen, B. Laurent, B. Heinold, and A. Macke (2007), A new Saharan dust source activation frequency map derived from MSG-SEVIRI IR-channels, *Geophysical Research Letters*, *34*(18), L18803, doi:10.1029/2007GL030168.

Shao, Y., K.-H. Wyrwoll, A. Chappell, J. Huang, Z. Lin, G. H. McTainsh, M. Mikami, T. Y. Tanaka, X. Wang, and S. Yoon (2011), Dust cycle: An emerging core theme in Earth system science, *Aeolian Research*, *2*(4), 181–204, doi:10.1016/j.aeolia.2011.02.001.

Todd, M. C., D. Bou Karam, C. Cavazos, C. Bouet, B. Heinold, J. M. Baldasano, G. Cautenet, I. Koren, C. Perez, F. Solmon, I. Tegen, P. Tulet, R. Washington, and A. Zakey (2008b), Quantifying uncertainty in estimates of mineral dust flux: An intercomparison of model performance over the Bodélé Depression, northern Chad, *Journal of Geophysical Research*, *113*(D24), D24107, doi:10.1029/2008JD010476.